Performance-Based Screening of Porous Materials for Carbon Capture

Amir H. Farmahini,* Shreenath Krishnamurthy, Daniel Friedrich, Stefano Brandani, and Lev Sarkisov*
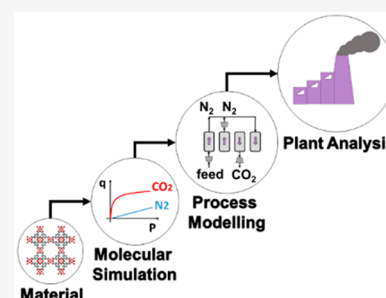
Read Online

ACCESS | Metrics & More | Article Recommendations

ABSTRACT: Computational screening methods have changed the way new materials and processes are discovered and designed. For adsorption-based gas separations and carbon capture, recent efforts have been directed toward the development of multiscale and performance-based screening workflows where we can go from the atomistic structure of an adsorbent to its equilibrium and transport properties at different scales, and eventually to its separation performance at the process level. The objective of this work is to review the current status of this new approach, discuss its potential and impact on the field of materials screening, and highlight the challenges that limit its application. We compile and introduce all the elements required for the development, implementation, and operation of multiscale workflows, hence providing a useful practical guide and a comprehensive source of reference to the scientific communities who work in this area. Our review includes information about available materials databases, state-of-the-art molecular simulation and process modeling tools, and a complete catalogue of data and parameters that are required at each stage of the multiscale screening. We thoroughly discuss the challenges associated with data availability, consistency of the models, and reproducibility of the data and, finally, propose new directions for the future of the field.

CONTENTS

1. INTRODUCTION

Recent discoveries in material science and advances in computational chemistry are having a profound impact on the way we approach design and optimization of chemical processes, devices, and technologies.

Traditionally, the workflow for the design of a process or a device would focus on a small number of materials available for experimentation and testing, as shown in the top panel of Figure 1. If performance of the material was not satisfactory, the experience gained in the process and the intuition of the investigator would guide the search for another material to be tried or suggest some modification of the existing material.

Unprecedented developments in material science in the last 20−30 years have challenged this approach. Indeed, over this period, several new classes of materials have been discovered with each class encompassing hundreds or even thousands of members. Testing all these materials in relevant experiments, according to the traditional workflow, is prohibitive in terms of cost and effort. Alternatively, performance of the materials can be first tested using a computer model with a view to focusing the experimental phase only on the most promising candidates. Moreover, using computational methods allows chemists and materials scientists to explore the performance of hypothetical, not yet synthesized materials. This is important both for the new classes of materials and for the well-known classes, where the phase space is significant (i.e., alloys). Within the new workflow,
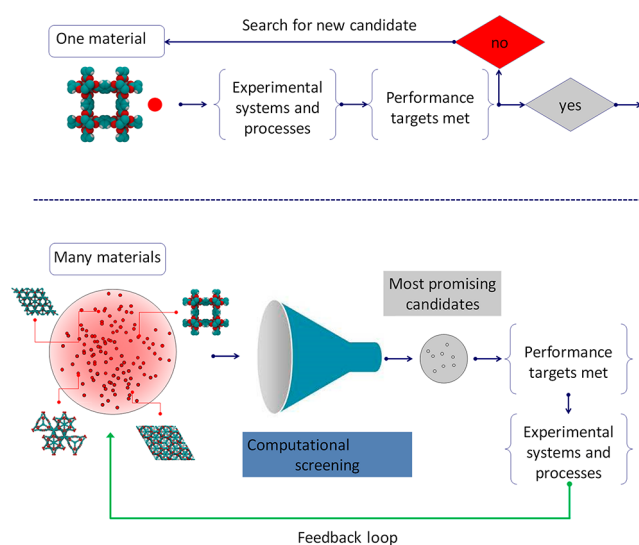
Figure 1. Traditional (top) and emerging (bottom) approaches to material selection for an application. Within the emerging approaches, a significant role is played by computational screening of a large database of materials, with the experimental effort focused only on the most promising candidates.

the process starts from the assembly of a large database of materials (real, hypothetical, or both), shown in the bottom of Figure 1 as a cloud of points. Their performance is then assessed using computational modeling. The most promising candidates are passed on to the experimental phase for validation and testing. In the feedback loop, the information obtained at the experimental stage is used to search for specific properties and functionalities within the database of materials to further enhance performance of the process.

This is a new strategy for *in silico* discovery of new materials and high-throughput screening of materials for various applications. A review by Curtarolo et al.[1] identifies the following areas where this strategy is likely to make the most significant impact: alloys, solar materials, photocatalytic water splitting, materials for carbon capture and sequestration, nuclear detection and scintillators, topological insulators, piezoelectric and thermoelectric materials, and materials for catalysis, energy storage and batteries. These developments also come with new challenges, for example, how to organize and share large material databases, how to navigate the clouds of materials properties to identify the most promising candidates, and how to relate material properties to their actual performance at the process level. Some of these challenges have been recognized through forming large scale collaborative projects, such as the Material Genome Initiative[2] and the Materials Cloud project.[3]

Carbon capture, reviewed in the article by Curtarolo et al., is an example of a chemical separation process.[1] Significant reduction of carbon emissions from power plants has been on the top of the agenda in the scientific and technology policies of the major economies in the world. Most decarbonization scenarios show that carbon capture is needed to reach net zero emissions.[4] The main challenge in the implementation of carbon capture technologies for existing plants is significant additional energy (and, ultimately, financial) cost associated with the process. Adsorption and membrane separations have been considered as energy efficient alternatives to the traditional amine-solution based processes. Similar factors have been driving developments in other chemical separation processes:
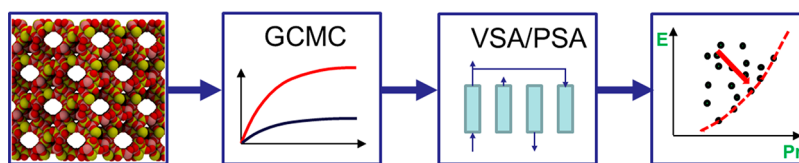
Figure 2. Multiscale workflow concepts in vacuum swing adsorption (VSA) and pressure swing adsorption (PSA) engineering. The starting point of the workflow is the structure of the porous material (either experimental or hypothetical, on the left). Molecular simulations are used to obtain equilibrium adsorption and kinetics data. Process simulations are performed for various cycle configurations. Finally, on the right, performance of the material is assessed in terms of energy (E)−productivity (Pr) trade-offs, with the red arrow in the graph indicating progression of this assessment toward the Pareto front (dashed red line).

as has been recently discussed by Sholl and Lively,[5] overall these processes consume 15% of the worldwide energy, and naturally, there is a significant incentive to reduce this impact by developing more efficient alternatives.

At the heart of an adsorption or a membrane process is the material used as an adsorbent or a membrane. The efficiency of the process hinges on the characteristics of this material and the interplay between the material characteristics and process configuration. Recently, several new families of porous materials, such as metal−organic frameworks (MOFs),[6−8] zeolitic imidazolate frameworks (ZIFs),[9] covalent organic frameworks (COFs),[10] porous organic cages (POCs),[11] porous aromatic frameworks (PAFs),[12] and polymers, including porous polymer networks (PPNs)[13] and polymers with intrinsic microporosity (PIMs),[14,15] have been discovered. A common motif associated with these families is a large number of (synthesized and hypothetical) members available within each family, as well as tunability and exquisite control of structural characteristics of the materials such as surface area, pore size distribution (PSD), and surface chemistry. This has prompted extensive research efforts to explore these new landscapes of structures to identify new porous materials with superior characteristics for adsorption applications, such as carbon capture.

The initial efforts in this field were led by the molecular simulation community, with various computational tools being used to obtain structural (e.g., surface area and porosity) and functional characteristics (e.g., equilibrium adsorption data) of the materials. These properties or metrics were then used to explore possible correlations between them and the function of the material in the actual application. An important question emerged from these early computational screening studies concerns the process descriptors or performance metrics: what descriptors and metrics should one actually adopt for ranking and selection of materials for a specific application? A useful metric must somehow reflect the essence of the process under consideration. For example, for methane storage, the realistic metric is the working capacity, in other words the specific amount of methane released by the material when pressure is reduced from the storage pressure to the lowest pressure in the device, as oppose to the absolute capacity, corresponding to the lowest pressure being zero.

If for some applications, such as gas storage, a single metric may suffice the selection process, for other more complex dynamic processes this is not possible. This was eloquently demonstrated by Rajagopalan et al.[16] by comparing a broad range of traditional and new separation performance metrics developed over the years with the actual performance of the material in the process simulation using postcombustion CO_2 capture as a case study.

In fact, a significant amount of literature and studies have been accumulated over the years on design and optimization of

pressure, vacuum, temperature, concentration, electrical properties, and microwave swing adsorption processes, from simplified equilibrium models to more advanced numerical approaches.[17−28] Typically, these studies focus on a particular process configuration, defined as the number of units, their arrangement, and the conditions. For each process, cycle configuration, defined as the specifications of individual steps in the cycle, is optimized to meet specific process objectives. In the case of the postcombustion carbon capture application, the objectives (or constraints of the process) are 90% recovery of the CO_2 from the feed with 95% purity, as recommended by the US Department of Energy (DOE) based on the emission control targets and storage requirements.[29] The efficiency of the process and hence performance of the material for the process can then be assessed from the perspective of two metrics: productivity, in other words the amount of CO_2 captured per unit of time by a unit of volume of the adsorbent, and energy penalty, which is the energy required to capture a mole of CO_2 in the process. These two metrics are in competition with each other and a complex trade-off between them cannot be captured using simplified equilibrium-based figures of merits.

The concurrent developments in computational screening based on molecular simulations and in advanced process simulations invariably led to the following proposition: what if the screening of porous materials for dynamic adsorption processes can be implemented using realistic process simulations while the microscale properties of materials are provided by molecular simulations? This multiscale screening protocol is schematically depicted in Figure 2. According to this diagram, molecular simulations can be used to obtain equilibrium data (e.g., adsorption isotherms), dynamic properties (e.g., micropore diffusivity), or other materials characteristics (e.g., thermal properties), if needed. This information is then fed into a process simulator and the performance of the materials is assessed using the metrics previously developed for dynamic adsorption process analysis.

The first examples of such a multiscale approach were published in two pioneering studies by Hasan et al.[30] for *in silico* screening of zeolite materials in the context of carbon capture and by Banu et al.[31] for computational screening of MOFs for hydrogen purification. The early endeavors into the field of performance-based materials screening also exposed a number of challenges. These challenges are associated with consistent and reliable transfer of data and information between the different levels of the simulation (e.g., from molecular simulations to process simulations), sensitivity of the process simulation predictions to the properties that cannot be obtained from molecular simulations, lack of experimental validation of the process simulation predictions, the accuracy of the produced material rankings, and propagation of errors, just to name a few.

Early studies also indicate that multiscale approaches where one is able to seamlessly progress from a material structure to its performance in the actual process or device will become of immense importance in the near future. With the advent of machine learning and quantum-mechanical methods, we are witnessing the dawn of material-driven process design, which will have a profound impact on a number of technologies and applications. Hence, this review is prompted by recognition of the importance of this emerging field for materials screening and discovery and the challenges that have been already encountered in the early studies. Here, we aim not only to provide a critical review of the topic by discussing previous contributions and developments of the field but also to offer a practical guide and a single source of information for both "users" and "developers" of the performance-based materials screening workflows. The users can include chemists and materials scientists working on the development and characterization of new adsorbents. They can simply use screening workflows to evaluate performance of their newly synthesized (or yet to be synthesized) materials in a target application. The developers, on the other hand, include computational chemists and molecular modelers (who develop molecular models and force fields for molecular simulations), experts in the field of process modeling and optimization (who develop new methods for simulation of the actual processes), and data scientists taking on the development of advanced machine-learning frameworks to better explore materials–performance space.

Although some of the background information provided as part of this review is also available in classical textbooks and field-specific review articles, it is not straightforward for various practitioners coming from different backgrounds to quickly extract, compile, and synthesize the information needed for the advancement of this highly interdisciplinary field. Moreover, it is important to put different elements of the materials screening workflow (being simulation methods or tools) into the same perspective and highlight their relations with respect to one another in order to demonstrate the difficulties that arise when they are integrated into a single workflow. Hence, we have undertaken the task to compile and synthesize all the elements and ingredients needed for the development of the afore-mentioned screening workflows for the wide range of readers of this review.

We note that although this review deliberately focuses on postcombustion carbon capture using Pressure Swing Adsorption (PSA) and Vacuum Swing Adsorption (VSA) processes, the multiscale workflow developed for this purpose and the challenges associated with advancement of this approach will be similar for a wide range of other separations processes such as hydrogen separation, oxygen purification, air separation, and so on.

Throughout this review, we aim to highlight the fact that development of accurate and efficient multiscale workflows for realistic screening of porous materials can only be successful if scientists working on different elements of these workflows are aware of the requirements of other parts. We also hope that the current review can encourage more cross-disciplinary collaborations in this emerging field and lead to the development of multiscale screening tools to be used in a variety of settings, from chemistry laboratories to chemical engineering pilot plants. With this in mind, the specific objectives of this review are as follows:

(i) Critically review recent contributions and major developments in the field of performance-based materials screening for postcombustion carbon capture using PSA or VSA processes.

(ii) Provide a practical guide and a single source of information on the principles of molecular and process simulations, a full list of data and parameters required at each stage, sources of data, and sources of uncertainties.

(iii) Review the key challenges in the implementation of the multiscale screening strategies and how they can be tackled.

(iv) Outline the existing gaps and propose directions for future developments and trends in this emerging field.

The review is divided into nine main sections. After this introduction, sections 2, 3, 4, and 5 will cover the application in question (postcombustion carbon capture), explain different elements of pressure and vacuum swing adsorption processes, discuss a hierarchy of metrics that can be used for selection and screening of porous materials for this application, and provide a historical perspective on how computational screening methods evolved over the last 10 years toward current multiscale workflows. We also critically review the methods proposed and used so far in application to materials screening. Section 6 mirrors in its structure the multiscale workflow depicted in Figure 2. Here, we will cover practical aspects associated with material databases and the tools available for structural characterization of materials that are currently collected by these databases. Next, we will move to introduce the fundamentals of molecular simulations and process modeling. We will explain how these elements should be used together and as part of a multiscale workflow for materials screening. For each method, we will also introduce available simulation tools and software packages that can be used for performing these types of simulations. Our emphasis will be on explaining what data are required at each stage and what information is obtained at each level, but we will also discuss the gaps in the methods that need to be addressed. In section 7, we review current progress and state-of-the-art in the process-level studies of VSA and PSA systems for carbon capture, including advanced process configurations for this task. In section 8, we explore the challenges associated with accuracy, model consistency, data availability and reproducibility of the results for materials screening, and provide our suggestions for addressing them, which we hope will stimulate further cross-disciplinary approaches and collaborations. Finally, in section 9, we reflect on the overall picture emerging so far, we discuss the roadblocks to industrial applications, and we finish with a brief discussion on future opportunities and possible directions of research in multiscale, performance-based screening of porous materials for carbon capture and other adsorptive separations.

2. POSTCOMBUSTION CARBON CAPTURE

Carbon capture and sequestration (CCS)[32−35] remains one of the key priorities in addressing the global climate change. This is the area where additional energy penalty associated with preventing carbon dioxide emission from power plants is the most significant barrier to the implementation of CCS technology, and any advance in this domain will likely have a profound impact on our ability to control atmospheric carbon dioxide levels. For this reason, CCS has been one of the most explored applications in the context of computational screening of new materials: zeolites, MOFs, ZIFs, and others.[36,37] This is also the area where the multiscale screening approaches have made the most significant progress. Hence, CCS and in
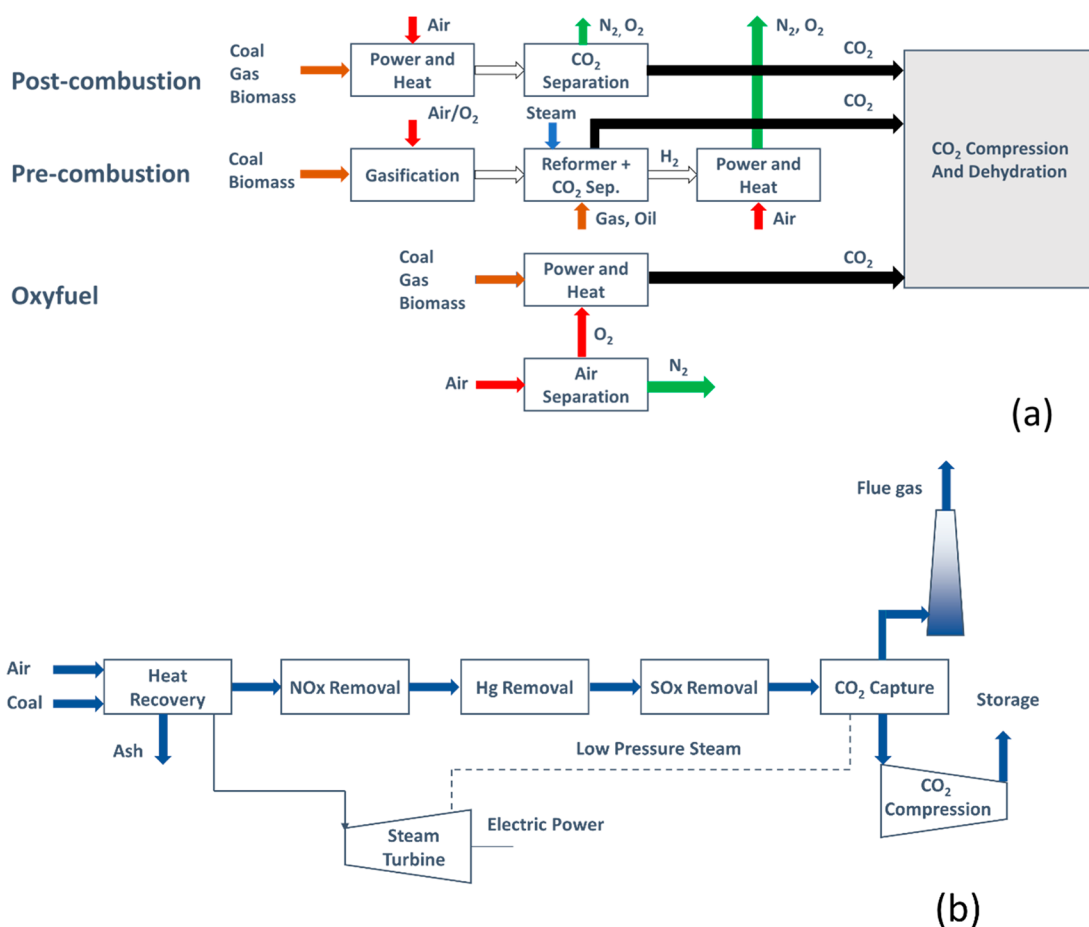
Figure 3. Different routes to carbon capture from power plants (a) and schematic illustration of postcombustion CCS plant (b).

particular postcombustion capture is the logical focus of this review.

Given the intended target audience of this review (as outlined in section 1), it is useful to introduce the basic concepts of postcombustion carbon capture, while referring the interested reader to the more specialized and extensive sources on the topic.[38−45]

The 2005 IPCC[4] committee identified three possible technologies for carbon capture from power plants, the most significant stationary CO_2 emitter globally: precombustion carbon capture, oxy-fuel process, and postcombustion carbon capture (Figure 3a). In the precombustion capture, fuel reacts with oxygen (or air) and steam. This produces so-called syngas (synthesis gas) composed predominantly of carbon monoxide and hydrogen. In the water-shift reactor, this mixture reacts with steam to produce carbon dioxide and more hydrogen. Carbon dioxide is then separated from the mixture, and the remaining purified hydrogen is used as a clean fuel in various processes. The idea of the oxyfuel process is to use pure oxygen for combustion. This oxygen is produced in the air separation step, which naturally comes with energy cost. However, as the process produces pure carbon dioxide during the combustion step, it does not require any carbon dioxide separation step, saving the costs down the line. Finally, in the postcombustion process carbon dioxide separation is applied to the flue gas from a standard power plant (Figure 3b).

Postcombustion capture is the only technology that can be retrofitted onto existing power plants and therefore is a promising approach in short and medium terms. In fact, detailed analysis of the US National Energy Technology Laboratory's (NETL) CCS database shows that there are currently more than 30 active postcombustion carbon capture plants around the world.[46] This is illustrated in Figure 4. In addition, postcombustion capture can be applied to hard-to-decarbonize emissions such as those from industrial processes and to power plants converted to bioenergy (BECCS), which would enable negative emissions.

The composition of the flue gas is typically 15−16 vol % CO_2, 5−7 vol % H_2O, 3−4 vol % O_2, and 70−75 vol % N_2 for coal-fired power plants. In addition, the flue gases may contain trace amounts (tens and hundreds of parts per million) of carbon monoxide, SO_x, and NO_x. This stream is at 1 bar and 50−75 °C.[47] We note, however, that most of the design efforts focus on a simplified separation operation involving only a binary mixture of CO_2 and N_2 at 1 bar and temperatures below 40 °C.

A viable carbon capture technology must remove 90% of carbon dioxide from this flue gas and produce it with 95% purity as proposed by the DOE.[29] Although these targets are not absolute requirements and may change depending on the economy of the process,[48] they provide a reasonable basis for the comparison of the technologies proposed for this task. In this context, the 95% purity constraint is mostly dictated by the requirement to compress the product CO_2 gas to 150 bar for further transportation or geological storage.[49,50] The recovery constraint of 90%, however, is rather an arbitrary choice of policy to encourage technologies that have higher success in large-scale mitigation of carbon dioxide.[48,51] In fact, there are compelling reasons that reducing the recovery target can be beneficial for
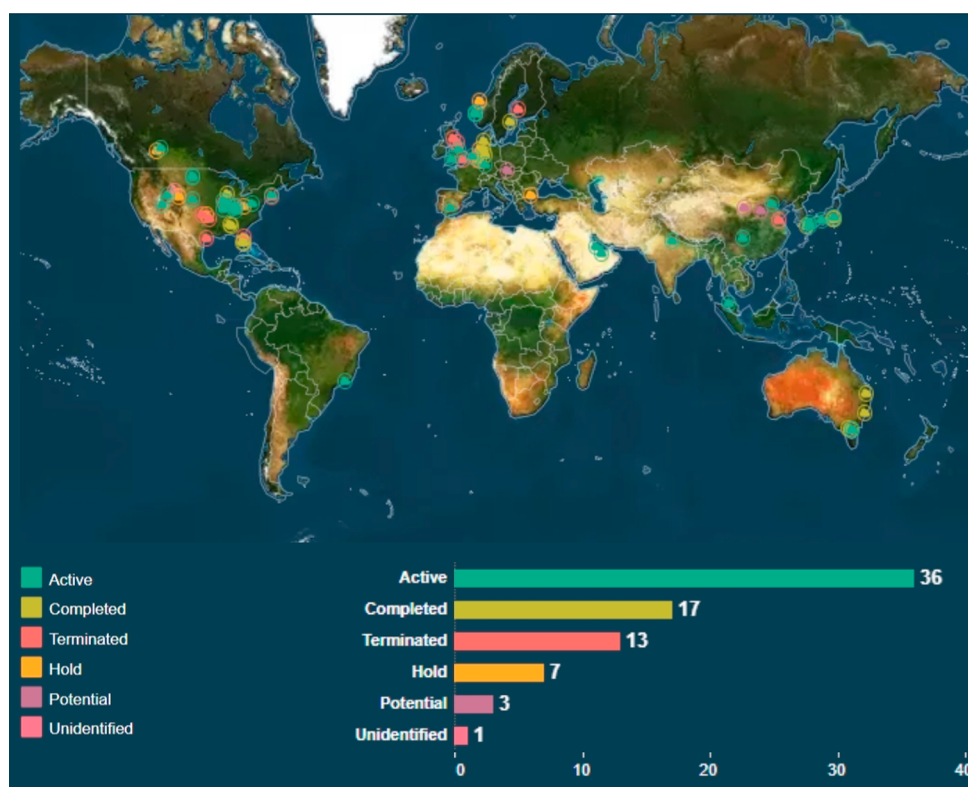
Figure 4. Active postcombustion carbon capture plants around the world as shown by green circles. Reprinted with permission from the NETL Carbon Capture and Storage (CCS) Database.[46] Copyright 2020 US Department of Energy.
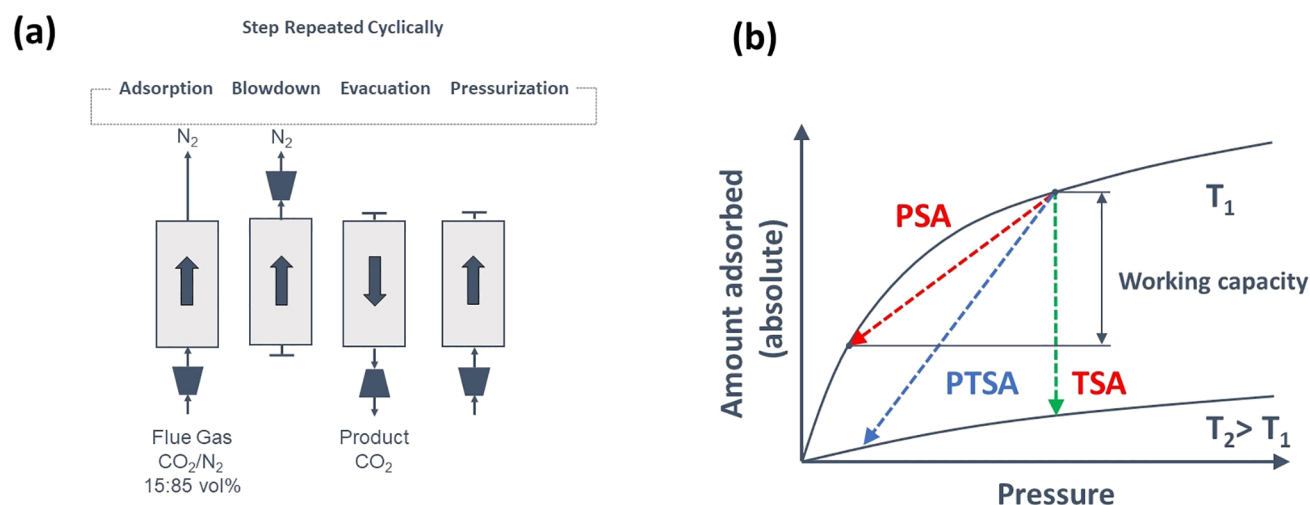
Figure 5. Schematic 4-step VSA cycle for separation of CO_2 and N_2 (a), difference of PSA/PTSA/TSA processes illustrated using equilibrium adsorption isotherms of CO_2 (b).

practical reasons especially for gas streams with higher concentrations of CO_2 (e.g., carbon capture from cement plants).[48,52−54] In this review, we mainly focus on the DOE's 95% purity and 90% recovery targets, considering they have been overwhelmingly used by the majority of materials screening studies conducted so far.

Traditional approaches for carbon capture from power plant streams employ solvent-based (e.g., amine) absorption processes. It is estimated that the best absorption technologies incur a parasitic energy penalty of about 1.3 MJ per kilogram of CO_2 captured.[55] This is associated with a significant energy demand of the solvent regeneration step. Any new technology

proposed for carbon capture must demonstrate that it is economically more viable (i.e., has lower energy penalty) than the reference, state-of-the-art amine absorption processes.

3. PRESSURE AND VACUUM SWING ADSORPTION FOR POSTCOMBUSTION CARBON CAPTURE

The main objective of this section is to introduce the key concepts and terminology associated with the pressure/vacuum and temperature swing adsorption processes that are required later in the article. The essential principle behind adsorption separation is that the components of the gas or liquid mixture somehow interact differently with the porous material and this

difference can be exploited to separate them. Depending on the nature of this difference, we can distinguish three classes of adsorption-based separation processes: (i) kinetic separations, in which diffusion of molecules of the gas mixture in and out of the material happens at significantly different rates; (ii) molecular sieving, where one of the components of the mixture is simply too bulky to fit in the pores of the structure while molecules of the other component are able to permeate through the porous structure; or (iii) equilibrium separations, where one of the components interacts more strongly with the porous structure via intermolecular interactions. The PSA and VSA processes under consideration in this review belong to this class of processes that constitute the largest group of the industrial adsorption-based separation processes.

To illustrate the principles of a PSA process, let us consider the diagram in Figure 5a, which shows different phases of a typical PSA cycle. The main element of this diagram is the adsorption column (schematically shown as just a rectangular box) filled with the porous material or *adsorbent*. In the first step (adsorption), the feed is introduced in the column. Stronger interacting components (called *heavy components*) are preferentially adsorbed by the porous material in the column, changing the composition of the gas phase. As a result, the product gas stream leaving the column on the other side (so-called, *raffinate*) is rich in the *light components* (weakly adsorbing components of the mixture). At some point in time, the adsorbent becomes saturated and will not be able to adsorb anymore of the heavy components. At this point, the adsorption step should be stopped, and the column should go through the regeneration or desorption phase. This phase may consist of a preliminary pressure reduction step (the blowdown step) followed by further reduction of pressure (the evacuation or extraction step), moving the process to the conditions associated with the low loadings on the isotherm and causing desorption of the heavy component (Figure 5b). The column is then repressurized and goes through the adsorption step again.

The difference in the equilibrium amount adsorbed between the adsorption and desorption cycle is called the *working capacity*. If the PSA system is cycling between ambient pressure and vacuum, then it is called a *vacuum swing adsorption* (VSA) process. The main additional energy cost of PSA and VSA processes is associated with pulling the vacuum (VSA) and compression (PSA). Hence, the work of vacuum pumps and compressors becomes a key ingredient in the assessment of economic viability of the PSA and VSA processes.

As can be seen from the simplistic description above, the PSA or VSA process is a cyclic process, where the basic unit of the process, the adsorption column, goes through repeating phases of adsorption and desorption. In the example above, we used pressure swing on the adsorption isotherm to regenerate the column as depicted in Figure 5b. Alternatively, we could have used higher temperature for regeneration. Indeed, as adsorption from the gas phase is an exothermic process, a higher temperature will shift the equilibrium to lower loadings, leading to desorption. This process is called *temperature swing adsorption* (TSA). A combination of pressure and temperature swing is also possible (PTSA), and the trajectory of conditions associated with this process is also shown in Figure 5b. Here, it is useful to note that Figure 5b represents an ideal case for PSA, VSA, and TSA processes. In reality, PSA and VSA processes are not completely isothermal, and TSA processes are not fully isobaric. This must be considered when idealized models are used for materials screening based on these processes.

For the PSA or VSA adsorption process to operate continuously, the actual plant consists of several columns going through various stages of the cycle. The number of units and how they are arranged is called *process configuration*. The types of steps involved, the timing of the steps within a single cycle, their duration, and other parameters constitute a *cycle configuration*. Developing process and cycle configurations in order to lower energy penalty and increase productivity constitute the main objective of the PSA or VSA design process.

In the case of the postcombustion separation process of a binary mixture, carbon dioxide is the heavy component and nitrogen is the light component. Unlike purification adsorption processes, such as hydrogen production from steam methane reformer off-gas, where the main product is the light component, in carbon capture, we are interested in the heavy component with specific constraints on its quality, and this makes design of the process more complex. Zeolite 13X is the most explored material for this application, both in process modeling and in pilot plant studies. This material is hydrophilic and will adsorb water present in the flue gas, leading to higher cost of the process.

Traditionally, PSA and TSA processes utilize packed bed configurations with the adsorbent being shaped in the form of beads or extrudates. For a separation process, the capture unit must be able to achieve the desired purity and recovery targets with a small footprint. For this, it is necessary to operate the process with fast cycling and higher flow rates. This poses challenges with respect to pressure drop and mass transfer. To overcome these issues, the use of structured sorbents such as laminates,[56,57] monoliths,[58,59] hollow fibers,[60,61] and 3D printed foams[62−64] is advocated. These sorbents have the potential for improved mass transfer and lower pressure drop.[65,66] While conventional packed bed systems are widely studied in literature, more recently 3D printing has attracted much attention due to its potential for manufacturing sorbents with controlled channel geometry.[62−64,67,68] Nevertheless, to the best of our knowledge, 3D printed adsorbents have not matured beyond laboratory scale, and the current technology is not yet ready for large scale deployment.

The brief introduction provided in this section serves only to establish the most essential elements of the PSA and VSA processes; for more extensive reviews of this technology for carbon capture, the reader is referred to more specialized and extensive sources.[43,69−72]

4. HIERARCHY OF PERFORMANCE METRICS FOR MATERIALS SCREENING

In section 2, we described the problem in hand: to capture CO_2 from flue gas of a power plant with 90% recovery and 95% purity. Imagine now that we want to identify the best adsorbent material for this from a cloud of many thousands of possible porous materials. To do so, we need a suitable performance indicator (i.e., metric) that can correctly quantify separation performance of porous materials and also is able to sufficiently discriminate between similar materials with different performance. A large number of performance indicators have been proposed for this purpose. In this section, we review the most important of these indicators as reported in the literature, focusing predominantly on their nature, classification, and availability. The information provided here will form the basis of the discussion in the next section where we will illustrate how application of these metrics in the field of computational

Table 1. Performance Indicators (performance evaluation metrics)[a]

index	metric class	screening metric	definition	reference
1	ISMM	pore volume		
2	ISMM	porosity		
3	ISMM	surface area		
4	ISMM	pore limiting diameter		
5	IFMM	enthalpy of adsorption		
6	IFMM	diffusivity		
7	IFMM	Henry selectivity	$\beta_{1,2} = \dfrac{K_{H,1}}{K_{H,2}}$	Bae and Snurr, 2011[95]
8	IFMM	adsorption selectivity	$\alpha_{1,2} = \dfrac{q_1^{ads}}{q_2^{ads}} \dfrac{C_2}{C_1}$	Bae and Snurr, 2011[95]
9	IFMM	working capacity	$WC = q_{ads,1} - q_{des,1}$	Bae and Snurr, 2011[95]
10	IFMM	regenerability	$R = \dfrac{WC_1}{q_1^{ads}} \times 100\%$	Bae and Snurr, 2011[95]
11	HMM	adsorbent figure of merit	$AFM = WC_1 \dfrac{(\alpha_{1,2ads})^2}{\alpha_{1,2des}}$	Baksh and Notaro, 1998[80]
12	HMM	sorbent selection parameter[b]	$SSP = \alpha_{1,2} \dfrac{WC_1}{WC_2}$	Rege and Yang, 2001[81]
13	HMM	separation factor	$SF = \dfrac{WC_1 C_2}{WC_2 C_1}$	Pirngruber et al., 2012[82]
14	HMM	adsorbent performance indicator	$API = \dfrac{(\alpha_{12}-1)^A WC_1{}^B}{\lvert \Delta H_{ads,1} \rvert^C}$	Wiersum et al., 2013[83]
15	HMM	adsorbent performance score	$APS = WC_1 \times \alpha_{1,2}$	Chung et al., 2016[84]
16	HMM	separation performance parameter (SPP)	$SPP = \dfrac{\left(\dfrac{M_{CH_4,raff}}{M_{CH_4,feed}}\right)}{\left(\dfrac{M_{ads}}{M_{CH_4,aff}}\right) \times \left(\dfrac{E}{M_{CH_4,raff}}\right)}$	Braun et al., 2016[85]
17	HMM	parasitic energy (PE)	$PE = (0.75 \eta_{T_{final}} \times Q) + W_{comp}$	Lin et al., 2012[86]
18	PLM	purity in PSA/VSA	$purity = \dfrac{\text{total mol } CO_2 \text{ in extract product}}{\text{total mol } CO_2 \text{ and } N_2 \text{ in extract product}} \times 100$	Rajagopalan et al., 2016[16]
19	PLM	recovery in PSA/VSA	$recovery = \dfrac{\text{total mol } CO_2 \text{ in extract product}}{\text{total mol } CO_2 \text{ fed into cycle}} \times 100$	Rajagopalan et al., 2016[16]
20	PLM	specific energy in PSA/VSA	$specific\ energy = \dfrac{\text{total energy used}}{\text{total mol } CO_2 \text{ captured}}$	Rajagopalan et al., 2016[16]
21	PLM	productivity in PSA/VSA	$productivity = \dfrac{\text{total mol } CO_2 \text{ in extract product}}{(\text{total volume of adsorbent}) \times (\text{cycle time})}$	Rajagopalan et al., 2016[16]
22	GEM	general evaluation metric	$GEM = \dfrac{WC_1}{WC_{2,mod}{}^{1.32} \times \alpha_{1,2des}{}^{0.25} \times \lvert \Delta H_{N_2} \rvert^{0.97}}$	Leperi et al., 2019[93]

[a]Subscripts 1 and 2 always denote stronger and weaker adsorbing components, respectively. For evaluation metrics 1−16, WC, α, β, C, K_H, and ΔH represent working capacity, adsorption selectivity, ideal selectivity, concentration, Henry's constant, and enthalpy of adsorption. For SPP, M_{ads}, $M_{i,k}$, and E denote mass of adsorbent, moles of species i in stream k, and total energy required for separation.[85] For PE, Q, η, and W_{comp} are the thermal energy requirement, Carnot efficiency, and compressor work, respectively. For GEM, ΔH_{N_2} and WC_{mod} stand for enthalpy of adsorption for nitrogen and the modified working capacity as defined in ref 93. [b]For Langmuir isotherms. For non-Langmuir systems, $SSP = \dfrac{(\alpha_{1,2ads})^2}{\alpha_{1,2des}} \dfrac{WC_1}{WC_2}$.[95]

material screenings evolved over the years leading to wider adoption of the process-level metrics for materials ranking.

Colloquially speaking, one would want to select the best material for a particular application simply by looking at its structure. The specific structural characteristics of a material may include its porosity, density, surface area, pore size distribution (PSD), and so on; see, for example, refs 73 and 74. These properties can be obtained either from experiments, as part of the standard characterization procedure for every newly synthesized material, or from the computational character-

ization methods that will be discussed later in this review. We call this group of metrics *intrinsic structural material metrics* (ISMMs). These structural metrics do not tell us anything about how the material interacts with its environment. The functional behavior of materials is described by adsorption equilibrium data (e.g., adsorption isotherms, Henry's constants of adsorption, adsorption capacity), transport characteristics (e.g., diffusivity), and thermal properties (e.g., heat capacity, thermal conductivity); see, for example, refs 75−78. These properties constitute
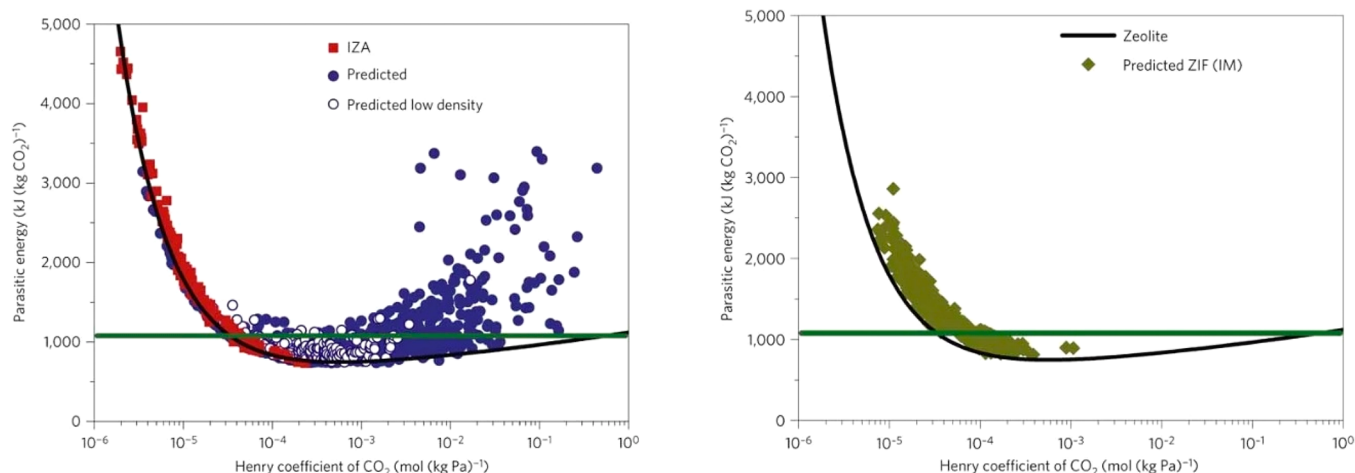
Figure 6. Parasitic energy as a function of the Henry's coefficient of adsorption of CO_2 for all-silica zeolites (left) and hypothetical ZIFs (right). The green lines are the parasitic energy of the current monoethanolamine (MEA) absorption technology. Reprinted with permission from Lin et al.[86] Copyright 2012 Springer Nature.

another group of metrics that can be termed *intrinsic functional material metrics* (IFMMs).

In separation applications, adsorption is a competitive process between two or more adsorbing species. Naturally, to characterize this competition, we need a metric that can compare the behavior of the material with respect to the competing species. For example, in the most general definition, selectivity is the ratio of the molar loadings of two competing components in the adsorbed phase q_i^{ads} in equilibrium with a bulk fluid phase mixture with respect to their partial fugacities, f_i, $\alpha_{1,2} = \dfrac{q_1^{ads}}{q_2^{ads}} \dfrac{f_2}{f_1}$.[79]

At low pressure, selectivity can be expressed simply as the ratio of the two Henry's constants. Selectivity is the simplest metric from the group of *hybrid material metrics* (HMMs), which combine various adsorbent metrics mentioned above to more accurately discriminate between adsorbents with different separation performances. Examples of these metrics include adsorption figure of merits (AFM),[80] sorbent selection parameter (SSP),[81] separation factor (SF),[82] adsorbent performance indicator (API),[83] and adsorbent performance score (APS).[84] Mathematical definitions of these metrics are provided in Table 1.

One important step in the development of more realistic metrics for material screening was the realization that selectivity and working capacity are not necessarily representative of the economic drivers of gas separation processes.[16] To address this limitation, new screening metrics were developed to exploit the correlations between adsorption characteristics of porous materials and the plant-wide economic appraisal of the separation process. A prominent example of such evaluation metrics is the separation performance parameter (SPP) by Braun et al.,[85] which was developed to represent the most important economic drivers for separation of CO_2 from natural gas mixtures. It assumes equilibrium adsorption and desorption in the PSA, TSA, or PTSA processes in order to calculate the value of an objective function, which accounts for the amount of captured target gas (e.g., CH_4), amount of adsorbent material used, and total energy required for the separation process.[85] The assumption of a process performing fully under equilibrium represents an ideal case scenario; however, this condition is not always achieved in dynamic separation processes such as PSA and VSA. Another limitation of the SPP metric is that instead of

using conventional cost indicators (e.g., capital and operating costs), SPP assumes that all process costs scale with the amount of adsorbent (M_{ads}) used in the separation unit.[85] As has been discussed in the same publication, there are cases where a large portion of the capital costs does not depend on the amount of material used in the process, and if these contributions of the capital cost become significantly larger, the amount of material used in the separation unit will become irrelevant.[85] Comparison of SPP, SSP, and API metrics with detailed process modeling indicates that for CO_2/CH_4 separation, SPP surpasses the other two evaluation metrics in terms of accuracy.[85]

Another important example of new evaluation metrics is the parasitic energy (PE), which was first used by Lin et al.[86] and Huck et al.[87] for evaluation of different classes or porous materials for postcombustion carbon capture. In their analysis, the additional energy required for the adsorption carbon capture process consists of (1) energy to heat the adsorbent material, (2) energy to supply the heat of desorption, which is equal to the heat of adsorption, and (3) energy needed to compress CO_2 to 150 bar, which is a standard requirement for transport and storage.[86] Based on this, the authors formulated a simplified expression for the parasitic energy of a CCS process as a combination of the thermal energy requirement and the compressor work.[86] In the definition of parasitic energy provided by Lin et al.[86] equilibrium adsorption and desorption is assumed. As mentioned before, this may not be always the case in dynamic PSA and VSA systems. The parasitic energy curve is however shown to be a useful metric for assessing performance of large groups of porous materials, examples of which are illustrated in Figure 6 for all-silica zeolites and hypothetical ZIFs.[86]

Inadequacy of screening metrics that are solely linked to the adsorbent properties and not their performance at the process level has been recently demonstrated by Rajagopalan et al.[16] using a case study for postcombustion CO_2 capture. Without intending to repeat the entire argument here, one may consider as an example selectivity of a candidate material for CO_2/N_2 separation using a PSA process. On its own, a high value of selectivity is unlikely to be enough to select the material for CO_2 separation. For instance, if the material has very low capacity, the operation is likely to be very costly, despite high selectivity of the material. This study clearly demonstrates that for complex,

dynamic adsorption processes, such as PSA and VSA processes for carbon capture, the realistic performance of a specific material must be assessed in the actual process, by performing process simulation and optimization under realistic conditions. For this purpose, a new class of evaluation metrics is required. The metrics used to assess performance of porous materials at the process level are therefore called *process-level metrics* (PLMs) in this review. In this case, a trade-off curve between overall energy penalty of the process and its productivity is used as an evaluation metric for materials screening.[16,88,89] Energy penalty and productivity not only are more realistic measures of process performance but also are more directly related to the economic drivers of the separation process. Therefore, the next natural step in developing realistic evaluation metrics for materials screening is to link the existing process modeling platforms to techno-economic analyses of the process because the ultimate goal of any separation unit is to achieve the design objective at the lowest cost.[90−92] Khurana and Farooq have extended this concept to include a comprehensive cost framework for the entire carbon capture plant.[90,91] Their integrated optimization framework looks at the separation cost in terms of $/ton of CO_2 captured or $/ton of CO_2 avoided, where the latter is defined as the difference between emissions of two power plants, one without a capture unit and the other with a capture unit but both producing the same net amount of electricity.[90] Fully integrated techno-economic analysis of carbon capture plants or any other industrial separation facility can be a daunting task for the purpose of screening of large groups of adsorbent materials that are currently available. As a result of this limitation, more recent studies have attempted to develop *general evaluation metrics* (GEMs) that are strongly correlated with the results of the detailed techno-economic analyses.[93] Usually, this is achieved by combining all previously known evaluation metrics into a more general one (i.e., GEM) and then reducing complexity of the GEM by removing the elements whose contribution into the correlation coefficient is insignificant.[93,94] Importance of each feature in the GEM developed by Leperi et al.[93] for evaluation of materials performance for postcombustion carbon capture is illustrated in Figure 7.

Leperi et al.[93] have shown that this approach is quite promising for the development of universal screening metrics that simultaneously take into account most important characteristics of the process associated with adsorbent material, process optimization, and overall economic cost of the plant. Development of new GEMs can particularly benefit from recent advances in machine-learning techniques, if adequately large data sets of techno-economic forecasts were available for training the GEM function.

From the review of the hierarchy of metrics provided in this section, one could make an impression that if the most accurate assessment of the material performance is achieved by the detailed process and plant models, then this should be the standard level of description in all materials screening protocols. This view, however, does not take into account, the computational cost associated with materials screening using these metrics. Once the equilibrium adsorption data are available, the hybrid metrics provide effectively an instant assessment of the material performance. Process simulation of a single cycle configuration for a PSA or VSA process may be done in a few minutes on a conventional CPU, whereas cycle optimization for the best performance may take many hours to complete. This computational price tag applied to thousands and tens of thousands of materials would still make routine use of screening
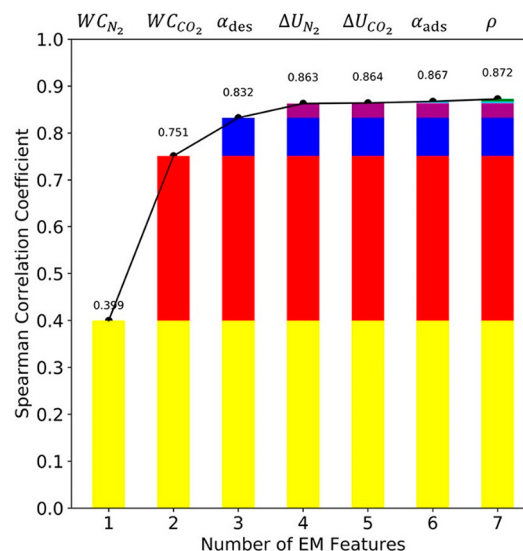
Figure 7. Importance of each feature in the GEM developed by Leperi et al.[93] for the Spearman correlation coefficient (SCC). The higher the value of SCC, the more reliable the metric is for predicting the cost of CO_2 capture. From right to left, the features are adsorbent density, selectivity at adsorption conditions, internal energy of adsorption for CO_2, internal energy of adsorption for N_2, selectivity at desorption conditions, working capacity of CO_2, and working capacity of N_2. SCC for each column is calculated with the feature listed on top plus the features listed in the previous columns. For example, the three GEM features used to calculate SCC in the third column are N_2 working capacity, CO_2 working capacity, and selectivity at desorption condition. Reprinted with permission from Leperi et al.[93] Copyright 2019 American Chemical Society.

of all materials at the process level unaffordable. Hence, this is still an ongoing area of research to develop a multistage screening process, where efficiency of process optimization are improved using novel numerical techniques or alternatively some preliminary screening is done using hybrid metrics and simplified process models, while accurate process modeling and optimization is only carried out for a selected group of promising materials. The role of emerging numerical techniques for process optimization and screening of large groups of materials is discussed in the following sections.

5. COMPUTATIONAL SCREENING OF POROUS MATERIALS: A HISTORICAL PERSPECTIVE

In the previous section, we discussed what metrics are available for material screening in adsorption applications through the prism of metric hierarchy from very simple "intrinsic" metrics to process-level metrics. In this section, we take a different, historical perspective on the development of computational screening strategies. This perspective will allow us to review how this field has evolved over time toward current multiscale workflows that incorporate elements of different types of simulation techniques and performance indicators.

The first material screening studies can be tracked back to more than 10 years ago.[96−98] In a pioneering study published in 2010,[75] Krishna and van Baten employed configurational-biased Monte Carlo (CBMC) and molecular dynamics (MD) simulations to examine adsorption, diffusion, and permeation selectivities for separation of CO_2/H_2, CO_2/CH_4, CO_2/N_2, CH_4/N_2, and CH_4/H_2 mixtures in a number of zeolite, MOF, ZIF, and carbon nanotube (CNT) structures. Their studies provided useful guidelines to the optimum choice of micro-
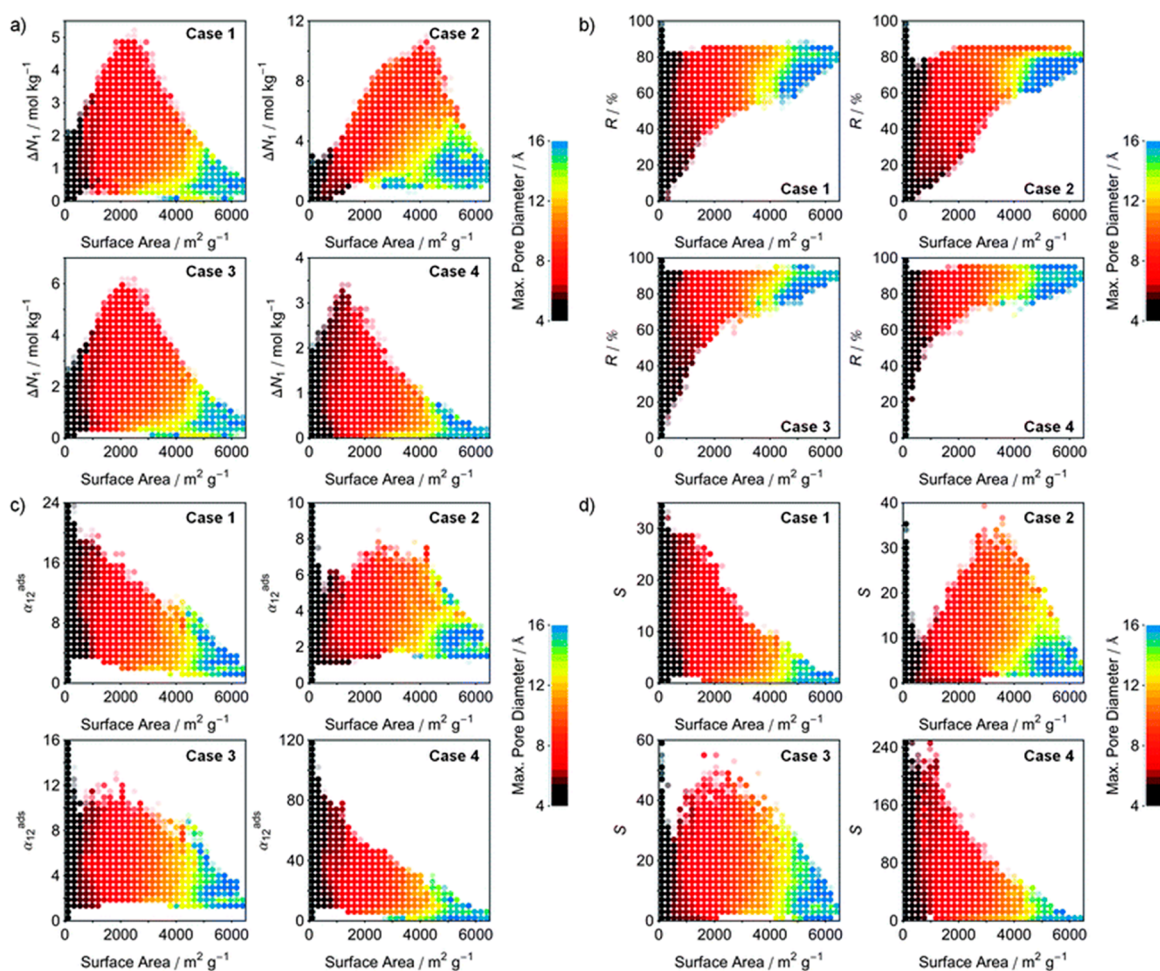
Figure 8. Structure−property relationships of MOFs as obtained from molecular simulations for CO_2 separation. Panels show the relations of working capacity (a), regenerability (b), selectivity (c), and sorbent selection parameter (d) with surface area for four different cases. Each plot is divided into 30 × 30 regions that are represented by a filled circle, if more than 10 (or 25 for selectivity and sorbent selection parameters) structures exist within that region. The four separation cases include case 1, natural gas purification using PSA, case 2, landfill gas separation using PSA, case 3, landfill gas separation using VSA, and case 4, flue gas separation using VSA. Reprinted with permission from Wilmer et al.[101] Copyright 2012 Royal Society of Chemistry.

porous layers that should be used in membrane separations representing a compromise between permeation selectivity and permeability. This study also emphasized the importance of correlations between pore space properties (pore volume, limiting pore diameter, etc.) and transport properties (e.g., diffusion and permeation) in these classes of porous materials.

Building on the importance of the pore structure characterization, Haldoupis et al.[74] analyzed pore sizes of more than 250 000 hypothetical silica zeolites to compute the size of the largest adsorbing cavity and pore-limiting diameter for all zeolites. This information can be used to reveal the range of adsorbate molecules that can possibly diffuse through each zeolite. Additionally, the authors computed Henry's constant of adsorption and diffusion activation energy for CH_4 and H_2 for a subset of 8000 zeolites using a computational method reported in their earlier study.[99] From the diffusion activation energies, they were able to estimate diffusivity of each adsorbate using a simple formulation of the transition state theory (TST). The method presented in this study for estimation of diffusion was limited to adsorption at infinite dilution. Calculation of transport properties at higher loadings is much more time-consuming, which may limit the ability of the employed method to screen large groups of porous materials. Nevertheless, within

the limitation of the methods, Haldoupis et al. could successfully demonstrate that using a combination of molecular simulation techniques, one can reasonably assess adsorption properties of a large group of nanoporous crystalline materials for a particular separation application.[74]

Application of computational materials screening approaches took another step forward in 2012 when two major studies were published. Namely, Snurr and co-workers used a library of 102 building blocks and a "tinker-toy" algorithm to assemble a database of 137 953 hypothetical MOFs.[100] Using geometric characterization tools and Monte Carlo simulations, they explored their database to identify the most promising structures for methane storage. From this perspective, this is the first example of a computational screening strategy applied to a large group of MOF materials. Later in the same year, Snurr and co-workers[101] simulated adsorption of CO_2, CH_4, and N_2 in more than 130 000 hypothetical MOFs from the same database and subsequently examined their potential for CO_2 capture using five different performance metrics including CO_2 uptake, working capacity, regenerability, adsorption selectivity, and sorbent selection parameter (as defined in Table 1). They showed that although the resulting structure−property relationship between pore size, surface area, pore volume, and chemical

functionality provide several leads for design of new porous materials, none of the above metrics is actually a perfect predictor of CO_2 separation performance. The studies of Snurr and co-workers introduced several concepts that are now central to the computational screening strategies of porous materials. These concepts can be formulated as follows:

(i) The modular nature of MOFs allows the use of simple tinker-toy algorithms to assemble new hypothetical structures simply by linking the building blocks along the appropriate topology. This idea can be extended to other new classes of materials (ZIFs, COFs, etc.).

(ii) Each material within the database can be explored in terms of structural properties and functional properties. These properties can be used to classify, compare, and organize materials within the database.

(iii) Computational screening studies calculate properties that are mentioned above. Two or more properties correlated to each other form clouds of data points, which can be explored to reveal some promising structure–property relations. An example of structure–property relationships for CO_2 separation in more than 130 000 MOFs is shown in Figure 8.

Further studies in this emerging field also identified several challenges and new directions of research, which can be summarized as follows:

(i) Structures assembled using the tinker-toy algorithms require further accurate structure optimization using quantum mechanical (QM) methods to be more realistic.

(ii) We need systematic approaches to organize structures into databases that can be used in molecular simulations.

(iii) Accurate molecular force fields are lacking for new classes of porous materials interacting with gases and liquids. A particularly striking manifestation of this was the failure of the conventional force fields to describe interaction of MOFs featuring open metal sites with carbon dioxide or unsaturated hydrocarbons. Interaction of adsorbents with water also presents a substantial challenge. This prompted the simulation community to put significant efforts into the development of a new generation of force fields based on the accurate QM potential energy surface. However, despite significant progress, many of these force fields are largely specialized and non-transferable; hence this is still very much a remaining challenge and an ongoing area of research.

(iv) Early studies would use several simple, well-known algorithms to obtain structural characteristics of porous materials. Later, a number of comprehensive and versatile tools were developed (Zeo++,[102] Poreblazer,[103] ZEOMICS/MOFomics[104,105]) to calculate geometric descriptors of porous materials. These descriptors can be used in the context of materials informatics for discovery and screening of emerging porous materials.

(v) Development of machine learning algorithms is needed to establish structure–property relationships within the databases and drive the discovery of new materials with desired functionalities.

Following the above studies, Smit and co-workers[86] also published a new study on screening of hundreds of thousands of zeolite and ZIF structures using the parasitic energy (PE) as a promising metric for evaluation of materials performance in the context of postcombustion carbon capture. At the molecular simulation level, they employed a combination of grand canonical Monte Carlo (GCMC) simulation, energy grid construction method, and Widom test particle insertion technique to obtain equilibrium adsorption characteristics of

materials. The PE metric was then used to search for materials that have the potential to reduce the parasitic energy by 30–40% compared to the conventional amine-based absorption technologies.[86] This study proposed a theoretical limit for the minimal parasitic energy that can be achieved for a particular class of porous materials.

A series of articles by Sholl and Keskin[98,106] and Keskin and colleagues[107–109] had laid the foundation of computational screening methods for membrane gas separations between 2007 and 2012. These studies were followed by Kim et al.[110] in 2013 after publishing a major study on screening of over 87 000 different zeolite structures for permeation separations. In this publication, the authors estimated the diffusion coefficients of CO_2, N_2, and CH_4 using free energy calculations and TST, and identified general characteristics of the best-performing structures for CO_2/CH_4 and CO_2/N_2 membrane separations. For CO_2/CH_4 separation, they predicted a structure that outperformed the best known zeolite by a factor of 4–7. Here, the performance was measured based on the required area of an ideal membrane, which is shown to be mainly dominated by and inversely proportional to the CO_2 permeability in the system.[110] In comparison with the results of Haldoupis et al.,[74] Kim et al. demonstrated that screening of porous materials based on purely geometric approaches may deviate from what is predicted from a more advanced energy-based analysis.[110]

The study of Kim et al.[110] was followed by two other publications with a greater emphasis on MOFs as an emerging group of porous solids for adsorption separation applications. The first study was published in 2014 by Sun et al.[76] where 12 materials including six MOFs, two ZIFs, and four zeolites were studied for removal of SO_2, NO_x, and CO_2 from the flue gas mixtures. They used grand canonical Monte Carlo (GCMC) simulations to predict mixture adsorption isotherms and selectivity of the candidate materials for separation of SO_2, NO_x, and CO_2 in a mixture containing N_2, CO_2, O_2, SO_2, NO_2, and NO. They compared the working capacity, absolute adsorption, and adsorption selectivity as three different performance indicators to select the best performing materials. It was concluded that Cu-BTC and MIL-47 were the best adsorbents for separation of SO_2 from the flue gas mixture. For the removal of NO_x, however, Cu-BTC was identified as the best performing material. Finally, for the simultaneous removal of SO_2, NO_x, and CO_2, Mg-MOF-74 was found to be the best candidate. The three performance indicators (namely, the working capacity, absolute adsorption, and adsorption selectivity) used for evaluation of materials performance in this study only focus on the ability of materials to adsorb different gases at equilibrium. They do not take into account the role of transport, which will be important in real dynamic processes. They also neglect the energy penalty associated with the regeneration of the bed.

The second study from this group was published by Huck et al.[87] in 2014 focusing on screening of more than 60 different synthesized and hypothetical materials including MOFs, zeolites, and porous polymer networks (PPNs) using a hybrid temperature–pressure swing adsorption (TPSA) process for postcombustion carbon capture. Acknowledging that several performance evaluation criteria have been already proposed, this publication emphasized the use of parasitic energy as a more realistic metric for materials screening. This is because parasitic energy takes into account the energy penalty associated with the compression process (needed for regeneration of the bed and geological storage of CO_2), as well as several essential
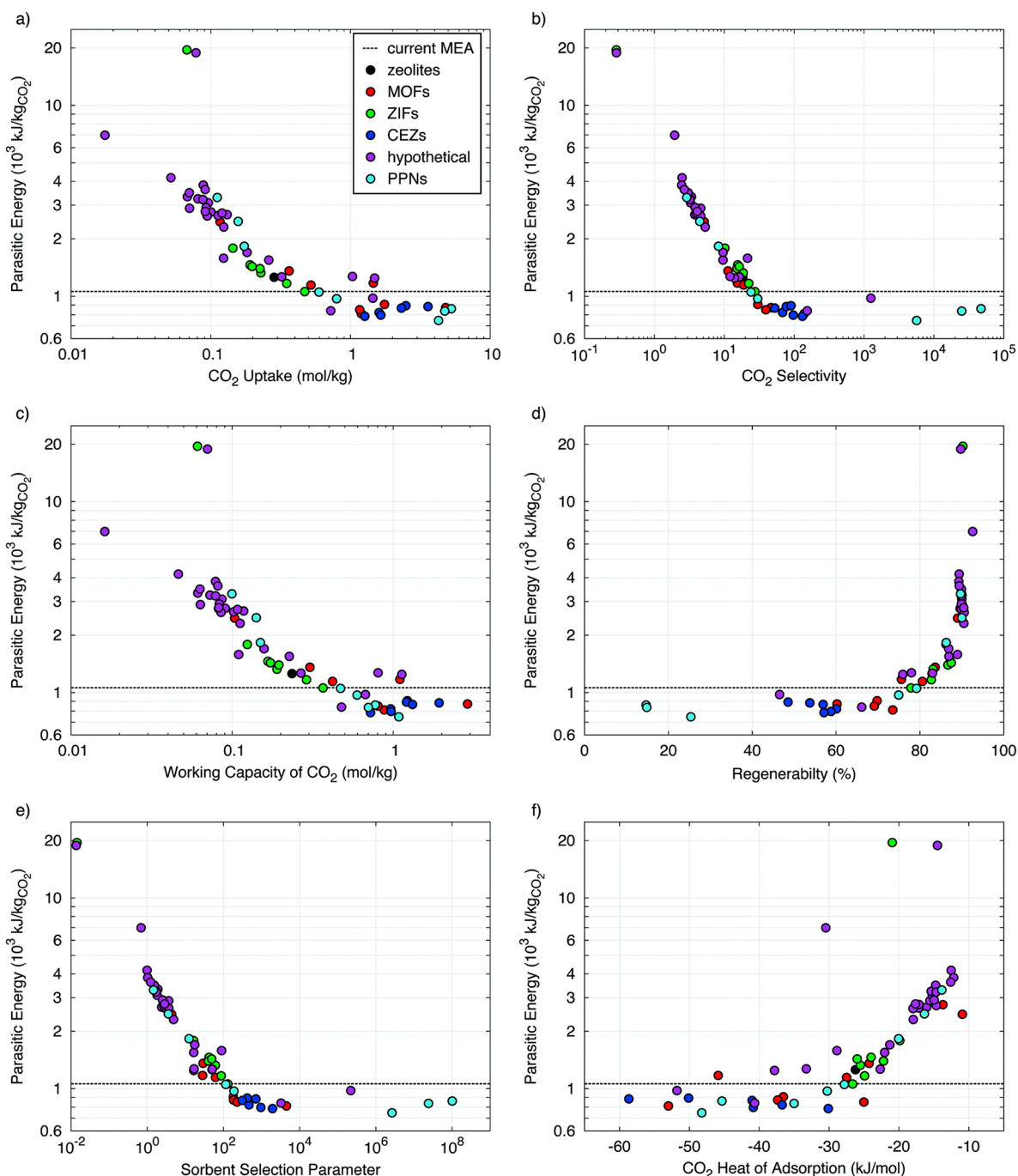
Figure 9. Correlation of parasitic energy with other performance indicators in a TPSA process for CO_2 capture. Reprinted with permission from Huck et al.[87] Copyright 2014 Royal Society of Chemistry.

thermodynamic properties such as the thermal energy required for heating up the adsorption bed, and the heat required to regenerate it.[87] The authors noted that the PSA and TPSA processes give better performance for all the materials in terms of the energy penalty compared to the TSA process. Figure 9 demonstrates the correlation of parasitic energy with other performance indicators calculated for separation of CO_2 using a TPSA process from a coal-fired power plant.

Using parasitic energy as the evaluation metric, the authors identified Mg-MOF-74, PPN-6-CH2TETA, and PPN-6-CH2DETA as the most promising materials for CCS in coal and natural gas fired power plants and for direct air capture, respectively.

In a more recent study focused on membrane separation, Qiao et al.[77] screened 137 953 MOFs in an attempt to identify the best performing candidates for separation of CH_4, N_2, and CO_2. In a four-stage strategy, the authors employed a combination of geometric pore characterization metrics (e.g., pore limiting diameter (PLD), pore size distribution) and equilibrium (Henry's constant) and transport properties (diffusivity and permeability) for materials screening showing that the PLD and pore size distribution are the two key factors governing diffusion and permeation of different gases in MOFs.[77]

In early 2016, Braun et al.[85] published a new study to explore performance of all-silica zeolites for CO_2 capture from natural gas where for the first time, the inadequacy of some of the above-

mentioned adsorbent metrics for materials screening was highlighted. This study suggested that selectivity and working capacity are not necessarily representative of the economic drivers that are considered for design of a chemical process.[85] The authors further argued that the use of these metrics can be even deceptive; hence they developed a new metric called separation performance parameter (SPP), which was designed to correctly represent the economic drivers behind CH_4/CO_2 separation. They applied this metric to explore separation performance and structure–property relationship of tens of thousands of all-silica zeolites recorded in the International Zeolite Association (IZA) database[111] and the Predicted Crystallography Open Database (PCOD) of hypothetical zeolites.[112]

The year 2016 also witnessed publication of more advanced screening studies. In particular, Snurr and co-workers reported on high-throughput screening of MOFs for CO_2 capture in the presence of water.[78] The article focused on the competitive co-adsorption of water as a potentially adverse issue in the deployment of adsorption-based CO_2 capture technologies. Here, computational screening was conducted to search for MOFs with high CO_2/H_2O selectivity. The screening workflow consisted of several steps as described below: initially, the framework charges were computed for 5109 MOFs using the extended charge equilibration method (EQeq),[113] which is an approximate, but computationally affordable technique for this purpose. In the next step, the Henry's constants of all MOFs were calculated using the Widom particle insertion. Following this step, the 15 most selective MOFs were identified based on the ratio of Henry's constant for CO_2 and H_2O. The resulting prescreened materials were investigated further using more rigorous simulation techniques. For these materials, partial atomic charges were computed using the repeating electrostatic potential extracted atomic (REPEAT) method,[114] which is more accurate compared to the EQeq technique and is based on the electron density distributions obtained from QM-DFT calculations. Further, GCMC simulations were carried out to calculate the binary and ternary adsorption of CO_2/H_2O and $CO_2/H_2O/N_2$ mixtures for the 15 preselected MOFs. GCMC-simulated adsorption isotherms were then used to identify MOFs with the highest CO_2 selectivity over both water and nitrogen. This study highlights the importance of electrostatic potentials in describing the H_2O–MOF interactions. On this basis, the authors suggested that accurate charge calculation methods are required to conduct similar screening studies. They also demonstrated a correlation between small pore sizes and strong binding of CO_2, which can limit adsorption of water at high humidity by preventing the formation of water clusters inside these pores.[78]

Later in 2017, Li et al.[115] published a new screening study to explore multivariate metal–organic frameworks (MTV-MOFs). The authors constructed a new database of ~10 000 MTV-MOFs with mixed linkers and functional groups. A GCMC-based high-throughput computational screening method was employed to identify the high-performing candidates for CO_2 capture. They showed that compared to their parent MOFs, functionalized structures consistently exhibit better CO_2/N_2 selectivity and in most cases even CO_2 capacity is improved. This work is particularly interesting as it demonstrated that arrangements of mixed linkers containing different functional groups can result in a combinatorial explosion in the number of possible structures, which can then be mined to increase structural diversity and surface heterogeneity of materials space.

This extended search space may contain candidate materials with higher potential for CO_2 capture.

Almost all studies reviewed up to this point had focused on the use of simple performance indicators (classes of ISMM, IFMM, and HMM), which are associated with structure or microscale function of adsorbents. These metrics normally consider simple properties such as the pore limiting diameter (PLD), pore size distribution (PSD), Henry's constant of adsorption (K_H), adsorption working capacity (WC), selectivity, and micropore diffusion. As discussed in section 4, one can use these performance indicators to reveal correlations between materials structure and functions at a microscale level, which is important for fundamental understanding of the system; however these metrics fail to realistically predict separation performance of materials at the process level for dynamic adsorption processes such as PSA or VSA. This realization gradually gave rise to the wider use of process-level metrics (PLMs) for materials screening leading to design of multiscale screening workflows, which combine various molecular simulation methods with process modeling and optimization.

The idea of constructing a multiscale simulation workflow through combining molecular simulations and process optimization for the purpose of materials screening was originally presented by Hasan et al. in 2013.[30] They used this method for cost-effective capture of CO_2 using zeolites as adsorbents. A similar multiscale approach was also adopted by Banu et al.[31] for hydrogen purification using MOFs. However, it was the studies of Farooq and co-workers[88,116] that brought to light the importance of multiscale performance-based methods for realistic materials screening especially in the context of postcombustion carbon capture. In their main screening study, Khurana and Farooq[88] evaluated the performance of 74 real and hypothetical adsorbents in a 4-step VSA process with light product pressurization (LPP). Process optimizations were carried out to minimize overall energy penalty of the process and maximize its productivity while simultaneously meeting the 95% CO_2 purity and 90% CO_2 recovery criteria for postcombustion carbon capture. As a result of this study, the authors identified several adsorbents with superior performance over zeolite 13X, the current benchmark and the most studied adsorbent for postcombustion carbon capture.

This new development also provided additional evidence that process-level metrics (PLMs) such as process productivity, overall energy consumption, and product purity do not directly correlate with the intrinsic properties of adsorbent materials[16,88,116–118] that have been widely used by scientists for materials screening over the past decade. The multiscale performance-based screening method discussed above addresses several important pitfalls associated with the traditional techniques where materials screening is performed solely based on intrinsic evaluation metrics: (1) This approach can confirm whether the important CO_2 purity–recovery requirement can be met. ISMM, IFMM, and HMM classes of evaluation metrics do not take this requirement into account. (2) It can identify the best performance for each adsorbent across a wide range of operating conditions while simultaneously satisfying the purity–recovery constraint. In contrast, adsorbent-based screening methods usually rank materials for a fixed set of operating conditions. (3) The process-level metrics (e.g., energy consumption and productivity) can be directly related to economic drivers of commercialized carbon capture plants (e.g., capital and operation cost).

Rank	WC	α	S	API$_1$	API$_2$	AFM$_1$	AFM$_2$	SF	GEM	Mod. Skars.	5-Step Cycle	FVSA
1	Ni-MOF-74	SIFSIX-3-Ni	SIFSIX-3-Ni	Mg-MOF-74	Mg-MOF-74	SIFSIX-3-Ni	SIFSIX-3-Ni	SIFSIX-3-Ni	UTSA-16	Zeolite 13X	UTSA-16	Cu-TDPAT
2	Mg-MOF-74	Zeolite 13X	Zeolite 13X	Zeolite 13X	Ni-MOF-74	Zeolite 13X	Zeolite 13X	UTSA-16	Cu-TDPAT	Cu-TDPAT	Zeolite 13X	UTSA-16
3	Co-MOF-74	Mg-MOF-74	UTSA-16	SIFSIX-3-Ni	UTSA-16	Mg-MOF-74	UTSA-16	Zeolite 13X	Zeolite 13X	UTSA-16	Cu-TDPAT	Zeolite 13X
4	UiO-66(OH)$_2$	UTSA-16	Cu-TDPAT	Ni-MOF-74	Zeolite 13X	Ni-MOF-74	Cu-TDPAT	Ni-MOF-74	SIFSIX-3-Ni	Ni-MOF-74	Ti-MIL-91	Zn-MOF-74
5	UTSA-16	Cu-TDPAT	Ni-MOF-74	UTSA-16	SIFSIX-2-Cu-i	UTSA-16	Ni-MOF-74	Cu-TDPAT	Ti-MIL-91	Mg-MOF-74	Zn-MOF-74	Ti-MIL-91
6	SIFSIX-2-Cu-i	Ni-MOF-74	Mg-MOF-74	Cu-TDPAT	Co-MOF-74		Cu-TDPAT	Mg-MOF-74	Ti-MIL-91	Zn-MOF-74	SIFSIX-2-Cu-i	SIFSIX-3-Ni
7	Zn-MOF-74	Ti-MIL-91	Ti-MIL-91	SIFSIX-2-Cu-i	UiO-66(OH)$_2$	SIFSIX-2-Cu-i	Ti-MIL-91	Mg-MOF-74	SIFSIX-2-Cu-i	SIFSIX-3-Ni	Mg-MOF-74	
8	Zeolite 13X	SIFSIX-2-Cu-i	SIFSIX-2-Cu-i	Zn-MOF-74	Zn-MOF-74	Zn-MOF-74	SIFSIX-2-Cu-i	SIFSIX-2-Cu-i	Ni-MOF-74	Zn-MOF-74		
9	Cu-TDPAT	Zn-MOF-74	Zn-MOF-74	UiO-66(OH)$_2$	Cu-TDPAT	Ti-MIL-91	Zn-MOF-74	Zn-MOF-74	Sc2BDC3	Ti-MIL-91		
10	Ti-MIL-91	Sc2BDC3	Sc2BDC3	Ti-MIL-91	UiO-66(OH)$_2$	Sc2BDC3	Sc2BDC3	Sc2BDC3	Mg-MOF-74			
11	Cu-BTTRi	UiO-66(OH)$_2$	UiO-66(OH)$_2$	Co-MOF-74	SIFSIX-3-Ni	Co-MOF-74	UiO-66(OH)$_2$	UiO-66(OH)$_2$	Cu-BTTRi			
12	NTU-105	Co-MOF-74	Co-MOF-74	Cu-BTTRi	Cu-BTTRi	Cu-BTTRi	Co-MOF-74	Co-MOF-74	UiO-66(OH)$_2$			
13	SIFSIX-3-Ni	Cu-BTTRi	Cu-BTTRi	NTU-105	NTU-105	NTU-105	Cu-BTTRi	Cu-BTTRi	ZIF-8			
14	MOF-177	NTU-105	NTU-105	Sc2BDC3	MOF-177	Sc2BDC3	NTU-105	NTU-105	Co-MOF-74			
15	ZIF-8	ZIF-8	ZIF-8	MOF-177	Sc2BDC3	MOF-177	ZIF-8	ZIF-8	NTU-105			
16	Sc2BDC3	MOF-177	MOF-177	ZIF-8	ZIF-8	ZIF-8	MOF-177	MOF-177	MOF-177			

Figure 10. Hierarchies of top-performing materials based on various adsorbent-based performance indicators as compared with detailed process modeling and optimization for three cycle configurations, namely, modified Skarstrom, 5-step PSA, and fractionated vacuum swing adsorption (FVSA) cycle. Adsorbent metrics from left to right include CO$_2$ working capacity, selectivity, sorbent selection parameter, adsorbent performance indicators (APS 1 and 2), adsorbent figures of merit (AFM 1 and 2), separation factor, and general evaluation metric (GEM). Reprinted with permission from Yancy-Caballero et al.[126] Copyright 2020 Royal Society of Chemistry.

The above approach for process-based screening of porous materials is particularly important in light of the available experimental evidence that supports the predictions of the proposed screening platform. In a pilot plant study, Krishnamurthy et al.[119] demonstrated that the 95% CO$_2$ purity and 90% CO$_2$ recovery targets for postcombustion carbon capture can be achieved in experiment using the same 4-step VSA cycle with light product pressurization that was investigated by Khurana and Farooq.[88,119] In a separate study, Estupiñan Perez et al.[120] also verified the ability of multiobjective optimization techniques to guide the design of PSA and VSA processes. In this study, it was shown that purity−recovery Pareto fronts of CO$_2$ as predicted by process modeling of the 4-step VSA-LPP cycle reasonably agree with the experimental results.[120] These promising observations attracted more attention to the newly proposed process-based materials screening approach and its combination with molecular simulation techniques. Several recent studies that have adopted this new materials screening approach are discussed below.

In 2018, Farmahini et al.[89] used a similar multiscale platform by combining GCMC simulation with process modeling and optimization of the 4-step VSA-LPP cycle to explore the challenges associated with the interface between molecular and process levels of description. In this study, the authors identified several sources of inconsistency in the implementation of the multiscale screening workflow that can potentially affect prediction of material performance at the process level. This includes the numerical procedures adopted to feed the equilibrium adsorption data into the process simulation, and the role of structural characteristics of adsorbent pellets including pellet porosity and pellet size.

In 2019, Subramanian Balashankar and Rajendran[121] employed a two-stage approach to screen 119 661 hypothetical zeolites, 1031 zeolitic imidazolate frameworks, and 156 zeolites catalogued by the International Zeolite Association.[111] In their study, the first stage was dedicated to the rapid screening of all materials under investigation using a computationally inexpensive batch adsorber analogue model to filter adsorbents that can meet 95% CO$_2$ purity and 90% CO$_2$ recovery targets. This stage was then followed by detailed process modeling of 15 top-performing candidates from the previous stage in addition to 24 synthesizable zeolites using the widely used 4-step VSA-LPP cycle to estimate the process level performance indicators more accurately. Out of the 39 adsorbents screened in the second stage, 16 material candidates outperformed zeolite 13X in terms of both productivity and energy consumption.[121]

A new generation of materials screening studies based on process performance metrics also appeared in 2020. In this year,

Farmahini et al.[122] explored the role of pellet morphology on materials performance. Pellet morphology belongs to the category of properties that cannot be evaluated at the molecular level and yet can greatly alter separation performance at the process level. The authors demonstrated that a series of competing mechanisms associated with diffusion into adsorbent pellets, convective mass transfer through the adsorption column, and pressure drop across the bed can be tuned through optimization of pellet size and pellet porosity to maximize separation performance of different classes of porous materials including zeolites and MOFs.[122]

Later, Park et al.[94] assessed separation performance of selected MOFs for subambient temperature postcombustion carbon capture based on (i) a selection of simple adsorbent metrics (e.g., CO_2 swing capacity, selectivity, and regenerability), (ii) performance in an idealized 2-step PSA model (adopted from Ga et al.[123]) consisting of adsorption and desorption steps, and (iii) performance in a rigorous model of 4-step Skarstrom cycle with light product pressurization. The results from this study showed that the order of high performing materials is different for the idealized 2-step model and the 4-step Skarstrom cycle. Moreover, it was illustrated that the simple adsorbent metrics that are strongly correlated with the predictions of the idealized model are not the same as those that are closely correlated with the predictions of the rigorous 4-step process model. This is an important observation, as it clearly demonstrates that the separation performance of porous materials is strongly influenced by the design of cycle configuration at the process level and that materials ranking based on simple adsorbent metrics are not directly correlated with materials performance at the process level.

Burns et al.[124] screened 1632 experimentally characterized MOFs using a multiscale platform that combines molecular simulations with process optimization and machine learning models. In their screening study, they employed the well-established 4-step VSA-LPP cycle and found that a total of 482 materials can meet the 95% CO_2 purity and 90% CO_2 recovery targets, out of which 365 materials have parasitic energies below that of commercial solvent-based CO_2 capture technologies.[124] Consistent with Danaci et al.,[125] this study also highlighted the fact that nitrogen adsorption behavior is an important factor for the prediction of materials ability to separate CO_2 with very high purity and recovery in postcombustion CO_2 capture.

Another screening study from 2020 was published by Yancy-Caballero et al.[126] who compared process level performance of 15 promising MOFs with zeolite 13X as a benchmark using three different process configurations including a modified Skarstrom cycle, a five-step PSA cycle, and a fractionated vacuum swing adsorption cycle. The results from this study suggest that UTSA-16 and Cu-TDPAT perform equally well or even better than zeolite 13X in all three process configurations mentioned above. The authors also compared process-level ranking of these MOFs with other rankings obtained based on simplified HMM and GEM metrics. They showed that the rankings suggested by these metrics may differ significantly from the one predicted by detailed process optimizations,[126] which is evident by various hierarchies of top-performing materials shown in Figure 10.

As an example, Cu-TDPAT and UTSA-16 are the two top performing materials according to FVSA cycle, but based working capacity they are the ninth and fifth in the list of top-performing materials. Based on selectivity, these materials are the fifth and fourth materials from the top. Interestingly, GEM seems to provide a closer estimation of materials performance

when compared with detailed process modeling for all three cycles. Another important observation here is the fact that the order of top-performing materials is a function of process configurations as shown by the first three columns from the right.

Another recent study was published by Pai et al.[127] in 2020 who developed a generalized and data-driven surrogate model that can reproduce operation of PSA/VSA processes at cyclic steady state with high accuracy. The multiscale screening framework developed here simultaneously optimizes adsorption isotherm properties and process operating conditions in order to estimate performance indicators of the process. The framework makes use of a dense feed forward neural network trained with a Bayesian regularization technique and is able to significantly reduce the simulation and optimization time required for multiscale screening of porous materials for postcombustion carbon capture.[127] Development of such material-agnostic machine-learning models is particularly useful, considering they can be employed for performance prediction of any arbitrary or hypothetical adsorbent as long as equilibrium adsorption isotherms of CO_2 and N_2 for that material can be sufficiently described by the implemented numerical adsorption model (e.g., a single-site Langmuir model in the case of this study).

Finally in 2021, Subraveti et al.[92] reported on a new attempt toward integration of techno-economic analyses with detailed modeling and optimization of adsorption process for postcombustion carbon capture. They estimated the capture cost of CO_2 using zeolite 13X, UTSA-16, and IISERP-MOF2 as adsorbent in a 4-step VSA-LPP cycle. Their study showed that application of IISERP-MOF2 in the above process leads to the lowest capture cost, while still being higher than the cost of carbon capture in an MEA-based absorption process as the current industrial benchmark. According to this study, zeolite 13X and UTSA-16 are respectively second and third material candidates in terms of the overall cost of the process. An important message conveyed by the authors in this study was that the minimum cost configurations obtained from techno-economic analyses do not necessarily correspond to the most optimum configurations obtained by minimizing energy penalty and maximizing productivity of a single-column VSA process, which is due to the complexities associated with scale-up of the process. This essentially means that realistic assessment of materials performance for industrial applications must go beyond optimization of the process itself and that the multiscale screening workflows should encompass considerations of techno-economic analyses for materials screening.

This section was meant to provide the reader with a historical perspective of the topic without going into technical details of the screening methods. At the end of this section, it is useful to reflect on some of the key observations from our overview. It is clear that multiscale materials screening strategies have advanced significantly over the past decade, evolving from screening of porous materials based on simple microscale properties toward development of more realistic approaches based on process modeling and optimization for evaluation of materials performance, and finally to incorporating techno-economic assessment of the whole separation plant into the screening workflows. Overview of the studies discussed in this section reveals lack of consistency among the hierarchies of top performing materials that are reported by different studies. This means that the screening studies conducted so far have not been able to propose a consistent set of materials as top performing
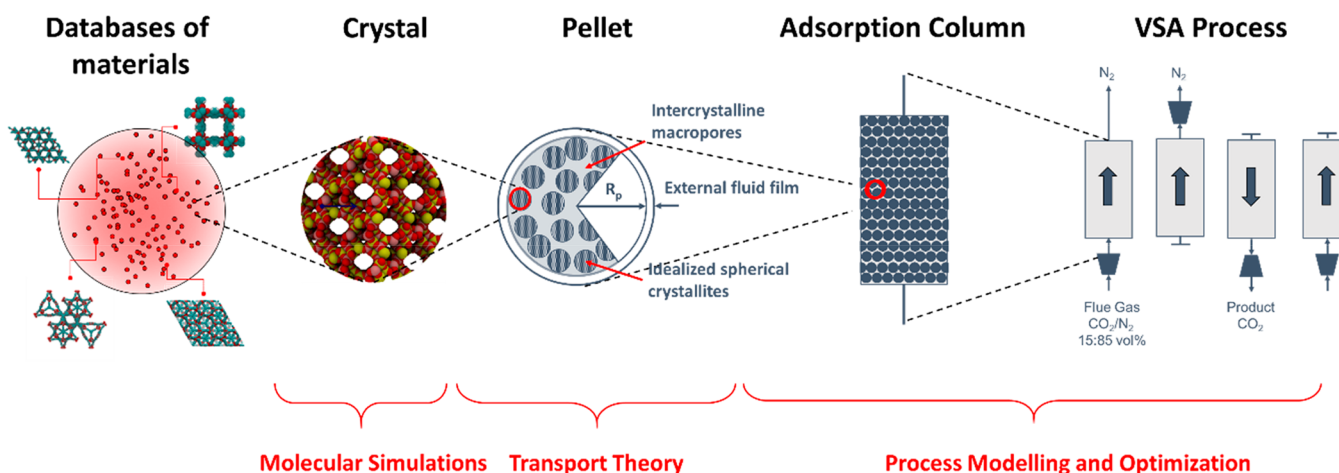
Figure 11. General structure of the multiscale screening workflow for materials screening.

candidates for postcombustion carbon capture. In fact, this is associated with the lack of consistency in model assumptions and in calculation of a series of parameters that are used in performance-based materials screening workflows including but not limited to the force fields used in molecular simulations for prediction of equilibrium adsorption data, the numerical methods used for fitting adsorption isotherms, various model assumptions applied in describing the kinetics of the process, application of different process and cycle configurations, and so on. Addressing the issue of consistency in ranking of porous materials requires detailed knowledge about the inner workings and implementation of all the modeling modules that are used in a materials screening workflow. This is the topic of the next section of this review.

6. MULTISCALE SCREENING WORKFLOW

In the previous sections, we briefly discussed why materials screening is important in the context of PSA and VSA technologies for postcombustion carbon capture. We also provided a historical perspective on the evolution of materials performance metrics and screening methods, which have been used so far. The main objective of these sections was to illustrate to the reader the importance and the gradual evolution of the research community toward adopting more complex multiscale screening workflows as the emerging way to evaluate separation performance of porous materials.

The objective of the current section is to introduce in an accessible, tutorial-style fashion the key elements and methods involved in multiscale screening workflows. Some of these elements, such as molecular simulations and process modeling, have been also comprehensively covered in several authoritative textbooks. The intention here is not to replace or replicate these sources but to highlight only the essential aspects of the methods while focusing on the data they require, information they produce, and the gaps at the interfaces between different elements. To achieve this objective, the structure of this section logically follows the multiscale workflow diagram, shown in Figure 11. The starting point of this workflow is a database of porous materials. In section 6.1, we review the currently existing databases and the computational tools required to characterize structural properties of the porous materials in these databases. Molecular simulations are used to obtain equilibrium and transport properties at a molecular level. These methods are introduced in section 6.2. Finally, following the workflow we

pass the information from molecular simulations to the process level modeling and optimization. Models, methods, and data required for this stage are reviewed in section 6.3.

6.1. Material Databases and Characterization Tools

This section corresponds to the first step in the multiscale material screening workflow. The aim here is to provide concise and practical reference to the reader on what databases are currently available, what materials and data they contain, and what tools are available to build geometric descriptors for materials in these databases.

6.1.1. Databases of Porous Materials. MOFs are the primary and most prominent example of the emerging families of materials,[6−8] and it is useful to briefly review what these materials are. Although the origins of MOFs can be traced as far back as the late 1950s, they were given their current name, metal−organic frameworks, in the seminal paper by Yaghi and Li in 1995.[128] To prepare a MOF, one uses two types of building blocks: metal centers and organic molecules capable of forming strong coordination bonds with these centers. In the synthesis process, the building blocks form a crystalline framework where metal complexes comprise the vertices of the framework, connected by the organic linkers. Several papers that followed in the late 1990s discovered a few more examples of these frameworks; however, most importantly, they demonstrated that these structures possessed permanent stable porosity and high surface area and that new materials could be designed simply by variation of the building blocks, leading to the concept of isoreticular material design.[129−131] Since then, tens of thousands of new MOFs have been discovered: the most current assessment of the Cambridge Structural Database (CSD) suggests ca. 100 000 reported structures that can be qualified as MOFs,[132] while the modular nature of these materials implies that in principle infinite variation of structures is possible (if we assume that the diversity of MOFs can approach the diversity of the organic chemical space).

ZIFs, discovered a few years later,[9,133,134] are a subclass of MOF materials that have zeolite framework topologies in which silicon atoms are replaced by transition metals and the bridging oxygens are substituted by imidazolate building units.[135] Currently, there are about 300 ZIFs reported in the CSD and potential application of these materials in the context of chemical separations has been recently reviewed by Pimentel et al.[136] In contrast to materials based on coordinative assembly and coordination bonds, covalent organic frameworks (COFs)

Table 2. Databases of Crystalline Porous Materials

index	database	number of entries	origin	cleaned	optimized	charges included
1	Wilmer-et-al.[100]	137 953	simulation	yes	no	no
2	Boyd-and-Woo[157]	324 426	simulation	yes	yes	yes
3	ToBaCCo[152,160]	13 512	simulation	yes	yes	no
4	CSD[150]	>1M	experiment	no	no	no
5	Goldsmith et al.[161]	4000	experiment	yes	no	no
6	CoRE-MOF-2019[165]	~14 000	experiment	yes	partially[a]	partially[b]
7	CSD-MOF-subset[c][154]	96 000	experiment	yes	no	no
8	hZeo[112,166]	2.6M	simulation	yes	yes	no
9	IZA[111]	253	experiment	yes	yes	no
10	hPPN[153]	18 000	simulation	yes	yes	no
11	hCOF[167]	69 840	simulation	yes	yes	no
12	CoRE-COF[168]	449	experiment	yes	yes	yes
13	CURATED-COFs[171]	482	experiment	yes	yes	yes
14	hZIFs[86]		simulation			
15	NE-DB[2]	530 243	simulation and experiment			
16	NMG[149,173]	>3M	simulation and experiment			
17	PRAM-DB[175]	205	simulation and experiment			partially

[a]879 MOFs underwent geometry optimization and were released as part of CoRE MOF-DFT optimized 2017.[164] [b]Partial atomic charges of 2932 MOFs were computed and were released as part of CoRE MOF-DDEC 2016.[163] [c]As of Aug 2019.[132,154]

do not feature metal complexes and are based on covalent bonds.[10,137] Since their discovery in 2005, a substantial number of 2D and 3D COFs have been reported with diverse structural and chemical properties.[137]

Crystalline materials, such as MOFs, ZIFs, and COFs, can be contrasted with several traditional and emerging classes of amorphous porous materials, such as activated carbons,[138] carbide-derived carbons,[139] and polymers with intrinsic microporosity (PIMs).[14,15,140] Porous aromatic frameworks (PAFs) are another class of porous materials with rigid aromatic open-framework structure constructed with covalent bonds.[12] Although PAFs are not crystalline, they are ordered with regular and high porosity.[141]

This wealth of new materials should not overshadow more traditional classes of porous materials such as zeolites, which, due to their stability, attractive cost, commercial availability, and maturity in industrial applications, will likely remain the primary adsorptive materials for years to come. There are currently more than 250 zeolite topologies recognized by the International Zeolite Association. From very early studies, efforts have been made to computationally realize and characterize these materials.[142−144] So far, millions of new zeolite structures have been hypothesized using computational methods.[112,145] Ongoing research is also directed toward understanding the magnitude and diversity of the materials landscape for adsorption science[146,147] and to evaluate what portion of this structural space is realizable in experiments.[148] Combined, these classes of materials provide enormous chemical and structural diversity, collectively described as the materials genome.[149] Several efforts have been made to assemble databases of experimentally synthesized or computationally constructed M O F s, Z I F s, o r p o r o u s p o l y m e r n e t w o r k s (PPNs).[86,100,150−154] Next, we review the most prominent examples of these databases which are also listed in Table 2.

6.1.1.1. Databases of Hypothetical MOFs. Hitherto, three main databases of hypothetical MOFs have been created which are discussed below:

(a) **The database by Wilmer et al.:** This database contains 137 953 structures and is generated by recombining a library of 102 building blocks including secondary building units (SBUs)

and organic linkers from crystallographic data of already synthesized MOFs using a "tinker-toy" algorithm.[100] The resulting hypothetical database is, however, composed of only a few underlying framework topologies.[155] By testing a limited set of MOFs including HKUST-1, IRMOF-1, PCN-14, and MIL-47, the authors suggested that their method can closely reconstruct molecular structures of the experimentally synthesized materials.[100] Nevertheless, generalization of this finding is subject to more comprehensive validations, considering no energy minimization was performed for any of the constructed structures in this database. The database originally published by Wilmer et al. did not include partial electrostatic charges on atoms of MOFs; hence its application was limited to very few adsorption cases where electrostatic interactions are not important (e.g., CH_4 adsorption).[100] The authors employed this database to search for MOFs that could be potentially used for methane storage and identified more than 300 MOFs with a predicted storage capacity larger than that of any previously known material.[100] In a later study, EQeq partial atomic charges[113] were computed for the above hypothetical MOFs and used for simulation of adsorption of charged molecules such as CO_2 and N_2.[101]

(b) **The database by Boyd and Woo:** This new database of hypothetical MOFs was constructed using the topology-based algorithm of Boyd and Woo[156] and contains 324 426 structures which are generated by assembling a set of secondary building units containing 8 inorganic and 94 organic SBUs resulting in 12 different topologies.[157] The set was further diversified by chemical modification of MOFs, in which available hydrogens were replaced by functional groups. All MOFs in this database are structurally optimized using classical force fields. Framework charges for all structures included in this database were also computed using the charge equilibration method (Qeq)[158] and the MOF electrostatic potential optimized (MEPO) parameters.[159]

(c) **ToBaCCo Database:** This database was constructed using the topologically based crystal constructor (ToBaCCo) algorithm and contains 13 512 MOF structures with 41 different edge-transitive topologies.[152,160] The database makes use of a top-down construction algorithm that uses topological blue-

prints and molecular building blocks as input to assemble MOF structures. The algorithm does not check for atom overlaps as part of the construction process; therefore the geometry of the resulting structures were optimized using generic force fields before being used in molecular simulations.[160] The database does not include partial atomic charges.

6.1.1.2. Cambridge Structural Database (CSD). The Cambridge Structural Database (CSD) contains more than a million organic and metal−organic small-molecule crystal structures that are obtained from X-ray or neutron diffraction analyses.[150] The MOF structures deposited in this database are experimentally realized; nevertheless, the use of CSD entries for high-throughput screening of porous materials is not straightforward. Checks must be performed to make sure that the candidate structures obtained from CSD are adequately porous and are free from residual substances that are leftover from the synthesis processes. As such, the first step in performing high-throughput screening of experimental MOFs is to construct curated subsets of CSD that can fulfill the above criteria (see more on the CSD-MOF Subset in section 6.1.1.5).

6.1.1.3. Goldsmith Database of Experimental MOFs. In 2013, Goldsmith et al.[161] constructed a MOF database containing 22 700 computation-ready structures which were derived from the CSD after the removal of unbonded guest molecules (e.g., residual solvents). By excluding disordered compounds and those with missing atoms, the total number of MOF structures were reduced to 4000,[161] which did not include those with interpenetrated frameworks and charge-balancing ions.[151] The materials included in the database were subsequently characterized by calculating porosity, surface area, and total theoretical H_2 uptake.[161] Goldsmith et al. used their MOF database to estimate the maximum theoretical uptake of hydrogen based on the so-called "Chahine rule" (see ref 162 for further reading) known for hydrogen adsorption in microporous carbons but also shown to be valid across a wide range of other porous materials including MOFs.[161]

6.1.1.4. CoRE-MOF Database. Construction of the computation-ready, experimental metal−organic frameworks (CoRE-MOF) database was a major attempt in development of a MOF database that can be directly used in molecular simulations. The first version of CoRE-MOF[151] contains 5109 3D MOF structures with pore-limiting diameter greater than 2.4 Å that are derived from CSD. The MOF structures were screened to make sure that all MOFs included in the database are crystalline (no disorder) and solvent-free. The database also reports helium void fractions of all MOFs in addition to their surface area, accessible volume, largest cavity diameter (LCD), and pore-limiting diameter (PLD). In the original version of the database, the structures were not optimized (except for very few MOFs that were manually edited).[151] Following the initial release of CoRE-MOF, two modified subsets of this database were released in 2016 and 2017. The first subset contains 2932 experimental MOFs whose partial atomic point charges were calculated using plane wave DFT and the DDEC charge partitioning methods.[163] The second subset focuses on the geometry optimization of 879 experimentally synthesized MOFs using a periodic density functional theory (DFT) method.[164] The latter publication demonstrated that although the majority of MOF structures undergo less than 10% change in their structural parameters (e.g., pore size, lattice parameters, unit cell volume, and helium void fraction) upon DFT optimization, many other MOF structures change significantly after geometry optimization especially those materials whose crystalline

structures were cleaned from solvent residue molecules. More importantly, it was shown that the DFT optimization had a large impact on simulated gas adsorption in some cases, even for materials whose crystalline structure did not change significantly.[164] This study has important implications for high-throughput materials screening approaches that rely on databases of experimentally synthesized materials such as CSD[150] or the original CoRE-MOF.[151] The CoRE-MOF database was recently expanded to include approximately 14 000 structures (CoRE MOF 2019). The updated database includes additional structures that were contributed by CoRE-MOF users, obtained from updates of the CSD database and a Web of Science search.[165] CoRE MOF 2019 was released in two different sets: (1) free solvent removed (FSR) database for which only the free solvent molecules have been removed from the structures; (2) all solvent removed (ASR) database for which both bound and free solvent molecules have been removed from the structures. CoRE-MOF 2019 also summarizes a list of MOF structures that contain open-metal sites.[165]

6.1.1.5. CSD-MOF Subset. In 2017, Moghadam et al.[154] constructed a new subset of CSD for solvent-free MOFs in which 69 666 1D, 2D, and 3D MOFs were listed out of which 54 808 structures are nondisordered. These materials were characterized using the Zeo++ code[102] based on the Voronoi decomposition technique to calculate the accessible surface area, accessible pore volume, LCD, and PLD. It was found that 46 420 structures have gravimetric surface area equal to zero, which essentially means that N_2 size molecular probes cannot access their pore spaces for geometric surface area calculations.[154] It is shown that the remaining 8388 MOFs have PLD values larger than 3.7 Å, which is approximately 3600 structures more than what was previously published by Chung et al.[151] in the initial version of the CoRE-MOF database. Currently, the MOF subset of CSD database contains approximately 100 000 MOFs.[132] The main advantage of the CSD-MOF subset is that it is integrated into the Cambridge Crystallographic Data Centre's (CCDC) structure search program. This not only allows for tailored structural queries (e.g., generation of MOF subsets based on secondary building units or selection of nondisordered materials), but it can also be used to automatically update the database with subsequent addition of new MOFs to CSD.[154]

6.1.1.6. Hypothetical Zeolites Database (hZeo-DB). hZeo is a database of computationally predicted zeolite-like structures that were generated by systematically exploring 230 space groups, unit cell dimensions between 3 and 30 Å, and T atom densities from 10 to 20 per 1000 Å³.[112,166] A computational procedure based on Monte Carlo search was employed to produce 3.3 million zeolite-like structures out of which 2.6 million topologically distinct structures were identified after energy minimization.[166] Roughly 10% of this number are the structures that are deemed to be thermodynamically accessible as aluminosilicates based on energy stability of the structures.[112]

6.1.1.7. Database of Zeolite Structures (IZA-DB). IZA-DB provides information about the structures of all the zeolite framework types that have been approved by the Structure Commission of the International Zeolite Association (IZA-SC). The database currently contains 242 ordered and 11 partially disordered topologies.[111]

6.1.1.8. Database of Hypothetical Porous Polymer Networks (hPPN-DB). The hypothetical PPN database constructed by Martin et al.[153] contains almost 18 000 hypothetical structures of porous polymer networks, which are predicted *in silico* using commercially available chemical fragments and two

experimentally known synthetic routes, hence aiming to provide a database of synthetically realistic PPNs.[153] All structures from this database have their structures optimized using semi-empirical electronic structure methods.[153] The structures are also characterized for their topological properties and methane adsorption characteristics.[153]

6.1.1.9. Hypothetical COF Database (hCOF-DB). This database is a collection of 69 840 hypothetical covalent organic frameworks (COFs) that were assembled from 666 distinct organic linkers and four established synthetic routes.[167] It contains 18 813 interpenetrated 3D structures, 42 386 non-interpenetrated 3D structures, and 8641 2D-layered structures. All materials are structurally relaxed using classical force fields. The database does not include partial atomic charges for the deposited COFs.

6.1.1.10. CoRE-COF Database. In 2017, Tong et al.[168] compiled a computation-ready database of experimental covalent organic frameworks (COFs) containing 187 structures. The original version of the database contained 19 3D-COFs and 168 2D-COFs. The structures collected in this database were reported to be disorder-free and solvent-free, which makes them ready for computational studies. Although most of the structures available in CoRE-COF database are cleaned versions of the experimentally reported CIF files, some of the COFs collected in the database are constructed computationally based on the information reported in the literature where synthesis of the corresponding COFs had been reported without any CIF file. CoRE-COF materials are structurally optimized using a two-step procedure[168] where optimization was initially performed using classical force fields and then later refined using the dispersion-corrected DFT method of Grimme (DFT-D2).[169] The database also reports on structural features of each COF including their largest cavity diameter, pore-limiting diameter, accessible surface area, and free volume. Since its first release, the CoRE-COF database has been updated regularly so that its most recent version (CoRE-COF, ver. 4.0)[170] contains 449 structures with the framework charges obtained from the charge equilibration (Qeq) method.

6.1.1.11. CURATED COF Database. Clean, uniform, refined with automatic tracking from experimental database (CURA-TED) of covalent organic frameworks (COFs) is another database of experimentally realized COFs.[171] The initial version of the database included 324 structures; however the database has been updated recently so that its most recent version (Feb 2020) contains 482 structures. All structures collected in the CURATED COFs are cleaned from solvent molecules and have no partial occupation or structural disorder. They are structurally optimized using DFT with the DDEC framework partial charges included.[171]

6.1.1.12. Hypothetical ZIFs Database (hZIF-DB). In 2012, Lin et al.[86] published a paper on computational screening of large number of zeolites and zeolitic imidazolate frameworks (ZIFs) for carbon capture. In this study, ZIF structures were generated computationally by using zeolite topologies of the International Zeolite Association (IZA) database. In doing so, the distance between zinc atoms and the center of imidazolate rings was set to be 1.95 times larger than the silicon–oxygen distance in zeolites. ZIF frameworks were then generated by scaling the corresponding zeolite structures by the same factor and replacing every oxygen atom with an imidazolate group and substituting every silicon atom with a zinc atom. The resulting ZIF geometries were validated by comparison against geometries of two experimentally known ZIF structures (i.e., ZIF-3

and ZIF-10).[86] This database is not available online or in a depository to further comment on its characteristics.

6.1.1.13. Nanoporous Explorer Database (NE-DB). Nanoporous explorer is an aggregated database of nanoporous materials including CoRE-MOF,[151] hypothetical MOFs,[100] and hypothetical PPNs.[153] The database is part of a larger database developed under the Materials Project program,[2] which is designed to provide a large collection of computed data for experimentally known and computationally predicted materials including nanoporous materials.[172] The NE-DB provides information about pore descriptors (e.g., PLD, LCD), adsorption properties (e.g., Henry's constant, adsorption isotherm, heat of adsorption), and simulated powder X-ray diffraction of many porous materials. At the time of writing this review, the Nanoporous Explorer database contained 530 243 entries.

6.1.1.14. Nanoporous Materials Genome Database (NMG-DB). NMG[149,173] is a collection of a growing number of materials databases that currently encompasses more than 3 million hypothetical and synthesized porous materials. Most prominent examples of these databases are already discussed in this review. For the sake of completeness, we provide a full list of the constituting databases for NMG, which includes hypothetical MOFs database,[100,157] computation-ready experimental MOFs database (CoRE-MOFs),[151,165] hypothetical zeolites,[112,166] ideal silica zeolites obtained from the International Zeolite Association (IZA) database,[111] hypothetical covalent organic frameworks (COFs),[167,174] computation-ready experimental COF database (CoRE-COFs),[168,171] hypothetical zeolitic imidazolate frameworks (ZIFs),[86] and hypothetical porous polymer networks (PPNs).[153]

6.1.1.15. Database of Porous Rigid Amorphous Materials (PRAM-DB). So far, the databases we reviewed comprised crystalline and ordered porous materials. In an important development, Thyagarajan and Sholl[175] have recently collected 205 atomistic models of amorphous nanoporous materials that had been previously published by various groups. This new database of porous rigid amorphous materials (PRAM-DB) contains several classes of materials with disordered porous structures including amorphous zeolite imidazolate frameworks (a-ZIFs),[176] activated carbons,[177] carbide-derived carbons,[178−183] polymers with intrinsic microporosity (PIMs),[184−187] hyper-cross-linked polymers (HCPs),[188−190] kerogens,[191] and cement,[192] which all have important applications in adsorption separation technologies. The database contains partial atomic charges for most of the materials. It also reports on a wide range of physical properties for each material. This includes pore limiting diameter (PLD), the largest cavity diameter (LCD), the accessible surface area and pore volume, pore size distribution (PSD), ray-tracing histograms, PXRD patterns, and radial pair distribution functions (RDF).[175] The new study also reports single-component and binary adsorption isotherms of several gases for these materials.[175]

6.1.2. Computational Tools for Structural Characterization of Porous Solids. As can be seen from the reviewed studies, classification of materials within the databases and early efforts in computational screenings are based on the geometric descriptors of porous materials, such as the accessible surface area, pore limiting diameter, and pore volume. As this is a practice-oriented review, we believe it is useful to mention the material characterization software available to obtain these geometric properties for crystalline and amorphous porous structures. To begin with, we refer the reader to several articles

Table 3. Computer Software Available for Pore Structure Characterizations

item	software	surface area	pore volume	PSD	PLD	RDF	cif format supported	code repository
1	Poreblazer[103]	yes	yes	yes	yes	no	no	https://github.com/SarkisovGroup/PoreBlazer
2	PorosityPlus[196]	yes	yes	yes	no	yes	no	https://data.csiro.au/collections/collection/CIcsiro:34838v1
3	Zeo++[102]	yes	yes	yes	yes	no	yes	http://zeoplusplus.org/

describing what properties of porous materials can be calculated and how they are related to the properties that can be measured and to the physical process of adsorption in porous materials.[102,103,193,194] In principle, calculation of selected properties, such as the solvent-accessible surface area (in application to porous materials often called simply the accessible surface area), is available within many commercial and free software packages. Three packages available for a more comprehensive assessment of the materials are Poreblazer,[103,193,195] Zeo++,[102] and PorosityPlus[196] (Table 3). From this list, Poreblazer developed by Sarkisov and Harrison[103,195] and PorosityPlus developed by Opletal et al.[196] are written in Fortran and are available as open-source packages. Zeo++, developed by Haranczyk and co-workers,[102] is a C++ package based on the Voronoi tessellation methods.[102] With Voronoi network being a dual graph of Delaunay network, the approach employed by Zeo++ is closely related to that of Foster et al.[197] The program is downloadable from the Web site of the developers, with the source code available upon request only.

All three codes mentioned above are able to calculate accessible surface area (equivalent to the area of the surface formed by the nitrogen probe rolling on the surface of the atoms of the structure), pore volume (using several alternative definitions of this property), and pore size distribution. Poreblazer and Zeo++ can also calculate pore limiting diameter (PLD) of the porous frameworks, while PorosityPlus is also able to compute radial distribution function (RDF) of the adsorbed phase in the system. One important feature of Zeo++ software is its ability to read framework structures in CIF format, while the other two programs can only use XYZ format as their input for the porous framework. A detailed comparison of Poreblazer, Zeo++, and RASPA[198] has been recently provided by Sarkisov et al.[195] for structural characterization of CSD-MOF Subset database.[154] Here, we note that RASPA is a molecular simulation software that is mainly known for its capabilities for Monte Carlo simulations. This program is presented in the following section where we discuss grand canonical Monte Carlo (GCMC) technique for simulation of equilibrium adsorption isotherms.

6.2. Molecular Simulation

The purpose of this section is to briefly introduce the two main and most widely used molecular simulation techniques, grand canonical Monte Carlo (GCMC) and molecular dynamics (MD) simulations, which are used for simulation of adsorption and transport properties, respectively, on a microscopic level. In the context of adsorption problems, comprehensive reviews on molecular simulations for metal–organic frameworks have been provided by Yang and co-workers[199] and for zeolites by Smit and Maesen.[200] In this section, however, we will discuss these techniques as two important elements of the multiscale screening workflows. In particular, we would like our intended reader to appreciate what parameters are required for these simulations, how they can be calculated, and what open-source software are available to researchers to perform these simulations.

In section 6.2.1, we introduce fundamentals of GCMC method followed by section 6.2.2, which presents the main publicly available simulation software for performing this type of simulation. Next, in section 6.2.3, fundamentals of molecular dynamics will be discussed, which will be followed by a section related to the open-source programs that can be used to run MD (section 6.2.4). Finally in section 6.2.5, we will briefly introduce molecular force fields, which are central to accurate simulation of molecular systems. The issues associated with the current gaps in the field of force field development and comments on their implications for multiscale materials screening studies will be reviewed later in section 8.1.

6.2.1. Grand Canonical Monte Carlo Simulation. In this section, we briefly review the grand canonical Monte Carlo (GCMC) simulation method, which is widely used for calculation of equilibrium adsorption data. For a more comprehensive review of Monte Carlo methods, we would refer the reader to reference books[201−203] and several excellent articles by Dubbeldam and co-workers on the Monte Carlo methods and the organization of computer codes associated with them.[198,204]

The problem of interest here is the adsorption of small molecules (carbon dioxide, nitrogen, methane, hydrogen) in crystalline porous materials. The volume (V) and temperature (T) of the system are fixed, and the specified value of the chemical potential (μ) establishes thermodynamic equilibrium between the system and the bulk reservoir, serving as a source and sink of adsorbate molecules. From the statistical-mechanical point of view, the system corresponds to the grand-canonical ensemble ($\mu V T$), for which the Metropolis Monte Carlo is a widely used method. This approach is suitable for rigid porous materials, which do not exhibit significant volume changes in response to external stimuli such as heat, pressure, and adsorption/desorption of guest molecules, although it is possible to incorporate in the simulations local movement of the atoms and groups, such as rotation of the ligands in MOFs. It is important to note that even for materials with almost rigid framework, there exists some intrinsic flexibilities.[205] This type of flexibility occurs without any change in unit cell volume and is associated with effects such as thermal vibrations at equilibrium or presence of adsorbed molecules inside pores. Recent studies have shown that the importance of intrinsic flexibility arising from thermal vibrations varies considerably for MOFs depending on the adsorption property of interest.[206,207] For example, it was shown that intrinsic flexibility can be more important where pore sizes are comparable to the kinetic diameter of adsorbate molecules.[206,208] For zeolites, however, the effect of thermal framework vibrations on molecular adsorption was shown to be negligible and the rigid framework assumption can be reliably used in GCMC simulation for these materials.[209] For simulation of flexible materials that undergo significant changes in unit cell volume, more advanced simulation methods such as the osmotic ensemble and Gibbs ensemble Monte Carlo should be used.[204]

A schematic diagram of the GCMC workflow is shown in Figure 12. According to this scheme, a Monte Carlo simulation of adsorption requires the following inputs:
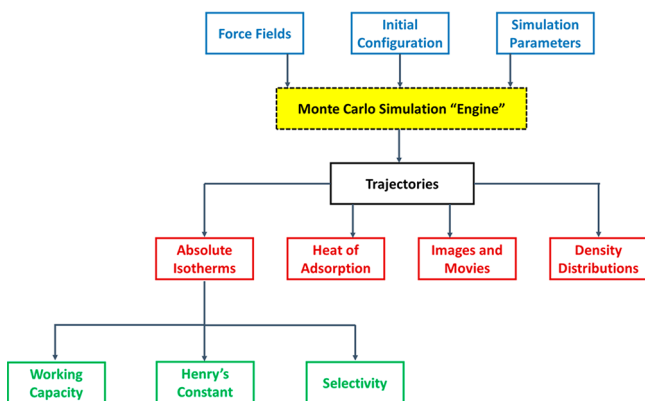
Figure 12. Schematic depiction of the workflow in the grand canonical Monte Carlo simulations. The blue boxes indicate the required input data and parameters for the simulations. In the most general terms, a simulation run generates a trajectory (a set of microstates of the system, corresponding to the particular ensemble). The red boxes indicate the primary properties that are directly calculated from the Monte Carlo trajectory. The green boxes are the secondary properties that can be calculated from the primary properties.

- Force field parameters: these parameters define what atoms and molecules are present in the system and describe how they interact with one another. This includes parameters associated with nonbonded van der Waals interactions, partial charges on the atoms of the structure and molecules, and geometry of the adsorbing molecules (distances and relative positions of the atoms within the molecule).

- Initial configurations of the species present in the system: this includes positions of the atoms of the porous structure and positions of any already adsorbed molecules.

- Simulation parameters, including details of the Monte Carlo protocol, number of steps allocated for the equilibration of the system, parameters associated with the statistical analysis of the simulation (i.e., number and size of blocks in the block-average analysis), temperature, and fugacities of the adsorbing components. This input data category may also prescribe particular specialized methods to calculate electrostatic interactions between partial charges on the atoms.

Let us consider what happens within the Monte Carlo simulation engine. A configuration of the system with a particular number of molecules (in case of GCMC) and their positions is called a *microstate*. In the actual physical system, these microstates occur according to the Boltzmann probability distribution. In a Monte Carlo simulation, these microstates are generated by stochastically perturbing the state of the system: we can add molecules to the system or remove them or change their position and orientation. These different ways to change the state of the system are called *Monte Carlo moves*. To ensure Boltzmann distribution of the microstates, the probability to accept a move is calculated according to eqs 1−4:

Translation:

$$P_{ACC}(S \rightarrow S') = \min\{1, \exp(-\beta \Delta U)\} \tag{1}$$

Rotation:

$$P_{ACC}(S \rightarrow S') = \min\left\{1, \exp\left(-\beta \Delta U \frac{\sin \theta_S}{\sin \theta_{S'}}\right)\right\} \tag{2}$$

Insertion:

$$P_{ACC}(N_a \rightarrow N_a + 1) = \min\left\{1, \frac{\beta f V}{N_a + 1} \exp(-\beta \Delta U)\right\} \tag{3}$$

Deletion:

$$P_{ACC}(N_a \rightarrow N_a - 1) = \min\left\{1, \frac{N_a}{\beta f V} \exp(-\beta \Delta U)\right\} \tag{4}$$

where U represents the potential energy of interaction, N_a and V are the number of molecules and volume, respectively, β is the reciprocal thermodynamic temperature, $1/k_B T$, with k_B being the Boltzmann constant, and θ is the Euler angle of the rigid body rotation. Here, f is the fugacity of the adsorbing species, which is related to the chemical potential as

$$f = \frac{q_{rot}}{\beta \Lambda^3} \exp(\beta \mu) \tag{5}$$

where q_{rot} is the rotational partition function for a single rigid molecule, and Λ is the thermal de Broglie wavelength:

$$\Lambda = \left(\frac{\beta h^2}{2\pi m}\right)^{1/2} \tag{6}$$

where h is Planck's constant and m is the molecule mass.

These probability factors depend on the potential energy of the system before and after the attempted move, ΔU; in the case of the insertion and deletion moves, they also depend on the chemical potential or fugacity of the adsorbing species. Therefore, it is clear that at a fixed volume, temperature, and chemical potential of the system and given the molecular structure of the porous solid, the state of the system is governed by the interaction energy, based on the employed force field. Hence, the key message of this section is that in Monte Carlo simulations (as in molecular dynamics), the force field is the main input information required to setup the physical description of the system, whereas everything else can be treated as technical details.

As the simulation progresses, the positions of the molecules change and the number of the molecules fluctuates, producing a set of microstates over which the average properties of the system can be calculated. This set of microstates is called a trajectory, and it is a common outcome of both Monte Carlo and molecular dynamic simulations (in the sense that it reflects the position of the system in the phase space), with the difference that the Monte Carlo trajectory is not a function of physical time and does not contain information about the velocities of the molecules.

The ensemble of microstates within the trajectory can be used to produce the relevant output properties of the system. In the context of adsorption studies, the most important property is the average number of molecules present in the system. For a single value of the chemical potential or fugacity, the simulation will produce an average adsorbed density. A series of simulations at increasing chemical potentials will produce an adsorption isotherm.

An important distinction has to be made between the absolute and excess amount adsorbed. The absolute amount adsorbed is the actual number of molecules present in the micropores at a particular fugacity. The excess amount is the difference between the absolute amount adsorbed and the number of molecules that would be present in the micropore volume according to the bulk gas density at the pressure and temperature of adsorption. The distinction between different definitions of adsorption and their connection to the experimental measurements has been discussed by Brandani et al.[210] Monte Carlo simulations report absolute amount adsorbed, whereas experimental measurements are more often presented as the excess amount. The process simulations discussed in the next section take as an input analytical models for the absolute amount adsorbed.

Another important property that can be obtained from GCMC simulation is the enthalpy of adsorption. As will be discussed in the process modeling section of this review, in real processes and in process models based on adiabatic considerations, heat effects may play a role in the performance of the cycle. In molecular simulations, this property can be calculated either using an expression based on the result from the statistical—mechanical fluctuation theorem[211] or, in direct analogy to the experimental methods, using the Clausius—Clapeyron equation. In the first case, a single isotherm is sufficient to calculate the heat of adsorption at each adsorption pressure, as described by eq 7:

$$\Delta H_{\text{ads}} = \frac{\langle N \times U \rangle_\mu - \langle N \rangle_\mu \langle U \rangle_\mu}{\langle N^2 \rangle_\mu - \langle N \rangle_\mu^2} - \langle U_g \rangle_{\text{IG}} - \langle U_s \rangle - RT \tag{7}$$

here ΔH_{ads} is enthalpy of adsorption, U represents combined total energy of the solid adsorbent and adsorbed molecules, N is the total of number of molecules adsorbed in the framework, $\langle U_g \rangle_{\text{IG}}$ refers to the average energy of a single molecule in the ideal gas phase, $\langle U_s \rangle$ is the average energy of the solid framework, and R is the gas constant. $\langle U_s \rangle$ will be equal to zero when the framework is assumed to be rigid, and $\langle U_g \rangle_{\text{IG}}$ is also zero if adsorbate molecules are treated as rigid. Thus, enthalpy of adsorption can be often calculated from the change in the potential energy of the system after adsorption. We note that the use of eq 7 in certain systems (e.g., adsorption of water in hydrophobic MOFs[212]) may result in large fluctuations of the values of ΔH_{ads}. In such cases, enthalpy of adsorption can be computed using the derivative of the total potential energy $\left(\frac{\partial \langle U \rangle}{\partial \langle N \rangle} \right)_T$, which will replace the first term on right-hand side of eq 7.[212] At high loadings, the reliability of eq 7 deteriorates. This is because this formula relies on the fluctuation of the number of adsorbed molecules in the system, and since at high loading the acceptance ratio for the insertion and deletion Monte Carlo moves is low, convergence of the method becomes problematic. This is not an issue for the approach based on the Clausius—Clapeyron equation;[211] however, this method requires adsorption isotherms at several temperatures. Finally, simplified expressions are available if one is interested in the heat of adsorption in the Henry's law (zero loading) regime.

In addition to the properties directly required by the process simulation data (adsorption equilibria, heats of adsorption), molecular simulations also generate a wealth of information by visualizing the adsorption process on a molecular level (e.g., visualizations and density maps). These properties help to elucidate, for example, the presence of specific binding sites and distribution of the molecules in the structure, which in turn can be used to construct new analytical models for adsorption.

So far, this brief introduction to the grand canonical Monte Carlo methods for adsorption problems implicitly assumed rigid crystal structures and rigid adsorbate molecules (with small gas molecules, such as nitrogen, carbon dioxide, and methane being adequately described by this approximation). Extension of GCMC simulations to larger flexible molecules (i.e., alkanes) requires more advanced techniques, such as the configurational-bias GCMC.[200] Adsorption behavior in flexible MOFs has also attracted significant attention over the years. To capture these phenomena, simulation in the osmotic ensemble is required as well as advanced force fields to correctly represent the internal degrees of freedom within the framework.[213]

6.2.2. Monte Carlo Simulation Codes. To make the review a practical reference, here we briefly introduce the open-source Monte Carlo codes for simulation of equilibrium adsorption isotherms in porous materials. These codes are listed in Table 4. We note here that a special issue of *Molecular*

Table 4. Monte Carlo Simulation Codes

software	ref	web site
Cassandra	Shah et al.[218]	https://cassandra.nd.edu/
DL_MONTE	Purton et al.[219]	https://www.ccp5.ac.uk/DL_MONTE
MuSiC	Gupta et al.[220]	https://github.com/snurr-group
RASPA	Dubbeldam et al.[198]	https://www.iraspa.org/RASPA/index.html
Towhee	Martin[221]	http://towhee.sourceforge.net/

Simulation journal invited the community to reflect on the codes and algorithms available for the Monte Carlo simulations and their accessibility and applicability, efficiency, and challenges.[214] In a recent study, we tasked ourselves with exploring the consistency of some of the most commonly used MC codes as listed in Table 4 and examined their relative efficiency.[215] For this, we concentrated on a specific case study of carbon dioxide adsorption in IRMOF-1 material at conditions for which previous simulation results and experimental data were available.[216] It was a significant reassurance for us to observe that the codes were indeed consistent with each other. To assess their relative efficiency, we employed analysis based on the statistical inefficiency of sampling to compare trajectories from different codes on a consistent basis of the rate at which they were generating a statistically novel configuration. Our analyses revealed some differences in the overall performance of various MC codes; nevertheless this variation was found to be relatively negligible.[215] RASPA, MuSiC, and DL_MONTE were overall the top performing programs in the analysis. Within the same article, we also generated consistent setups and scripts for all the codes for the above test case, which can be used by the molecular simulation community as a template for consistency tests and validation of future MC codes. These materials are available from our online GitHub repository.[215,217] Consistency and efficiency of MC codes are particularly important in the context of materials screening and multiscale simulation workflows.

Here, we briefly introduce the codes listed in Table 4.

6.2.2.1. Cassandra. Cassandra is a MC program developed in Maginn's research group at the University of Notre Dame. It is a software package written in FORTRAN for simulation of the thermodynamic properties of fluids and solids.[218] Cassandra supports canonical (NVT), isothermal—isobaric (NPT), grand canonical (μVT), osmotic (μpT), Gibbs (NVT and NPT

versions), and reactive (RxMC) ensembles. The code can be compiled to run in parallel using OpenMP.[218]

6.2.2.2. DL_MONTE. DL_MONTE is another Monte Carlo simulation software written in FORTRAN that can also be run in parallel.[219] It was originally developed by Purton and co-workers at Daresbury Laboratory in the U.K. with special emphasis at materials science. It is now being developed as a multipurpose simulation package in collaboration with the Wilding (University of Bristol) and Parker (University of Bath) research groups. The code can simulate systems in canonical (NVT), isobaric–isothermal (NPT), grand canonical (μVT), semi-grand canonical, and Gibbs ensembles.[219] DL_MONTE is a twin sister code of the DL_POLY package, a molecular dynamics simulation software that will be introduced later in this review. With regard to parallelization of MC codes such as DL_MONTE and Cassandra, Gowers et al.[215] have demonstrated that the measured performances of existing implementations show poor efficiency due to various reasons. At least in the context of adsorption simulations and computational screening of porous materials, parallel execution of multiple MC runs offers higher efficiency and larger overall speed up compared to parallelization of MC codes.[215]

6.2.2.3. MuSiC. Multipurpose simulation code (MuSiC) is an object-oriented software written in FORTRAN that was developed in Snurr's research group from Northwestern University.[220] The code supports grand canonical (μVT), canonical (NVT), and isobaric–isothermal (NPT) ensembles. It can also be used to perform hybrid MC and molecular dynamics (MD) simulations.[222]

6.2.2.4. RASPA. RASPA is a molecular simulation program written in C language that was designed for simulation of adsorption and diffusion processes in nanoporous materials, including flexible structures.[198] The code was originally started in Snurr's research group at Northwestern University in active collaboration with Calero's group from the University Pablo de Olavide, and with David Dubbeldam from the University of Amsterdam being the lead developer of the code.[198] RASPA supports a variety of ensembles including microcanonical (NVE), canonical (NVT), isobaric–isothermal (NPT), iso-enthalpic–isobaric (NPH), Gibbs (NVT and NPT versions), and isobaric–isothermal ensembles with a fully flexible simulation cell (NPTPR).[198] It can be used to perform both Monte Carlo and molecular dynamics simulations; however it is best known for its capability as a MC software. The code also supports configurational bias Monte Carlo (CBMC) and continuous fractional component Monte Carlo (CFMC) for rigid and flexible molecules.[198,204]

6.2.2.5. MCCCS Towhee. The Monte Carlo for complex chemical systems (MCCCS) program was originally developed in Siepmann's research group at the University of Minnesota. It is currently being developed and maintained by Martin.[221,223] The bulk of Towhee is written in FORTRAN 77. The code was initially designed for the prediction of fluid-phase equilibria; however, it has been extended later to simulate different systems including porous materials. Towhee supports a variety of ensembles including NVT, NPT, μVTm and Gibbs ensembles.[221]

6.2.3. Molecular Dynamics Simulation. In this section, we turn our focus to molecular dynamics, which is widely employed for calculation of time-dependent phenomena across different fields from gas separation to materials science, geological sequestration of gases, biomolecular science, and drug discovery.[199,224−229] The brief description provided here

solely concerns molecular diffusion of simple gases in crystalline porous materials. We also note that although MD has been extensively used for simulation of molecular diffusion in porous solids, there are other techniques that might be more suitable for simulation of diffusion processes depending on different specific aspects of the system of interest. For example, simulation of very slow diffusion processes may not be fully attainable in conventional MD. For these systems, more advanced simulation methods such as transition path sampling[230] and dynamically corrected transition state theory,[231] which are particularly designed for sampling the sequence of rare events, should be used. Therefore, the section provided here is only meant to serve as introductory material for nonexpert readers. For more in-depth discussion of this technique, the reader is referred to numerous resources available in the literature.[201,229,232−235]

In contrast to Monte Carlo method where the microstates of the system are generated stochastically, in MD, we consider evolution of the system in space and time by numerically solving Newton's classical mechanics equations of motion.[234] In a system of particles interacting with each other and their environment, the total force exerted on each particle is given by[234,236]

$$F_i(t) = m_i a_i(t) = m_i \frac{dv_i}{dt} = m_i \frac{d^2 r_i}{dt^2} = -\nabla_i U(r_i)$$

$$i = 1, 2, 3, ..., N \tag{8}$$

where F_i, v_i, m_i, a_i, and r_i denote the force, velocity, mass, acceleration, and position, respectively, of the ith particle and U and t stand for the potential energy of interaction and time. The above equation is normally solved from a Taylor series expansion about initial position and velocity of particles in the system.[234,237] There are several algorithms in the literature for time integration of eq 8 such as the Leapfrog[238] and Verlet.[236] In the latter one, which is not only one of the simplest methods but also one of the most widespread algorithms,[232] the position of the particle at each time step is calculated by

$$r_i(t + \Delta t) \approx 2r_i(t) - r_i(t - \Delta t) + \frac{F_i(t)}{m_i}\Delta t^2 \tag{9}$$

The above estimate of the new position of particle i contains an error that is on the of order Δt^4, where Δt is the time step in the MD simulations.[232]

In the context of gas adsorption where diffusion of particles in porous materials is monitored, MD simulations are normally carried out in the canonical (NVT) ensemble where volume (V), temperature (T), and the number of particles in the system (N) are conserved. This approach is suitable for molecular diffusion in materials whose porous framework exhibits negligible flexibility; hence crystalline structure of these materials can be safely assumed as rigid. Nevertheless, in frameworks where pore sizes are close to the kinetic diameter of adsorbing molecules, the assumption of a rigid framework can result in diffusivity values that are largely incorrect.[239,240] For materials with considerable framework flexibility, simulations can be performed in NPT ensemble where pressure (P) is constant instead of the system volume (V).[241,242] This would allow volume of the system to change under constant pressure, which is often the case in diffusion experiments.

Figure 13 depicts the schematic diagram of the MD workflow and the properties that can be calculated from typical MD simulations. In MD, we need to define a set of starting (i.e., initial) configurations for the system, which are often obtained
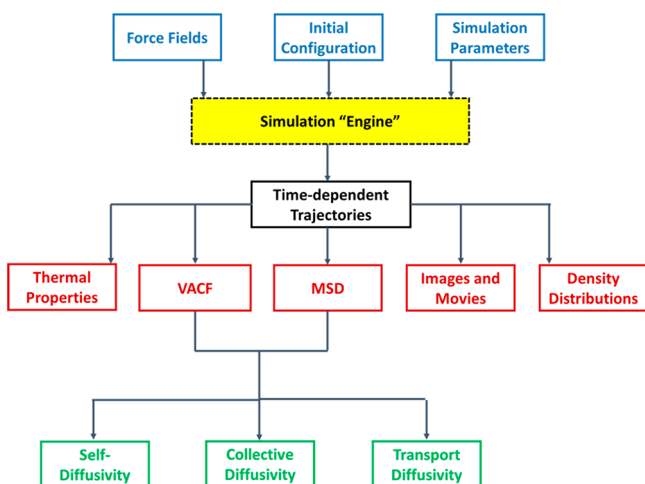
Figure 13. Schematic depiction of the workflow in the molecular dynamic simulations. The blue boxes indicate the required input data and parameters for the simulations. MD simulation generates a time-dependent trajectory from which the primary properties (red squares), such as mean-squared displacement (MSD) and velocity autocorrelation function (VACF), are calculated. The green boxes are the secondary properties that can be calculated from the primary properties.

from GCMC simulation. Similar to the MC method, interatomic interactions of all particles must be defined using an appropriate set of force fields along with other simulation parameters that are normally supplied to an MD program as input data (e.g., time step, temperature, and pressure). MD generates a time trajectory of the system containing positions of all particles and their associated potential energies. From these data, a number of transport[200,229,243] and thermal properties[224,244−246] can be calculated. Similar to the key message of the GCMC method, here we emphasize again that given a set of physical constraints (e.g., NVT) these properties are a function of how molecules interact with each other, whereas all other parameters can be treated as technical details of the protocol. These technical details may influence the efficiency of sampling and convergence of the results but not the physical properties of the system. Hence, the force field is the main input property that defines the physics and the behavior of the system of interest.

From the perspective of multiscale workflows, the key data we are interested to obtain using MD are transport properties of multicomponent mixtures. Indeed, obtaining information on multicomponent diffusion from experiments is not trivial and requires advanced techniques. Similarly to the GCMC simulation, extension of simulation from a single component system to multicomponent mixtures does not make the MD simulations significantly more complicated, and this is the main advantage of molecular simulations. It is also important to recognize that "transport properties" is an umbrella term for several distinct diffusion phenomena and frameworks of description associated with them. Below we consider these phenomena using the single component and multicomponent cases. In the process, we comment on what properties associated with these phenomena can be obtained from MD and what properties are required in process modeling.

6.2.3.1. Diffusion in Single-Component Systems. Self-diffusivity, collective diffusivity, and transport diffusivity are three types of diffusion phenomena that are commonly studied by molecular simulations.[200,229,235,243,247,248] Self-diffusivity

(D_s) describes the motion of individual labeled molecules through a fluid in the absence of the chemical potential or concentration gradients. In experiments, this property is measured using tracer diffusivity techniques, such as pulsed field gradient (PFG) NMR. In simulation, equilibrium molecular dynamics (EMD) is extensively used to calculate self-diffusivity of adsorbate molecules in different types of porous frameworks.[249−254] Self-diffusivity can be conveniently computed from the mean-squared displacement of particles using the Einstein relationship given by

$$D_s = \frac{1}{2Nd} \lim_{t \to \infty} \frac{1}{t} \left\langle \sum_{i=1}^{N} |r_i(t) - r_i(0)|^2 \right\rangle \tag{10}$$

where d is dimensionality of the system. D_s can also be computed from the time integral of the velocity autocorrelation function (VACF) defined by

$$D_s = \frac{1}{Nd} \int_0^{\infty} \left\langle \sum_{i=1}^{N} v_i(t) \cdot v_i(0) \right\rangle \, dt \tag{11}$$

here, $v_i(t)$ is the center of mass velocity vector of molecule i. The brackets in eqs 10 and 11 indicate an ensemble average taken over the simulation run time. As diffusion in porous materials is an activated process, temperature dependence of D_s is typically captured in the well-known Arrhenius relation $D_s = D_0 \exp\left(-\frac{E_a}{k_B T}\right)$, where D_0 is the pre-exponential constant and E_a is the activation energy.

In contrast to self-diffusivity, the transport (D_t) and collective, or corrected (D_c), diffusivities are associated with the macroscopic flux of molecules arising from the spatial concentration gradient in the fluid.[199,234] The transport diffusivity, also referred to as the Fickian or chemical diffusivity, is related to net flux in the system, which is described by Fick's first law:

$$J(q) = -D_t(q)\nabla q \tag{12}$$

here, J and ∇q are the flux and concentration gradient in the adsorbed phase, respectively.

Equation 12 can also be described in terms of the chemical potential gradient, $\nabla \mu$:[234]

$$J(q) = -L(q)\nabla \mu = -\frac{q}{k_B T} D_c(q)\nabla \mu \tag{13}$$

where, L is the Onsager transport coefficient and D_c is the corrected, or collective, diffusivity.[234]

The transport diffusivity (D_t) is related to the collective diffusivity (D_c) through a term associated with curvature in the adsorption isotherm.[200,243] This parameter is called the thermodynamic or Darken correction factor, Γ, described by

$$\Gamma \equiv \frac{1}{k_B T} \left(\frac{\partial \mu}{\partial \ln q} \right)_T \tag{14}$$

Given the relation of fugacity with chemical potential, $\Delta \mu \equiv k_B T \ln\left(\frac{f}{f_o}\right)$, one can rewrite eq 14 in the following form.[200,234]

$$\Gamma \equiv \left(\frac{\partial \ln f}{\partial \ln q} \right)_T \tag{15}$$

where f represents the fugacity of the bulk fluid in equilibrium with the adsorbed phase and q denotes the concentration of the adsorbed phase. The thermodynamic correction factor can be calculated from the adsorption isotherm, which itself is obtained from GCMC simulation as explained in section 6.2.1.

Therefore, the relation between D_t and D_c can be rewritten as[234]

$$D_t(q) = \frac{k_B T}{q} L(q)\Gamma = D_c(q)\Gamma \tag{16}$$

The collective and transport diffusivities can be calculated from both equilibrium molecular dynamics (EMD) and nonequilibrium molecular dynamics (NEMD) simulations. In the latter approach, the chemical potential gradient is the driving force for transport, which is imposed on the system in the dual control volume grand canonical molecular dynamics (DCV-GCMD).[255,256]

In EMD, the collective diffusivity can be computed from either of the following equations:[199,234]

$$D_c = \frac{1}{2Nd} \lim_{t \to \infty} \frac{1}{t} \left\langle \left| \sum_{i=1}^{N} [r_i(t) - r_i(0)] \right|^2 \right\rangle \tag{17}$$

$$D_c = \frac{1}{Nd} \int_0^\infty \left\langle \left(\sum_{i=1}^{N} \nu_i(t) \right) \cdot \left(\sum_{i=1}^{N} \nu_i(0) \right) \right\rangle dt \tag{18}$$

In process modeling, the mass balance equations are formulated using Fick's description of transport phenomena, and therefore, it is the data and models for the transport diffusion coefficient, D_t, that are required to set up a process simulation.

6.2.3.2. Diffusion of Multicomponent Systems. To this point, we have discussed methods required for the calculation of different types of diffusion in single-component systems. Diffusion in multicomponent systems is generally an advanced topic with extensive literature available on the fundamentals and practical applications.[257] Here, we mention only essential concepts to illustrate what properties can be obtained from molecular simulations and challenges associated with the incorporation in the process models.

Several equivalently rigorous formulations of multicomponent diffusion exist, for example, Onsager, Maxwell–Stefan, and the generalized Fick's approach.[258,259] Briefly, for an *n*-component system, the generalized Fick's law can be formulated as

$$[J] = [D_t][\nabla q] \tag{19}$$

here, $[J]$ is the column vector of diffusion fluxes of the components in the system and $[\nabla q]$ is the column vector of the diffusion gradients in the adsorbed phase. The mutual diffusion matrix, $[D_t]$, is given by

$$[D_t] = [B]^{-1}[\Gamma] \tag{20}$$

where

$$B_{ii} = \frac{x_i}{Đ_{in}} + \sum_{\substack{k=1 \\ k \neq i}}^{n} \frac{x_k}{Đ_{ik}}, \quad B_{ij(i \neq j)} = -x_i \left(\frac{1}{Đ_{ij}} - \frac{1}{Đ_{in}} \right) \tag{21}$$

with $Đ_{ij}$ being the Maxwell–Stefan diffusion coefficients, and $[\Gamma]$ a matrix of thermodynamic correction coefficients. Equivalently, eq 21 could be formulated using a matrix of

Onsager coefficients $[L]$, which can be shown to be related to $[B]^{-1}$.[257,260]

In principle, all properties in eq 20 can be obtained from molecular simulations. Mutual diffusion coefficients and the components of the Onsager matrix can be obtained using expressions, similar to eq 17 for a multicomponent system:

$$L_{ij} = \frac{1}{2N_j d} \lim_{t \to \infty} \frac{d}{dt} \left\langle \left(\sum_{l=1}^{N_i} [r_l^i(t) - r_l^i(0)] \right) \right. \\ \times \left. \left(\sum_{k=1}^{N_j} [r_k^j(t) - r_k^j(0)] \right) \right\rangle \tag{22}$$

whereas elements of $[\Gamma]$ could be obtained from GCMC simulations of multicomponent systems. This immediately points to two challenges. First, construction of the comprehensive data for multicomponent diffusion requires a substantially larger number of simulations, with properties, such as L_{ij} difficult to converge. The complete matrix of thermodynamic correction factors also requires GCMC simulation of multicomponent systems, which may be associated with substantial parameter space (i.e., the variation of the composition of the gas and adsorbed phases). Second, the process simulations require a continuous analytical model of the transport and equilibrium properties. Hence, the data obtained from molecular simulations for the properties above would need to be fitted to some simplified models (e.g., the Darken approximation of Maxwell–Stefan coefficients) or be amiable to interpolation within the process model. This will be further complicated if one wants to incorporate temperature dependence of the diffusion coefficients, since in the micropores it is an activated process.

6.2.3.3. What Data on Transport Properties Are Required in Process Simulations? The general theoretical framework for multicomponent transport phenomena may require a substantial number of parameters that are difficult to obtain in both experiments and simulation. However, to construct a process model such a level of description may not be actually needed. To understand this, it is useful to broadly identify three regions of the process where transport of the components of the mixture take place: the bulk space between the pellets of the porous material in the adsorption column, the macropores within the pellets, and the micropores in the small crystal grains (crystallites) constituting the pellets.

In the gas phase of the interstitial space between the pellets and in the macropores, concentration dependent diffusion coefficients would be required for the cases when the number of components is more than two and when the system is expected to significantly deviate from the ideal gas. This is not the case for low pressure binary mixtures of N_2 and CO_2. Hence, as we will see in the process modeling section 6.3, for the diffusion in these regions we have a range of classical models, such as the Chapman–Enskog model for molecular diffusivity, that provide concentration independent Fickian diffusion coefficients.

What about the micropores? In the same section on process modeling, we will also explain why in the commonly adopted process models for PSA postcombustion carbon capture, the diffusion in micropores of the crystal is not considered at all. The assumption is that for micropores larger than the size of adsorbing molecules (for species such as CO_2 and N_2, the micropores should be larger than 4 Å), the micropores are in instant equilibrium with the gas phase in the macropores of the

pellet, and we will provide a comment on why it is a reasonable assumption.

Hence, the remaining domain of processes and applications where the multicomponent data are indeed required in sufficient detail is associated with kinetic separations, for example, the separation of oxygen and argon in molecular sieves or propane–propylene separation using 4A zeolites. However, even in the kinetically controlled systems, single component diffusivities coupled with the gradients of the chemical potential will provide a reasonably good model for process simulations in the most cases. Molecular simulations, however, could be useful to probe under what conditions these assumptions are correct, to test when models of additional intermediate complexity may be required and identify reliable approaches to calibrate them. In summary, we are not aware of process modeling studies that incorporated the description of the multicomponent diffusion in its full complexity, although some studies employed simple models for micropore diffusion based on concentration independent single component data.[31,261,262]

6.2.4. Molecular Dynamics Codes. In this section, we briefly introduce some of the most widely used open-source molecular dynamics simulation software. There are numerous MD codes developed by various research groups and commercial developers,[204,263] some of which are purpose-built software that are developed with particular applications in mind, such as large biological systems (e.g., NAMD,[264] CHARMM[265]). In this section, however, we only focus on MD packages that offer many useful features for simulation of fluid transport in nanoporous materials. These software packages are listed in Table 5 and are briefly described here.

Table 5. Molecular Dynamics Simulation Codes

software	ref	web site
LAMMPS	Plimpton[266]	https://lammps.sandia.gov
GROMACS	Abraham et al.[267]	http://www.gromacs.org
DL_POLY	Todorov et al.[268]	http://www.ccp5.ac.uk/DL_POLY

6.2.4.1. LAMMPS. The large-scale atomic-molecular massively parallel simulator (LAMMPS) is a highly efficient and scalable classical molecular dynamics simulation code developed by the US Sandia National Laboratories with a focus on materials modeling.[266] It can be used for simulation of solid-state materials (metals, semiconductors), soft matter (biomolecules, polymers), coarse-grained, and mesoscopic systems.[266] LAMMPS can be employed as a parallel particle simulator at the atomic, meso, or continuum scales.[266] LAMMPS is written in C++. Many features of the code support accelerated performance on CPUs, GPUs, Intel Xeon Phis, and OpenMP.[266]

6.2.4.2. GROMACS. The Groningen machine for chemical simulations is a MD simulation software primarily designed for simulation of biochemical molecules;[267] however, due to its computational efficiency it is also highly popular in the domain of materials modeling and simulation of transport processes in porous media. The code is written in C/C++. It was originally developed at the Department of Biophysical Chemistry in the University of Groningen. Since 2001, two teams at the Royal Institute of Technology (KTH) and the Uppsala University in Sweden have been responsible for development and maintenance of the GROMACS software.

6.2.4.3. DL_POLY. DL_POLY, which was developed at Daresbury Laboratory in the U.K., is another classical MD

simulation software. It is a massively parallel code written in Fortran that is suitable for simulation of macromolecules, polymers, ionic systems, solutions, and transport in porous media.[204,268]

6.2.5. Force Fields. A comprehensive review of the current state-of-the art in force fields for adsorption phenomena in nanoporous materials has been recently provided by Dubbeldam and co-workers.[269] Here, we mention only essential elements required in the context of the multiscale workflows. A force field is a set of equations and parameters that describe how molecules interact with each other and with their environment, and governing the thermophysical properties of the system of interest.

Let us consider adsorption of CO_2 in a rigid porous material. Small molecules such as CO_2 can be also treated with reasonable accuracy as rigid structures. The total energy of interaction in this case is associated only with nonbonded (not involving a chemical bond) contributions and can be seen as composed of two terms: molecules of the gas interacting with each other (we call this for simplicity *fluid–fluid* interactions) and with the atoms of the porous structure (*fluid–solid* interactions):

$$U_{\text{nonbonded}} = U_{\text{fluid–fluid}} + U_{\text{fluid–solid}} \tag{23}$$

In their turn, each of these terms can be seen as composed of the short-range dispersion/repulsion interactions and the long-range polar interactions. The commonly adopted mathematical model to describe short-range interactions (the so-called van der Waals interactions) between two atoms is the Lennard-Jones (LJ) potential model:

$$u_{\text{LJ},ij} = 4\varepsilon_{ij}\left[\left(\frac{\sigma_{ij}}{r_{ij}}\right)^{12} - \left(\frac{\sigma_{ij}}{r_{ij}}\right)^{6}\right] \tag{24}$$

where ε, σ, and r are the potential well-depth, collision diameter, and distance, respectively, and the indices ij indicate that these properties are obtained for a pair of atoms i and j. The above model consists of a repulsive term, $4\varepsilon_{ij}\left(\frac{\sigma_{ij}}{r_{ij}}\right)^{12}$, and an attractive term, $-4\varepsilon_{ij}\left(\frac{\sigma_{ij}}{r_{ij}}\right)^{6}$ representing the dispersion interactions.[201] In contrast, the polar interactions are usually captured by placing partial charges on the specific atoms within the molecule. The interaction between the two partial charges is then obtained using the usual Coulomb equation:

$$u_{\text{Coul},ij} = \frac{q_i q_j}{4\pi\varepsilon_0 r_{ij}} \tag{25}$$

where q_i and q_j are individual partial charges on atoms i and j and ε_0 is the vacuum electrical permittivity. The total Lennard-Jones and electrostatic interaction energy in the system are then simply a sum of all pairwise terms according to eqs 24 and 25 between atoms and charges in the system. In practice, these calculations are performed within a particular cutoff distance around each individual atom. For short-range interactions such as the Lennard-Jones potential, the calculated value quickly converges as a function of distance, leading to a small error if the cutoff is equal to a few atom diameters. This is not the case for the long-range Coulombic interactions and advanced techniques such as the Ewald summations have to be employed to account for this.

For rigid porous materials and small rigid adsorbate molecules, the collection of all Lennard-Jones parameters of

the atoms in the system, partial charges assigned to them, and the particular rules associated with the calculation of the cross-term for unlike atoms constitute the simplest force field.

If one wants to consider more complex systems featuring, for example, flexible molecules or flexible porous structures, additional energy terms to describe internal degrees of freedom (bond and angle vibrations, dihedral rotations, etc.) will be required as defined by eq 26:[204,269]

$$
\begin{aligned}
U_{total} = &\sum_{bonds} u_b(r) + \sum_{bends} u_\theta(\theta) + \sum_{tortion} u_\phi(\phi) \\
&+ \sum_{out-of-plane-bends} u_\chi(\chi) + \sum_{nonbonded} u_{nb}(r) \\
&+ \sum_{bond-bond} u_{bb'}(r, r') + \sum_{bond-bend} u_{b\theta'}(r, \theta) \\
&+ \sum_{bend-bend} u_{\theta\theta'}(\theta, \theta') + \sum_{bond-torsion} u_{r\phi}(r, \phi, r') \\
&+ \sum_{bend-torsion} u_{\theta\phi}(\theta, \phi, \theta') + ...
\end{aligned}
\tag{26}
$$

In this case, it is the collection of all functions and parameters involved in eq 26 that constitute a complete force field.

Over the years, a substantial number of force fields have been developed. They differ in the functional forms employed in eq 26, target properties they reproduce, specialization, and numerical procedures used to optimize the force field parameters to capture the target properties. Important characteristics of the force fields are (1) availability (the force field has parameters available for a particular group of molecules and species of interest), (2) accuracy (the force field is able to reproduce particular properties of the system) and (3) transferability (the same force field can be applied to another class of molecules, while retaining its accuracy).

From this perspective, it is useful to distinguish very specialized force fields, such as AMBER[270−276] for biological systems, which are very accurate for specific properties within a specific group of chemical species but may not be available for other classes of chemicals or have limited transferability. The other example is generic force fields, such as the universal force field (UFF)[277−279] and DREIDING,[280] that are based on a small number of basic elements, are able to describe a broad range of chemicals and species, but also for the same reason may lack consistent accuracy in description of the properties of interest.

A special comment should be also made on the assignment of the point charges within a particular force field. There is currently no universally accepted system of point charge assignment, because point charges are not experimentally observable properties. As a result, different force fields adopt different strategies on how to assign partial charges on the molecules under consideration. For example, the UFF model was originally calibrated to work with no charges assigned or charges obtained using the Qeq charge equilibration method.[277] For porous materials, the common practice is to assign charges in a separate step as these charges are not readily available from the standard force fields. For this, again, many algorithms were developed over the years, including empirical approaches, based on fitting some target properties, and a wide range of methods based on information from quantum-mechanical (QM) calculations, including the Mulliken population analysis,[281] density derived electrostatic and chemical (DDEC) charges,[282] repeating electrostatic potential extracted atomic (REPEAT) charges,[114] and ChelpG[283] to name a few. What is important to

recognize here is that this large variety of methods differ in their fundamental principles, in the level of theory they use, and in the system they consider to calibrate the charges (periodic systems, fragments). Although methods such as DDEC and REPEAT are often found to be more reliable for reproducing adsorption isotherms,[284,285] the ambiguity involved in the assignment of partial point charges in nanoporous materials still prevails. For example, in one case it was shown that results based on the use of REPEAT point charges reproduce experimental adsorption data more accurately compared to DDEC charges; however at the same time the REPEAT method leads to assignment of charges that are sometimes unphysical.[284] To avoid the ambiguity involved in assignment of partial charges, Watanabe et al.[284] have developed a method to directly incorporate the electro-static potential energy surface (EPES) derived from DFT calculations into molecular simulation, hence removing the need to assign partial charges to framework atoms explicitly. The above method can be only used for adsorption simulation of rigid frameworks in which framework atoms are nonpolarizable with respect to adsorbate molecules.[284] For flexible frameworks, it would be computationally impractical to perform DFT for every configuration of the framework during simulation.[284] The complexity of charge assignment for materials such as MOFs has been recently explored by Sladekova et al.,[285] who also provided a useful introduction to the previous studies investigating the influence of the choice of the charge assignment scheme on the adsorption properties of the material. More recently, new charge assignment schemes have been developed based on machine learning (ML) techniques where the ML model is trained on a collection of high-quality DFT-derived charges such as DDEC.[286,287] An example of these models is developed by Kancharlapalli et al.[286] for MOFs and was shown to be transferable to other porous materials such as zeolites and porous molecular crystals. The ML-based charge assignment schemes are more beneficial for screening of large databases of porous materials where application of DFT-derived partial charges such as REPEAT or DDEC can be computationally very expensive.

In the context of adsorption in porous materials, a number of force fields have been developed for zeolites. In particular, accurate force fields have been developed to describe adsorption of hydrocarbons in all-silica zeolites.[288] These force fields stem from the transferable potentials for phase equilibria force field (TraPPE) model that has been developed to accurately capture phase equilibria of alkanes and other organic species.[289−294] Reasonably accurate force fields for CO_2, N_2, and some other small gases in zeolites are also available from García-Sánchez et al.[295] and from Martin-Calvo et al.[296] Force fields derived from first-principles calculations such as DFT-D2[169] and DFT/CC[297] have been also developed and have proved to be accurate in prediction of CO_2 adsorption in siliceous,[298] cation-ex-changed,[299,300] and NH_4-containing zeolites.[301] One important feature of these force fields is that they can be developed completely from first-principles and independent of any experimental data, while at the same time being able to accurately reproduce experimental measurements of adsorption isotherms and heats of adsorption.[299,301]

In the case of MOFs, the situation is more complex due to significant chemical heterogeneity of these materials. Early molecular simulation studies adopted generic force fields such as UFF and DREIDING for the sole reason that these force fields contained some parameters for metal atoms, required to describe MOFs.[302] These force fields in fact proved quite

reasonable in description of adsorption of simple nonpolar molecules, such as methane, and noble gases.[73] The situation became more difficult as the focus of the research community shifted to adsorption of polar molecules, such as carbon dioxide and water. Adsorption of these molecules in MOFs and ZIFs requires assignment of partial charges on the atoms of the structure. As we discussed above, the number of possible methods to assign these charges is significant, and there is not yet a single, agreed procedure for this step.

An additional challenge is posed by MOFs with open metal sites. The exposed metal sites interact quite strongly with molecules such as CO_2, water, and unsaturated carbons, and this is where generic force fields fail.[303] Accurate description of interactions of these molecules with open-metal-site MOFs has been the subject of intensive investigation in recent years.[304−309] The employed approaches involved accurate QM calibration of the functional forms of the potentials and associated parameters and led to several specialized force fields for certain groups of MOF materials, such as the MOF-74 family.[306,307,309,310] These specialized force fields have, however, low transferability to other MOFs and so far have been focused on specific adsorbate molecules, such as CO_2, whereas the comprehensive implementation of the multiscale frameworks requires accurate description of adsorption of all components in the multicomponent mixture, including nitrogen. As flue gas also contains some water, modeling of water adsorption in addition to CO_2 and N_2 would also allow one to construct more accurate and realistic process models. However, accurate molecular simulation of water adsorption in all materials, regardless their nature, is still a very challenging problem.

Finally, we note that although the developed force field may be reliable in the prediction of equilibrium adsorption properties, it does not necessarily imply accurate prediction of transport properties using the same force field.

In summary, even within the constraints of rigid structures and small rigid gas molecules, accurate force fields for CO_2 and N_2 adsorption are available and have been validated only for a handful of materials. Later in this review, we will discuss this challenge and its implications for the computational screening workflows.

6.2.5.1. Beyond Rigid Structures: Force Fields for Prediction of Structural Transitions and Lattice Vibrations. Molecular simulations typically assume adsorbent materials to have rigid frameworks. Recently, novel porous materials have been discovered that exhibit structural flexibility.[311,312] Development of force fields that can correctly capture this behavior is an ongoing area of research.[313−317] This is particularly important for the studies of MOFs, as all MOFs exhibit *some* forms of structural flexibility[213,269,311] ranging from lattice vibrations at equilibrium to large-scale structural transformations upon external stimuli,[269] such as temperature,[318] guest adsorption,[319] and electric field.[320] Among different types of structural flexibilities, structural vibrations and phonon properties of the lattice determine specific heat capacity of porous solids,[244,321,322] whose importance for performance-based materials screening has been recently demonstrated.[122,125]

As elucidated by Kapil et al., thermal properties of the lattice can be described by a quantum harmonic treatment.[322] However, the heat capacity of loaded porous frameworks requires a combination of quantum and anharmonic treatment.[322] Analysis of phonon properties for estimation of thermal properties of materials requires costly quantum mechanical calculations,[323] which are not affordable for routine screening of

large numbers of porous materials. To address this limitation, development of purpose-built and computationally affordable force fields has been recently undertaken by several groups;[323−326] nevertheless, further developments for improved accuracy and transferability of these force fields are required.[327]

6.3. Process Modeling and Optimization

The main objective of this section is to give an accessible guide on PSA and VSA process modeling from fundamentals to practical implementation. We begin with the basics of the mass, energy, and momentum balances in the adsorption column packed with pellets of adsorbent material (section 6.3.1). We will introduce the hierarchy of models, differing in the level of details in their description and in the assumptions involved. We will briefly review the commonly involved methods in the solution of the introduced balance equations under the appropriate boundary conditions.

Setting up a process model requires a number of parameters and properties. For a nonpractitioner, it can be overwhelming to see the process model in its full complexity, and hence in section 6.3.2 we tasked ourselves with explaining what parameters are required and how their values can be obtained.

A pressure swing adsorption process involves several columns, each of them going through a cyclic sequence of steps. In section 6.3.3, we will use a simple 4-step cycle to introduce the PSA process and the key concepts associated with its cycle, such as cyclic steady state (CSS), and performance of the cycle in terms of purity, recovery, productivity, and energy consumption. Furthermore, using this example of the 4-step process, we will briefly explore the concentration profiles during different steps at CSS and how to interpret them.

A specific cycle configuration may not operate at the optimal conditions. Hence, a significant part of process modeling research is focused on cycle optimization. In section 6.3.4, we introduce currently used optimization methods, such as genetic algorithms, and essential concepts associated with process optimization.

As has been already discussed in the section on process metrics, in general process simulations are time-consuming. This prompted significant research efforts into development of more efficient alternatives for process performance evaluation that work in tandem with detailed process simulations. These developments are reviewed in section 6.3.5.

Finally, following the spirit of the review, we conclude the section on process modeling with a brief overview of the available codes for this type of modeling and their capabilities and access (section 6.3.6).

6.3.1. Fundamentals. An adsorption column is the basic unit of the adsorption process. In this section, we provide a brief summary of the mass, energy, and moment balances around this unit, which either are solved numerically in the process simulations or serve as starting points for simplified analytical models. For a more comprehensive analysis, we refer the reader to the seminal books by Ruthven et al.[328,329] on fundamentals of adsorption and PSA processes.

Consider the schematic of a packed column in Figure 14. The column has length of L_c, z is used as the position within the column in the axial direction, and the feed is introduced to the column from the bottom at $z = 0$. The column is packed with pellets of adsorbent material. The pellet consists of microporous crystallites that are held together by an inert binder. Thus, the pellet has intercrystalline macropores and intracrystalline micropores. In the description of the various transport
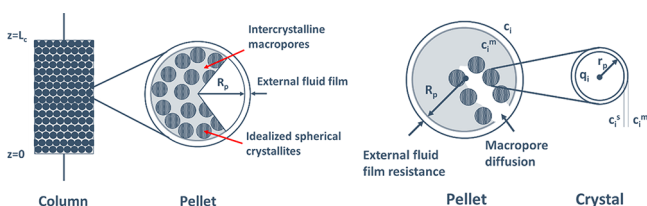
Figure 14. Schematic depiction of the adsorption system under consideration. The column is treated as a vessel filled with pellets of porous materials (on the left). Each pellet can be seen as an agglomerate of crystallites held together by inert binder. Other properties and processes are explained in the text.

processes, we adopt the following convention: *macropore* refers to the pore space between the crystallites and *micropore* refers to the pores inside the crystallites. On the right of Figure 14, we show an idealized spherical pellet of radius R_p and volume V_p. In the model, we can also assume that crystallites are spherical particles of radius r_p. The pellet volume consists of the macropore volume, V_{macro}, and crystal volume, V_{cr}, which in turn consists of the micropore volume, V_{micro}, and the skeletal volume, V_{skel}:

$$V_p = V_{macro} + V_{cr} \tag{27}$$

$$V_{cr} = V_{micro} + V_{skel} \tag{28}$$

The bulk density (ρ_{bulk}), pellet density (ρ_p), crystal density (ρ_{cr}), and skeletal density (ρ_{skel}) are defined as follows:

$$\rho_{bulk} = \frac{m_p}{V_C} = \frac{m_p}{V_{gas} + V_p} \tag{29}$$

$$\rho_p = \frac{m_p}{V_p} = \frac{m_p}{V_{macro} + V_{cr}} \tag{30}$$

$$\rho_{cr} = \frac{m_p}{V_{cr}} = \frac{m_p}{V_{micro} + V_{skel}} \tag{31}$$

$$\rho_{skel} = \frac{m_p}{V_{skel}} \tag{32}$$

Here, V_{gas} is the volume of the gas phase in the column and m_p is the total mass of the adsorbent pellets. This mass includes both the mass of the adsorbent crystals and the mass of the binder. Thus, it is assumed that the binder volume is part of the skeletal volume of the pellet. Therefore, the saturation capacity of the adsorbent has to be corrected for the mass of the binder if the adsorption isotherms were measured for the nonpelletized adsorbent crystals. The bed void fraction (ε), pellet void fraction (ε_p), and crystal void fraction (ε_{cr}) are defined as follows:

$$\varepsilon = \frac{V_{gas}}{V_C} = 1 - \frac{V_p}{V_C} = 1 - \frac{\rho_{bulk}}{\rho_p} \tag{33}$$

$$\varepsilon_p = \frac{V_{macro}}{V_p} = 1 - \frac{V_{cr}}{V_p} = 1 - \frac{\rho_p}{\rho_{cr}} \tag{34}$$

$$\varepsilon_{cr} = \frac{V_{micro}}{V_{cr}} = 1 - \frac{V_{skel}}{V_{cr}} = 1 - \frac{\rho_{cr}}{\rho_{skel}} \tag{35}$$

A common starting point for many process modeling approaches is the material balance in the column based on the axial dispersed plug flow model (although more complex and complete formulations are also possible, that is, including radial dispersion term, etc.):

$$\frac{\partial c_i}{\partial t} + \frac{(1 - \varepsilon)}{\varepsilon} \frac{\partial \bar{Q}_i}{\partial t} + \frac{\partial (c_i v)}{\partial z} + \frac{\partial J_i}{\partial z} = 0 \tag{36}$$

Here, c_i is the gas phase concentration of component i, c_i^m is the macropore concentration of component i in the adsorbent pellet, v is the interstitial velocity, and J_i is dispersive flux of component i. In this equation, the first and the second terms are the accumulation terms in the gas phase and in the pellets, respectively. The amount adsorbed in the pellet, Q_i, can be seen as the composite of the amount as gas in the macropores of the pellet, $\varepsilon_p c_i^m$, and the absolute amount adsorbed in the micropores of the adsorbent material, $(1 - \varepsilon_p)q_i$:

$$Q_i = \varepsilon_p c_i^m + (1 - \varepsilon_p)q_i \tag{37}$$

where q_i is the sorbate concentration of component i in the micropores of the adsorbent. In the column mass balance, the average amount adsorbed in the pellet is needed:

$$\bar{Q}_i = \frac{3}{R_p^3} \int_0^{R_p} Q_i r^2 \, dr \tag{38}$$

and, similarly the average adsorbed amount in a crystallite can be defined:

$$\bar{q}_i = \frac{3}{r_p^3} \int_0^{r_p} q_i r^2 \, dr \tag{39}$$

The third term in eq 36 describes the convective flow of the gas across the bed, and the final term describes the dispersion process relative to the bulk flow. The dispersive flux is given by

$$J_i = -D_i^L c_T \frac{\partial x_i}{\partial z} \tag{40}$$

where D_i^L is the axial dispersion coefficient, c_T is the total gas concentration, and x_i is the mole fraction of component i. For the axial dispersion coefficient (D_i^L), correlations are available,[329] such as

$$D_i^L = 20 \frac{D_i^m}{\varepsilon} + 0.5 V_0 \frac{2R_p}{\varepsilon} \tag{41}$$

here, D_i^m is molecular diffusivity, which is defined later in this section, and V_0 is the average superficial fluid velocity through the packed bed.

Although eq 36 provides the overall mass balance in the column, it does not describe the actual process of diffusion into the pellets. For this, a separate set of material balance equations can be formulated around the pellet. In the most general case, the model will contain terms associated with the external film resistance at the pellet surface, macropore diffusion from the bulk gas phase into the pellet, barrier and film resistance at the adsorbent crystal boundary, and micropore diffusion in the adsorbent crystals. A schematic of an adsorbent pellet with relevant properties is shown on the right of Figure 14. Let us consider these processes in more detail.

First, let us focus on the overall material balance for the pellet. The amount adsorbed in the pellet is governed by the following mass-balance equation, based on the second Fick's law formulated for the spherical pellet geometry:

$$\varepsilon_p \frac{\partial c_i^m}{\partial t} + (1 - \varepsilon_p) \frac{\partial \bar{q}_i}{\partial t} - \frac{1}{r^2} \frac{\partial}{\partial r}\left(D_{macro,i}^e r^2 \frac{\partial c_i^m}{\partial r}\right) = 0,$$

$$0 < r < R_p \tag{42}$$

Here, $D_{macro,i}^e$ is the effective macropore diffusion coefficient. The first term of eq 42 represents the accumulation in the macropores, the second term describes the accumulation in the micropores, and the last term describes diffusive mass transport due to the concentration gradients inside the pellet (the second Fick's law).

At the surface of the pellet, diffusion from the bulk gas phase into the pellet can be described via a mass-transfer process across the film at the surface:

$$D_{macro,i}^e \frac{\partial c_i^m}{\partial r}\bigg|_{r=R_p} = k_{i,f}(c_i - c_i^m) \tag{43}$$

where $k_{i,f}$ is the external fluid film mass transfer coefficient. This equation sets the boundary condition at R_p, whereas at $r = 0$, the boundary condition is $\frac{\partial c_i^m}{\partial r}\big|_{r=0} = 0$, which is required due to the assumption of spherical symmetry.

The effective diffusion coefficient reflects various mass-transfer mechanisms into the pellet and is obtained by combining the molecular diffusion (D_i^m), Knudsen diffusion (D_i^K), surface diffusion (D_i^S), and viscous diffusion coefficients (D_i^V):

$$D_{macro,i}^e = \frac{\varepsilon_p}{\tau}\left[\left(\frac{1}{D_i^m} + \frac{1}{D_i^K}\right)^{-1} + D_i^S + D_i^V\right] \tag{44}$$

where the individual diffusion coefficients are estimated using the well-known expressions:

$$D_i^m = 1.86 \times 10^{-7} \frac{\sqrt{T^3(MW_1^{-1} + MW_2^{-1})}}{P\sigma_{12}^2\Omega_{12}} \tag{45}$$

$$D_i^K = 97 r_{pore}\sqrt{\frac{T}{MW_i}} \tag{46}$$

$$D_i^S = \frac{1 - \varepsilon_p}{\varepsilon_p} K D_i^{S_0} \exp\left(\frac{-E}{RT}\right) \tag{47}$$

$$D_i^V = 10^{-5}\frac{P r_{pore}^2}{8\mu_i} \tag{48}$$

here, MW_i is the molecular weight in g mol^{-1}, σ_{12} is the collision diameter from the Lennard-Jones potential in Å, Ω_{12} is a function depending on the Lennard-Jones force constant and temperature, r_{pore} is the mean macropore radius in m, K is the Henry's constant of adsorption, and E is the diffusional activation energy. These expressions along with the theories behind them and the values of the parameters are discussed in the classical textbooks on transport phenomena.[328,330] We further note that typically in the process models the values are obtained at some fixed, representative conditions, while in reality the conditions change dynamically in the actual process, and hence, these properties would also vary in time in a more accurate model.

Similarly, for the diffusive process in the micropores inside the crystallites, modeled as spherical particles of size r_p, we can formulate a similar general mass-balance equation, based on the second Fick's law of diffusion:

$$\frac{\partial q_i}{\partial t} - \frac{1}{r^2}\frac{\partial}{\partial r}\left(D_i^\mu r^2 \frac{\partial q_i}{\partial r}\right) = 0, \quad 0 < r < r_p \tag{49}$$

Here, D_i^μ is the effective diffusion coefficient in micropores and other terms are asdescribed before. Similar to the processes at the pellet surface, the diffusion into the crystallite particle from the surface can be described using transfer resistances across the surface:

$$D_i^\mu \frac{\partial q_i}{\partial r}\bigg|_{r=r_p} = k_{i,f}^\mu(c_i^m - c_i^s) = k_{i,b}(q_i^*(c_i^s) - q_i|_{r_p}) \tag{50}$$

Here, q_i^* is the adsorbed concentration of component i in equilibrium and c_i^s is the concentration of component i at the crystal boundary. In eq 50, we equivalently consider fluxes across the external fluid film, governed by the mass-transfer coefficient $\kappa_{i,f}^\mu$, or across the crystal boundary, governed by the mass-transfer coefficient $k_{i,b}$. Equation 50 defines a boundary condition for $r = r_p$, whereas at $r = 0$, it is $\frac{\partial q_i}{\partial r}\big|_{r=0} = 0$ (again similar to the boundary condition of the pellet).

A similar hierarchy of equations can be formulated for the energy balance in the column. In the most general non-isothermal case, the following equation governs the heat-transfer processes:

$$\varepsilon\frac{\partial \check{U}_f}{\partial t} + (1-\varepsilon)\frac{\partial \check{U}_p}{\partial t} + \varepsilon\frac{\partial(\check{H}_f v)}{\partial z} + \frac{\partial J_T}{\partial z}$$
$$+ \varepsilon\sum_{i=1}^N \frac{\partial(J_i\tilde{H}_i)}{\partial z} + h_w\frac{A_c}{V_c}(T_f - T_w) = 0 \tag{51}$$

here, $\check{U}_f$ is the internal energy in the fluid phase per unit volume, $\check{U}_p$ is the internal energy in the pellet per unit volume, $\check{H}_f$ is the enthalpy in the fluid phase per unit volume, J_T is the thermal diffusive flux, and $\tilde{H}_i$ is the partial molar enthalpy of component i in the fluid phase. T_f and T_w are temperatures of the fluid and the wall, respectively, while h_w is the heat transfer coefficient between the wall and the surroundings. A_c and V_c are the surface area and the volume of the column, respectively. The first two terms in eq 51 are accumulation terms for the gas phase and the solid phase, respectively; the third term is associated with the convective flux of the fluid stream, with enthalpy $\check{H}_f$. The next two terms are the axial dispersion terms. The first one, $\frac{\partial J_T}{\partial z}$, describes thermal flux due to the temperature gradients along the z axis, whereas the second term is associated with the diffusive fluxes due to the concentration gradients along z axis (and hence enthalpy fluxes coupled with them). The last term on the left in eq 51 describes heat transfer from the fluid to the wall of the column.

The heat transfer across the wall of the column can be described as

$$\rho_w\hat{c}_{P,w}\frac{\partial T_w}{\partial r} + h_w\frac{A_c}{V_c}(T_f - T_w) + U\alpha_{wl}(T_w - T_\infty) = 0 \tag{52}$$

where T_∞ is the temperature of the surroundings. The column wall is defined by the column wall density ρ_w and specific heat

capacity $\hat{c}_{P,w}$. The ratio of the logarithmic mean surface area to volume of the column wall, α_{wl}, is given by

$$\alpha_{wl} = \left[(2R_c + \delta_w) \ln\left(\frac{2R_c + \delta_w}{2R_c}\right) \right]^{-1} \tag{53}$$

where R_c and δ_w are the radius of the column and the thickness of the wall, respectively.

At the level of the pellet, a uniform temperature profile is typically assumed across the pellet (no temperature gradients), and this has been shown to be consistent with the experimental observations.[331]

The overall energy balance for the pellet can be then formulated as

$$\frac{\partial \check{U}_P}{\partial t} = \varepsilon_p \frac{\partial \check{U}_{P,f}}{\partial t} + (1 - \varepsilon_p) \frac{\partial \check{U}_{P,s}}{\partial t}$$

$$= h_p(T_f - T_p)\frac{V_P}{A_P} + \sum_{i=1}^{N_c} \frac{\partial \bar{Q}_i}{\partial t}\bar{H}_{i,f} \tag{54}$$

Here, the first equality simply indicates that the total energy change in the pellet can be seen as a sum of the change in energy in the fluid phase in macropores and change in energy associated with the adsorbed phase (solid + micropores). The second equality links this change to the heat transfer across the pellet boundary with heat transfer coefficient h_p and heat flux associated with the adsorption of the components in the system, where $\bar{H}_{i,f}$ is the partial molar enthalpy of the component i.

Finally, the thermal axial dispersion flux, J_T, is given by

$$J_T = -\lambda_f^L \varepsilon \frac{\partial T_f}{\partial z} - \lambda_p^L (1 - \varepsilon) \frac{\partial T_p}{\partial z} \tag{55}$$

Here, the axial thermal conductivity in the fluid and pellet are given by λ_f^L and λ_p^L, respectively. There are also alternative ways to formulate the energy balance, for an example of which we refer the reader to the article by Zhao et al.[332]

The momentum balance is described by the Ergun pressure drop equation:

$$-\frac{dP}{dz} = \frac{150\mu(1 - \varepsilon)^2}{\varepsilon^2 4R_p^2}v + \frac{1.75(1 - \varepsilon)^2\rho_f}{\varepsilon 2R_p}v|v| \tag{56}$$

where μ is the fluid viscosity and ρ_f is the fluid density.

The equations above provide a complete and general description of the mass and energy balances in the column. These equations serve as a starting point for more simplified models. Indeed, Figure 15 illustrates the hierarchy of the models
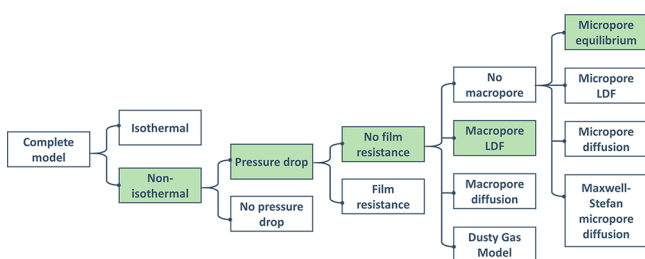

Figure 15. Hierarchy of the models available for the mass and energy balances in the adsorption column (not an exhaustive list). Squares shaded green reflect the combination of the models employed in the studies by Farmahini et al.[89,122] and also commonly adopted by other practitioners in the field.

with each model based on its own set of assumptions and resulting simplifications of the governing equations. Reading this diagram from left to right, the system can be considered as isothermal (hence no energy balance equations are required) or nonisothermal. Then, within each branch, we can either include or ignore the pressure drop across the system. For each branch, we can further consider whether we include film resistance at the surface of the pellet or not and so on. This hierarchy demonstrates that we can construct on order of 10^2 models depending on the combination of the assumptions we use. The boxes shaded green in Figure 15 represent the choice of the assumptions adopted in the studies of Farmahini et al.,[89,122] as well as in many other previous studies.[117,333,334] In this case, the following assumptions are considered:

(1) The system is modeled as non-isothermal with heat transfer allowed between the packed bed and its wall, but the pellets and gas phase are kept at the same temperature.

$$T_f = T_p \tag{57}$$

(2) Pressure drop is considered across the bed. The pressure drop is modeled using the Ergun equation, eq 56.

(3) No external film resistance is considered. In this case, eq 43 vanishes, and the following condition applies:

$$c_i^m(R_p, z, t) = c_i(z, t) \tag{58}$$

(4) The macropore resistance is modeled using the linear driving force (LDF) approximation. Effectively, all the resistances to diffusion are lumped into a single effective parameter, while the driving force of the process is simply the difference between the concentration of species i in the gas phase (c_i) and that in the macropores (c_i^m). As a result, eq 42 can be replaced with a simplified model:

$$\varepsilon_p \frac{\partial c_i^m}{\partial t} + (1 - \varepsilon_p)\frac{\partial \bar{q}_i}{\partial t} = k_i^P \frac{A_P}{V_P}(c_i - c_i^m) \tag{59}$$

Here, k_i^P is the LDF coefficient for the pellet. This parameter can be calculated using the effective macropore diffusivity with the Glueckauf approximation, which is equivalent to assuming a parabolic concentration profile:[335]

$$k_i^P = \frac{5D_{macro,i}^e}{R_p} \tag{60}$$

(5) Micropore equilibrium is assumed. This assumption implies that the crystallites are in instant equilibrium with the gas phase in the macropores of the pellet. This would be the case when the overall mass transfer into the pellets is controlled by macropores and not micropores. Although this seems counterintuitive, the validity of this assumption for materials with pore sizes that do not impose significant kinetic constrains on diffusion of small molecules (larger than 4 Å) has been discussed on several occasions.[328,336] To illustrate this point, let us return to the eq 42 describing the mass balance around the pellet. If we make an assumption that the isotherm is linear ($\bar{q}_i = K_{H,i}c_i^m$ where $K_{H,i}$ is the Henry's constant for component i), eq 42 can be rearranged as

$$[\varepsilon_p + K_{H,i}(1 - \varepsilon_p)]\frac{\partial c_i^m}{\partial t} = \frac{1}{r^2}\frac{\partial}{\partial r}\left(D_{macro,i}^e r^2 \frac{\partial c_i^m}{\partial r}\right) \tag{61}$$

which can be further rearranged to obtain the Fick's diffusion equation and the effective pore diffusivity of component i, $D_e^{P,i}$:

$$\frac{\partial c_i^m}{\partial t} = \frac{1}{r^2}\frac{\partial}{\partial r}\left(D_{P,i}^e r^2 \frac{\partial c_i^m}{\partial r}\right) \tag{62}$$

$$D_{P,i}^e = \frac{D_{macro,i}^e}{[\varepsilon_p + K_{H,i}(1 - \varepsilon_p)]} \tag{63}$$

While it is obvious that D_i^μ is always smaller than $D_{P,i}^e$, what is important in determining the controlling mass transfer mechanism is the comparison of the molar fluxes. In particular, the two diffusional time constants that should be compared to each other are then the macropore diffusion constant $(R_p^2/D_{P,i}^e)$ and the micropore diffusion time constant, (r_p^2/D_i^μ). Small crystals (small r_p^2), relatively large beads (large R_p^2) and large value of the effective Henry's constants lead to $\frac{R_p^2}{D_{P,i}^e} \gg \frac{r_p^2}{D_i^\mu}$, or in other words mass transfer controlled by the macropore diffusion.

Hence, we assume that the micropores are in instantaneous equilibrium with the gas phase in the macropores, described by the concentration c_i^m. This assumption is equivalent to the following condition:

$$q_i(z, t) = q_i^*(c_i^m) \tag{64}$$

Instead of the condition above, one may wish to include a more detailed model of micropore diffusion using the LDF approximation. Then, the following simplification can be employed to describe transport into the crystallites:

$$\frac{d\overline{q}_i}{dt} = k_i^{cr}\frac{3}{r_p}(q_i^* - \overline{q}_i) \tag{65}$$

The LDF coefficient k_i^{cr} can be calculated from the effective micropore diffusivity by

$$k_i^{cr} = \frac{5D_i^\mu}{r_p} \tag{66}$$

Regardless of the details of the model, the combined mass and energy balance equations form a system of differential algebraic equations (DAEs). These equations are usually discretized in the spatial domain by an appropriate numerical method such as finite difference, finite element, orthogonal collocation, or finite volume method. This produces a system of ordinary differential equations (ODEs), which can be solved using a number of approaches, such as the internal functions within the available simulation packages (e.g., MATLAB), or existing numerical solution libraries (e.g., SUNDIALS[337]). Here, it is also useful to reflect on the simplified LDF-based models versus detailed diffusion equation models. The motivation to develop simplified LDF models is driven primarily by the numerical efficiency. Indeed the simplified LDF model with 30 axial volumes and 2 components corresponds to 120 DAEs, while the same system with the diffusion equation would be approximately 600 DAEs. Including also diffusion in the micropores would lead to ca. 3000 equations. The computational costs would be at least proportional to the total number of equations N if the code is well written and N^2 for a not-so-well written code.

6.3.2. Complete Hierarchy of Data Required for Multiscale Process Simulation.

One of the primary aspirations of this review is to provide a useful guide on PSA and VSA process models for nonpractitioners. Reading a standard research paper on process modeling of adsorption processes can often be overwhelming because of the number of parameters and properties one needs to specify, with their sources not necessarily being obvious. Here, we also emphasize that even after reading our review we do not expect a novice in process modeling to be able to setup their own simulations. However, we hope they will be able to understand the requirements for these simulations and be aware of the potential sources of data. Broadly, we can split the data required for setting PSA or VSA process simulations into the following categories: Column properties describe the geometric dimensions of the column, its length, diameter, and thickness of the walls. These properties are either taken to reflect the actual experimental unit, or given some specific, physically meaningful values. For example, certain parameters of the column have been used in several studies, and they have now become commonly employed by several groups to ensure consistent comparison of the process modeling results.[88,89,93,116,120−122,124] The balance equations described in section 6.3.1 also imply that to solve these equations we need values of the properties associated with the thermophysical characteristics of the material of the column and how it interacts with its environment (e.g., heat capacity, heat transfer coefficient, etc.).

In the next category, we have all properties associated with the pellet: pellet size, pellet porosity, and pellet tortuosity. In the same category, we also include properties associated with the transport in macropores of the pellets, such as different contributions to the overall macropore diffusivity (e.g., molecular diffusion, Knudsen diffusion, etc.).

Further down in the hierarchy of scales shown in Figure 15 is crystallites, and hence the next category of properties is associated with the properties of the adsorbent material crystals: crystal density, crystal thermal and transport properties, etc. In principle, the pellet is made out of crystallites and binder, and properties of the pellet, such as the specific heat capacity or thermal conductivity, are a composite property of the two materials, binder and crystallites. However, the common convention is to assume these properties of the binder to be equivalent to the properties of the adsorbent crystals.

Generally, equilibrium adsorption data should also belong to the category of the crystal properties. However, this requires a special consideration. Adsorption data, both in experiments and in simulations, are typically obtained as single component adsorption isotherms comprised of discrete data points. However, process simulations require an analytical expression describing adsorption equilibria in order to be able to solve the mass-balance equations described in section 6.3.1. Moreover, the accuracy of process modeling also depends on how well the supplied models describe the multicomponent equilibria; hence accurate interpolation of single component isotherms may not be sufficient for the correct behavior of the model in the actual process simulations. A common approach is to use the dual-site Langmuir (DSL) adsorption model to obtain an analytical description of adsorption isotherms. For a single component system, the DSL isotherm for species i is defined by

$$q_i^* = \sum_{j=1}^{2}\left[q_{j,i}^s \frac{b_{j,i}P}{1 + b_{j,i}P}\right] \tag{67}$$

Here, $q_{i,j}^s$ is saturation capacity of site j with respect to species i, and $b_{j,i}$ is the affinity of each site described by the van't Hoff equation: $b_{j,i} = b_{oj,i}\exp\left(\frac{-\Delta H_{j,i}}{RT}\right)$. In the van't Hoff equation, $\Delta H_{j,Ij}$ is the heat of adsorption at adsorption site j and $b_{oj,i}$ is the pre-exponential factor.

Table 6. Complete Set of Input Parameters for Process Simulation

parameter	symbol	source
Column Properties		
wall (ambient) temperature (K)	T_w	design specification
column length (m)	L_c	design specification
inner column radius (m)	$R_{c,i}$	design specification
outer column radius (m)	$R_{c,o}$	design specification
column void fraction	ε	heuristic values
specific heat capacity of column wall (J/(kg·K))	$\hat{C}_{P,w}$	literature data
density of column wall (kg/m³)	ρ_w	literature data
wall heat transfer coefficient (J/(m²·K·s))	h_w	literature data
outside heat transfer co-coefficient (J/(m²·K·s))	U	heat-transfer engineering correlations, available from the literature
Pellet Properties		
pellet porosity	ε_p	mercury porosimetry experiment
pellet radius (m)	R_p	geometric measurement using conventional callipers
pellet tortuosity (τ)	τ_p	often heuristic values are used; however, dynamic tortuosity can be obtained from the measurement of the effective pellet diffusivity at different temperatures and pressures[345]
pellet heat transfer coefficient (J/(m²·K·s))	h_p	analytical correlations[328]
average macropore diameter (m)	r_{pore}	mercury porosimetry experiment
molecular diffusivity (m²/s)	D^m	predicted from kinetic theory of gases or measured in bulk gas mixtures; eq 45 corresponds to the Chapman–Enskog theory
Knudsen diffusivity (m²/s)	D^K	predicted from the standard kinetic theories, eq 46
surface diffusivity (m²/s)	D^S	measured experimentally; several methods exist,[346] eq 47
viscous diffusivity (m²/s)	D^V	eq 48
Crystal Properties		
crystal density (kg/m³)	ρ_{cr}	experimental crystallographic data
microporosity (−)	ε_{cr}	helium pycnometry experiment on powder, interpretation of nitrogen and argon adsorption isotherms at 77 and 87 K, respectively, or CO_2 adsorption isotherm at 273 K
crystal radius (m)	r_p	optical microscopy
specific heat capacity (J/(kg·K))	$\hat{C}_{P,cr}$	experimental calorimetry, empirical group contribution methods, ab initio simulation methods based on QM
micropore diffusivity (m²/s)	D^μ	molecular dynamic simulation, NMR experiments, other experimental techniques[347]
activation energy (kJ/mol)	E_a	molecular dynamics, NMR experiments, other experimental techniques[347]
Properties of Competitive Adsorption Isotherms[a]		
saturation capacity for site 1 of the DSL model (mol/m³)	q_{s1}	DSL fit to experimental adsorption or GCMC simulation data
pre-exponential constant for site 1 of the DSL model (bar⁻¹)	b_{01}	DSL fit to experimental adsorption or GCMC simulation data
enthalpy of adsorption on site 1 for site 1 of the DSL model (J/mol)	$-\Delta H_1$	DSL fit to experimental adsorption or GCMC simulation data
saturation capacity for site 2 of the DSL model (mol/m³)	q_{s2}	DSL fit to experimental adsorption or GCMC simulation data
pre-exponential constant for site 2 of the DSL model (bar⁻¹)	b_{02}	DSL fit to experimental adsorption or GCMC simulation data
enthalpy of adsorption on site 2 for site 1 of the DSL model (J/mol)	$-\Delta H_2$	DSL fit to experimental adsorption or GCMC simulation data
Fluid Properties		
viscosity (Pa·s)	μ	literature data
fluid thermal conductivity (J/(m·K·s))	λ_f^L	literature data
axial dispersion coefficient (m²/s)	D_i^L	eq 41
Feed Properties		
feed composition (−)	$c_{F,i}$, $x_{F,i}$	design specifications
feed temperature (K)	T_F	design specifications

[a]For example, in the case of the DSL model.

As seen here, there are six parameters ($q_{1,i}^s$, $q_{2,i}^s$, $b_{o1,i}$, $b_{o2,i}$, $\Delta H_{1,i}$, and $\Delta H_{2,i}$) for each gas component i that can be obtained. Thermodynamic consistency requires that the saturation capacity of each site is the same for all adsorbing species (for example, for the binary CO_2/N_2 adsorption, this implies $q_{1,N_2}^s = q_{1,CO_2}^s$ and $q_{2,N_2}^s = q_{2,CO_2}^s$), unless adsorbing molecules differ significantly in size. In an early study, Myers showed that these conditions are essential for the accuracy of the multicomponent DSL model.[338] This poses additional constraints on the fitting of eq 67 to the reference adsorption data using nonlinear least-squares regression. Adsorption of species A from a binary gas mixture of A and B at fixed temperature is described by the extended version of the dual-site Langmuir model (extended DSL), which is given by

$$q_A^* = \left[q_{1,A}^s \frac{b_{1,A} P y_A}{1 + (b_{1,A} P y_A) + (b_{1,B} P y_B)} \right]$$
$$+ \left[q_{2,A}^s \frac{b_{2,A} P y_A}{1 + (b_{2,A} P y_A) + (b_{2,B} P y_B)} \right] \quad (68)$$

where y_A and y_B are mole fractions of components A and B in the gas phase. To obtain physically meaningful parameters for the DSL model, normally the fitting algorithm is guided through a set of mathematical constraints, which also help the algorithm to converge.[89] The quality of the DSL model is ultimately tested by its ability to predict binary adsorption equilibria. This data may not be readily available from experiment; however in molecular simulations, it is relatively easy to implement and carry out these tests. In our previous publications, we explored systematic ways to obtain parameters of the DSL model, and we refer the reader to the original publication.[89]

It should be noted that for many new materials such as phase-change adsorbents it is not easy to propose a suitable functional form that can properly describe equilibrium adsorption data.[339,340] The alternative approach here is to describe the equilibrium relationship between adsorbed phase and fluid phase as a set of discrete points. Haghpanah et al.[341] have proposed a method to obtain discrete equilibrium data from single-component breakthrough experiments and include it into computer simulations so that a continuous functional form is no longer required. In this method, adsorbed phase concentration (q) is defined for a set of discrete values of the fluid phase concentration (c) within the range of the feed concentration. The adsorbed phase concentration of any point between two adjacent discrete points is then calculated by interpolation.[341] To extract discrete equilibrium data, single-component breakthrough experiments are performed for different fluid phase concentrations. The actual values of the corresponding solid loadings are found by solving an optimization problem and reducing the error between the experimental breakthrough results and predictions of the process model.[341] The above computational technique has been further developed by other research groups.[342,343] For example, Rajendran et al.[343] have extended this method by incorporating discrete single-component equilibrium data into the ideal adsorbed solution theory (IAST)[344] in order to describe binary equilibrium data.

The final category of parameters that are required for process modeling includes properties of the feed such as its temperature and composition, which are typically specified by the design problem at hand (e.g., postcombustion carbon capture). Table 6 summarizes the full set of properties needed to set up a PSA or VSA process simulation along with their sources according to the categories provided above.

From Table 6, it is clear that setting up a model requires a combination of properties that can be measured experimentally (e.g., adsorption isotherms, properties of the pellet) or for which well-established thermophysical models exist (e.g., molecular diffusivity, Knudsen diffusivity). Some other properties have well-known literature values (e.g., heat conductivity of steel). In general, the large number of parameters required to set up the model in combination with the large number of potential models (hierarchies used as described in Figure 15) often makes comparison and reproduction of data between various research groups a challenging task; hence we strongly advocate detailed disclosure of the sources, parameters, and algorithms used for every simulation.

A separate challenge is the implementation of the complete *in silico* workflows. As can be seen from Table 6, only a limited set of properties can be obtained from molecular simulations (e.g., equilibrium adsorption data, micropore diffusivity, heat capacity, and thermal conductivity of adsorbent crystals). For other properties, particularly those pertaining to the morphology of the pellets, we can either adopt some conventional estimates based on what is known from previous experimental measurements or use these parameters as optimization variables within a specified range of known values. The former approach is however prone to inaccuracy and inconsistency, considering that pellet morphology is not standardized and various manufacturers produce adsorbent materials with different characteristics (e.g., different size and porosity, various types of binder). Optimization of these parameters however has proved to be a more promising approach in some cases. In a recent study, Farmahini et al.[122] have demonstrated that size and porosity of pellets can be used as decision variables during process optimization not only to achieve maximum theoretical performance of adsorbent materials but also for consistent comparison of different screening studies. To fully understand the impact of these two approaches, we advocate for sensitivity and error propagation analyses of the multiscale materials screening workflows for the parameters that cannot be calculated from molecular simulations or any other theoretical methods. The results of such analyses will show whether the use of estimated reference values for these properties has a significant impact on the overall predictions of the multiscale workflows.

6.3.3. PSA and VSA Process and Cycle Configuration.
In section 3, we briefly introduced the PSA and VSA processes. In the previous sections, we also covered the mass, energy, and momentum balance equations governing the behavior of the adsorption column and the data needed to set up the process model. Here, we consider in more detail a particular 4-step VSA cycle and essential elements of cycle configuration. For the sake of concreteness and consistency, we continue with the same case study of the postcombustion feed, comprised of carbon dioxide (15%) and nitrogen (85%).

Figure 16 shows a 4-step cycle that first appeared in the work of Ko et al.,[348] who referred to this as the fractionated vacuum swing adsorption cycle. The first step of the process is the adsorption step. The feed is introduced to the column at a pressure close to atmospheric. This is followed by a concurrent blowdown step: the column is closed at the feed end, and the pressure is reduced to remove excess nitrogen present in the column in order to increase the purity of the product. Next is the counter-current evacuation step, where the pressure is reduced further, causing desorption of carbon dioxide. The product of this step is a carbon dioxide-rich stream. Finally, this step must be followed by bringing the pressure of the column back to the adsorption pressure, which is done in the repressurization step. In principle, repressurization can be done using the feed stream. However, previous studies demonstrated that counter-current repressurization with the light product stream, as schematically depicted in Figure 16 leads to much better process performance.[119,349] This effect stems from the counter-current repressurization helping to concentrate carbon dioxide closer to the feed end of the column as it will increase purity and recovery of carbon dioxide during the evacuation step later in the sequence. As can be seen from Figure 16, each step in this process is associated with a particular pressure profile and duration. These parameters, namely, time of the adsorption step (t_{ads}), time of the blowdown step (t_{bd}), and time of the
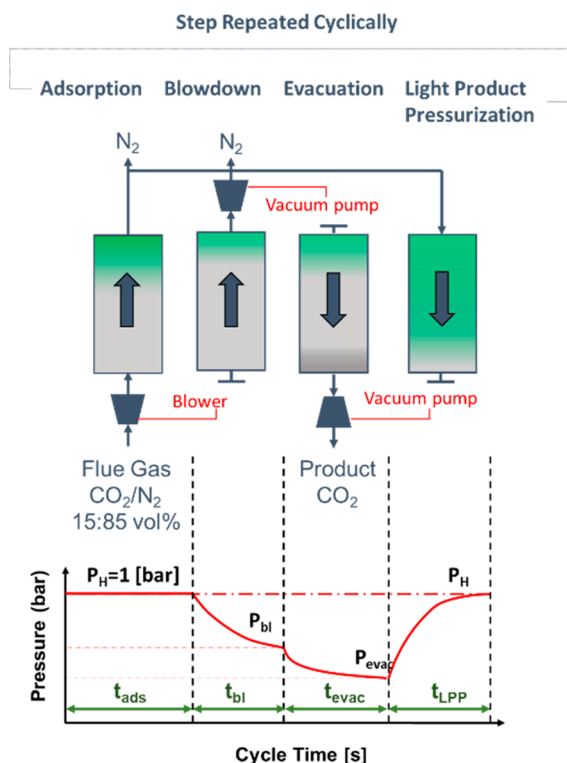
Figure 16. Schematic depiction of a four-step process with light product pressurization (LPP). From left to right, the column goes through adsorption, cocurrent blowdown, counter-current evacuation, and LPP steps. The bottom panel shows the pressure profiles during the steps and their duration within the cycle time. The green color within the column unit schematically indicates distribution of nitrogen at the end of each step. The figure has been adapted from Burns et al.[124]

important example. In practical systems, 0.2−0.3 bar would be a reasonable value for this parameter, but often much lower values are used in process simulations in order to achieve the required purity and recovery targets.

Adsorption processes operate at the cyclic steady state (CSS), and equations described in section 6.3.1 can be solved iteratively to arrive to the CSS. Alternatively, time can be discretized, and the CSS in this case is calculated directly, but this approach results in a large set of nonlinear equations and is not necessarily faster.[350] Although the actual industrial process features several adsorption units in a different stage of the cycle at any given moment, as they all go through the same steps, it is possible to consider modeling of this process with only one unit. This so-called *unibed* approach was originally described by Kumar et al.[351] This in general allows one to study a multicolumn process at a similar numerical cost as a simple Skarstrom cycle. The numerical procedure starts with some initial conditions and solution of the balance equations in the adsorption step. This produces concentration profiles for each component of the system in the adsorbed phase and in the gas phase. These concentration profiles and the composition of the product stream serve as the initial conditions for the next step in the adsorption cycle (in this case, the blowdown step), and so on. The iterative process continues until the numerical CSS is reached: this happens when the state variables start to depend only on the spatial position in the system and the time relative to the start of the cycle. One can employ several mathematical criteria to establish whether the solution has reached the CSS.[352,353] We note, however, that this is not a simple problem especially for non-isothermal systems or ones with one very strongly adsorbed component (for example, water): in this case, convergence may require thousands of cycles. Complexity of the PSA and VSA processes is very well illustrated by the concentration, temperature, and pressure profiles that are calculated for each process cycle. Figure 17 depicts concentration profiles of CO_2 at the end of each step for the 4-step VSA-LPP cycle shown in Figure 16. The corresponding cycle variables are provided in Table 7.

Correct interpretation of the bed profiles is vital for the analysis of the performance and efficiency of the PSA and VSA

evacuation step (t_{evac}), blowdown pressure (P_{bd}), and evacuation pressure (P_{evac}), along with feed pressure (P_H) and feed flow rate, are called cycle variables for this particular process and their specific values define the cycle configuration. The cycle variables are typically constrained by a number of considerations. For example, P_H cannot be set too high otherwise the compression of the dilute gas makes the process not viable. P_{evac} is another

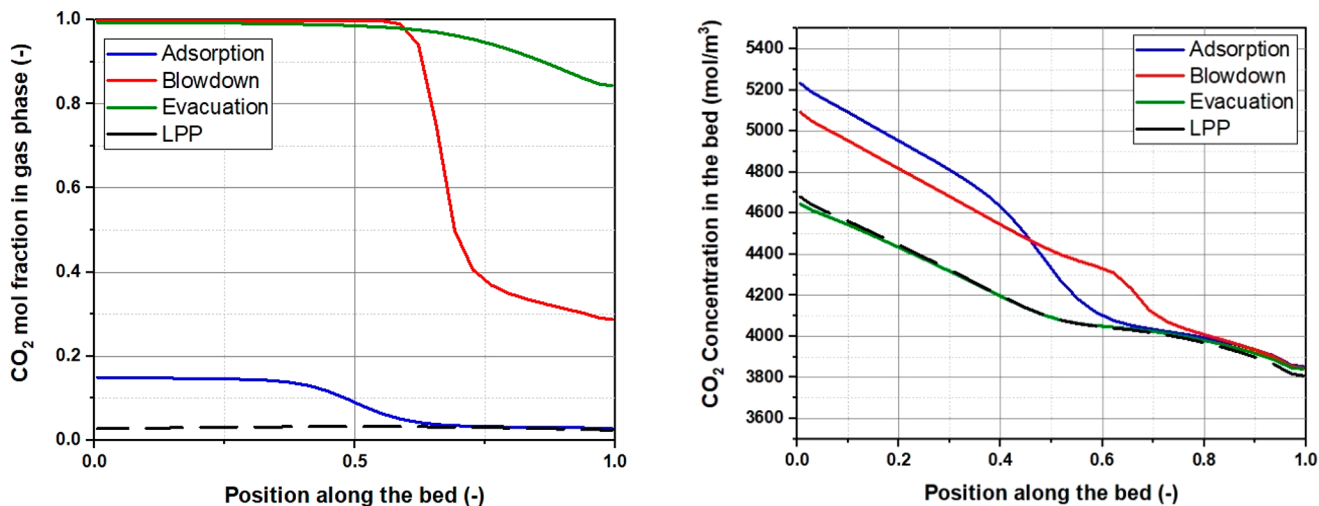**Figure 17.** Examples of the concentration profiles for carbon dioxide in the column as a function of the dimensionless position along the bed. The profiles correspond to the end of adsorption, blowdown, evacuation, and LPP steps in the gas phase (on the left) and in the adsorbed phase (on the right) at the cyclic steady state condition. The conditions and other parameters of the process are provided elsewhere.[122]

Table 7. Cycle Variables Used for Simulation of Figure 17

decision variable	feed (mol/s)	t_{ads} (s)	t_{bd} (s)	t_{evac} (s)	P_{bd} (bar)	P_{evac} (bar)
value	0.793	79.9	15.8	85.3	0.085	0.02

processes. The CSS implies that these profiles do not change anymore (within the numerical convergence criteria) as we continue with the numerical iterations and they will remain looking like this at the end of their respective steps.

Let us focus on these profiles in a step by step fashion. The LPP step prepares the bed for the next adsorption step, and the LPP profile reflects the state of the column before the adsorption step is started. In the gas phase, the concentration of carbon dioxide is very low. In the adsorbed phase, the concentration of carbon dioxide is also low; however some carbon dioxide remains in the adsorbed phase close to the feed end of the column (dimensionless bed position = 0). At the end of the adsorption step, the profile in the adsorbed phase reflects the higher amount of carbon dioxide now present in the solid. It starts with saturation values at the feed end slowly diminishing toward the light product end of the column (dimensionless bed position = 1). This reduction in saturation value is due to a nonuniform temperature distribution along the column: at the adsorption front, the heat of adsorption increases the temperature, which in turn reduces the saturation value; behind the adsorption front, the temperature reduces gradually and, in turn, the saturation value increases toward the feed end. In the gas phase, the concentration of carbon dioxide is low at the end of the adsorption step. The main purpose of the blowdown step is to remove the remaining nitrogen in the gas phase. At the end of the blowdown, some carbon dioxide is released from the porous material, and it is concentrated at the feed end of the column in the gas phase. The available carbon dioxide at the end of the blowdown step will contribute to the heavy product, that is, CO_2-rich stream, during the counter-current evacuation step. At the end of this step, the gas phase consists almost of pure CO_2, while in the adsorbent phase, the concentration of CO_2 is lowered. It is important to note from the profiles discussed that the porous material is never fully regenerated: the amount of carbon dioxide it captures is represented by the difference between blue (adsorption) and green (evacuation) lines, indicating that the working capacity of the material is only a fraction of the absolute capacity. From the same graph, it is also clear that the adsorption step is stopped before complete breakthrough occurs and the portion of the bed between 0.75 and 1.00 in the dimensionless coordinates along the bed length is never used.

To quantify performance of PSA and VSA processes, the following properties are normally evaluated:

(1) Purity, Pu_{CO_2}, this property characterizes the composition of the final product. It is the ratio of the number of moles of carbon dioxide evacuated to the total number of moles of gas mixture evacuated during a single cycle:

$$Pu_{CO_2} = \frac{\text{moles of } CO_2 \text{ recovered in evacuation}}{\text{total moles out in evacuation}} \tag{69}$$

(2) Recovery, Re_{CO_2}, this property describes the amount of carbon dioxide recovered as part of the product stream compared to what was originally fed into the column.

$$Re_{CO_2} = \frac{\text{moles of } CO_2 \text{ recovered in evacuation}}{\text{total moles of } CO_2 \text{ in the feed}} \tag{70}$$

The other two properties include energy penalty and productivity of the process, which have been already defined in Table 1; however, we will explain them here again:

(3) Specific energy penalty (En) is defined as the total amount of energy used for separation of 1 mol of CO_2 from the feed.

$$En = \frac{\text{total energy used}}{\text{moles of } CO_2 \text{ captured}} \tag{71}$$

(4) Productivity (Pr) is the amount of CO_2 captured in the product stream per unit volume of adsorbent per unit time.

$$Pr = \frac{\text{total moles of } CO_2 \text{ in product}}{(\text{total volume of adsorbent}) \times (\text{cycle time})} \tag{72}$$

Here, it is also instructive to reflect on the nature of the energy used in the process. In the PSA or VSA cycle, this work is associated with either compression or pulling vacuum. In the 4-step process considered here, the most significant energy penalty comes from pulling vacuum during the evacuation step; however it may shift to other steps in more complex processes.[354]

The complexity of this picture, its dynamic nature, and the fact that it depends on a number of parameters, including the configuration variables of the cycle, explains why it is difficult to find some simplified metrics that would comprehensively capture the efficiency of PSA and VSA separation processes.

6.3.4. Process Performance and Optimization. In the previous section, we considered a single cycle configuration with specific values ascribed t_{ads}, t_{bd}, t_{evac}, P_{bd}, P_{evac}, and flow rate of the feed, F. However, in reality, the resulting process may or may not be able to meet the design objectives to recover more than 90% of CO_2 with at least 95% purity. It also may not operate optimally, hence incurring additional energy penalties. The objective of the optimization process is to adjust the values of the cycle parameters in such a way that the process can meet its design constraints while operating at the highest possible productivity and minimum energy penalty. Normally, most optimizations consider a fixed process configuration (e.g., column size and connections) and only modify the cycle configuration. For the fixed process configuration case, it is essential to include the feed flow rate as a decision variable in the optimization because it directly influences the pressure drop and residence time of the system. If the feed flow rate was fixed, the optimization would have to modify the column dimensions, which would lead to a more complicated optimization problem.

In the optimization language, the cycle parameters described above become decision variables, while mathematically the optimization problem can be formulated as follows:

$$\Theta_{min} = \min_{t_{ads}, t_{bd}, t_{evac}, P_{bd}, P_{evac}, F} \Theta_i \qquad i = 1, 2 \tag{73}$$

$$\Theta_1 = \text{energy}/100 \tag{74}$$

$$\Theta_2 = -\text{productivity}$$

$$\text{subject to } Re_{CO_2} \geq 90\%; \ Pu_{CO_2} \geq 95\% \tag{75}$$

The optimization conditions above form an optimization problem with two objective functions and two constraints. Here, it is important to realize that the two optimization targets, minimal energy penalty and high productivity, are in competition with each other. Indeed, higher productivity may be achieved using higher flow rates given the same amount of the active adsorbent material in the column. However, this approach may require faster cycles and lower evacuation pressures, which
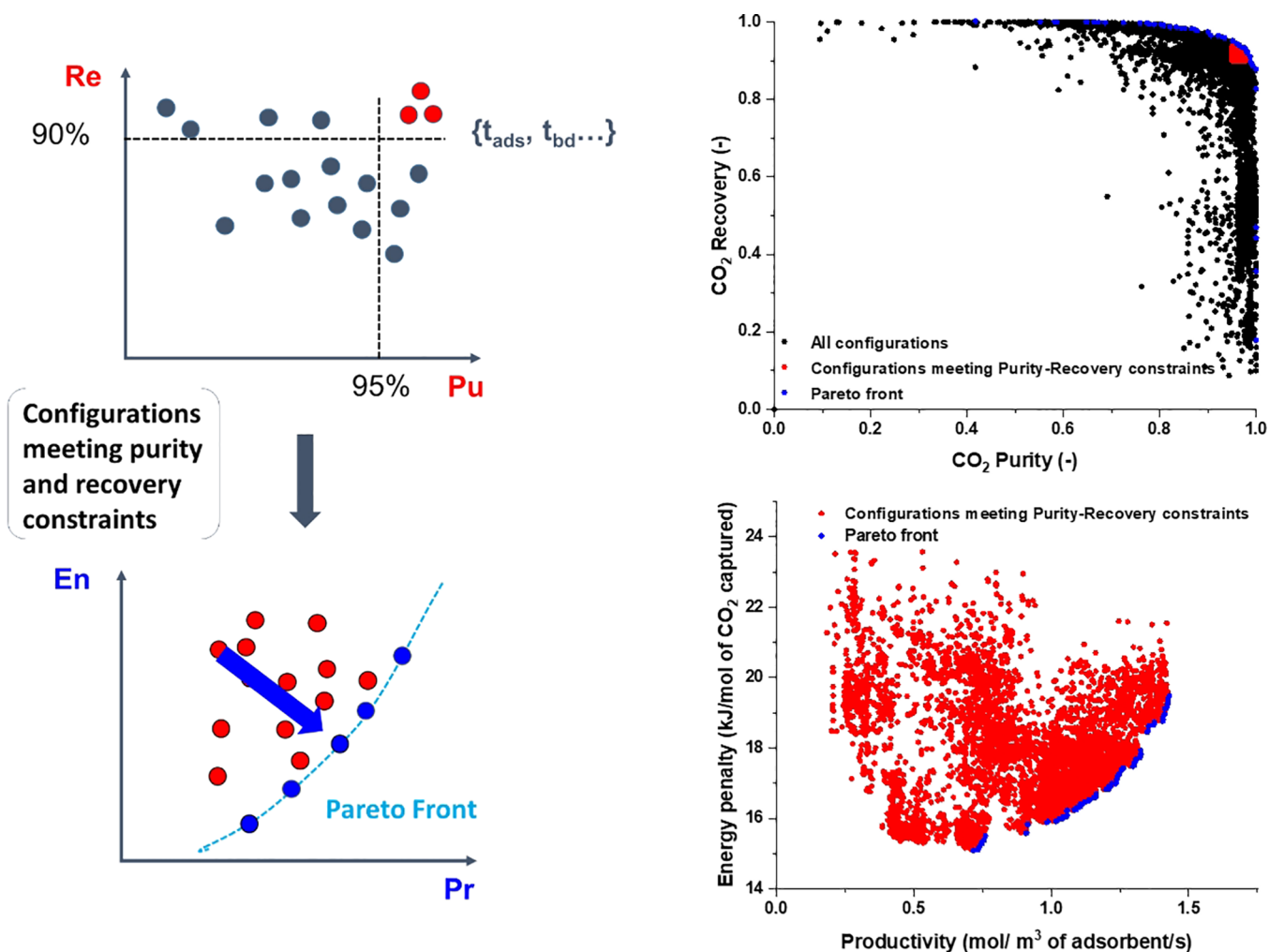
Figure 18. Process performance characterized in terms of purity−recovery coordinates (constraints, top graph) and energy penalty−productivity coordinates (Pareto front, bottom graphs); graphs on the left are schematics for the illustration, whereas graphs on the right correspond to a case studied in our recent publication.[122]

will lead to higher energy penalties. In contrast, lower energy penalty can be achieved with more moderate vacuum during the evacuation step, but it will be achieved at a cost of processing lower flow rates in the system or having to resort to longer individual steps, leading to lower productivity. As a result, the actual solution to the optimization problem is not a single set of values of the cycle parameters but multiple combinations of these parameters, each of them associated with a particular combination of purity, recovery, energy penalty, and productivity values.

From the mathematical perspective, the problem above corresponds to a multiobjective optimization. In general, this is a challenging problem as the search for the solution takes place in a multidimensional space of the decision variables, which can form clusters of feasible solutions, separated by nonfeasible regions. The study of Fiandaca et al.[355] showed that the objective function is nonsmooth and nonconvex and also that the design space is nonconvex. Several approaches have been proposed to deal with this problem over the years, with ref 355 briefly reviewing available approaches up to 2009. However, in recent years, the conventional practice became to invoke the evolutionary genetic algorithms (GAs) because of their ability to achieve global convergence, and a large number of tools available to implement them. In particular, a set of methods associated

with the second and third generations of nondominated sorting genetic algorithm (NSGA-II,III) has been a popular choice. It has been implemented in many commercial packages such as MATLAB and also available as a set of free libraries.[356−358]

The initial step in the optimization problem is to identify a range of values within which each decision variable can change. A number of initial operating conditions (so-called, *population* in GA terms) is selected from this range (either randomly or using more sophisticated approaches such as Latin hypercube sampling). For each combination of the decision variables, the PSA process is simulated as described in section 6.3.3. Promising candidates are identified, and their features are combined (using mutations and crossover moves) to give a new generation of operating conditions. As the optimization process evolves from generation to generation, the cloud of points representing the cycle configurations on the energy penalty−productivity plot progresses toward higher values of productivity and lower values of energy (subject to purity and recovery constraints) until this process effectively stops (further progress of the cloud is not visible within the convergence criteria). At this point, the optimization has converged to its final set of solutions.

This process can be illustrated with two useful graphs commonly employed in the process simulation and optimization studies. The first plot has purity and recovery as *X* and *Y* axes. It

identifies the proportion of cycle configurations that are able to meet the 95%−90% constraints for purity and recovery of carbon dioxide. The second plot shows the evolution of the cycles in energy penalty−productivity coordinates. Figure 18 illustrates typical examples of these graphs.

The front edge of the clouds shown in Figure 18 are called the Pareto fronts. These are the set of cycle configurations that combine the highest purity−recovery and energy−productivity for a given process configuration subject to its predefined process constraints.

As already mentioned, this implies that for each material there is a number of possible operating conditions to choose from (points on the Pareto front). High productivity processes will incur higher energy cost, but lower footprint and capital cost of the plant. Low energy processes, on the other hand, will benefit from lower energy penalties but may incur larger capital costs due to larger required footprint of the plant.

Assessment of the performance of two materials then invariably becomes the comparison of their corresponding Pareto fronts. For example, if two specific values of energy penalty are provided as indicators of the performance of two materials, it is important to specify to what conditions these values correspond, the lowest productivity on the Pareto front or the highest productivity.

6.3.5. Emerging Numerical Techniques for Process Optimization.
The process simulations that we have covered so far are computationally expensive: a single process simulation for a given set of design variables takes minutes to complete. Process optimization to obtain a Pareto front as described in Figure 18 requires thousands or tens of thousands of simulations, leading to an overall cost of the process optimization exercise to be around 10^2−10^3 CPU hours for a single material. Clearly, routine screening of tens, hundreds, or thousands of materials at the process level is prohibitive.

This promoted the development of several strategies to reduce the cost of process modeling and optimization stage. These strategies can be split into three main categories:

(1) Reducing the pool of candidate materials by low cost, preliminary screening strategies

(2) Reducing the computational complexity of the individual process simulations through following steps:

(a) Accelerating the convergence to CSS

(b) Using a simpler model from the model hierarchy

(c) Replacing the high-fidelity model with a surrogate model trained on the high-fidelity one

(3) Reducing the computational effort of the optimization process

The above three approaches can be combined together, although each of them has its own disadvantages and limitations which can compromise the screening process so that the optimal material and cycle configuration may be missed. Here we review studies that focus on accelerating process modelling and optimization using the strategies outlined above.

Strategies in the first category use simple performance metrics to reduce the number of candidates in pre-screening steps so that the expensive computational efforts can be only spent on the most promising materials. As described in section 4, simple performance metrics are not able to correctly and accurately rank materials for the complex and highly dynamic adsorption processes where performance is defined by a balance between the competing objectives of energy penalty and productivity as well as the competing constraints of purity and recovery. Thus, it is crucial to have very conservative exclusion criteria so that

potentially promising candidates are not removed from the candidate pool. On the other hand, a number of these metrics can be computed very quickly so that the least promising candidates can be removed for a low computational cost.

Burns et al.[124] performed a detailed multiobjective process optimization and ranking for a large range of materials for postcombustion carbon capture. Afterward, they trained machine learning (ML) classifiers to predict the objectives, that are, purity, recovery, energy penalty, and productivity, based on 29 sorbent metrics such as working capacity, selectivity, and isotherm parameters. They showed that the N_2 adsorption behavior is crucial for the correct classification of materials that meet the 95% purity−90% recovery constraints and achieved a prediction accuracy of 91% for this. However, the prediction of energy penalty and productivity for materials that met the 95% purity−90% recovery constraints had very low accuracy. They concluded that full process simulations are required for accurate prediction of energy penalty and productivity. An interesting approach was followed by Khurana and Farooq[88] who trained a classification neural network based on five equilibrium isotherm characteristics, which cover the parameter space of the dual-site Langmuir isotherm. Their model can predict with 94% accuracy whether a material can meet the 95%−90% purity-recovery constraints for postcombustion carbon capture using the VSA-LPP cycle. For the materials that met the 95%−90% purity-recovery constraints, they developed a metamodel to predict the energy penalty and productivity and achieved R^2 values of around 0.9 for minimum energy penalty and maximum productivity.

The second category is split into three methods to reduce the computational complexity of the individual process simulations. First, instead of simulating cycle after cycle to reach CSS, so-called successive substitution, several studies have explored methods to accelerate the convergence to CSS. For example, Smith and Westerberg[359] and Ding and LeVan[360] used Newton and quasi-Newton steps to reduce the cyclic deviation. This method requires the calculation of the Jacobian and can achieve about an order of magnitude faster convergence. Alternatively, derivative-free extrapolation methods such as the epsilon extrapolation used by Friedrich et al.[361] can reduce the required number of cycles to CSS by a factor of 3. Pai et al.[362] used artificial neural networks to predict the bed profiles at CSS and used this to initialize the high-fidelity simulations. In their tests, the model reduces the average number of cycles that need to be simulated to reach CSS by a factor of 6.

Second, simpler but still physics-based models are used instead of the high-fidelity models. These simplified models should be fast to calculate while still capturing the main physics of the separation process. Subramanian Balashankar et al.[363] used a batch adsorber analogue model as a simplification for the full VSA model with spatial discretization. The simplified model assumes that the system is isothermal and well-mixed and has no mass transfer resistance but still captures part of the physics of the separation and can be solved in seconds. The authors compared the output from the simplified model with the detailed process optimizations and developed a classifier that achieved a Matthew correlation coefficient of 0.76 in the classification of materials that meet the 95% purity−90% recovery constraints. In addition, they calculated a linear regression for the energy penalty, which estimated the energy penalty with reasonably good accuracy, that is, within 15% for 83% of the materials. However, Biegler et al.[364] evaluated the use

of simplified models for process optimization and concluded that it can lead to convergence failure and even to false optima.

Third, surrogate models are built based on the output of the high-fidelity models. These models are faster to evaluate and are usually embedded into optimization methods. Agarwal et al.[24] used proper orthogonal decomposition (POD) to replace the detailed spatial discretization with a reduced order model (ROM), leading to a system of differential algebraic equations (DAEs) of a significantly lower order. The ROM was trained on a number of bed profiles for different cycle conditions simulated to CSS. Because only the largest singular values are used for the ROM, the size of the discretized model is reduced by an order of magnitude. The ROM is accurate close to the training cycle conditions but loses accuracy further away from these points. This means that the ROM needs to be retrained if the optimization moves away from the original training points.

In recent years, the focus has moved to directly using the optimization objectives and constraints to build ROMs instead of using the ROM of the bed profiles. This approach replaces the process simulation (reduced order or high-fidelity) with fast-to-calculate surrogate models (also called ROMs, metamodels, or emulators), which directly calculates the optimization objectives based on the optimization variables. These models are built from the input−output relations generated with the high-fidelity models and can be used with any black-box optimization algorithm. This enables the interfacing with state-of-the-art multiobjective optimization methods to handle the trade-off between competing objectives and constraints. Below, we review the principles of these models and discuss recent studies that have used this approach.

The process of surrogate optimization starts with an initial design of experiments (DoE), which should cover the entire design space. The high-fidelity model is used to simulate the responses for these initial designs. Then the optimization loop starts by building a surrogate model based on these input−output relations. The optimization method operates on this fast-to-calculate surrogate model to find promising design points. The choice of the next design point is a balance between exploring the design space and exploiting the best-predicted design or designs. The new design point is evaluated with the high-fidelity model and added to the input−output relations, and a new iteration of the optimization loop starts, that is, we build a new surrogate model. The optimization loop is stopped once a stopping criterion, which is often a computational budget, is fulfilled.

Beck et al.[25,334] used Kriging regression based surrogate models with the NSGA-II optimizer to simultaneously optimize the CO_2 purity and recovery for postcombustion capture. The Kriging regression models the input−output relation as a Gaussian process and gives the best linear unbiased prediction. In addition, it also provides confidence bands for the prediction, which can be used to explore the design space. They achieved a 5-times reduction in computational effort and also investigated the specific energy penalty.[334]

The rapid development of machine learning methods and, in particular, artificial neural networks (ANNs) is mirrored in the application of machine learning to adsorption process optimizations. Sant Anna et al.[365] developed a three layer neural network (input layer, one hidden layer, and output layer) surrogate model for the separation of nitrogen and methane. They trained the neural network on around 500 training samples and performed a multiobjective optimization of N_2 purity and recovery on the trained network without further updating the

surrogate model. Comparing the optimal values with the high-fidelity simulations showed that the maximum relative difference was 1.4% for N_2 purity and 4% for N_2 recovery.

Instead of directly approximating the optimization objectives and constraints, Leperi et al.[366] used ANN based surrogate models to approximate each basic step, for example, counter-current pressurization and cocurrent feed, of the PSA cycles. This approach enabled them to build arbitrary PSA cycles and to include cycle synthesis in the optimization procedure without the need to retrain the ANN for each process configuration. They built 12 surrogate models for each step: one ANN for the state variables at 10 locations along the column and one for each end of the column to predict the inflow/outflow during the step. The ANNs are trained with high-fidelity simulations for 300 Latin hypercube samples and used to predict the column profiles as well as purity and recovery for three process configurations and two adsorbents for postcombustion carbon capture. The predictions were used in an optimization loop to find the purity-recovery Pareto front. The solutions on the Pareto front were used to test the accuracy of the ANN prediction and to retrain the ANN in case the prediction is too far from the high-fidelity simulation. After retraining, the relative errors for both purity and recovery were below 1.5% for all cases.

Subraveti et al.[367] used a surrogate model based on ANN in the multiobjective optimization of purity and recovery of precombustion CO_2 separation and achieved a 10-fold reduction in computational effort. For the first five generations of the multiobjective NSGA-II algorithm, they used the high-fidelity model. This generated training data for the ANN, which would already be biased toward the optimal region of the design space and should improve the prediction accuracy in the optimal region. The ANN with one hidden layer and 10 neurons was trained on the generated input−output data. The remaining 45 generations of the optimization were performed on the ANN. The Pareto front was close to the one generated with the high-fidelity model but had a relative error around 1% in both objectives. In a subsequent paper, the group compared a range of machine learning methods and showed that Gaussian process regression achieves an R^2 value above 0.98 for purity, recovery, energy penalty, and productivity with a training set of 400 randomly sampled high-fidelity simulations.[362] Their optimization on this surrogate model (without further refinement) was within 3% of the high-fidelity simulation for purity and recovery as well as for energy penalty and productivity. However, the latter optimization was tested subject to reduced 95%−80% purity-recovery constraints.

Pai et al.[127] developed a material-agnostic surrogate model called MAPLE that fully emulates operation of the 4-step VSA-LPP cycle at the cyclic steady state. The framework is based on a dense feedforward neural network trained with a Bayesian regularization technique. The framework accepts the adsorbent properties, the Langmuir adsorption isotherm parameters, and operating conditions as input. It predicts key performance indicators of the process including CO_2 purity and recovery in addition to productivity and overall energy consumption of the process as output. The model was trained with a set of data generated using detailed process modeling. In order to reduce computational time of the multiobjective optimization, MAPLE was used to calculate the CSS performance indicators and feed them back to the optimizer. The fully trained model predicts each performance indicator with less than 2% error compared to the detailed process modeling. The computational time required for simulation and optimization of the process was also reduced

from 1500 core-hours per adsorbent to ≤1 core-minute for each adsorbent, which shows a significant improvement for screening of large databases of porous materials.[127]

Strategies in the third category include a range of methods to reduce the computational requirements of the optimization itself, that is, reducing the number of required iterations to reach an optimal value or Pareto front. Here, the first strategy is the reduction of the search space. This includes the removal of parameters that have no or only a small impact on the performance, and the reduction of design space, that is reducing the evacuation pressure range. For example, Subramanian Balashankar et al.[363] removed the blowdown and evacuation times from the list of optimization variables. This was acceptable in their optimization because these variables have very limited impact on the purity and recovery. However, they have a large effect on productivity and energy penalty.

Yancy-Caballero et al.[126] performed a hierarchical, multi-objective optimization with NSGA-II. They first optimized purity and recovery to screen for materials that achieve the 95%−90% purity-recovery constraints and then optimized the promising materials for energy penalty and productivity. The energy penalty and productivity optimization was seeded with the results from the initial optimization and was performed in two steps: the first step used a low spatial resolution, which reduces the computational complexity, and the second step used a high spatial resolution and was preseeded with the low resolution results.

Finally, Ding et al.[368] and Jiang et al.[369] presented a strategy that combines the reduction of the computational complexity of individual simulations with a reduction of the computational complexity of the optimization. They included the CSS condition as a constraint in the constrained single-objective optimization problem so that both the objective and approach to CSS were optimized simultaneously. This approach, called the simultaneous tailored approach by Biegler and co-workers,[17] removes the expensive calculation of CSS for each iteration and has reduced the computational time by a factor of 10 for single-objective optimizations of air separation VSA cycles.[369]

6.3.6. Available Tools and Software for Process Modeling and Optimization. The objective of this section is to introduce the reader to several software packages and libraries that are available for PSA/VSA process simulations. Broadly, these can be divided into two main categories: codes developed by different academic groups, and commercial software packages with built-in adsorption process simulators. From this classification we can also identify the most significant challenge in a consistent description of these tools: they are not open source software (with one exception discussed below) and we do not have direct access to the organization, functionality, implemented models or capabilities of these codes to make the comparison consistent. Hence, from the onset we admit that this section is likely to be incomplete, however our main objective is to provide the reader with an overview of the options available for PSA/VSA simulations.

6.3.6.1. Commercial Software. 6.3.6.1.1. gPROMS: The process builder developed by Siemens Process Systems Engineering (PSE) has an adsorption process library that has been used for simulation of pressure and temperature swing adsorption processes.[370] In the adsorption process library, it is possible to use the dispersed plug flow or the plug flow model. The adsorption isotherms of Langmuir, dual-site Langmuir, and virial isotherms can be used in gPROMS. Here, the flow sheet can be built by joining individual units such as valves, header

mass flow controllers, sources and sinks, and adsorption columns. The adsorption process model is a system of partial differential equations that are discretized in the spatial domain using either finite difference (backward, forward, and central), finite element, finite volume, or orthogonal collocation with finite element. The flow controllers supply a constant amount of gas, while the sources and sinks are used to specify initial and final operating conditions. gPROMS also has a facility to account for column headers to distribute flow, and these are modeled as continuous stirred tank reactors. Building a flow sheet enables one to schedule various steps operating in multiple columns. In principle, within gPROMS, it is possible to perform optimization and scheduling of VSA processes using in house libraries.[371,372] Nevertheless, gPROMS only supports single-objective deterministic optimisations. For multiobjective optimisation, the software can be interfaced with MATLAB where it is possible to use evolutionary genetic algorithms. PSA processes have been optimized in gPROMS for the maximization of CO_2 product purity and recovery, with the number of beds, process configuration, feed pressure, particle diameter, length to diameter ratio, and feed flow rate as the decision variables. An example of such studies is provided by Nikolaidis et al.[373] The same approach has been also used in an earlier study by Nikolić et al.[374] for H_2 recovery from steam methane reformer off-gas. However, it should be noted that these studies have not reported any Pareto fronts.

6.3.6.1.2. Aspen Adsorption: Aspen Adsorption is a flow sheet simulator that can design, simulate, and optimize adsorption processes.[375,376] Few studies exist in literature that have simulated PSA and dual-reflux PSA processes for CO_2 capture using this program.[377−380] In Aspen Adsorption, it is possible to simulate multibed PSA processes with an isothermal or a non-isothermal model and to use nonideal gas equations of states. In most publications with Aspen Adsorption, a Langmuir model has been used. Moreover, it is also possible to use finite difference or finite volume numerical schemes to solve the model equations. To the best of our knowledge, no cycle optimization studies have been published using Aspen Adsorption software, although it is possible to couple Aspen products with MATLAB.[381]

6.3.6.1.3. ProSim DAC. ProSim DAC is a dynamic simulation software from ProSim.[382] It is capable of simulating adsorption and desorption steps using TSA, PSA, and VTSA processes. From the model hierarchy point of view, the process model can be isothermal or non-isothermal, it can further include a pressure drop, while transport in macropores is modeled using the LDF approach. Data for a wide variety of adsorbents is available (e.g., activated carbon and zeolites) and is accompanied by many different models for equilibrium data (adsorption isotherms) and mass transfer models. DAC is a relatively new addition to the ProSim family of process simulation tools which have been so far employed predominantly in solvent recovery and in adsorption of volatile organic compounds. We are not aware of any academic article on carbon capture simulation and optimization that have used ProSim DAC.

6.3.6.2. Academic codes. Several academic research groups have been developing simulation codes for adsorption process modeling since the 1980s, including SAXS (Swing Adsorption X = Pressure, Temperature Software) from Da Silva and Rodrigues, dynamic adsorption process simulator (DAPS) by Ebner and Ritter, PSA SW from Mazzotti and co-workers, MINSA by Webley and co-workers, and CySim by Brandani and co-workers. The key challenge in the discussion of the process

modelling codes developed by various academic groups is similar to the issues associated with the commercial software: the codes are usually not open-source, and full details of the algorithms, implementation and capabilities are not readily available. Below we briefly review the information available on MINSA, our own process simulator, CySim, and a recently published open-source code from Fengqi You's research group (Cornell-PEESE).

6.3.6.2.1. MINSA (Monash Integrated Numerical Simulator for Adsorption): MINSA is a generalized cycle simulator that was developed by Webley and co-workers for PSA simulations using the VODE integration scheme of Brown et al.[383] written in FORTRAN.[384−387] This simulation package solves mass and energy balance equations that have been discretized by the finite volume method.[386,387] The software has been used extensively for various adsorption processes and verified against experimental data over the past two decades[385,388−390]

6.3.6.2.2. CySim (Cycle Simulator): CySim is a modular computer program for simulation of adsorption processes that was developed by Brandani and co-workers[561,391] at the University of Edinburgh. CySim can be used to simulate breakthrough curves, ZLC experiments,[391] dual piston PSA,[392] and other PSA processes. The user defined structure is translated into a system of differential algebraic equations, which are solved with the SUNDIALS library. This can be interfaced with either MATLAB or Python's genetic algorithm packages such as *gamultiobj,*[393,394] *inspyred,*[395] and *Platypus*[356] to perform process optimization. Recently Farmahini et al. have used CySim to simulate and optimize the 4-step VSA process with LPP for postcombustion carbon capture.[89,122] CySim is regularly updated with new models and applications, for example, for monolithic adsorbents to include inlet and flow maldistributions.[353,396]

6.3.6.2.3. Cornell-PEESE Simulator: Recently, Yancy-Caballero and co-workers published a MATLAB code for simulation of PSA/VSA processes.[126] In particular, the code uses the finite volume method with the weighted essentially nonoscillatory (WENO) scheme to discretize the PSA model, and the ode15s solver within MATLAB to solve the resulting ODEs. NSGA-II algorithms within MATLAB are employed for process optimization. In the most recent study, this code has been employed for performance ranking of several MOF materials in postcombustion carbon capture processes, using three different cycles: a modified Skarstrom cycle, a fractionated vacuum swing adsorption (FVSA) cycle, and a five-step PSAcycle. A notable feature of the code is that it is open-source and is publicly available from the github depository of the Cornell-PEESE group. Table 8 provides a list of process simulation software that has been discussed in this section.

7. CARBON CAPTURE WITH ADVANCED PROCESS CONFIGURATIONS

The main objective of this section is to introduce the reader to more complex PSA/VSA process configurations and review recent studies on application of process modeling to assess the viability of PSA/VSA technologies for carbon capture.

In the previous section, we used the 4-step VSA-LPP process to introduce several essential concepts and fundamentals of the PSA/VSA process and optimization. One of the issues associated with this specific process is that it can meet the required purity/recovery constraints only by going to very low evacuation pressures (e.g., 0.01 bar). Although from the Pareto front analysis this process is very competitive compared to other

Table 8. List of Academic and Commercial Software for PSA/VSA Simulation

software	reference	web site
Commercial Software		
gPROMS	PSE[370]	https://www.psenterprise.com/products/gproms
Aspen Adsorption	AspenTech[375]	https://www.aspentech.com/en/products/pages/aspen-adsorption
ProSim DAC	ProSim[382]	https://www.prosim.net/en/product/prosim-dac-dynamic-adsorption-column-simulation/
Academic Software		
MINSA	Webley and co-workers[384,385]	http://users.monash.edu.au/~webley/minsa.htm
CySim	Friedrich et al.[361]	https://www.carboncapture.eng.ed.ac.uk/lab/cysim
Cornell-PEESE Simulator	Yancy-Caballero et al.[126]	https://github.com/PEESEgroup/PSA

alternatives, in practice it is not viable, as the standard industrial pumps do not typically go below the range of 0.13−0.2 bar.[397] This necessitates a search for more complex process configurations. One option is to consider a two-stage process.[336] In this case, the first stage focuses on maximizing the recovery, while the second smaller polishing unit would aim to achieve the required purity. Indeed, Abanades et al. summarized recent studies of 2-stage PSA processes.[336] According to their summary, it is clear that most process simulations arrive at VSA configurations that require approximately 0.5−0.75 MJ/kg and that they can operate at evacuation pressures between 0.05 and 0.1 bar, which is more comparable to the industrial standards.

Alternatively, we can consider more complex multibed multistep configurations. Below we review several studies that explore more complex process configurations in the context of postcombustion carbon capture. In particular, Reynolds et al.[398,399] studied the capture of CO_2 from a flue gas mixture containing 15% CO_2 and 10% H_2O with the rest being N_2 using potassium-hydrotalcite as the adsorbent. They had studied 9 different cycles with heavy and light reflux steps in 4-bed, 5-bed, and 6-bed configurations. Two examples of such advanced PSA or VSA processes are shown in Figure 19. A parametric study was then carried out and the best performing cycle was the 5-bed 5-step cycle with light reflux (LR) and heavy reflux (HR) from the counter current depressurization (CnD) as shown in Figure 19 on the left. The purity and recovery values were 98.7% with a productivity of 0.11 mol/(m³·s). The next best cycle was that shown in Figure 19 on the right, which, although showed a much lower recovery of 71%, had a high throughput of 1.11 mol/(m³·s). It should be noted that this was a parametric study that did not show the optimum performance of these cycles; in other words, detailed process optimization was not carried out to identify conditions corresponding to maximum productivity while meeting purity and recovery targets.

Zhang and Webley[388] constructed a pyramidal hierarchy of cycles. In this work, experiments were conducted initially using a 3-column PSA system (1 m long columns with 7.7 cm internal diameter). The experimental data collected from this system was then used to validate an adsorption process model on which basis the authors constructed the pyramid of cycles. Here, the pyramid consisted of cycles ranging from a simple 2-step cycle to complex cycles that included heavy reflux, light reflux, pressure equalization, etc. They carried out a parametric study on the
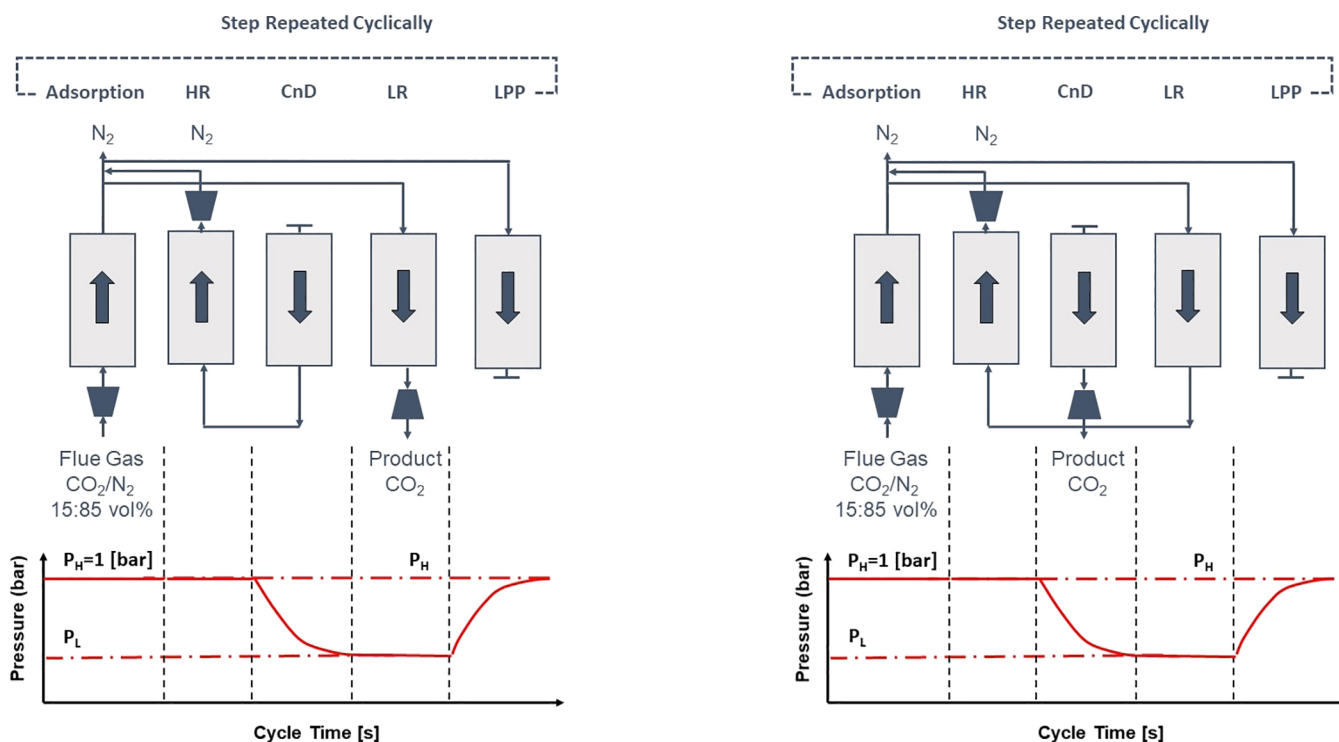
Figure 19. Examples of more complex process configurations: 5-bed 5-step cycle with light reflux and heavy reflux from counter-current depressurization on the left; 5-bed 5-step cycle with light reflux and heavy reflux from light reflux purge on the right.[399] HR: heavy reflux; CnD: counter-current depressurization; LR: light reflux; LPP: light product pressurization.

effect of feed step duration, pressure equalization, heavy reflux (rinse), evacuation, and purge steps on the purity and recovery values. Although their model was a simple one, it provided some useful insights on the performance. In particular, they had studied the effect of feed time, light reflux, pressure equalization, and heavy reflux steps on the purity, recovery, and specific energy consumption. One of the main conclusions was that the addition of heavy reflux improved the purity from 85.7% to 95.2% in their experiments.

A two-stage vacuum pressure swing adsorption (VPSA) process was studied both theoretically and experimentally by Shen et al. using activated carbon as adsorbent.[400] The two-stage VPSA system was composed of two columns. The first stage employed a 4-step Skarstrom cycle comprising the following steps: pressurization with feed, adsorption, blowdown, and counter-current evacuation (light product purge). In the second stage, a 5-step cycle comprising pressurization with feed, adsorption, pressure equalization, blowdown, and pressure equalization was used. The work mimicked a 2-stage operation where the first stage concentrates CO_2 from 15% to 40−50%, while the second stage is to achieve high values of CO_2 purity. Here, the first stage used a feed under ambient pressure, while the second stage required a compression up to 3.5 bar. With a vacuum pressure of 0.1 bar, the two stage process produced 95% pure CO_2 product with 74.4% CO_2 recovery. The specific energy and productivity values were 0.72 MJ/kg and 0.23 mol/(m^3 ads/ s). Deepening the vacuum to 0.05 and 0.03 bar improved the purity to 96.3% and 96.6% respectively, while the recovery increased to 80.7% and 82.9%, respectively. This also improved the productivity to 0.25 and 0.26 mol/(m^3 ads/s). The increase in energy consumption was significant and the values were 0.83 and 0.9 MJ/kg for pressure values of 0.05 and 0.03 bar.

Through a combination of experiments and simulations, Wang et al.[401] studied CO_2 capture from dry flue gas containing 15%−17% CO_2. They used a two-stage process with the first stage containing 3 columns packed with zeolite 13X and the second stage containing 2 columns packed with activated carbon. In the first stage, the cycle chosen was an 8-step cycle comprising pressurization with feed, adsorption, concurrent evacuation, heavy reflux, depressurizing pressure equalization, counter-current evacuation, light reflux, and pressure equalization. The CO_2 product was collected from the counter-current evacuation and the reflux step. For the second stage, a six-step cycle comprising pressurization with feed, adsorption, heavy reflux, depressurizing pressure equalization, light reflux, and pressurizing pressure equalization was used. The vacuum pressures of the first and second stage were 0.08 and 0.2 bar, respectively. In the first stage, CO_2 purity of 70% was achieved. This stream containing 70% CO_2 was then compressed and sent to the second stage, and here the product contained over 95% CO_2. The overall recovery was over 90%. From the experiments and the simulations, the values of the energy consumption were found to be 2.44 and 0.76 MJ/kg respectively. The large differences in the reported energy consumption values could have been a consequence of the low pressure used in the first stage, which would have resulted in a lower vacuum pump efficiency as shown by Krishnamurthy et al.[119] The other possibility is the use of a constant efficiency for the vacuum pump, whereas pump efficiency is a function of the suction pressure.[92]

Haghpanah et al.[349] also performed detailed process optimization on 7-different cycles, ranging from 4 to 6 steps, to identify the optimal configuration of postcombustion CO_2 capture using zeolite 13X as adsorbent. The genetic algorithm-based optimization was carried out in two steps: (a) to maximize

Table 9. Summary of Selected Process Configurations Studies for Post-combustion Capture in Chronological Order from 1993 to 2021

process	adsorbent	y_{CO_2} (%)	P_{high}/P_{low} (kPa)	purity (%)	recovery (%)	minimum specific energy[h] (MJ/kg)	source[l]	reference
4-step VSA	AC, CMS	17	120/10	99.99	68.4	*i*	sim	Kikkinides et al.[405]
7-step PSA	13X	16, 26	110/6.7	99	70	*i*	sim	Chue et al.[406]
dual reflux PSA	13X	15	101.3/8.1	95	95	*i*	exp	Diagne et al.[403]
2 bed PTSA/PSA	13X	15	NA/5−15	99	90	2.02 mix[j]	exp	Ishibashi et al.[407]
VSA	13X	10	115/6.7	50−70	30−90	0.9−1.1	sim	Park et al.[408]
2 bed, 2 stage PVSA	13X	10.5	1st NA/6.7, 2nd NA/13	99	80	2.3−2.8	exp	Cho et al.[510]
4-step PVSA	13X	15	652/10−70	88.9	96.9	1.5	sim	Ko et al.[348]
TSA	5A	10	423 K	>94	75−85	6.12−6.46 th[k]	lab	Merel et al.[409]
VSA	13X	12	100/3	95	>70	0.54	sim	Xiao et al.[387]
6-step PVSA (3 beds)	13X	12	130/5	82	60−80	0.34−0.69	exp	Zhang et al.[410]
9-step PVSA (3 beds)	13X	12.1	130/5	90−95	60−70	0.51−0.86	exp	Zhang et al.[410]
3-step PVSA	13X	12[a]	118/4	72.4	60	*i*	exp	Li et al.[411]
PVSA	13X	12.6	120/5−6	90−95	60−70	0.52−0.86	lab	Zhang and Webley,[388]
5-bed, 5-step PVSA	hydrotalcite	15[b]	139.7/11.6	96.7	71.1	*i*	sim	Reynolds et al.[399]
6-step PVSA	13X, F200 alumina	13[c]	140/3	89.6	74.9	0.72	exp	Zhang et al.[412]
9-step PVSA	13X	13[c]	140/3	98.9	78.7	0.57	exp	Zhang et al.[412]
9-step PVSA	13X	13[d]	140/3	98.9	82.7	0.65	exp	Zhang et al.[412]
9-step PVSA	13X	15[c]	140/3	86.1	60	1.07	sim	Zhang et al.[412]
9-step PVSA	13X	15[d]	140/3	90	62	0.89	sim	Zhang et al.[412]
2-bed, 4-step	13X	15	276/21.4	90.74	85.94	2.3	sim	Agarwal et al.[54]
4-step VPSA	AC	15	202.6/10	93.7	78.2	*i*	exp	Shen et al.[413]
2-stage PVSA	5A	15	150/10	96.1	91.1	0.65	sim	Liu et al.[371]
TSA	5A	10	433 K	95	81	3.23 th[k]	sim	Clausse et al.[414]
VSA	13X	13	100/2	93.8	91.5	0.43	sim	Delgado et al.[415]
2-stage VPSA	AC	15	350/10	95.3	73.6	0.73	sim	Shen et al.[400]
2-stage VPSA	AC	15	350/5	96.4	80.4	0.83	sim	Shen et al.[400]
2-stage VPSA	AC	40−60	202/10	94.1	85.1	*i*	exp	Shen et al.[400]
VTSA	13X	15	101/363K, 3 kPa	98.5	94.4	*i*	exp	Wang et al.[416]
2-stage PVSA	13X APG	15	150/10	96.5	93.4	0.53	sim	Wang et al.[417]
2-stage PVSA	13X APG	15	150/6	96.6	97.9	0.59	sim	Wang et al.[417]
VSA	5A	15	101.3/5.5	71−81	79−91	2.64−3.12	exp	Liu et al.[418]
2-stage VSA	1st 13X APG 2nd AC beads	16	1st 123/7.5, 123/20	95.2	91.3	0.76	sim	Wang et al.[401]
4-step VSA	13X	15	101/2	90	90	0.53	sim	Haghpanah et al.[117]
VSA	13X	15	101/3	90−97	90	0.55	sim	Haghpanah et al.[117]
VSA	13X, AC, MOF-74, chemisorbent	15	120/5−10	45−95	35−95	0.95−1.2	sim	Maring and Webley[118]
1-stage and 2-stage VSA	CMS	15	101/3	90	90	0.99	sim	Haghpanah et al.[262]
4-step PVSA	13X	15	150/2.2	95.9	86.4	1.7	exp	Krishnamurthy et al.[119]
4-step PVSA with LPP	13X	15	150/2.2	94.8	89.7	1.71	exp	Krishnamurthy et al.[119]
2-bed, 4-step VSA with LPP	13X, silica gel	15[e]	101/3	95	90	0.63	sim	Krishnamurthy et al.[333]
4-step VSA with LPP	13X, rho-ZMOF	15	101/3	95	90	0.56−0.7	sim	Nalaparaju et al.[116]
2-bed, 6-step VSA	13X, AC, MOF-74	15	101/2	95	90	0.76−0.83	sim	Nikolaidis et al.[419]
4-bed, 9-step cycle	13X	15	105/3,5	70.5−92.4	62.9−91.3	0.22−0.3	exp	Ntiamoah et al.[377]
Skarstorm cycle	13X, HKUST, 5A, MOF-74	15[f]	1st 101/10 2nd 126/10	90	90	0.99−1.3	sim	Leperi et al.[420]
4-step VSA with LPP	74 real and hypothetical materials	15	101/2	95	90	0.43−0.53	sim	Khurana and Farooq[88]

Table 9. continued

process	adsorbent	y_{CO_2} (%)	P_{high}/P_{low} (kPa)	purity (%)	recovery (%)	minimum specific energy[h] (MJ/kg)	source[i]	reference
4-step VSA with LPP	UTSA-16, 13X	15	101/0.02−0.1	95	90	0.43−0.86	sim	Khurana and Farooq[354]
4-step VSA with LPP	UTSA-16, 13X	15	101/2−10	95	90	0.56−1.85	sim	Khurana and Farooq[354]
4-step VSA	13X, UTSA-16, AC, MOF-74	15	101/2−3	95	90	0.41−0.63	sim	Rajagopalan et al.[16]
4-step VSA	UTSA-16, 13X, hypothetical material	15	101/2	95	90	0.38−0.59	sim	Khurana and Farooq[421]
6-step VSA	UTSA-16, 13X, hypothetical material	15	101/10	95	90	0.41−0.66	sim	Khurana and Farooq[421]
4-step VSA	13X	15	100/1−2	95	90	0.57−0.85	sim	Farmahini et al.[89]
4-step TSA	13X + alumina	12[g]	440 K	95	90	4.86 th[k]	sim	Hefti and Mazzotti[422]
4-step VSA	13X, hypothetical materials	15	100/2	95	90	0.4−1.38	sim	Rajagopalan and Rajendran[423]
4-step VSA	13X, diamine appended MOFs	15	100/3−10	95	90	0.51−0.63	sim	Pai et al.[340]
4-step VSA with LPP	13X, UTSA-16 and hypothetical materials	15	101/3	95	90	0.8−0.9	sim	Burns et al.[124]
4-step VSA with LPP	13X, UTA-16, AC, hypothetical material	15	101/1−10	95	50−90	0.36−0.86	sim	Maruyama et al.[48]
4-step VSA with LPP	13X, silicalite, HKUST, Ni MOF-74	15	101/1−2	95	90	0.5−0.9	sim	Farmahini et al.[122]
MBTSA	13X, Ni MOF-74	5	101, 480 K, 405 K	95.8, 98.9	98.2, 92.6	1.42, 1.89 th[k]	sim	Mondino et al.[372]
modified Skarstrom, 5-step, and FVSA	13X, 15 MOFs	15	100−1000/10−50	90	90	0.55−2.5	sim	Yancy-Caballero et al.[126]
4-step VSA with LPP	13X, UTSA-16, IISERP-MOF2	20	100/1	95	90	0.55−0.72	sim	Subraveti et al.[92]
4-step VSA with LPP	36 materials	0.05−0.7	100/1	95	90	0.42	sim	Pai et al.[127]
6-step VSA	supported amine sorbent	15[c]	101/10	95	90	1	sim	Krishnamurthy et al.[424]
6-step VSA	supported amine sorbents with PEI, benzyl, amine, and amino silane	15[c]	101/10	95	90	1	sim	Krishnamurthy et al.[425]
4-step VSA with FP or LPP	13X, UTSA-16, IISERP-MOF2	5, 15, 25, 35	100−500/1−100	95	90	0.1−1.1	sim	Pai et al.[426]

[a]In the presence of 3.4% H_2O. [b]In the presences of 10% H_2O. [c]In the presence of 5% H_2O. [d]In the presence of 7% H_2O. [e]In the presence of 3% H_2O. [f]In the presence of 5.5% H_2O. [g]In the presence of 1.5%, 3.1%, and 4.5% H_2O. [h]All energy values are electric, that is, the energy consumed by the vacuum pumps and the compressors. [i]Not available. [j]mix = electric + thermal, the electric energy consumed by vacuum pumps in the 2nd stage PSA process and heat needed to recover the CO_2 from the 1st stage PTSA process of Ishibashi et al.[407] [k]th = thermal, the heat supplied to desorb the CO_2 in TSA/PSA process. [l]Sim and Exp refer to simulation and experimental studies, respectively.

purity and recovery; (b) to minimize energy consumption and maximize productivity for cycles satisfying 90% purity and recovery constraints. The decision variables were the step durations, evacuation pressures, and the feed flow rate. The adsorption step pressure was kept constant at 1 bar, and the feed was a 15% CO_2/85% N_2 mixture at 298 K. The optimization results from the first step showed that 4 cycles, namely, a 4-step cycle with LPP, a 5-step cycle with light reflux (LR) and LPP, and two 6-step cycles satisfied the 90% purity−recovery targets. The next step was to minimize energy and maximize productivity, and in this case, the 4-step cycle with LPP was the best performing cycle in terms of the energy consumption. The minimum energy consumption was 0.47 MJ/kg for a productivity of 0.57 mol/(m^3·s) and with an evacuation pressure of 0.03 bar. The 6-step cycle with LR and HR was the best in terms of the purity and recovery, and in this cycle over 98% purity and recovery were achieved. However, this cycle had much higher energy consumption. The 4-step cycle with LPP was also able to achieve the 95% purity and 90% recovery targets, and in this case the energy and the productivity values were

0.554 MJ/kg and 0.44 mol/(m^3·s), respectively. The 4-step cycle with LPP was shown to meet the 95% purity and 90% recovery targets through a pilot plant study by Krishnamurthy et al.[119]

Later, in a fully computational investigation, Haghpanah et al.[262] studied CO_2 capture using a carbon molecular sieve by the optimization of 1-stage and 2-stage VSA processes. The 2-stage process was basically a 4-step cycle with LPP carried out twice where the product from the counter-current evacuation step from the first stage served as the feed for the adsorption step in the second stage. In the 1-stage process, 5-step cycles with heavy reflux and with feed and light product pressurization were used. It was seen that the 2-stage VSA process was the best in terms of energy and productivity. However, the productivity was about 50% smaller than that of zeolite 13X mentioned above, considering that carbon molecular sieve is a kinetically selective adsorbent.

It should be noted that in both the studies by Haghpanah et al.[262,349] the evacuation pressures were from 0.01 to 0.05 bar, and this, as we have already discussed, may not be industrially achievable. In a recent study by Khurana and Farooq,[354] it was

shown that with a 6-step cycle it was possible to achieve evacuation pressures of 0.1 bar and above. The 6-step cycle is essentially the 5-bed 5-step cycle with heavy reflux from light reflux product of Reynolds et al. with the addition of a concurrent evacuation step.[399] The authors have compared the performance of this cycle with that of the 4-step cycle with LPP and used two adsorbents, namely, zeolite 13X and UTSA-16. Through detailed process optimization, it was seen that the 6-step cycle was able to achieve similar productivity values as the four-step cycle but at a much higher evacuation pressure of 0.1 bar.

Another cycle that has shown promise for producing both CO_2 and N_2 in high purities is the dual reflux pressure swing adsorption (DRPSA) cycle. The concept of the dual reflux PSA process first appeared in the 1990s in the experimental studies of Diagne et al.,[402,403] who had obtained 95% CO_2 purity and recovery from a stream containing 20% CO_2. The DRPSA contains two columns, one operating at high pressure and the other at low pressure at a given instance. Feed can be introduced from the bottom or from an intermediate position, both at low and high pressures. The enriched gas from low pressure feed is then compressed and sent to the column at high pressure to perform the heavy reflux. The light product from this heavy reflux step can be used to recover the heavy component simultaneously during the feed step. After this step, the column roles reverse, and the same sequence of steps are carried out. Over the years, variations of the dual reflux PSA cycle have been studied by a few authors.[378−380,404] One among them is that of Li et al.,[379] who had studied the CO_2 capture from a binary mixture containing 15% CO_2 and 85% N_2 at 2 bar and 20 °C feed using silica gel adsorbent. They were able to achieve over 99% purity and recovery for CO_2 and N_2. A follow up study by Shen et al.[380] presented a detailed experimental and simulation investigation of the same cycle and the adsorbent in which the process achieved over 95% purity and recovery with energy consumption of 2.5 MJ/kg.

In Table 9, we complement the summary of Abanades et al.[336] with a summary of the recent studies of various process configurations for postcombustion capture. We note that although the table contains two TSA cycles, in reality the productivity of these cycles will be low compared to the PSA and VSA processes. Lower productivity of TSA processes is a result of longer cycle times that are required for heating and cooling steps. To be competitive in the postcombustion capture from coal-fired plants, larger columns (or a larger number of them) are required in TSA processes. They may however find application in the carbon capture from natural gas fired power plants, where the concentration of CO_2 in the flue gas is much lower.

8. CHALLENGES OF MULTISCALE MATERIALS SCREENING: ACCURACY, DATA AVAILABILITY, AND REPRODUCIBILITY

In this section, we outline what we believe are the key challenges in the development and implementation of realistic multiscale workflows for performance-based screening of porous materials. Our awareness of these challenges evolved over time as we, being a collaborative group of molecular simulators and process modelers, navigated this emerging field of research. Through experience, we have come to a conclusion that the main obstacle in development of realistic materials screening approaches is not the number of materials and the magnitude of phase space that must be explored, but the main pitfalls lie in the accuracy,

reproducibility, consistent implementation, and validation of these workflows. In this section, we pay special attention to these issues and aim to discuss them in a practical way.

Let us imagine that two articles from two different academic groups have reported ranking of two sets of porous materials for a particular separation application (e.g., CO_2 capture) using the multiscale workflows discussed in this review. Are these two different rankings compatible and consistent with each other? In other words, can we combine the results of the above two studies into one ranking and therefore identify the best material out of the combined group of candidates? As we will see in section 9.1, in general, the answer is "no"! This is because different groups employ different hierarchies of models and assumptions, use different sources and values of parameters, and apply different conditions to the process. Such an inconsistent approach to materials screening results in prediction of performance indicators that are largely different. Therefore, in this section, we will explore the importance of data availability, reproducibility, and consistency in materials screening simulations.

There are many concerns about accuracy and transferability of the force fields that are used for prediction of equilibrium adsorption data in molecular simulations. Reproducibility of experimental adsorption isotherms (as reported in the literature) is another source of concern. Adsorption isotherms obtained from experiment are routinely employed for validation of atomic force fields that are used in GCMC simulation. As such, any concern about reproducibility and accuracy of experimental adsorption data will manifest itself in our confidence about accuracy of the predictions made based on simulated adsorption isotherms. The two issues concerning accuracy of molecular force fields and reproducibility of experimental adsorption data are discussed in sections 8.1 and 8.2.

Another challenge in development of reliable multiscale screening workflows concerns the issue of data availability and consistent implementation of models. As has been discussed throughout this review, not all of the data required for setting up the multiscale simulation workflows are available in the literature or can be calculated from classical molecular simulations. This is in fact a limiting factor for multiscale materials screenings to be performed consistently and fully *in silico*. Some of the macroscopic properties required for process modeling, such as diffusion in macropores, can be constructed using appropriate, well-established theories and models. For other data however, some assumptions have to be made. In order to be able to compare different material rankings consistently, similar assumptions for implementation of the models and estimation of input parameters should be made. Recent studies have probed the influence of some of these assumptions on the actual process performance predictions and are discussed in section 8.3.

The next important question here concerns the reliability of material rankings produced by the multiscale screening workflows. Can these workflows realistically predict relative performance of high-performing material candidates, which are then going to be tested and used in real applications? How accurate such predictions are when compared against lab- or pilot-scale experiments? How big is the error in the final predictions, and how must propagation of such errors be understood? All of these questions will be discussed in sections 8.4 and 8.5.

Finally in section 8.6, we will discuss the efficiency of process optimization techniques for comprehensive screening of
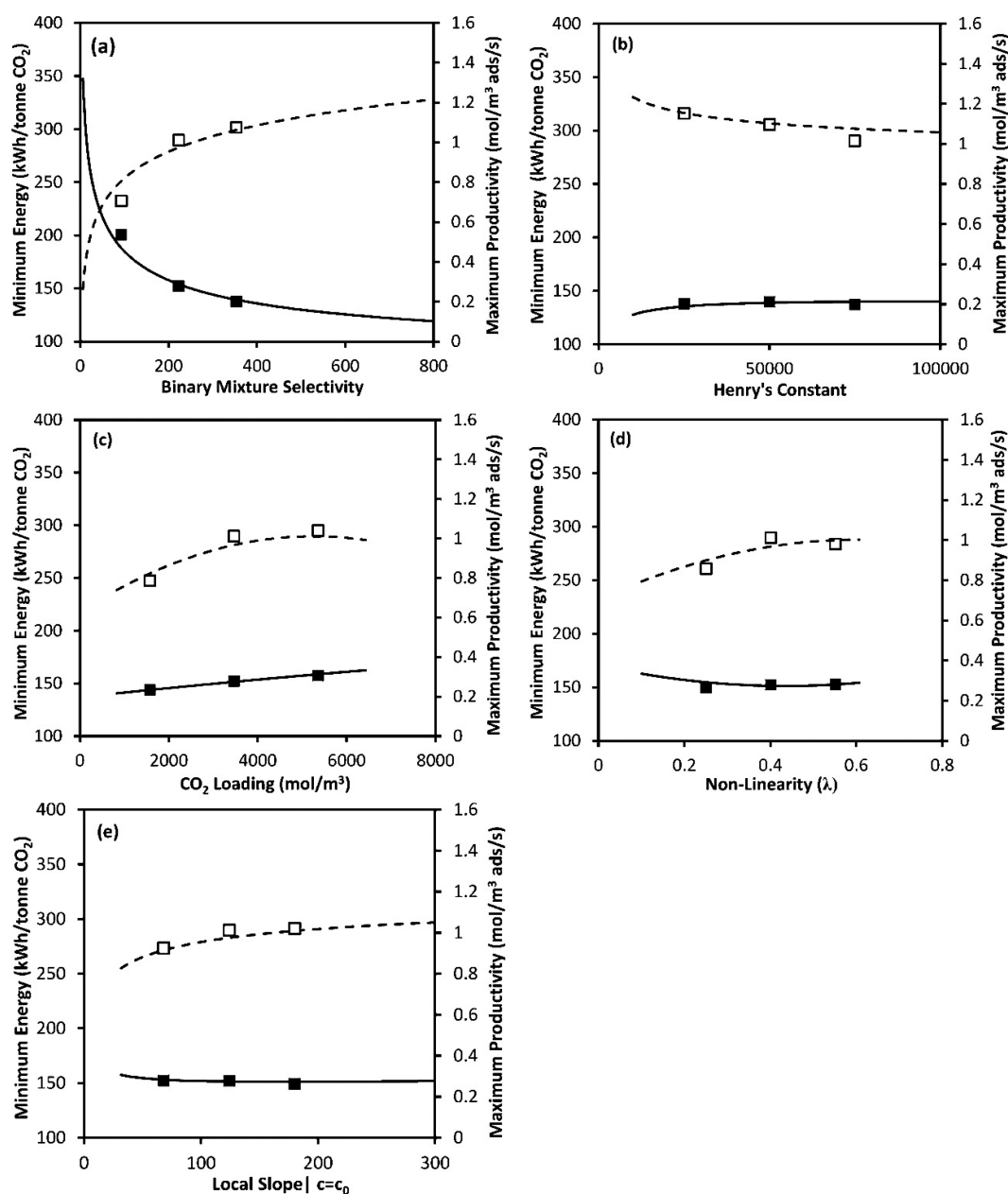
Figure 20. Variation of minimum energy penalty and maximum productivity in a 4-step VSA-LPP process with respect to different isotherm characteristics. The symbols (closed symbols for minimum energy and open symbols for maximum productivity) are associated with the results of detailed process modeling and optimization, and lines (continuous lines for minimum energy and dashed lines for maximum productivity) represent the predictions from a meta-model, which is discussed in the original publication. Reprinted with permission from Khurana and Farooq.[88] Copyright 2016 American Chemical Society.

materials space, and outline some of the challenges associated with screening of unconventional adsorbents.

8.1. Accuracy and Transferability of the Molecular Force Fields

Accurate adsorption equilibrium models are the basis for equilibrium driven separations, such as those considered here for postcombustion carbon capture. From the perspective of a process modeler, the most immediate advantage of having access to accurate molecular simulation tools is gained by having the ability to predict multicomponent adsorption equilibria. This requires force fields for the mixture constituents that are validated against pure component adsorption data of good quality. As discussed in section 6.2.5 about force fields, van der

Waals and electrostatic interactions are two important classes of molecular interactions that are relevant to adsorption and diffusion phenomena. It was also noted that the ability of molecular simulations to correctly predict adsorption behavior is limited by the ability of force fields to correctly model these interactions. In this section, we highlight the existing issues around accuracy of molecular force fields for predicting adsorption isotherms and emphasize the need for consistent implementation of them in multiscale workflows for materials screening.

8.1.1. van der Waals Interactions. An important concern regarding the use of molecular force fields is availability and transferability of model parameters for calculation of van der Waals interactions (e.g., Lennard-Jones parameters). Currently
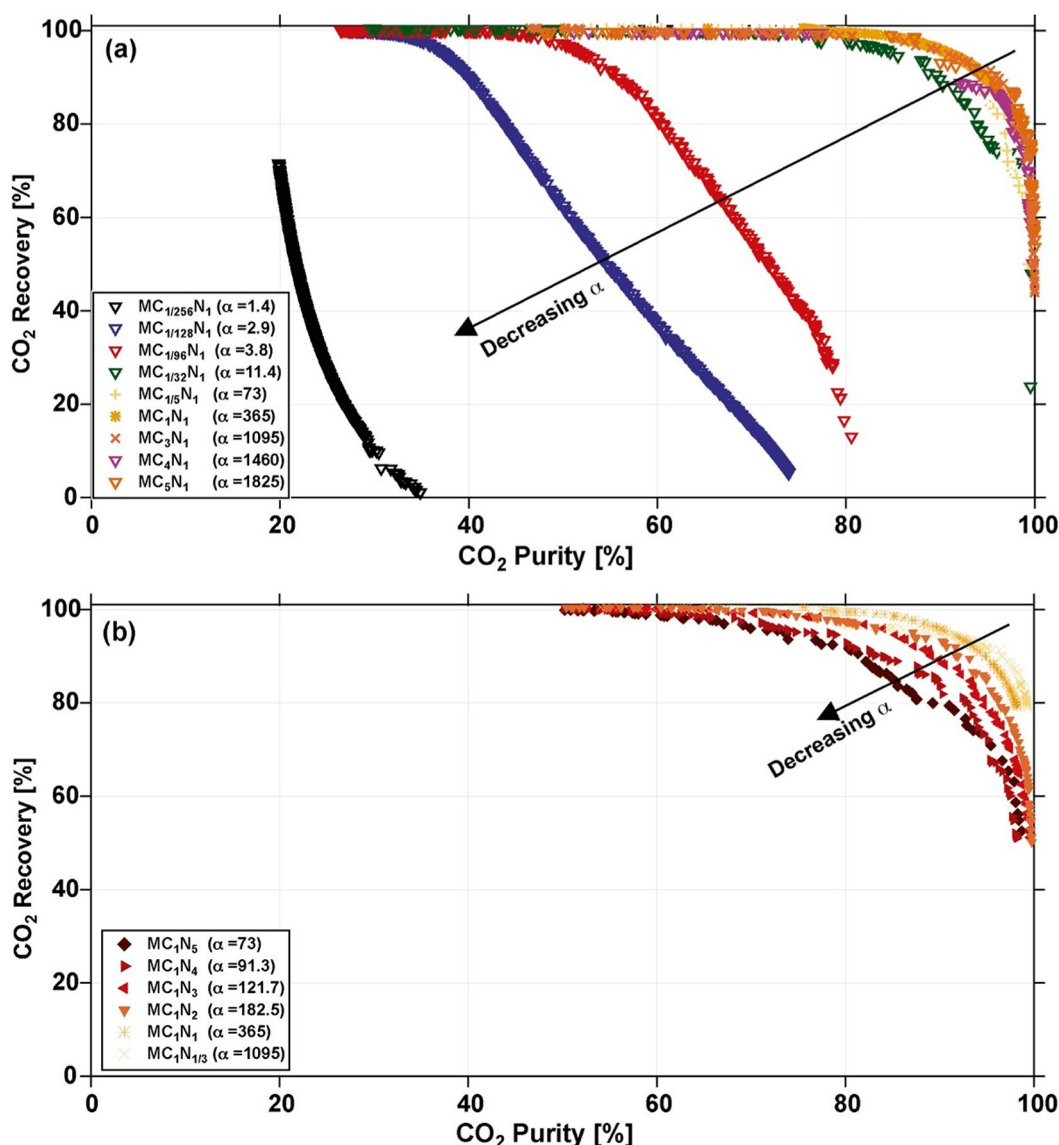
Figure 21. Purity and recovery Pareto fronts for different hypothetical adsorbents (MC_cN_n) with fixed N_2 isotherm (a) and fixed CO_2 isotherm (b). MC_1N_1 represents zeolite 13X as a reference material, α is binary selectivity of CO_2/N_2 for each material, and ratio of c/n is equal to selectivity of MC_cN_n normalized by selectivity of zeolite 13X ($\alpha_{13X} = 365$). Reprinted with permission from Rajagopalan and Rajendran.[423] Copyright 2018 Elsevier.

and for practical reasons, high-throughput screening of large materials databases heavily relies on the use of generic force fields that are commonly used for framework atoms.[76−78,86,93,99,153,427] As mentioned before, the most commonly used generic force fields include DREIDING,[280] UFF,[277] and OPLS-AA.[428] Despite their widespread use, generic force fields fail to accurately reproduce experimental adsorption data in many cases[429−431] particularly for gas adsorption in MOFs with coordinatively unsaturated metal sites.[305,310,432] Even for the systems where generic force fields are deemed suitable, prediction of experimental adsorption isotherms is rather qualitative in which simulated isotherms only capture the general shape of their experimental counterparts.[433−436] Therefore, the use of generic force fields for screening of large and diverse databases of porous materials should be approached with caution. These issues have been raised in several excellent studies in the past.[433,437,438] In fact, many groups have already started to develop specialized force fields for challenging systems

such as those involving adsorption of water[431,439] or MOFs containing open metal sites.[306−310]

At this point, it is also useful to reflect on what is considered to be "good agreement" between a simulated adsorption isotherm and experimental data, as this terminology can mean different things for a molecular modeler and a process modeler. While correctly reproducing the overall shape of the isotherm may seem a good achievement in molecular simulations (particularly for challenging cases such as water or other polar species), in process modeling, accurate estimation of Henry's constant, nonlinearity, saturation capacity, and other quantitative features of the adsorption data are important, considering they will impact separation performance of adsorbent materials at the process level (i.e., their energy−productivity or purity−recovery Pareto fronts). An illustrative example here is provided by Khurana and Farooq[88] where the influence of isotherm characteristics on minimum energy penalty and maximum productivity of a 4-step VSA-LPP cycle is demonstrated (Figure 20).

As shown in this figure, both minimum energy penalty and productivity of the process are highly sensitive to variation of binary mixture selectivity. For the case studied here, the local slope, nonlinearity, and Henry's constant of CO_2 isotherms seem to have rather small effects on the minimum energy and maximum productivity of the process. Nevertheless, one should consider these results with caution because in the above example only one isotherm characteristic has been allowed to vary for each case, while other isotherm characteristics are held constant. In reality, it is not rare to see GCMC simulated isotherms that do not adequately reproduce multiple characteristics of experimental adsorption isotherm; hence the combined effect on the performance of the material at the process level will be larger than what is shown in the above figure. Finally, the effect of isotherm characteristics of nitrogen is not considered in the analysis provided in Figure 20 (i.e., this figure is only related to characteristics of CO_2 adsorption isotherm).

While molecular simulations often focus on the behavior of a single component of interest (CO_2 in carbon capture), in process modeling, it is recognized that the separation performance depends on the behavior of the mixture and accurate equilibrium data for all components is important. Several studies have shown that adsorption of nitrogen plays a significant role in separation performance of the PSA and VSA processes for postcombustion carbon capture.[16,88,89,93,118,124,125,423] In fact, an important concern regarding the quality of available force fields is associated with the role of nitrogen in process simulation. To date, significant efforts have been made to develop more reliable force fields for adsorption of CO_2; however, the impact of other components in the flue gas mixture has been somehow overlooked. A quick review in the literature shows that specialized QM-derived force fields for nitrogen adsorption are scarce,[304,440,441] although the accuracy of generic force fields for prediction of nitrogen adsorption is not satisfactory for many materials. Some examples of this include adsorption of nitrogen in STT, CHA all silica zeolites,[442] FAU and MFI type zeolites with different Si/Al ratios,[89,442] Mg-MOF-74[304] and Ni-MOF-74,[122] ZIF-68,[443] Zn-MOF, and Cu-BTC.[444]

From a process simulation perspective, it is the nitrogen adsorption behavior that most significantly determines whether the process can produce CO_2 with 95% purity and 90% recovery.[16,93,124,423] A recent study by Rajagopalan and Rajendran[423] has clearly demonstrated that purity—recovery Pareto fronts obtained using a 4-step VSA-LPP cycle for separation of CO_2 and N_2 are very sensitive to variation of nitrogen adsorption. This observation is illustrated in Figure 21.

As shown here, reducing selectivity by more than 160 times (from 1825 to 11.4) through changing CO_2 adsorption isotherms, while N_2 isotherm is held constant (Figure 21a) has less impact on purity and recovery of the process compared to the case where selectivity is reduced only by 15 times (from 1095 to 73) through changing N_2 adsorption isotherm, while CO_2 isotherm is fixed (Figure 21b).[423]

In a separate study from Leperi et al.,[93] it was shown that heat of adsorption of nitrogen plays a crucial role on the maximum CO_2 purity that can be achieved in a fractionated vacuum pressure swing adsorption (FVPSA) cycle. It was shown that if N_2 heat of adsorption is greater than 16 kJ/mol, the process cannot produce CO_2 with 90% purity.[93] This is illustrated in Figure 22.

Even for those materials that meet 95%—90% targets for purity and recovery of CO_2, inaccurate prediction of N_2
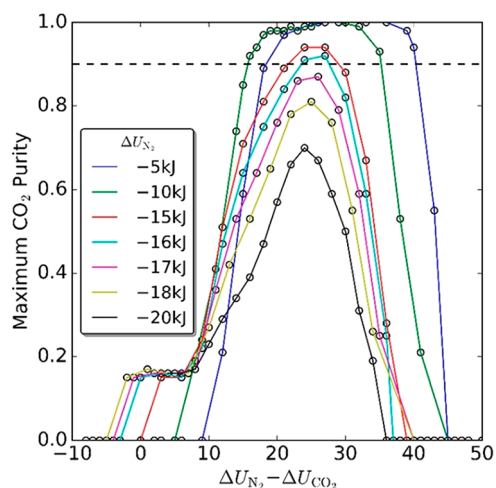

Figure 22. Optimal heats of adsorption for the FVPSA cycle using a generic adsorbent with density of 1.1 g/cm³. Each point represents the highest CO_2 purity that can be achieved while recovering 90% of CO_2. Each line depicts a different N_2 internal energy of adsorption. The dashed horizontal line is CO_2 purity of 90%. Reprinted with permission from Leperi et al.[93] Copyright 2019 American Chemical Society.

adsorption data is shown to affect energy and productivity of the process.[89] These observations in turn highlight the importance of having access to accurate molecular force fields for realistic prediction of nitrogen adsorption data using molecular simulations, a topic whose importance has been overlooked so far. Force field development for nitrogen is, however, a challenging task for two related reasons. Initially, one would consider QM methods to develop a detailed picture on the potential energy surface for nitrogen in various porous materials including MOFs, in a similar fashion that has been done for several CO_2—MOF systems. What is important to remember is that nitrogen is a weakly adsorbing component (heat of adsorption 10—20 kJ/mol, but likely to be closer to 10—12 kJ/mol). Relative error in QM estimates of energy of binding is likely to have a much stronger impact on nitrogen adsorption than on stronger adsorbing carbon dioxide. For a similar reason, the uncertainty in the experimental adsorption isotherms of nitrogen (which are used for validation of QM-based force fields) is also greater, considering the amount adsorbed tends to be much smaller for N_2 compared to CO_2 under the conditions of interest.

8.1.2. Electrostatic Interactions. As mentioned in section 6.2.5, there are several computational schemes to assign partial charges to the atoms of porous materials. The overwhelming majority of material databases constructed so far do not include partial atomic charges, and there is no universal agreement in the scientific community on what scheme should be adopted to assign these charges. The effect of framework atomic charges on gas adsorption has already been demonstrated in several studies.[285,445] It was shown that application of different charge calculation schemes in molecular simulation can lead to substantial variation in the adsorption data.[285,445] For example, Sladekova et al.[285] have compared adsorption isotherms of carbon dioxide and water in several MOFs using different sets of partial atomic charges, which were obtained from different charge calculation methods such as DDEC,[282] ChelpG,[283] LoProp,[446] EQeq,[113] and REPEAT.[114] As shown in Figure 23, the use of various charge calculation schemes can lead to significantly different adsorption behavior of CO_2 and water in
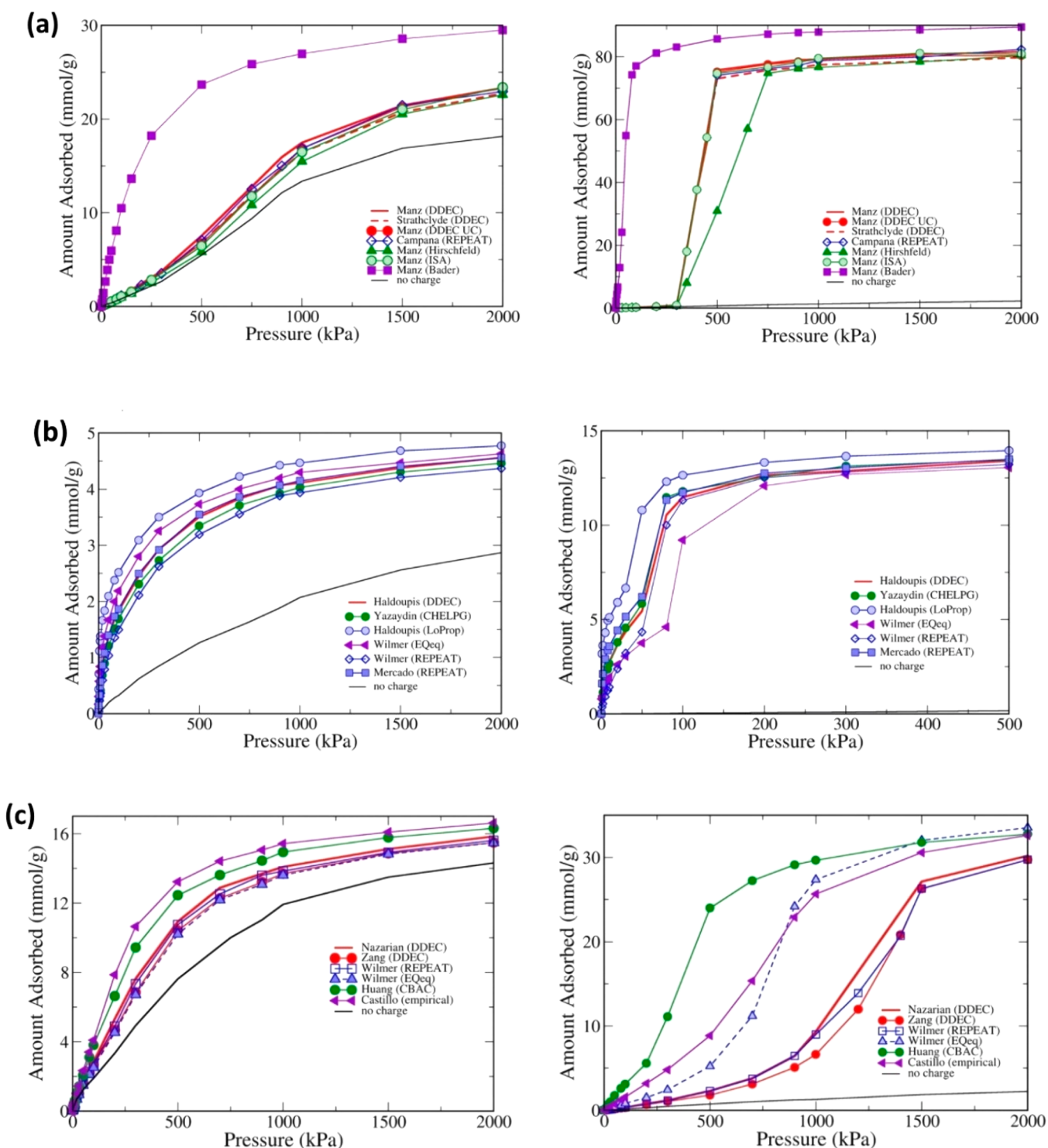
Figure 23. Adsorption isotherms of CO_2 and water in IRMOF-1 (a), Co-MOF-74 (b), and Cu-BTC (c) as obtained from different charge calculation schemes. Reprinted with permission from Sladekova et al.[285] Copyright 2020 Springer Nature.

these materials. This in turn will have a profound impact on separation performance of these materials at the process level. As we previously mentioned, the flue gas contains water, and if we wished to include water adsorption in the process model, obtaining accurate equilibrium data from molecular simulations would be challenging.

Li et al.[78] provide another good example for the use of two different charge calculation techniques for screening of MOFs for CO_2 capture in the presence of water. They use the extended charge equilibration (EQeq)[113] and the REPEAT[114] methods to compute atomic partial charges of porous frameworks for adsorption of CO_2/H_2O and $CO_2/H_2O/N_2$ mixtures in a large group of MOFs, which were selected from the CoRE-MOF database. It was demonstrated that water adsorption behavior can be greatly influenced by the choice of methods used for calculation of electrostatic interactions.[78] This is evident in Figure 24, which compares CO_2/H_2O selectivities of various

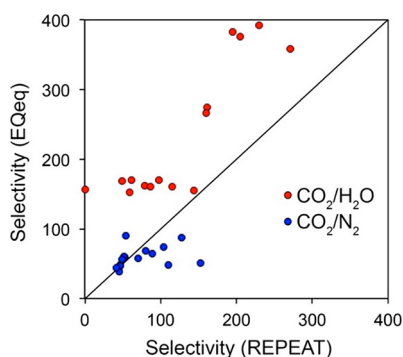MOFs based on two different sets of partial charges obtained from EQeq and REPEAT methods.

Figure 24. Comparison between the Henry selectivities obtained for the structures with EQeq partial atomic charges (y-axis) and REPEAT partial atomic charges (x-axis). Red circles are related to CO_2/H_2O selectivity, and blue circles are associated with CO_2/N_2 selectivity. Reprinted with permission from Li et al.[78] Copyright 2016 American Chemical Society.

In a more recent study, Altintas and Keskin[447] discussed the role of partial charge assignment methods in high-throughput screening of MOFs for CO_2/CH_4 separation. They employed a quantum-based density-derived electrostatic and chemical charge method (DDEC)[282] and an approximate charge equilibration method (Qeq)[158] to predict adsorption of CO_2/CH_4 mixtures in 1500 MOFs. The authors demonstrate that gas uptake, working capacity, selectivity, adsorption performance score (APS), and regenerability of MOFs vary considerably depending on the charge assignment methods used in molecular simulations, as shown in Figures 25 and 26.[447] The authors also report that the rankings of the best-performing MOFs are also different depending on the method used for charge calculations.[447]

The fact that application of different charge calculation schemes in molecular simulations can lead to very different results in prediction of adsorption properties (as shown by a number of studies discussed in this section) suggests that none of these methods can actually reproduce the electron density of real materials very accurately. As previously discussed in section 6.2.5, point charges are not experimentally observable properties and different charge assignment methods are only approximate techniques to mimic the actual electron density of porous solids. Having said that, various studies have demonstrated that techniques such as REPEAT and DDEC are more reliable or at least can reproduce experimental adsorption data more consistently.[284,285] Therefore, these methods should be preferably used in application to screening of porous materials.

8.2. Availability and Reproducibility of the Experimental Adsorption Data

To develop molecular force fields we need experimental adsorption data. While reproducibility of computational studies is generally expected and is easier to achieve (as long as the details of the models and computer codes are provided), ensuring replicability of the data obtained from experimental measurements is more challenging. Two research groups measuring the same adsorption data on the same material and under the same conditions may produce different adsorption isotherms. This is often associated with the two samples of the same material having different properties, different activation
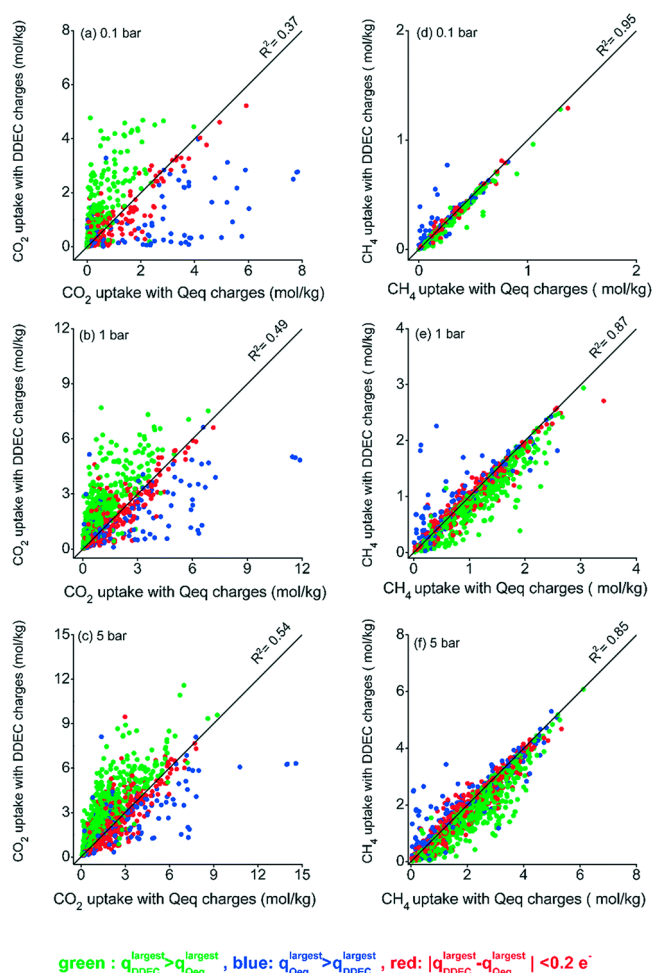

Figure 25. CO_2 (a–c) and CH_4 (d–f) uptake obtained from simulations using Qeq and DDEC charges at 0.1, 1.0, and 5.0 bar for the 10%–90% CO_2/CH_4 mixture. Reprinted with permission from Altintas and Keskin.[447] Copyright 2020 Royal Society of Chemistry.

procedures involved, accuracy of the equipment used, and errors of the measurements. Now, the question is which data should be used for the development and validation of molecular models in such cases? This is a principal question for the implementation of multiscale screening workflows, as the ultimate performance of the materials depends on the adsorption data against which the models are calibrated.

Although a number of general recommendations have been made to improve reproducibility of data in scientific research,[448−452] recent observations have raised many concerns about reproducibility of experimental measurements in materials-oriented research especially in the areas of materials synthesis and adsorption measurements.[453,454]

An interesting study from Agrawal et al.[454] has recently explored the reproducibility of 130 experimentally synthesized MOFs from the CoRE-MOF database.[151] The authors analyzed literature metadata of more than 4300 papers and demonstrated that only a small fraction of the above materials have been resynthesized repeatedly. Analysis of BET surface area of these materials demonstrated large variability indicating significant structural differences of the resynthesized materials. This observation is attested in Figure 27.

This figure demonstrates variation of experimentally measured BET surface area for six MOFs whose replicate synthesis
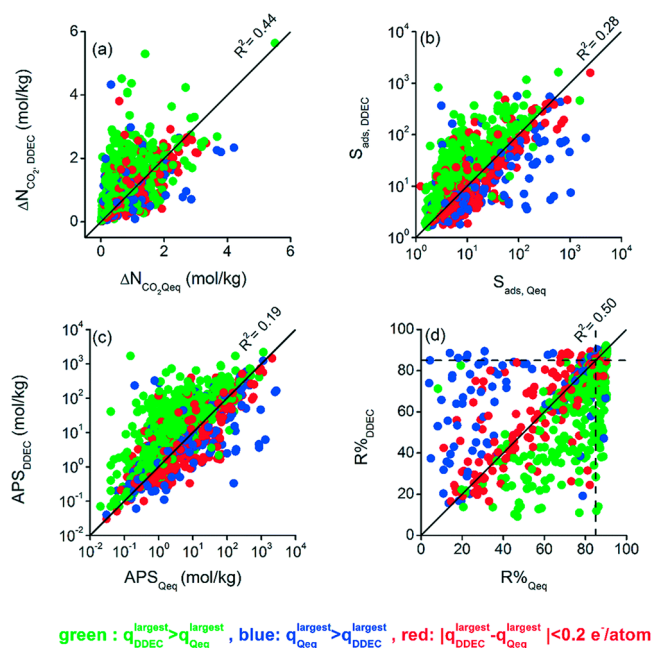
green : $q_{DDEC}^{largest} > q_{Qeq}^{largest}$, blue: $q_{Qeq}^{largest} > q_{DDEC}^{largest}$, red: $|q_{DDEC}^{largest} - q_{Qeq}^{largest}| < 0.2$ e$^-$/atom

Figure 26. Calculated adsorbent performance evaluation metrics using Qeq and DDEC charges under VSA conditions at 298 K for 10%−90% CO_2/CH_4 mixture: (a) CO_2 working capacity, (b) selectivity, (c) adsorbent performance score, and (d) regenerability. Reprinted with permission from Altintas and Keskin.[447] Copyright 2020 Royal Society of Chemistry.

has been reported more frequently among the materials studied by the authors. Wide distribution of BET surface area implies significant structural differences between the synthesized samples especially once we remember that this parameter is highly correlated with pore volume of the material.[454] The above irreproducibility of structural properties could be due to many

factors including exposure of the samples to moisture, degradation, incomplete removal of solvents, and so on.[454]

Round robin testing and investigation of literature metadata have provided even more evidence for large variabilities of adsorption measurement data.[453,455−462] Two recent studies conducted by Sholl and co-workers particularly provide useful insights into the scale of the reproducibility problem in this area.[457,458] In one example, Park et al.[458] examined thousands of experimental adsorption isotherms reported in the NIST/ ARPA-E Adsorption Database[463] and collected all CO_2 adsorption isotherms for MOFs. First of all, they found that even for the widely studied case of CO_2 adsorption, there are only 15 MOFs with adequate replicates in the literature that can be used in a reproducibility test. More importantly, the authors showed that from all the isotherms analyzed, more than one in five (i.e., 21%) were not consistent with other reported data for the same adsorbent at the same temperature and hence must be classified as outliers. A reproducibility map for all CO_2 isotherms analyzed in this study is provided in Figure 28.

In this figure, MOFs for which the strongest conclusions about their reproducibility can be made are located further to the right, and MOFs with the smallest number of outliers are located at the top. The font size implies the number of independent measurements that are available after removing outliers.[458]

In a similar study, Bingel et al.[457] analyzed reproducibility of 510 experimental adsorption isotherms for alcohols in 176 adsorbents including MOFS and zeolites as reported in NIST/ ARPA-E Adsorption Database.[463] The results from this study demonstrate that despite numerous examples of alcohol adsorption isotherms in the literature, there are only a small number of them that have been replicated independently and hence can be used for reproducibility analyses. These results also suggest that almost 20% of all adsorption isotherms for alcohol must be classified as outliers. Interestingly, this value is very similar to the fraction of outliers identified for adsorption of CO_2
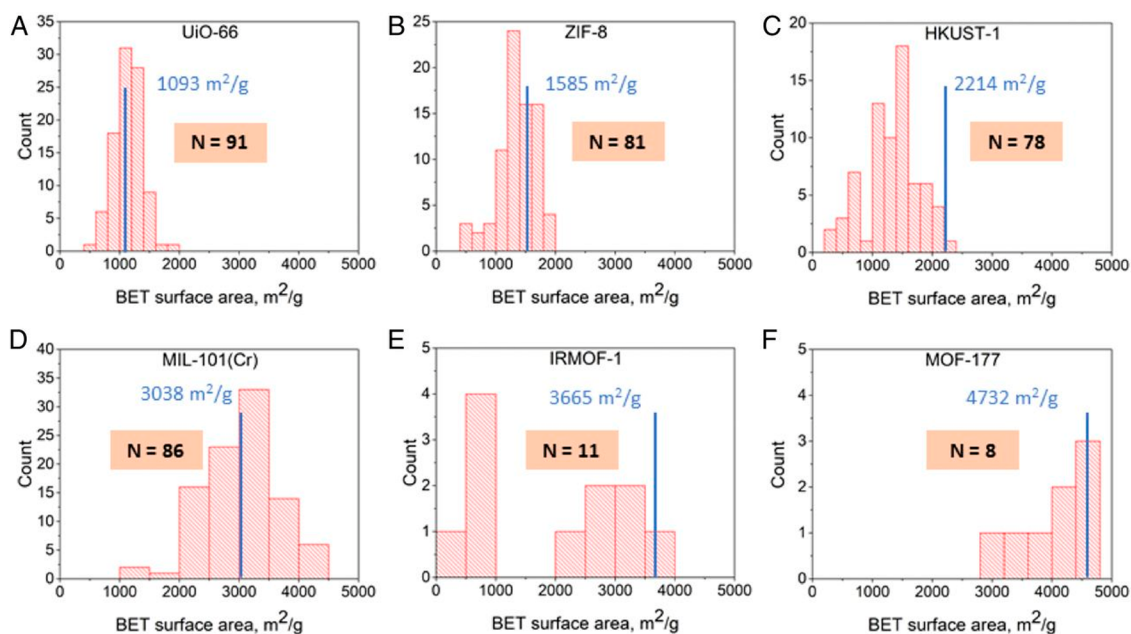
Figure 27. Distribution of experimentally reported BET surface areas for UiO-66, ZIF-8, HKUST-1, MIL-101(Cr), IRMOF-1, and MOF-177. Here, N denotes the number of reported surface areas for each material. Computationally calculated values of surface area for defect-free/cleaned crystal structures is shown by a vertical blue line and text for each material. Reprinted with permission from Agrawal et al.[454] Copyright 2020 National Academy of Sciences.
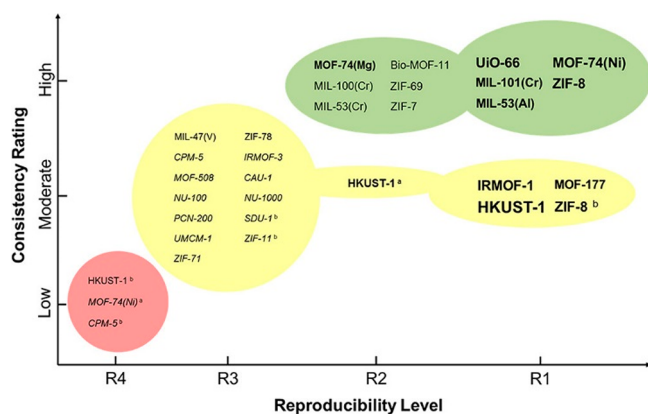
Figure 28. Reproducibility map of experimental CO_2 adsorption isotherms in MOFs. The definitions of reproducibility level and consistency rating can be found in the original article. Outlier levels are indicated by the font size. Most of the isotherms are measured at 298 ± 5 K except for data at 313 ± 5 K (superscript a) and 273 ± 5 K (superscript b). Reprinted with permission from Park et al.[458] Copyright 2017 American Chemical Society.

in MOFs as reported by Park et al.[458] In addition to that, the authors observed considerable variability in the adsorbed amounts even for materials that are not considered as outliers.[457] Figure 29 depicts the reproducibility map of alcohol isotherm in various porous materials. As shown here, 42 out of 61 systems analyzed by the authors were only moderately consistent (R3).
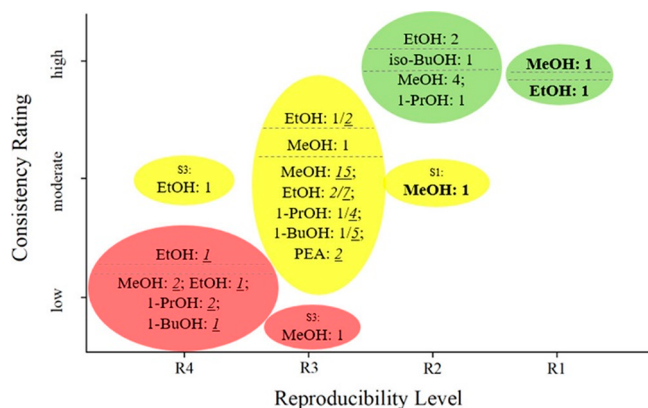

Figure 29. Reproducibility map of experimental adsorption isotherms for alcohols in different porous materials. The numbers indicate the quantity of systems for the given molecule that were classified at the corresponding consistency and reproducibility level. The distinction between the different outlier levels is provided by different type of fonts (O1, bold; O2, regular; and O3, italic underlined). The replicate strength decreases from S1 (top) to S3 (bottom) within ovals with different strengths. The definitions of reproducibility (R) and outlier (O) levels, consistency rating, and replicate strength (S) can be found in the original article. Reprinted with permission from Bingel et al.[457] Copyright 2020 American Chemical Society.

Analysis of literature metadata for mixture adsorption measurements also conveys the same picture about availability of replicate data and reproducibility of experimental adsorption isotherms.[464] Recently, Cai et al.[464] analyzed a collection of 900 gas mixture experiments consisting of 125 different binary mixtures, 60 different adsorbates, and 333 different porous materials as adsorbent and showed that the number of replicate experiments for which adsorption was measured independently

at similar temperatures, pressures, and compositions for a given binary mixture and adsorbent is very scarce.

To summarize, the picture that starts to emerge from the studies discussed in this section about the extent of the irreproducibility of experimental adsorption measurements is alerting. Now, we know that a non-negligible portion of experimental adsorption data reported in the literature is not reproducible. Moreover, even if we decide to cross check the reproducibility of the available data by comparing them against similar measurements, there is not enough replicate data in the literature to allow sufficient checks. These observations have important implications for the materials screening community especially for modelers who use experimental adsorption isotherms for validation of atomic force fields and simulated isotherms. They also emphasize the need for implementation of a series of recommendations[453] especially aimed at experimental research to enhance reproducibility and quality of adsorption measurements.

8.3. Data Availability and Consistent Implementation of Multiscale Screening Workflows

As briefly mentioned in the introduction part of this section, there are several parameters that are required for process modeling but are not available in the literature or from classical molecular simulations. We also need to make certain assumptions for implementation of various models across the simulation workflow. All of these are important for consistent comparison of materials rankings. In this section, we probe the influence of some of these parameters and model assumptions on the actual performance of the process.

8.3.1. Heat Capacity of the Adsorbents. Traditionally, it has been assumed that heat effects play a secondary role in the adsorption column and will not significantly influence the performance of the process or ranking of the material. Adsorbent heat capacity is also a property scarcely measured or available for the new classes of porous materials, such as MOFs. Therefore, as a pragmatic approach, some studies have assumed the heat capacity of all adsorbents to be equal to the heat capacity of a reference material, such as zeolite 13X.[88,116] Nevertheless, a recent preliminary sensitivity study of the influence of this parameter painted a somewhat different picture.[122] As shown in Figure 30, performance of Cu-BTC with the value of the heat capacity equal to that of reference zeolite 13X was considerably different from the performance of the same material using its actual experimental value for this property.[122]

Recently, Danaci et al.[125] have also analyzed sensitivity of three process-level performance indicators, namely, purity, recovery, and capture cost to variation of specific heat capacity for Mg-MOF-74 and UTSA-16 using a 0-dimensional equilibrium-based PVSA model. As shown in Figure 31, all of the above indicators show considerable sensitivity to variation of specific heat capacity for Mg-MOF-74. For UTSA-16 however, the sensitivity to variation of heat capacity is negligible.

Therefore, it seems for a diverse group of porous materials (MOFs, zeolites), it would be prudent to procure more heat capacity data, explore the heat effects in more details, and use more accurate values of C_p in process modeling. How can this be accomplished in purely *in silico* workflows? With some compromise, we can use empirical group contribution methods where heat capacity of an adsorbent is estimated by summing the molar fraction contributions of its functional groups (e.g., metal nodes and organic ligands in MOFs).[125,465,466] Kloutse et al.[466] have recently calculated specific heat capacities of MOF-5, Cu-
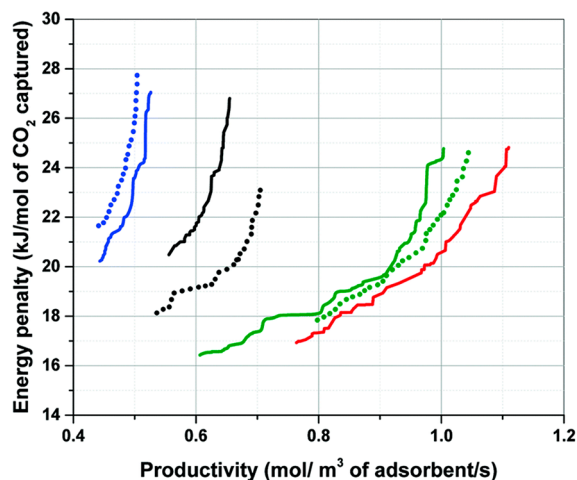
Figure 30. Effect of specific heat capacity (C_p) on position of the Pareto fronts for Cu-BTC (black), Ni-MOF-74 (green), silicalite-1 (blue), and zeolite 13X (red) obtained from optimization of a 4-step VSA−LPP cycle. Dashed lines illustrate a case where experimental C_p of each material is used for process simulations. Solid lines represent another case where C_p for all materials is assumed to equal 920 J·kg^{-1}·K^{-1}. Reprinted with permission from Farmahini et al.[122] Copyright 2020 Royal Society of Chemistry.

BTC, Fe-BTC, MOF-177, and MIL-53 (Al) at a single temperature (323 K) using this method. The results are compared with experimental heat capacity data showing relative difference errors between 2.58% and 14.77%.[466] Nevertheless, in the absence of experimental data for many porous adsorbents, the results from this method should be considered with caution especially for flexible materials such as MOFs. As correctly pointed out by Danaci et al.,[125] the group contribution method for calculation of heat capacity does not take into account the contribution of vibrational modes of crystalline materials. This will lead to underestimation of the heat capacity. In contrast, atomic vibrations of ligands may be reduced upon coordination, which is due to the loss of some degrees of freedom. This is also not considered in the group contribution method, resulting in overestimation of the heat capacity.[125] To fully evaluate reliability of the group contribution method, a separate computational study is needed to investigate the relative contributions of these factors for a range of different materials including MOFs.

An alternative technique for estimation of heat capacity while taking into account the vibrational modes of the structure is the so-called phonon analysis method.[323,324,467,468] Togo and Tanaka[469] have accurately estimated specific heat capacity of aluminum lattice using the quasi-harmonic approximation (QHA) in the context of first-principles phonon calculations. This approach was later expanded to a large group of inorganic solid crystals by Nath et al.[467] who could reliably predict thermal properties of these materials. Figure 32 demonstrates the results obtained by Nath et al.[467] for a set of inorganic solid crystals showing a maximum of 20% error in prediction of experimental heat capacity data.

Analysis of phonon properties of porous solids often requires time-consuming quantum mechanical calculations to capture the full range of harmonic/anharmonic behaviors that are pertinent to thermal properties of these materials.[468,470] At the same time, the use of QM-based methods is not affordable for routine screening of large groups of materials. One way forward would be the development of transferable force fields that are
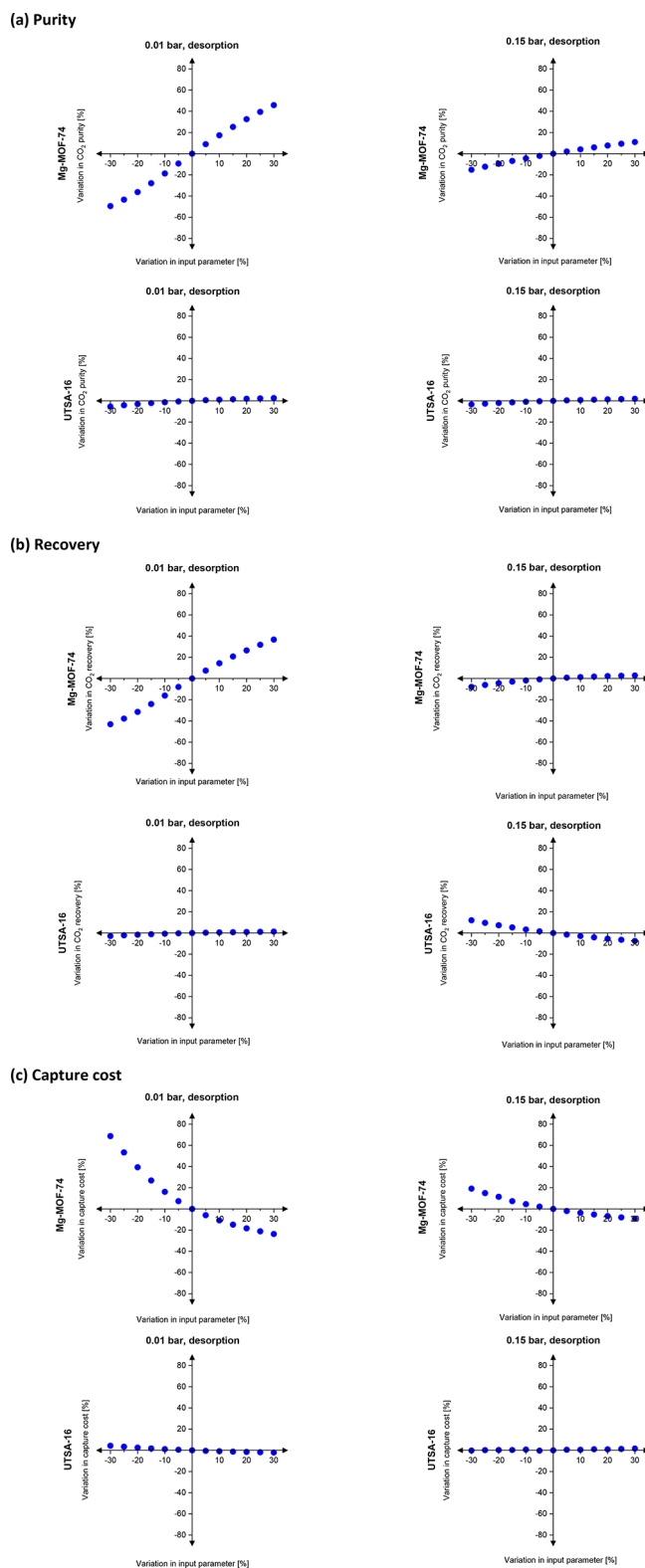
Figure 31. Sensitivity analysis of purity (a), recovery (b), and capture cost (c) to variation of heat capacity for Mg-MOF-74 and UTSA-16 at 0.01 and 0.15 bar desorption pressure in a PVSA process. Reproduced with permission from Danaci et al.[125] Copyright 2020 Royal Society of Chemistry.

especially tuned to reproduce lattice dynamics of porous solids. These force fields can be affordably used in classical simulations for calculation of heat capacity. An example of such force fields
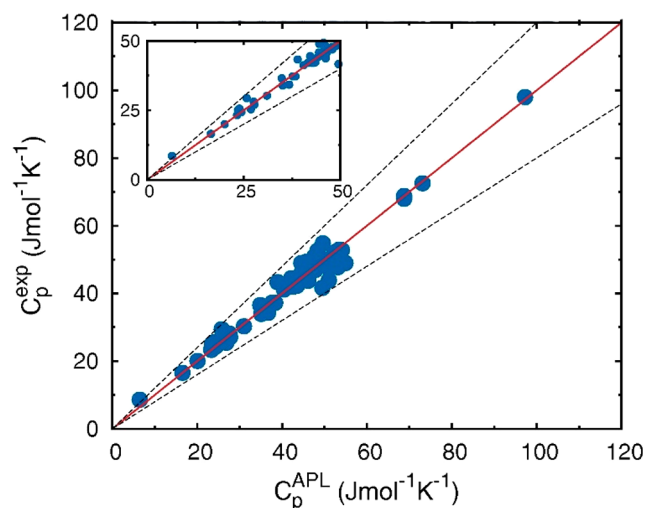
Figure 32. Comparison of experimental and predicted values of specific heat capacity, C_p for a selected set of inorganic solid crystals. The dashed black lines represent ±20% error. Reprinted with permission from Nath et al.[467] Copyright 2016 Elsevier.

Figure 33. Pareto fronts of Cu-BTC (black triangle), Ni-MOF-74 (green square), silicalite-1 (blue circle), and zeolite 13X (red diamond) obtained using fixed values of pellet size and pellet porosity (solid symbol) and optimized values of pellet size and pellet porosity (open symbol) in process optimization of a 4-step VSA−LPP cycle. Reprinted with permission from Farmahini et al.[122] Copyright 2020 Royal Society of Chemistry.

has been recently developed by Bristow et al.[323,324] for a few MOFs. In this study, the authors show close agreement of specific heat capacity data calculated using the QHA method with the values obtained using the new force field. Unfortunately, due to the lack of reliable experimental data for heat capacity of these MOFs, the values of heat capacity computed in this study were not compared against experiment. As mentioned earlier, there is a huge gap in availability of experimental data for thermal properties of porous materials, which is now considered as a major challenge for validation of any computational technique that seeks to accurately predict these properties.
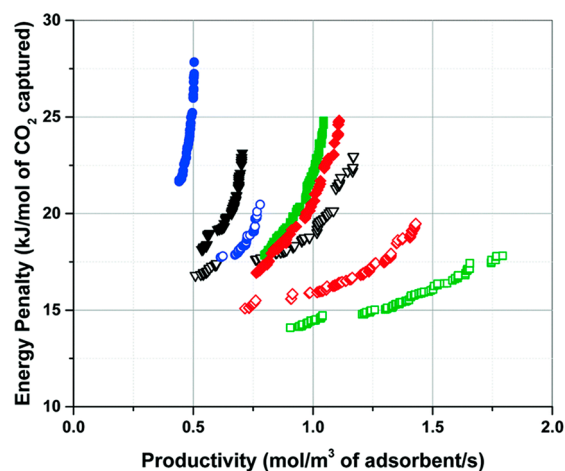
8.3.2. Pellet Size and Pellet Porosity. In the process modeling literature, the values of pellet size and pellet porosity are typically obtained from experiment for a specific sample of the material under consideration. However, for an *in silico* study, these values must be somehow estimated. A pragmatic approach adopted in previous studies has been to use the values available for a reference material (such as zeolite 13X) universally for all the other materials under consideration. However, in the context of the ranking of porous materials, a question can be asked whether optimal performance of a material can be achieved only at specific values of pellet size and pellet porosity (within the range of feasible experimental values)? In this case, shall the ranking be performed under the constraint of specific values of pellet size and porosity or shall these properties also become some optimization parameters? Farmahini et al.[122] have explored these questions in a recent study and observed that depending on the protocol adopted (i.e. pellet size and porosity constrained to some reference values versus being free optimization parameters), performance of the materials as well as the order of the top-performing candidates indeed change.[89,122] This effect is illustrated in Figure 33 for flour materials including Cu-BTC, Ni-MOF-74, silicalite-1 and zeolite 13X.

Therefore, consistent comparison of the materials' performance at the process level must take into account opportunities for the optimization of pellet morphology.

8.3.3. Numerical Models for Adsorption Isotherms. Adsorption models for process simulations are trained on the available experimental or simulation data, and they should be able to give consistent and accurate representation of multi-component adsorption equilibria. This is however not always the case and two different models trained on the same data may give different predictions of the binary (or multicomponent) adsorption equilibria (depending on the training protocols adopted) and hence, process level predictions.[89,471] For example, Farmahini et al.[89] have recently demonstrated that the use of different recipes for fitting adsorption data to the DSL model can affect position of the energy−productivity Pareto fronts obtained from the process optimization. The authors have therefore proposed and validated a rigorous numerical protocol for consistent fitting of the widely used DSL model, in which the choice of temperature range, fitting constraints, and calculation of Henry's constant are standardized.[89] Similarly, several other studies have attempted to establish consistent routines for fitting equilibrium adsorption data;[471−473] nevertheless none of the proposed procedures have been universally adopted by other groups, as a result of which consistency of various materials rankings that have been produced so far remains uncertain. As has been also discussed by Farmahini et al.,[89] the ultimate test of the analytical models used in the process level simulations is their ability to predict binary and multicomponent adsorption data. This can be easily done using molecular simulations, as simulation of multicomponent systems come with relatively small additional effort compared to the simulation of single component systems. Recently, Cai et al.[464] has developed a database of 900 gas mixture adsorption experiments using literature meta-analysis, which will be also very useful for cross validation of the analytical models and the fitting protocols adopted for describing adsorption isotherms. Hence, we propose this validation step to be adopted as a routine practice in the simulation community in order to probe the accuracy of the analytical adsorption models before performing any process simulation.

8.3.4. Consistency between Various Simulation Packages. As mentioned in section 8.2, reproducibility of computational studies is generally expected and perhaps easier to achieve compared to experimental investigations. Whether a computational study is fully reproducible or not largely depends on the
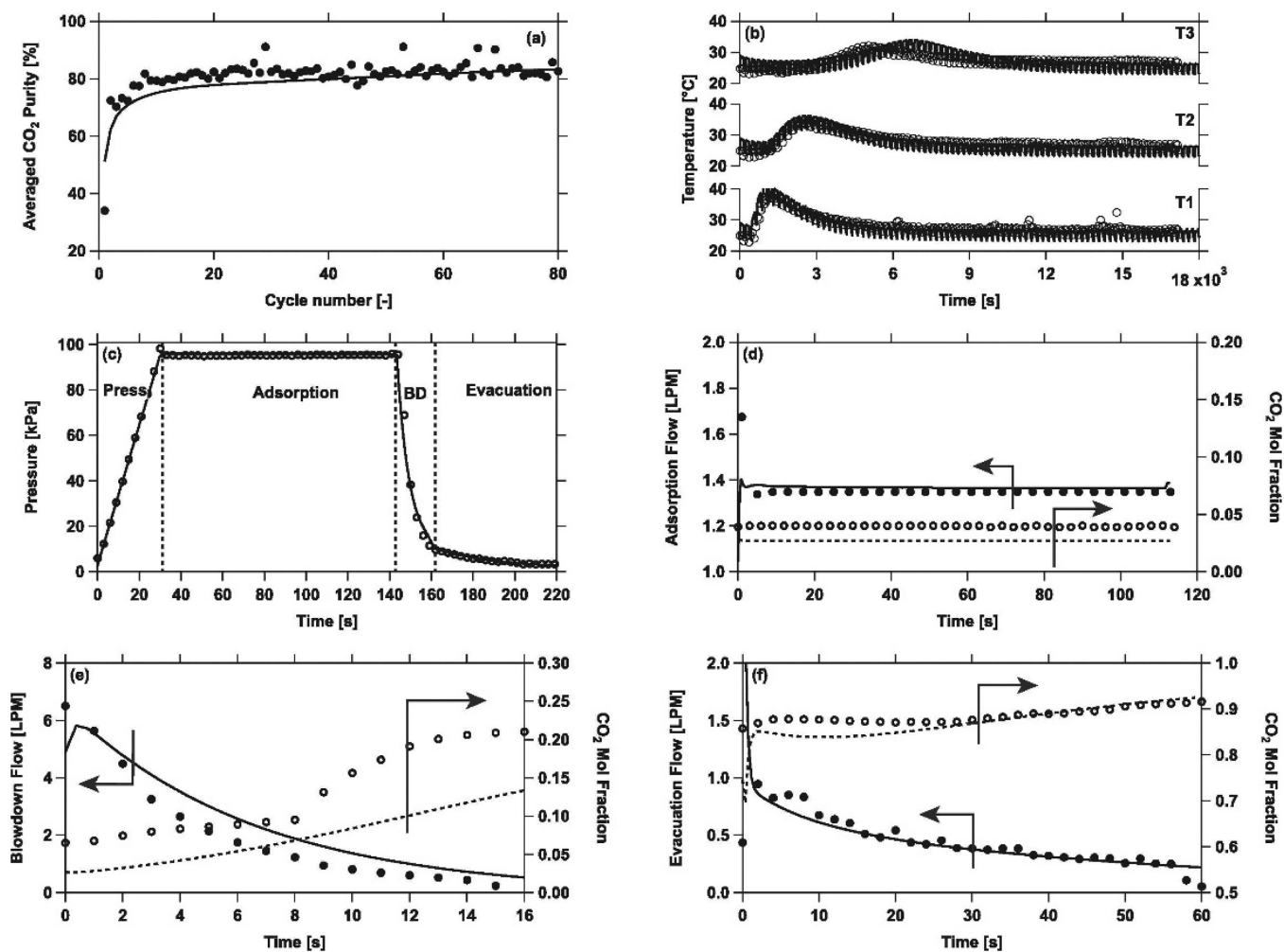
Figure 34. Example of validation of simulated transient histories against experimental data for adsorption of CO_2 and N_2 in zeolite 13X using a basic 4-step VSA cycle. Evolution of CO_2 purity (a), temperature histories at three locations in the column (b), pressure history for one cycle at CSS (c), CO_2 composition and flow rate at the outlet of the adsorption step (d), CO_2 composition and flow rate at the outlet of the blowdown step (e), CO_2 composition and flow rate at the outlet of the evacuation step (f). Symbols represent experimental data and lines indicate numerical simulations. Reprinted with permission from Estupiñan Perez et al.[120] Copyright 2019 Elsevier.

availability of the codes, methods, assumptions, and data. In order to improve reproducibility, replicability, and reusability of computer-based experiments, a set of useful recommendations have been made.[474,475] Unfortunately, not all of these recommendations have been adopted universally.

In the context of computational materials screening, one important aspect in the development of consistent multiscale workflows with reproducible results is having access to widely used and validated open-source software and case studies. As discussed in sections 6.1.2, 6.2.2, and 6.2.4, there are a number of open-source molecular simulation packages for which several benchmark and case studies have been produced.[195,215,263] However, this has not been done for process simulation packages mainly because the majority of these software are not available as open-source. In fact, among all the software introduced in section 6.3.6, only one computer code has been released as open source.[126] As has been shown by the molecular simulation community over the last two decades, access to open-source simulation software and clear case studies has facilitated the development of new generations of computer codes and modeling tools leading to significant advancement of the field of computational materials science. We believe this will be also the case for the process simulation community, and hope that the

current review has been successful in demonstrating the importance of any efforts that can address the current gap.

8.4. Validation of Multiscale Screening Workflows

Despite recent advances in development of more sophisticated multiscale screening workflows, validation of the materials rankings produced by these frameworks is still an outstanding issue. As illustrated throughout this review, multiscale screening workflows have a modular structure in which various computational modules are put together to perform different types of simulations. The simplest multiscale workflow contains three modules in order to perform (1) GCMC simulation, (2) process modeling, and (3) process optimization. This can be further extended, if one decides to include quantum mechanical or MD simulations in the workflow. Normally, results of each module can be validated separately. For example, adsorption isotherms generated using GCMC simulation are routinely compared against equilibrium adsorption data obtained from experiments to ensure the accuracy of the predictions. At the process level, validation tests are conventionally carried out by reproducing column breakthrough curves, or temperature, pressure, and concentration profiles from experiments,[119,120,361,476,477] an

example of which is illustrated in Figure 34 for a basic 4-step VSA cycle.

Efforts for validation of genetic algorithms that are used for multiobjective optimization of PSA and VSA processes are more recent and less widespread. In one recent example, the ability of multiobjective optimization techniques to guide the design of PSA and VSA processes has been shown by Estupiñan Perez et al.[120] In this study, purity and recovery of CO_2 predicted through numerical optimization of a basic 4-step VSA cycle and a 4-step VSA cycle with LPP were replicated by experiment for postcombustion carbon capture using zeolite 13X as adsorbent,[120] which is shown in Figure 35.
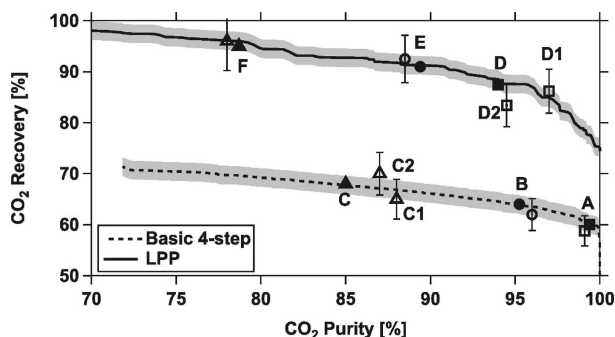

Figure 35. Pareto fronts corresponding to a basic 4-step VSA cycle (dashed line) compared to a 4-step VSA−LPP cycle (solid line). Closed symbols correspond to the optimized set of operating conditions that were implemented in experiment. Open symbols represent the corresponding purity and recovery values obtained from the experiment. The shaded region around the Pareto front denotes the 1.8% confidence region arising due to a 10% uncertainty of selected model inputs. Reprinted with permission from Estupiñan Perez et al.[120] Copyright 2019 Elsevier.

Unfortunately, it was not possible in this study to carry out any measurement to verify total energy consumption of the process against experimental data.[120] A pilot plant study conducted by Krishnamurthy et al.[119] for CO_2 capture using the same 4-step processes with zeolite 13X reported significant discrepancies between theoretical and experimental values of energy consumptions, while their analyses show overall quantitative agreement for purity and recovery and somewhat modest agreement for productivity data (Figure 36).[119]

Other pilot- or lab-scale studies also report reasonable agreement between experimental and theoretical values of purity and recovery at the given feed concentrations for separations of CO_2 using VSA and PSA processes,[417,418] while the discrepancy reported for the total energy consumption is still considerable.[418] This becomes especially crucial, if we remember that energy−productivity Pareto fronts obtained from multiobjective optimization of the process play a central role in performance-based ranking of porous materials. Here, it should be noted that estimation of total energy consumption of the process from simulation is particularly problematic due to the difficulty of including exact characteristics of the valves, heat losses across the system, and the performance at a variable flow rate of the vacuum pumps and compressors.

With the surge in development of machine-learning approaches for modeling and optimization of separation processes, one would also need to consider additional tests for validation of these novel techniques. Some recent studies have reported promising cases where machine-learning based
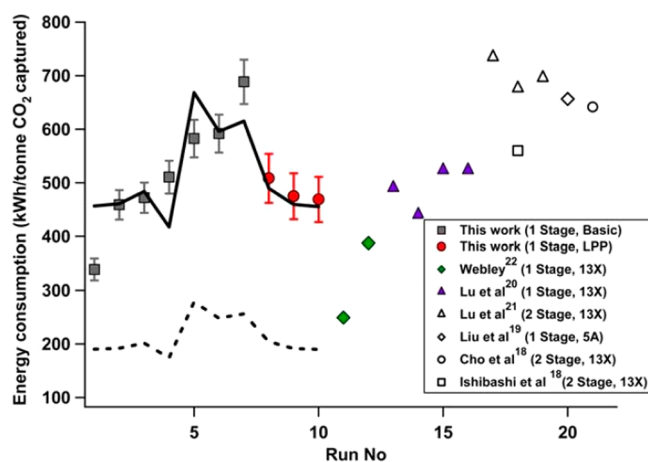

Figure 36. Energy consumption of pilot plant experiments conducted by Krishnamurthy et al.[119] compared with other data extracted from literature. The dotted line represents an efficiency of 72% for the VSA process, while the solid line denotes an efficiency of 30%. Note that all the experiments shown in this figure resulted in different purity−recovery values; thus care should be taken in comparing their corresponding energy values directly (The references in the inset are available from the original publication). Reprinted with permission from Krishnamurthy et al.[119] Copyright 2014 John Wiley and Sons.

surrogate models developed for the optimization of PSA/VSA processes have been validated against Pareto fronts and cyclic steady state (CSS) column profiles that are mainly obtained from detailed process simulations[127,362,366] but some also from lab-scale experiments.[362]

Despite all these efforts for validation of different computational modules of multiscale screening workflows, there is no single material ranking study in which the order of top performing materials has been confirmed experimentally. In fact, unless this final level of validation is achieved, it is unlikely that the top-performing materials proposed by various computational screening studies are going to find their way into any industrial application.

8.5. Sensitivity Analysis and Propagation of Errors

From the studies reviewed so far, it is clear that the overall process performance and ranking of porous materials depend upon calculation of a large group of parameters and model assumptions at both molecular and process level of descriptions (see Table 6). Despite some studies on the sensitivity of process performance to various input parameters and data,[89,122,125,126,423,478] it is yet to be established what level of accuracy is required for the full spectrum of parameters and models to guarantee consistent and comparable ranking of porous materials between different studies. One crucial element of such a study would be the investigation of error propagation from molecular level all the way through to process modeling and optimization. For example, we need to understand how the errors arising from the use of inaccurate molecular force fields in GCMC simulations for prediction of adsorption isotherms are combined with the errors resulting from the use of numerical models for fitting adsorption data and what impact they will have together on the overall performance of the process. Shih et al.[479] have recently employed a hierarchical Bayesian approach to quantify the inconsistency among experimental adsorption data reported in the literature for similar materials. Analogous methods can be also used, for example, to investigate the inconsistency between adsorption isotherms obtained from

Table 10. Ranking of Top 10 Materials Based on Minimum Energy Penalty

index	4-step VSA with LPP[a] (Khurana and Farooq[88])	4-step Skarstrom PSA[b] (Park et al.[94])	4-step VSA with LPP[a] (Subramanian Balashankar and Rajendran[121])	4-step VSA with LPP[a] (Burns et al.[124])	modified Skarstrom[c] (Yancy-Caballero et al.[126])	FVSA[c] (Yancy-Caballero et al.[126])	5-step PSA[c] (Yancy-Caballero et al.[126])
1	h8155527	TASXIW	h8116500	IISERP-MOF2	UTSA-16	UTSA-16	UTSA-16
2	NAB	BIBXUH	h8297545	IGAHED02	zeolite 13X	Cu-TDPAT	Ti-MIL-91
3	UTSA-16	TERFUT	h8210285	XAVQIU01	SIFSIX-3-Ni	zeolite 13X	Cu-TDPAT
4	NaA	FAKLOU	h8180594	YEZFIU	Ti-MIL-91	Ti-MIL-91	zeolite 13X
5	h8124767	MODNIC	h8116694	NaA	Cu-TDPAT	SIFSIX-3-Ni	SIFSIX-3-Ni
6	ZIF-36-FRL	ZESFUY	IZA-WEI	ZIF-36-FRL	Ni-MOF-74	Zn-MOF-74	Zn-MOF-74
7	h8291835	RAXCOK	h8329775	UTSA-16	SIFSIX-2-Cu-i		Mg-MOF-74
8	ZIF-82	SENWIT	IZA-BIK	HUTTIA	Zn-MOF-74		
9	ZIF-78	CUHPUR	ZIF-Im-h8127937	QIFLUO	Mg-MOF-74		
10	ZIF-68	SENWOZ	IZA-MON	GAYFOD			

[a]4-step VSA with LPP using a packed-bed adsorbent system. Feed composition: 15% CO_2/85% N_2 at 298 K. Optimization constraints: 95% CO_2 purity and 90% CO_2 recovery. [b]4-step PSA using a hollow fiber adsorbent model. Feed composition: 14% CO_2/86% N_2 at 243 K. No optimization constraint imposed on purity and recovery. [c]PSA cycles using packed-bed adsorbent system. Feed composition: 15% CO_2/85% N_2 at 313 K. Optimization constraints: 90% CO_2 purity and 90% CO_2 recovery.

molecular simulations using different force fields or calculated from different numerical adsorption models. Sensitivity analysis of the simulated systems should be expanded to contain all sources of errors and uncertainties in the multiscale workflow so that the impact of the combined error on variation of purity−recovery and energy−productivity Pareto fronts can be understood. In this case, separation performance of each material will be represented by a range of Pareto fronts, rather than a single Pareto front. The results from this analysis are likely to change our perspective on what are currently perceived as the top performing candidates for postcombustion carbon capture in VSA and PSA processes.

8.6. Other Challenges

8.6.1. Improving Efficiency of Process Optimization for Comprehensive Screening of Materials Space. Multiscale simulation of PSA/VSA processes for screening of large databases of porous materials requires extensive computational resources. In the screening workflow, process optimization is usually considered as a bottleneck where significant computational efforts are incurred.[367] Attempts have been made to improve computational efficiency of process optimization through reducing dimensionality of the variable space in process optimization, by development of novel machine-learning methods (section 6.3.5). These methods pave the way not only for faster screening of large databases of porous materials but also for identifying the most efficient process configurations for a particular separation process. This can lead to better understanding of the material−process−performance relationships. Nevertheless, the remaining challenge is yet to tackle the magnitude of the material−process phase space. Currently, these methods have only been tested for screening of small sets of porous materials (<2000),[124,127] which is infinitesimal compared to the huge number of materials that have been discovered so far, as mentioned in section 6.1.1. Also, experimental evidence for validation of numerical techniques that are used for expedited optimization of PSA/VSA processes are still scarce,[362] and it is for the future studies to address this important limitation.

8.6.2. Multiscale Workflows for Unconventional Adsorbents. In addition to what has been discussed in this section, development of more advanced multiscale workflows for PSA/VSA/TSA processes can be envisioned where behavior of more complex materials is simulated. An important example of such cases is the prediction of separation performance of novel porous materials[311,312,480] with gating effects and phase-change behavior that exhibit step-shaped adsorption isotherms.[339,481−483] Atomistic structures of these materials undergo considerable structural changes in response to external stimuli such as heat, pressure, humidity, and adsorption of guest molecules.[213,481] Simulation of adsorption processes in this class of materials must capture the interplay between the presence of adsorbate molecules and the structural deformation of the framework using computational methods that go beyond conventional GCMC (e.g., the osmotic Monte Carlo method or hybrid MC/MD methods).[194,484] In addition to simulation of structural flexibility of these materials that must be handled at the molecular level, it is also crucial to develop more sophisticated analytical adsorption models that can capture stepwise shape of the isotherms in these materials as required for process simulation.[339,485,486] These two issues alone pose a significant challenge to the development of future generations of multiscale simulation workflows for screening of flexible materials.

9. CURRENT PERSPECTIVE AND THE FUTURE OUTLOOK

9.1. Current Perspective

In this article, we reviewed the recent progress in the application of performance-based multiscale workflows for material screening in postcombustion carbon capture. To make it useful for our wide range of audience consisting of material scientists, computational modelers, and chemical engineers, we introduced the basic principles involved in each element of the workflow and provided references to the available computational tools. We outlined what data are required at each level and showed how they can be calculated computationally without resorting to experiment. We also highlighted the issue of availability and completeness of the data, as well as the consistency of implementations for multiscale workflows. The article also summarized all the recent studies in the field, and as such can serve as a starting point for further developments. Before we can close this review with our concluding remarks, it is important to highlight the current perspective of the field and explain what actually the multiscale materials screening approach has achieved. Naturally, two questions emerge here:

Table 11. Ranking of Top 10 Materials Based on Maximum Productivity

index	4-step VSA with LPP[a] (Khurana and Farooq[88])	4-step Skarstrom PSA[b] (Park et al.[94])	4-step VSA with LPP[a] (Subramanian Balashankar and Rajendran[121])	4-step VSA with LPP[a] (Burns et al.[124])	modified Skarstrom[c] (Yancy-Caballero et al.[126])	FVSA[c] (Yancy-Caballero et al.[126])	5-step PSA[c] (Yancy-Caballero et al.[126])
1	UTSA-16	SENWOZ	h8315144	GAYFOD	UTSA-16	Cu-TDPAT	UTSA-16
2	NaA	SENWIT	h8328529	WUNSII	zeolite 13X	UTSA-16	zeolite 13X
3	h8155527, h8124767	WONZOP	IZA-MON	IISERP-MOF2	Cu-TDPAT	Zn-MOF-74	Cu-TDPAT
4	ZIF-36-FRL	UTEWUM	IZA-RRO	UTSA-16	Ni-MOF-74	zeolite 13X	Zn-MOF-74
5	NAB	OJICUG	IZA-JBW	YEZFIU	Mg-MOF-74	Ti-MIL-91	Ti-MIL-91
6	CaX	BIBXUH	h8206103	IGAHED02	SIFSIX-3-Ni	SIFSIX-3-Ni	SIFSIX-3-Ni
7	ZIF-78	SENWAL	IZA-WEI	XAVQIU01	SIFSIX-2-Cu-i		Mg-MOF-74
8	h8272272	FEFDAX	h8313037	NaA	Ti-MIL-91		
9	Zn-MOF-74	RAXCOK	ZIF-Im-h8055553	HUTTIA	Zn-MOF-74		
10	MgX	CUHPUR	ZIF-Im-h8164555	ZEGSUB			

[a]4-step VSA with LPP using a packed-bed adsorbent system. Feed composition: 15% CO_2/85% N_2 at 298 K. Optimization constraints: 95% CO_2 purity and 90% CO_2 recovery. [b]4-step PSA using a hollow fiber adsorbent model. Feed composition: 14% CO_2/86% N_2 at 243 K. No optimization constraint imposed on purity and recovery. [c]PSA cycles using packed-bed adsorbent system. Feed composition: 15% CO_2/85% N_2 at 313 K. Optimization constraints: 90% CO_2 purity and 90% CO_2 recovery.

(1) What processes and materials have been identified so far as the most promising candidates for postcombustion carbon capture?

(2) Have we already reached the limit of performance that could be achieved through design of new materials?

To answer these questions, we have compiled the top performing material candidates that have been identified so far by the most comprehensive screening studies using detailed process modeling and optimization for postcombustion carbon capture from binary CO_2/N_2 flue gas mixtures. This is summarized in Tables 10 and 11 where the top 10 materials from each study have been listed in order of performance. The tables contain the results of 7 screening studies performed using 5 different PSA or VSA process configurations. Table 10 summarizes top-performing materials based on minimum energy consumption of the process, while Table 11 lists the top candidates based on their maximum productivity.

Evidently, the answer to the first question raised at the beginning of this section does not seem to be straightforward. This is because different screening studies have employed various process and cycle configurations for assessment of materials performance at the process level. We also need to be aware that these studies draw their candidates form different databases of materials, so the fact that a particular material does not appear in a top ranked group, may simply indicate that it was not included in the original screening set. For the studies listed in Tables 10 and 11, the processes include 4-step VSA cycle with LPP, 4-step Skarstrom-based PSA cycle, modified 5-step Skarstrom cycle, FVSA cycle, and 5-step PSA cycle. The use of different process configurations inevitably makes direct comparison of materials performance problematic. For example, according to Yancy-Caballero et al.,[126] Mg-MOF-74 appears to be among the top performing materials in the modified Skarstrom and 5-step PSA cycles but not in the FVSA cycle (as seen in Tables 10 and 11). Nevertheless, the issue is beyond the use of different process configurations, because the hierarchy of materials rankings are not consistent even within those studies that have used a similar cycle (e.g., 4-step VSA with LPP). A prominent example here is the position of UTSA-16 in Table 10 in which UTSA-16 outperforms NaA according to the ranking by Khurana and Farooq,[88] but its performance is found to be poorer compared to the same material according to the study conducted by Burns et al.[124] The same is true if we compare the position of UTSA-16 with ZIF-36-FRL in the two studies

mentioned above in Table 10. This could be due the use of different model assumptions at the molecular or process levels (e.g., different force fields used for molecular simulations or different numerical protocols employed for fitting adsorption isotherms). These observations clearly demonstrate our point about the importance of consistent implementation of multi-scale screening workflows, which is highlighted throughout this review and particularly discussed in sections 8.1 and 8.3.

On the other hand, in Tables 10 and 11, we deliberately did not include the actual values of the energy penalty or productivity as we believe it would be an inconsistent comparison of studies that are conducted on different bases. However, without the actual numbers, we also need to be careful in our criticism of the consistency of rankings: the data presented in Tables 10 and 11 do not tell us *how close* materials are in terms of the numerical performance. Therefore, a more comprehensive discussion of the meaning of the rankings is not possible without the accompanying analysis of the propagation of uncertainties.

So what is the impact of the studies reviewed above? From an engineering point of view, they have identified several candidates that are very promising for postcombustion carbon capture. From Tables 10 and 11, many materials have energy consumption and productivity values that are superior to those of zeolite 13X, which is the current industrial benchmark. Examples of these materials include NAB, UTSA-16, NaA, and ZIF-36-FRL.[88] IISERP-MOF2 is another example whose energy consumption is less than that of amine-based absorption technology, while its productivity surpasses zeolite 13X.[124] This new MOF is known to have excellent stability against moisture and acid gas environments.[487] This list of top-performing candidates also includes other MOFs with high kinetic stability in the presence of water such as UTSA-16 and SIFSIX-2-Cu-i.[488] As a Linde type A (LTA) zeolite, NaA is another promising candidate that is currently synthesized at industrial scales;[124,489] hence its application for carbon capture from dried flue gas can be more economical compared to other candidates that are not currently mass produced.[124]

In addition to identifying promising materials and processes, application of performance-based screening strategies has led to important learning outcomes, a prominent example of which is the role of nitrogen adsorption for material performance. Now, we know that we do not need to limit our search for ideal

adsorbents to materials with high CO_2 capacity, but rather we should look for the candidates that have low nitrogen uptake.

Considering what is discussed in this section, it is reasonable to state that performance-based screening of porous materials has significantly improved our ability to realistically identify a range of promising materials that can be considered for lab-scale and pilot-plant examinations. This will be especially true if the research community focuses on addressing the challenges that were identified and discussed in section 8 of this review to improve consistency and accuracy of the multiscale screening workflows.

The second question posed at the beginning of this section is also crucial in deciding whether (and how) we should proceed with materials engineering and screening studies for carbon capture. We can view this problem as an inverse engineering problem. Indeed, imagine we could design and synthesize an ideal adsorbent for carbon capture. Of course, its properties must be located within the limits of physically meaningful and realistic values. Having said that, what would be the performance of such an ideal material for a carbon capture process? We could then look at the differences (both in the performance and properties) of this ideal adsorbent from the actual materials reviewed in Tables 10 and 11 as the current innovation gap. In other words, a potential improvement in performance that could be achieved through the engineering of new materials could be identified in this way. A large innovation gap would suggest that our current collection of materials is still far away from what is theoretically possible in terms of performance, and it would be worthwhile to continue our efforts for design and screening of porous materials to close this gap. A small innovation gap, however, would indicate a likely plateau in what is achievable through material optimization in the process, and hence the focus should shift to other processes and conditions. This is precisely the question that was recently posed by Pai et al.[426] in their study about practically achievable limits of process performance for carbon capture using PVSA processes. For this, the authors considered a 4-step cycle with light product pressurization and with feed pressurization using realistic pump efficiencies. One important aspect of this study is that the authors explored performance of these processes as a function of the evacuation pressure, concentration of CO_2 in the feed, pressure of the feed, and broader limits of purity/recovery constraints, while comparing the resulting performance with the thermodynamic minimum energy required for gas separation, and with the conventional reference absorption process.[490] Overall, the study indicates that for the standard case of 15% CO_2 in the feed, adsorption processes are competitive in terms of energy penalty only if the process invokes very low evacuation pressures (0.01−0.1 bar, which is not realistic in practice). Moreover, the current top-performing materials (zeolite 13X, UTSA-16, IISERP-MOF2) are already quite close to the performance of the ideal material (innovation gap in performance is about 20%). The PVSA processes seem to be much more competitive (and operate under more realistic conditions) at higher CO_2 concentrations of the feed. However, at the same time, the innovation gap under these conditions becomes very small, meaning the existing materials already perform close to what will be realistically achievable.

9.2. Roadblocks to the Industrial Application of New Materials for Carbon Capture

In the previous section, we provided a summary of several recent screening studies that collectively identified a group of materials with promising properties for carbon capture. Now, the key question is what the impact of these findings will be on the industrial practices. Can any of the above material candidates find their way into industrial applications and be commercialized?

As it happens, there are multitude of barriers between identifying some promising materials for carbon capture and their actual implementation as new technologies on an industrial scale. It should be boldly stated that these barriers have not been overcome yet! Although, this review aimed to predominantly focus on the principles of the multiscale workflows and on the screening of porous materials using these workflows, it is vital to discuss the above-mentioned technological barriers in order to provide a realistic picture about the potential of the adsorptive carbon capture technologies.

9.2.1. Stability. The flue gas typically contains small amounts of water vapor and trace amounts of acid gases, such as SO_x and NO_x. For a material to be suitable for large scale industrial applications, it should be stable against the presence of these gases. Many of the early MOFs reported would not be stable under the conditions of interest for any extensive period of time. An excellent example of this situation is Mg-MOF-74 (or Mg-DOBDC or CPO-27-Mg). It has one of the highest CO_2 capacities at 0.1 bar because of the strong interaction of its open metal sites with the gas.[435,491] For the same reason, this material has been extensively investigated as a benchmark adsorbent for carbon capture.[491,492] Nevertheless, it has been shown that the structure of Mg-MOF-74 collapses irreversibly in the presence of even a small amount of water, as its open magnesium sites strongly interact with water.[493,494] Furthermore, as the column experiences gradients in temperature and pressure, the industrial adsorbent must be stable under multiple repeating cycles of these conditions over the expected lifespan of the unit (scale of years). There is evidence that mechanical stability of flexible MOFs is far from this threshold.[495]

In recent years, the situation has moved on with an increasing number of thermally, mechanically, and water stable MOFs being discovered, for which we refer the reader to some appropriate reviews.[488,496−498] Prominent recent examples of stable new materials with promising carbon capture properties include CALF-20 from Shimizu and co-workers,[499] IISERP-MOF2 from Nandi et al.,[487] Al-PMOF from Boyd et al.,[157] and MUF-17 from Qazvini and Telfer.[500] This, however, also draws attention to an important issue of defining stability. It is crucial to know how the stability of materials is defined and measured, as depending on the community and application, the condition and the definition of stability may widely vary. Retaining CO_2 capacity under cyclic conditions reflecting the actual PSA process for carbon capture would be the most useful definition of stability in the context of the application of interest. Stability tests however are very time-consuming processes. As noted by Gibson et al.,[477] the zero length column (ZLC) technique can be used to test the stability of adsorbents with respect to flue gas contaminants, such as SO_x, NO_x, and water. In this method, the sample is exposed to a mixture containing the contaminants for a few hours, and after regeneration, the normal test is carried out to determine its CO_2 uptake. The experiment is then repeated cyclically to determine the variation of the CO_2 uptake as a function of the amount of contaminants that have been eluted on the sample. Because of the small amount of material used in ZLC, results can be obtained rapidly to determine whether the sample is stable or whether pretreatment of the flue gas is needed before the carbon capture unit. As an alternative to time-

consuming experimental procedures, Batra et al.[501] recently proposed the use of machine learning techniques to search for water stable MOFs. In summary, it can be said that stability testing requires further research to establish the necessary standards in terms of consistency and reliability of the test methods.

9.2.2. Cost and Availability. To understand the importance of the cost of materials, it is useful to reflect on the scale of the carbon capture process from a typical coal power plant. For this, let us consider one of the baseline cases published by the US National Energy Technology Laboratory (NETL).[502] In particular, case B12A in the study represents the performance of a pulverized coal based plant without CO_2 capture. The plant has gross electrical output of 580 MW and net electrical output of 550 MW and generates ca. 10^4 kmol/h of CO_2. In other words, this relatively small scale plant generates 440 tons of CO_2 every hour. The NETL study also provides important reference figures of the cost of carbon capture using the conventional absorption technologies (Shell Cansolv capture system). The report indicates that the gross power of the power plant had to increase to 640 MW to have net power 550 MW after capture, while the levelized cost of electricity (LCOE) increased from $80.4/MWh without carbon capture to $133.2/MWh with capture. Khurana and Farooq[90] used this case study from NETL to provide a techno-economical analysis of the same carbon capture process using adsorption technologies with the gross and net power of plant being 665 and 630 MW, respectively. To capture the desired amount of CO_2, their representative case based on a 6-step PSA process required 104 trains each of which consisted of 6 columns. Although the LCOE numbers seemed promising (LCOE without capture $79.6/MWh and with capture 114.9$/MWh for the optimal adsorbent), the required footprint of the adsorption area was 8800 m^2. With each column being 6.8 m in length and about 2.3 m in diameter, the required amount of the adsorbent material would be on the order of 10^4 tons. As mentioned above, the plant considered in this example is of a rather small scale. For comparison, capacity of the largest coal power plant in the world (Datang Tuoketuo, China) is ten times higher than the plant considered in this case study (~6.7 GW).[503] Assuming a linear relationship between the capacity of the plant and the adsorption area, installing adsorptive carbon capture at the 10 largest coal power stations in the world would require 10^6 (one million) tons of adsorbent.

Clearly, industrial applications of this scale cannot rely on expensive adsorbents. The back-of-the envelope calculations provided above raise concerns about the feasibility of using new materials such as MOFs in adsorptive technologies for carbon capture from power plants. In the study of Khurana and Farooq, the indicative cost of Zeochem zeolite 13X as adsorbent was taken to be $0.5/kg.[90] The cost of MOFs is much greater than that of zeolite 13X, although it has been projected to drop significantly for some of the materials (from tens of thousands or thousands of dollars per kilogram to tens of dollars per kilogram) as new synthetic routes, solvents, and conditions become available.[504,505] One particularly notable example is CALF-20 (already mentioned in this section), which is claimed to be available at $20−30/kg.[506] Another issue closely related to the cost of materials is the availability of new adsorbents. There are now several companies that commercially produce MOFs, including BASF, MOF Technologies, novoMOF, NuMat, Immaterial, MOFWORX, and framergy. However, the production capacity of these companies is still limited to a few tons of materials per year (i.e., kilograms per hour), and this is far away

from meeting the global demands for building new carbon capture plants at industrial scales.

These findings, combined with the analysis of Pai et al.[426] reviewed in the previous section, raise serious concerns about the prospects of new materials such as MOFs for carbon capture from power plants. More promising avenues seem to be associated with capture units for other industrial applications which are 1−2 orders of magnitude smaller compared to power plants. These applications have been reviewed by Abanades et al.[336] For example, the good stability of CALF-20 and its attractive cost led to efforts to increase its production to "ton scale" and to use it for carbon capture from a cement plant.[507] What is however important to emphasize for the purpose of this review is that a comprehensive analysis of promising porous materials (such as that provided by Pai et al.[426]) is only possible through the use of advanced multiscale screening workflows that were introduced and discussed in this review. From this perspective, the multiscale workflows described here will also be able to play an important role in evaluating the potential of adsorbent materials for carbon capture in the context of other applications, such as those reviewed by Abanades et al.[336]

9.3. Future Outlook

After reflecting on the state-of-the-art in the field, here we provide our concluding remarks and proposals for the future direction of multiscale performance-based materials screening studies.

9.3.1. Beyond Postcombustion Carbon Capture. In this review, we focused on postcombustion carbon capture as it is a very challenging, societally relevant, and most investigated process. However, we believe the multiscale screening approaches reviewed here will become a new way to design and appraise material options for other separation applications as well. Decarbonization of the chemical industry by 2050 cannot be achieved with carbon capture from power plants alone and will require a wider range of technologies. These technologies will deal with different process conditions (primarily different levels of carbon dioxide concentration) and will be operating on relatively small scale processes, compared to postcombustion capture (meaning, smaller amounts of materials will be required). For these processes, it is likely that faster cycles will be used to reduce the footprint of the units, especially in retrofit applications. This will in turn lead to larger effects of mass transfer and heat transfer limitations, precisely the challenges that need to be explored within the multiscale framework.

Air separation is a very useful case to consider for benchmarking multiscale modeling approaches. Production of oxygen is an equilibrium driven separation where the light component is produced. Therefore, simpler process configurations will work well in this case and advances are more likely to be in the definition of the ideal structural properties of the formed materials. Production of nitrogen is a kinetic separation that requires materials with small pore openings. Again, although this process is well-established, the data accumulated over the years can provide a benchmark to understand whether accurate a-priori predictions based on force fields that are efficient in equilibrium calculations can be also used in predicting diffusivities.

Finally, we envision that other separation processes, such as membrane separations, where the performance of the process is defined by the material used, will also benefit from multiscale

screening workflows in producing more realistic, performance-based rankings of the available materials.

9.3.2. The Role of ML Methods Will Grow. It is already evident that the scope of multiscale screening methods will be expanding along with the range of available materials. This, combined with a large number of parameters, leads to a multidimensional "material−process configuration−performance" space, which is very challenging for conventional optimization algorithms to deal with. Machine learning methods have already been used successfully to accelerate the optimization problems in this field. The growing availability of data across all scales opens exciting opportunities to use ML not only to explore the search space, but also for other aspects of the multiscale workflow such as the design of new force fields and the prediction of the best material structure.[508] This direction is both very promising and still widely uncharted. Hence, there is a strong incentive to fully explore the potential of ML models to accelerate process-level screenings.

9.3.3. Quality Data, Reproducibility of Results, and Consistency of Comparisons. We believe these aspects will be a singular, most important barrier for the multiscale approaches to make an actual impact through identifying both better and realistic options for carbon capture. The molecular simulation community has already produced a substantial number of screening studies for carbon capture. Similarly, the process simulation community has been examining various options for both processes and materials (but not in a large scale screening mode) for this task. The multiscale methods emerging from the combination of these two realms have been reviewed here. However, these studies use different assumptions, models, and conditions, which makes systematic comparison of their results difficult. One possible proposal for the simulation community would be an open call for systematic comparison of the currently existing process modeling codes (including commercial ones) and the model assumptions using a reference case study. This will be a significant step toward building confidence in ranking of the materials.

9.3.4. Techno-economic Analysis and Scale-Up of the Process. Development of multiscale screening studies should eventually go beyond the process-level. This is because, similar to any technology, the ultimate driver for commercialization of adsorption-based carbon capture is the cost. Therefore, the screening studies at the process level must be linked with techno-economic analyses where the ultimate design objective is to reduce the overall cost of CO_2 capture and concentration (CCC) at industrial scales. Although there have been some attempts in this direction,[90−92,125] there is still a dire need for integrated adsorbent-process optimizations that are properly linked with techno-economic assessments of the CCC technology. Such studies, must realistically assess capital and operating costs of the process including the cost of adsorbent, operational lifetime of key components of the cyclic process, realistic efficiencies of vacuum pumps, process scheduling, and finally the costs associated with scale-up of the technology and its footprint requirements.[90,92,125]

From the few techno-economic studies conducted so far, it seems that the cost of the CO_2 capture using VSA or PSA technology is generally higher than that of the current technological benchmark, which is the amine-based absorption separation (despite the promising values of energy penalty reported[92,125]). Recent studies have consistently noted that the cost of adsorbent has a major impact on the ultimate cost of the CO_2 capture process.[92,125] As discussed in section 9.2, this is

indeed the case for some materials (such as MOFs) whose synthesis is still expensive and limited for large-scale productions. In the case of VSA processes, another major challenge is the limitation of maximum feed velocities that can be employed in beaded or pelletized adsorbents.[92] Apparently, this results in the requirement for a large number of adsorption columns and multiple parallel trains, which in turn poses other technological challenges associated with practicality of deploying large and complex capture plants.[90,92] From this perspective, future efforts in the domain of adsorption-based carbon capture technology must focus on addressing the following technological barriers:

- Development of monolith adsorbents[65,66] or parallel-passage contactors[509] that can increase productivity of the process through reducing pressure drop and enhancing kinetics.[90,92]

- Development of better and cheaper adsorbents that can be economically mass produced.

- Development of adsorbents with improved thermal and mechanical stabilities and higher resistance to moisture that can operate under rapid cyclic conditions of PSA and VSA processes with reasonable operational lifetime.

In this context, the following should be particularly undertaken by the simulation community for future materials screening studies using the multiscale workflows:

- Materials screening using structured adsorbents[65] (as opposed to pelletized adsorbents) in PSA/VSA systems. These adsorbents exhibit lower pressure drop compared to traditional packed bed systems and do not suffer from fluidization at high feed velocities; hence they can be used for cycle intensification and increasing productivity. Recent studies have also shown that it is possible to operate monolithic VPSA processes at a higher productivity than the traditional methyldiethanolamine (MDEA)-based absorption processes.[353] A number of recent studies have already developed new models for implementation of structured adsorbents in PSA and VSA simulations.[353,396]

- Focusing the computational efforts on screening of materials that are known to meet the essential criteria stated in this section (e.g., low price, water resistant, and thermally and mechanically stable materials).

9.3.5. The Ultimate Challenge in Postcombustion Carbon Capture Still Remains. It is important to recognize, that despite 15 or so years of computational materials screening studies for postcombustion carbon capture, there is no pilot-scale plant that is designed to operate using a MOF or ZIF as an adsorbent. While the aim of developing an *in silico* route to finding optimal materials is a sound aspiration, there is the need to include in the selection process, also the ability to synthesize new materials and assess their stability against thermal cycling and exposure to contaminants and moisture. Predicting the stability of the materials is a challenging area. There are also other technical issues associated with scale-up that were mentioned earlier in this review. Hence, it is clear that there are still significant challenges toward industrial implementation of carbon capture technologies based on novel porous materials. Notwithstanding, we believe development of more advanced and realistic multiscale screening methods (such as those reviewed in this work) is an important step in accelerating our progress toward our ultimate goal.

AUTHOR INFORMATION

Corresponding Authors

Amir H. Farmahini − *Department of Chemical Engineering and Analytical Science, School of Engineering, The University of Manchester, Manchester M13 9PL, United Kingdom;* orcid.org/0000-0002-6686-8588; Email: a.farmahini@manchester.ac.uk

Lev Sarkisov − *Department of Chemical Engineering and Analytical Science, School of Engineering, The University of Manchester, Manchester M13 9PL, United Kingdom; School of Engineering, Institute of Materials and Processes, The University of Edinburgh, Edinburgh EH9 3FB, United Kingdom;* orcid.org/0000-0001-7637-7670; Email: Lev.Sarkisov@manchester.ac.uk

Authors

Shreenath Krishnamurthy − *Process Technology Department, SINTEF Industry, Oslo 0373, Norway;* orcid.org/0000-0002-9584-6804

Daniel Friedrich − *School of Engineering, Institute for Energy Systems, The University of Edinburgh, Edinburgh EH9 3FB, United Kingdom;* orcid.org/0000-0002-3951-2201

Stefano Brandani − *School of Engineering, Institute of Materials and Processes, The University of Edinburgh, Edinburgh EH9 3FB, United Kingdom;* orcid.org/0000-0001-9470-6837

Complete contact information is available at:
https://pubs.acs.org/10.1021/acs.chemrev.0c01266

Notes

The authors declare no competing financial interest.

Biographies

Amir H. Farmahini is currently a research associate at the University of Manchester, U.K. He received his BEng in Mechanical Engineering from Islamic Azad University in Iran. Subsequently, he completed his M.Sc. and Ph.D. studies in University of Bergen (Norway) and University of Queensland (Australia). Dr. Farmahini's expertise and research interests span across multiscale and multiphysics modeling and simulation of chemical engineering systems (from atoms to processes), molecular systems engineering, and adsorption in crystalline and amorphous nanoporous materials.

Shreenath Krishnamurthy graduated from the National University of Singapore in 2014 with a Ph.D., focused on CO_2 Capture by Vacuum Swing Adsorption Process. He worked as postdoctoral research fellow at the University of Edinburgh and now has been with the process technology department at SINTEF Industry in Oslo since 2018. He has extensive experience in adsorbent characterization, laboratory and pilot scale vacuum swing adsorption experiments, and simulation and optimization of cyclic adsorption processes.

Daniel Friedrich is a Senior Lecturer in Mathematics for Engineering Applications in the School of Engineering at the University of Edinburgh, which he joined in 2009. He did his undergraduate studies in Technomathematik at the Universität Karlsruhe (TH) and his Ph.D. research at the University of Southampton. His research interests are in mathematical modeling, simulation, and optimization of engineering processes in the energy area, particularly for dynamic systems. This includes the accurate and efficient simulation of specific components, for example, adsorption columns for gas separation, as well as process optimization. In 2020, he was appointed to the RSE Young Academy of Scotland.

Stefano Brandani is the Chair of Chemical Engineering at the University of Edinburgh since 2007. He is the recipient of a Royal Society-Wolfson Research Merit Award and a Philip Leverhulme Prize, a Fellow of the IChemE, and a Director of AIChE's Separations Division. His research activity focuses on gas separations based on novel nanoporous materials including design of novel adsorption experiments in combination with advanced dynamic process simulations to determine adsorption equilibrium and kinetic properties of nanoporous materials, material scale-up and testing from milligram to kilogram scale, and optimization of integrated carbon capture systems.

Lev Sarkisov is Professor in Chemical Engineering at the University of Manchester and a visiting Professor in the School of Engineering at the University of Edinburgh. In Manchester, his group specializes in multiscale simulations of adsorption process for carbon capture, theoretical modeling of membrane transport processes, computational structure characterization tools, and material informatics, among other themes.

REFERENCES

(1) Curtarolo, S.; Hart, G. L.; Nardelli, M. B.; Mingo, N.; Sanvito, S.; Levy, O. The High-Throughput Highway to Computational Materials Design. *Nat. Mater.* **2013**, *12*, 191−201.

(2) Jain, A.; Ong, S. P.; Hautier, G.; Chen, W.; Richards, W. D.; Dacek, S.; Cholia, S.; Gunter, D.; Skinner, D.; Ceder, G.; Persson, K. A. Commentary: The Materials Project: A Materials Genome Approach to Accelerating Materials Innovation. *APL Mater.* **2013**, *1*, 011002.

(3) Talirz, L.; Kumbhar, S.; Passaro, E.; Yakutovich, A. V.; Granata, V.; Gargiulo, F.; Borelli, M.; Uhrin, M.; Huber, S. P.; Zoupanos, S.; Adorf, C. S.; Andersen, C. W.; Schütt, O.; Pignedoli, C. A.; Passerone, D.; VandeVondele, J.; Schulthess, T. C.; Smit, B.; Pizzi, G.; Marzari, N. Materials Cloud, a Platform for Open Computational Science. *Sci. Data* **2020**, *7*, 299−311.

(4) *Ipcc Special Report on Carbon Dioxide Capture and Storage*; Working Group III of the Intergovernmental Panel on Climate Change: Cambridge, UK, and New York, USA, 2005; p 442.

(5) Sholl, D.; Lively, R. Seven Chemical Separations to Change the World. *Nature* **2016**, *532*, 435−437.

(6) Zhou, H.-C.; Long, J. R.; Yaghi, O. M. Introduction to Metal-Organic Frameworks. *Chem. Rev.* **2012**, *112*, 673−674.

(7) Li, J.-R.; Sculley, J.; Zhou, H.-C. Metal-Organic Frameworks for Separations. *Chem. Rev.* **2012**, *112*, 869−932.

(8) Safaei, M.; Foroughi, M. M.; Ebrahimpoor, N.; Jahani, S.; Omidi, A.; Khatami, M. A Review on Metal-Organic Frameworks: Synthesis and Applications. *TrAC, Trends Anal. Chem.* **2019**, *118*, 401−425.

(9) Chen, B.; Yang, Z.; Zhu, Y.; Xia, Y. Zeolitic Imidazolate Framework Materials: Recent Progress in Synthesis and Applications. *J. Mater. Chem. A* **2014**, *2*, 16811−16831.

(10) Geng, K.; He, T.; Liu, R.; Dalapati, S.; Tan, K. T.; Li, Z.; Tao, S.; Gong, Y.; Jiang, Q.; Jiang, D. Covalent Organic Frameworks: Design, Synthesis, and Functions. *Chem. Rev.* **2020**, *120*, 8814−8933.

(11) Hasell, T.; Cooper, A. I. Porous Organic Cages: Soluble, Modular and Molecular Pores. *Nat. Rev. Mater.* **2016**, *1*, 16053.

(12) Tian, Y.; Zhu, G. Porous Aromatic Frameworks (Pafs). *Chem. Rev.* **2020**, *120*, 8934−8986.

(13) Lu, W.; Yuan, D.; Zhao, D.; Schilling, C. I.; Plietzsch, O.; Muller, T.; Bräse, S.; Guenther, J.; Blümel, J.; Krishna, R.; Li, Z.; Zhou, H.-C. Porous Polymer Networks: Synthesis, Porosity, and Applications in Gas Storage/Separation. *Chem. Mater.* **2010**, *22*, 5964−5972.

(14) McKeown, N. B. Polymers of Intrinsic Microporosity (Pims). *Polymer* **2020**, *202*, 122736.

(15) McKeown, N. B.; Budd, P. M. Polymers of Intrinsic Microporosity (Pims): Organic Materials for Membrane Separations, Heterogeneous Catalysis and Hydrogen Storage. *Chem. Soc. Rev.* **2006**, *35*, 675−683.

(16) Rajagopalan, A. K.; Avila, A. M.; Rajendran, A. Do Adsorbent Screening Metrics Predict Process Performance? A Process Optimisation Based Study for Post-Combustion Capture of CO_2. *Int. J. Greenhouse Gas Control* **2016**, *46*, 76−85.

(17) Biegler, L. T.; Jiang, L.; Fox, V. G. Recent Advances in Simulation and Optimal Design of Pressure Swing Adsorption Systems. *Sep. Purif. Rev.* **2005**, *33*, 1−39.

(18) Grande, C. A. Advances in Pressure Swing Adsorption for Gas Separation. *ISRN Chem. Eng.* **2012**, *2012*, 982934.

(19) Riboldi, L.; Bolland, O. Overview on Pressure Swing Adsorption (Psa) as CO_2 Capture Technology: State-of-the-Art, Limits and Potentials. *Energy Procedia* **2017**, *114*, 2390−2400.

(20) Hedin, N.; Andersson, L.; Bergström, L.; Yan, J. Adsorbents for the Post-Combustion Capture of CO_2 Using Rapid Temperature Swing or Vacuum Swing Adsorption. *Appl. Energy* **2013**, *104*, 418−433.

(21) Wiheeb, A. D.; Helwani, Z.; Kim, J.; Othman, M. R. Pressure Swing Adsorption Technologies for Carbon Dioxide Capture. *Sep. Purif. Rev.* **2016**, *45*, 108−121.

(22) Ribeiro, R. P. P. L.; Grande, C. A.; Rodrigues, A. E. Electric Swing Adsorption for Gas Separation and Purification: A Review. *Sep. Sci. Technol.* **2014**, *49*, 1985−2002.

(23) Zhu, X.; Li, S.; Shi, Y.; Cai, N. Recent Advances in Elevated-Temperature Pressure Swing Adsorption for Carbon Capture and Hydrogen Production. *Prog. Energy Combust. Sci.* **2019**, *75*, 100784.

(24) Agarwal, A.; Biegler, L. T.; Zitney, S. E. Simulation and Optimization of Pressure Swing Adsorption Systems Using Reduced-Order Modeling. *Ind. Eng. Chem. Res.* **2009**, *48*, 2327−2343.

(25) Beck, J.; Friedrich, D.; Brandani, S.; Guillas, S.; Fraga, E. S. Surrogate Based Optimisation for Design of Pressure Swing Adsorption Systems. In *Computer Aided Chemical Engineering*; Bogle, I. D. L., Fairweather, M., Eds.; Elsevier: 2012; Vol. *30*, pp 1217−1221, DOI: 10.1016/B978-0-444-59520-1.50102-0

(26) Andersen, A.; Divekar, S.; Dasgupta, S.; Cavka, J. H.; Aarti; Nanoti, A.; Spjelkavik, A.; Goswami, A. N.; Garg, M.O.; Blom, R. On the Development of Vacuum Swing Adsorption (Vsa) Technology for Post-Combustion CO_2 Capture. *Energy Procedia* **2013**, *37*, 33−39.

(27) Chronopoulos, T. Microwave Swing Adsorption for Post-Combustion CO_2 Capture from Flue Gases Using Solid Sorbents. Doctoral Thesis, Heriot-Watt University, ROS Theses Repository, 2016.

(28) Plaza, M. G.; Rubiera, F. Development of Carbon-Based Vacuum, Temperature and Concentration Swing Adsorption Post-Combustion CO_2 Capture Processes. *Chem. Eng. J.* **2019**, *375*, 122002.

(29) *Compendium of Carbon Capture Technology*; US Department of Energy/National Energy Technology Laboratory: 2018.

(30) Hasan, M. M. F.; First, E. L.; Floudas, C. A. Cost-Effective CO_2 Capture Based on in Silico Screening of Zeolites and Process Optimization. *Phys. Chem. Chem. Phys.* **2013**, *15*, 17601−17618.

(31) Banu, A.-M.; Friedrich, D.; Brandani, S.; Düren, T. A Multiscale Study of Mofs as Adsorbents in H_2 Psa Purification. *Ind. Eng. Chem. Res.* **2013**, *52*, 9946−9957.

(32) de Coninck, H.; Benson, S. M. Carbon Dioxide Capture and Storage: Issues and Prospects. *Annual Review of Environment and Resources* **2014**, *39*, 243−270.

(33) Bui, M.; Adjiman, C. S.; Bardow, A.; Anthony, E. J.; Boston, A.; Brown, S.; Fennell, P. S.; Fuss, S.; Galindo, A.; Hackett, L. A.; Hallett, J. P.; Herzog, H. J.; Jackson, G.; Kemper, J.; Krevor, S.; Maitland, G. C.;

Matuszewski, M.; Metcalfe, I. S.; Petit, C.; Puxty, G.; Reimer, J.; Reiner, D. M.; Rubin, E. S.; Scott, S. A.; Shah, N.; Smit, B.; Trusler, J. P. M.; Webley, P.; Wilcox, J.; Mac Dowell, N. Carbon Capture and Storage (Ccs): The Way Forward. *Energy Environ. Sci.* **2018**, *11*, 1062−1176.

(34) Sood, A.; Vyas, S. Carbon Capture and Sequestration- a Review. *IOP Conference Series: Earth and Environmental Science* **2017**, *83*, 012024.

(35) Vitillo, J. G.; Smit, B.; Gagliardi, L. Introduction: Carbon Capture and Separation. *Chem. Rev.* **2017**, *117*, 9521−9523.

(36) Yu, J.; Xie, L.-H.; Li, J.-R.; Ma, Y.; Seminario, J. M.; Balbuena, P. B. CO_2 Capture and Separations Using Mofs: Computational and Experimental Studies. *Chem. Rev.* **2017**, *117*, 9674−9754.

(37) Phan, A.; Doonan, C. J.; Uribe-Romo, F. J.; Knobler, C. B.; O'Keeffe, M.; Yaghi, O. M. Synthesis, Structure, and Carbon Dioxide Capture Properties of Zeolitic Imidazolate Frameworks. *Acc. Chem. Res.* **2010**, *43*, 58−67.

(38) Nakao, S.-I. *Advanced CO_2 Capture Technologies: Absorption, Adsorption, and Membrane Separation Methods*; Springer: Cham, 2019.

(39) *Process Systems and Materials for CO_2 Capture: Modelling, Design, Control and Integration*; Wiley: Hoboken, NJ, 2017.

(40) *Post-Combustion Carbon Dioxide Capture Materials*; Royal Society of Chemistry: London, 2019.

(41) *Carbon Capture and Storage*; Royal Society of Chemistry: Cambridge, U.K., 2020.

(42) Wang, Y.; Zhao, L.; Otto, A.; Robinius, M.; Stolten, D. A Review of Post-Combustion CO_2 Capture Technologies from Coal-Fired Power Plants. *Energy Procedia* **2017**, *114*, 650−665.

(43) Bhattacharyya, D.; Miller, D. C. Post-Combustion CO_2 Capture Technologies — a Review of Processes for Solvent-Based and Sorbent-Based CO_2 Capture. *Curr. Opin. Chem. Eng.* **2017**, *17*, 78−92.

(44) Zaman, M.; Lee, J. H. Carbon Capture from Stationary Power Generation Sources: A Review of the Current Status of the Technologies. *Korean J. Chem. Eng.* **2013**, *30*, 1497−1526.

(45) Gao, W.; Liang, S.; Wang, R.; Jiang, Q.; Zhang, Y.; Zheng, Q.; Xie, B.; Toe, C. Y.; Zhu, X.; Wang, J.; Huang, L.; Gao, Y.; Wang, Z.; Jo, C.; Wang, Q.; Wang, L.; Liu, Y.; Louis, B.; Scott, J.; Roger, A.-C.; Amal, R.; He, H.; Park, S.-E. Industrial Carbon Dioxide Capture and Utilization: State of the Art and Future Challenges. *Chem. Soc. Rev.* **2020**, *49*, 8584.

(46) *Netl Carbon Capture and Storage (Ccs) Database*. 04/2018 ed.; the US National Energy Technology Laboratory: online, 2018.

(47) D'Alessandro, D. M.; Smit, B.; Long, J. R. Carbon Dioxide Capture: Prospects for New Materials. *Angew. Chem., Int. Ed.* **2010**, *49*, 6058−6082.

(48) Maruyama, R. T.; Pai, K. N.; Subraveti, S. G.; Rajendran, A. Improving the Performance of Vacuum Swing Adsorption Based CO_2 Capture under Reduced Recovery Requirements. *Int. J. Greenhouse Gas Control* **2020**, *93*, 102902.

(49) Lackner, K. S. A Guide to CO_2 Sequestration. *Science* **2003**, *300*, 1677.

(50) Smit, B.; Reimer, J. A.; Oldenburg, C. M.; Bourg, I. C. *Introduction to Carbon Capture and Sequestration*; Imperial College Press: London, 2014; Vol. *1*.

(51) Brandl, P.; Bui, M.; Hallett, J. P.; Mac Dowell, N. Beyond 90% Capture: Possible, but at What Cost? *Int. J. Greenhouse Gas Control* **2021**, *105*, 103239.

(52) Nikolaidis, G. N.; Kikkinides, E. S.; Georgiadis, M. C. An Integrated Two-Stage P/Vsa Process for Postcombustion CO_2 Capture Using Combinations of Adsorbents Zeolite 13x and Mg-Mof-74. *Ind. Eng. Chem. Res.* **2017**, *56*, 974−988.

(53) Turner, M.; Iyengar, A.; Woods, M. Cost and Performance Baseline for Fossil Energy Plants Supplement: Sensitivity to CO_2 Capture Rate in Coal-Fired Power Plants;. NETL-PUB-22695; US National Energy Technology Laboratory (NETL): 2020.

(54) Agarwal, A.; Biegler, L. T.; Zitney, S. E. A Superstructure-Based Optimal Synthesis of Psa Cycles for Post-Combustion CO_2 Capture. *AIChE J.* **2010**, *56*, 1813−1828.

(55) Ramezan, M.; Skone, T. J.; Nsakala, N. Y.; Liljedahl, G. N. Carbon Dioxide Capture from Existing Coal-Fired Power Plants. DOE/

NETL-401/110907; National Energy Technology Laboratory, US Department of Energy: 2007.

(56) Akhtar, F.; Ogunwumi, S.; Bergström, L. Thin Zeolite Laminates for Rapid and Energy-Efficient Carbon Capture. *Sci. Rep.* **2017**, *7*, 10988.

(57) Ojuva, A.; Akhtar, F.; Tomsia, A. P.; Bergström, L. Laminated Adsorbents with Very Rapid CO_2 Uptake by Freeze-Casting of Zeolites. *ACS Appl. Mater. Interfaces* **2013**, *5*, 2669−2676.

(58) Grande, C. A.; Rodrigues, A. E. Electric Swing Adsorption for CO_2 Removal from Flue Gases. *Int. J. Greenhouse Gas Control* **2007**, *2*, 194−202.

(59) Zhao, Q.; Wu, F.; Men, Y.; Fang, X.; Zhao, J.; Xiao, P.; Webley, P. A.; Grande, C. A. CO_2 Capture Using a Novel Hybrid Monolith (H-Zsm5/Activated Carbon) as Adsorbent by Combined Vacuum and Electric Swing Adsorption (Vesa). *Chem. Eng. J.* **2019**, *358*, 707−717.

(60) Rezaei, F.; Subramanian, S.; Kalyanaraman, J.; Lively, R. P.; Kawajiri, Y.; Realff, M. J. Modeling of Rapid Temperature Swing Adsorption Using Hollow Fiber Sorbents. *Chem. Eng. Sci.* **2014**, *113*, 62−76.

(61) Lively, R. P.; Bessho, N.; Bhandari, D. A.; Kawajiri, Y.; Koros, W. J. Thermally Moderated Hollow Fiber Sorbent Modules in Rapidly Cycled Pressure Swing Adsorption Mode for Hydrogen Purification. *Int. J. Hydrogen Energy* **2012**, *37*, 15227−15240.

(62) Grande, C. A.; Blom, R.; Middelkoop, V.; Matras, D.; Vamvakeros, A.; Jacques, S. D. M.; Beale, A. M.; Di Michiel, M.; Anne Andreassen, K.; Bouzga, A. M. Multiscale Investigation of Adsorption Properties of Novel 3d Printed Utsa-16 Structures. *Chem. Eng. J.* **2020**, *402*, 126166.

(63) Thakkar, H.; Eastman, S.; Hajari, A.; Rownaghi, A. A.; Knox, J. C.; Rezaei, F. 3d-Printed Zeolite Monoliths for CO_2 Removal from Enclosed Environments. *ACS Appl. Mater. Interfaces* **2016**, *8*, 27753−27761.

(64) Middelkoop, V.; Coenen, K.; Schalck, J.; Van Sint Annaland, M.; Gallucci, F. 3d Printed Versus Spherical Adsorbents for Gas Sweetening. *Chem. Eng. J.* **2019**, *357*, 309−319.

(65) Rezaei, F.; Webley, P. Structured Adsorbents in Gas Separation Processes. *Sep. Purif. Technol.* **2010**, *70*, 243−256.

(66) Rezaei, F.; Mosca, A.; Webley, P.; Hedlund, J.; Xiao, P. Comparison of Traditional and Structured Adsorbents for CO_2 Separation by Vacuum-Swing Adsorption. *Ind. Eng. Chem. Res.* **2010**, *49*, 4832−4841.

(67) Thakkar, H.; Eastman, S.; Al-Naddaf, Q.; Rownaghi, A. A.; Rezaei, F. 3d-Printed Metal-Organic Framework Monoliths for Gas Adsorption Processes. *ACS Appl. Mater. Interfaces* **2017**, *9*, 35908−35916.

(68) Wang, S.; Bai, P.; Sun, M.; Liu, W.; Li, D.; Wu, W.; Yan, W.; Shang, J.; Yu, J. Fabricating Mechanically Robust Binder-Free Structured Zeolites by 3d Printing Coupled with Zeolite Soldering: A Superior Configuration for CO_2 Capture. *Advanced Science* **2019**, *6*, 1901317.

(69) Leung, D. Y. C.; Caramanna, G.; Maroto-Valer, M. M. An Overview of Current Status of Carbon Dioxide Capture and Storage Technologies. *Renewable Sustainable Energy Rev.* **2014**, *39*, 426−443.

(70) Yu, C.-H.; Huang, C.-H.; Tan, C.-S. A Review of CO_2 Capture by Absorption and Adsorption. *Aerosol Air Qual. Res.* **2012**, *12*, 745−769.

(71) Ben-Mansour, R.; Habib, M. A.; Bamidele, O. E.; Basha, M.; Qasem, N. A. A.; Peedikakkal, A.; Laoui, T.; Ali, M. Carbon Capture by Physical Adsorption: Materials, Experimental Investigations and Numerical Modeling and Simulations - a Review. *Appl. Energy* **2016**, *161*, 225−255.

(72) Wilcox, J.; Haghpanah, R.; Rupp, E. C.; He, J.; Lee, K. Advancing Adsorption and Membrane Separation Processes for the Gigaton Carbon Capture Challenge. *Annu. Rev. Chem. Biomol. Eng.* **2014**, *5*, 479−505.

(73) Düren, T.; Sarkisov, L.; Yaghi, O. M.; Snurr, R. Q. Design of New Materials for Methane Storage. *Langmuir* **2004**, *20*, 2683−2689.

(74) Haldoupis, E.; Nair, S.; Sholl, D. S. Pore Size Analysis of > 250000 Hypothetical Zeolites. *Phys. Chem. Chem. Phys.* **2011**, *13*, 5053−5060.

(75) Krishna, R.; van Baten, J. M. In Silico Screening of Zeolite Membranes for CO_2 Capture. *J. Membr. Sci.* **2010**, *360*, 323−333.

(76) Sun, W.; Lin, L.-C.; Peng, X.; Smit, B. Computational Screening of Porous Metal-Organic Frameworks and Zeolites for the Removal of SO_2 and NO_x from Flue Gases. *AIChE J.* **2014**, *60*, 2314−2323.

(77) Qiao, Z.; Peng, C.; Zhou, J.; Jiang, J. High-Throughput Computational Screening of 137953 Metal-Organic Frameworks for Membrane Separation of a $CO_2/N_2/CH_4$Mixture. *J. Mater. Chem. A* **2016**, *4*, 15904−15912.

(78) Li, S.; Chung, Y. G.; Snurr, R. Q. High-Throughput Screening of Metal-Organic Frameworks for CO_2 Capture in the Presence of Water. *Langmuir* **2016**, *32*, 10368−10376.

(79) Krishna, R.; van Baten, J. M. Elucidation of Selectivity Reversals for Binary Mixture Adsorption in Microporous Adsorbents. *ACS Omega* **2020**, *5*, 9031−9040.

(80) Baksh, S. A. B.; Notaro, F. Method for Production of Nitrogen Using Oxygen Selective Adsorbents. U.S. Patent US005735938A, 1998.

(81) Rege, S. U.; Yang, R. T. A Simple Parameter for Selecting an Adsorbent for Gas Separation by Pressure Swing Adsorption. *Sep. Sci. Technol.* **2001**, *36*, 3355−3365.

(82) Pirngruber, G. D.; Hamon, L.; Bourrelly, S.; Llewellyn, P. L.; Lenoir, E.; Guillerm, V.; Serre, C.; Devic, T. A Method for Screening the Potential of Mofs as CO_2 Adsorbents in Pressure Swing Adsorption Processes. *ChemSusChem* **2012**, *5*, 762−776.

(83) Wiersum, A. D.; Chang, J.-S.; Serre, C.; Llewellyn, P. L. An Adsorbent Performance Indicator as a First Step Evaluation of Novel Sorbents for Gas Separations: Application to Metal-Organic Frameworks. *Langmuir* **2013**, *29*, 3301−3309.

(84) Chung, Y. G.; Gómez-Gualdrón, D. A.; Li, P.; Leperi, K. T.; Deria, P.; Zhang, H.; Vermeulen, N. A.; Stoddart, J. F.; You, F.; Hupp, J. T.; Farha, O. K.; Snurr, R. Q. In Silico Discovery of Metal-Organic Frameworks for Precombustion CO_2 Capture Using a Genetic Algorithm. *Sci. Adv.* **2016**, *2*, No. e1600909.

(85) Braun, E.; Zurhelle, A. F.; Thijssen, W.; Schnell, S. K.; Lin, L.-C.; Kim, J.; Thompson, J. A.; Smit, B. High-Throughput Computational Screening of Nanoporous Adsorbents for CO_2 Capture from Natural Gas. *Mol. Syst. Des. Eng.* **2016**, *1*, 175−188.

(86) Lin, L. C.; Berger, A. H.; Martin, R. L.; Kim, J.; Swisher, J. A.; Jariwala, K.; Rycroft, C. H.; Bhown, A. S.; Deem, M. W.; Haranczyk, M.; Smit, B. In Silico Screening of Carbon-Capture Materials. *Nat. Mater.* **2012**, *11*, 633−641.

(87) Huck, J. M.; Lin, L.-C.; Berger, A. H.; Shahrak, M. N.; Martin, R. L.; Bhown, A. S.; Haranczyk, M.; Reuter, K.; Smit, B. Evaluating Different Classes of Porous Materials for Carbon Capture. *Energy Environ. Sci.* **2014**, *7*, 4132−4146.

(88) Khurana, M.; Farooq, S. Adsorbent Screening for Postcombustion CO_2 Capture: A Method Relating Equilibrium Isotherm Characteristics to an Optimum Vacuum Swing Adsorption Process Performance. *Ind. Eng. Chem. Res.* **2016**, *55*, 2447−2460.

(89) Farmahini, A. H.; Krishnamurthy, S.; Friedrich, D.; Brandani, S.; Sarkisov, L. From Crystal to Adsorption Column: Challenges in Multiscale Computational Screening of Materials for Adsorption Separation Processes. *Ind. Eng. Chem. Res.* **2018**, *57*, 15491−15511.

(90) Khurana, M.; Farooq, S. Integrated Adsorbent Process Optimization for Minimum Cost of Electricity Including Carbon Capture by a Vsa Process. *AIChE J.* **2019**, *65*, 184−195.

(91) Susarla, N.; Haghpanah, R.; Karimi, I. A.; Farooq, S.; Rajendran, A.; Tan, L. S. C.; Lim, J. S. T. Energy and Cost Estimates for Capturing CO_2 from a Dry Flue Gas Using Pressure/Vacuum Swing Adsorption. *Chem. Eng. Res. Des.* **2015**, *102*, 354−367.

(92) Subraveti, G. S.; Roussanaly, S.; Anantharaman, R.; Riboldi, L.; Rajendran, A. Techno-Economic Assessment of Optimised Vacuum Swing Adsorption for Post-Combustion CO_2 Capture from Steam-Methane Reformer Flue Gas. *Sep. Purif. Technol.* **2021**, *256*, 117832.

(93) Leperi, K. T.; Chung, Y. G.; You, F.; Snurr, R. Q. Development of a General Evaluation Metric for Rapid Screening of Adsorbent Materials for Postcombustion CO_2 Capture. *ACS Sustainable Chem. Eng.* **2019**, *7*, 11529−11539.

(94) Park, J.; Rubiera Landa, H. O.; Kawajiri, Y.; Realff, M. J.; Lively, R. P.; Sholl, D. S. How Well Do Approximate Models of Adsorption-Based CO_2 Capture Processes Predict Results of Detailed Process Models? *Ind. Eng. Chem. Res.* **2020**, *59*, 7097−7108.

(95) Bae, Y.-S.; Snurr, R. Q. Development and Evaluation of Porous Materials for Carbon Dioxide Separation and Capture. *Angew. Chem., Int. Ed.* **2011**, *50*, 11586−11596.

(96) Feng, B.; An, H.; Tan, E. Screening of CO_2 Adsorbing Materials for Zero Emission Power Generation Systems. *Energy Fuels* **2007**, *21*, 426−434.

(97) Babarao, R.; Jiang, J. Molecular Screening of Metal-Organic Frameworks for CO_2 Storage. *Langmuir* **2008**, *24*, 6270−6278.

(98) Keskin, S.; Sholl, D. S. Efficient Methods for Screening of Metal Organic Framework Membranes for Gas Separations Using Atomically Detailed Models. *Langmuir* **2009**, *25*, 11786−11795.

(99) Haldoupis, E.; Nair, S.; Sholl, D. S. Efficient Calculation of Diffusion Limitations in Metal Organic Framework Materials: A Tool for Identifying Materials for Kinetic Separations. *J. Am. Chem. Soc.* **2010**, *132*, 7528−7539.

(100) Wilmer, C. E.; Leaf, M.; Lee, C. Y.; Farha, O. K.; Hauser, B. G.; Hupp, J. T.; Snurr, R. Q. Large-Scale Screening of Hypothetical Metal-Organic Frameworks. *Nat. Chem.* **2012**, *4*, 83−89.

(101) Wilmer, C. E.; Farha, O. K.; Bae, Y.-S.; Hupp, J. T.; Snurr, R. Q. Structure-Property Relationships of Porous Materials for Carbon Dioxide Separation and Capture. *Energy Environ. Sci.* **2012**, *5*, 9849−9856.

(102) Willems, T. F.; Rycroft, C. H.; Kazi, M.; Meza, J. C.; Haranczyk, M. Algorithms and Tools for High-Throughput Geometry-Based Analysis of Crystalline Porous Materials. *Microporous Mesoporous Mater.* **2012**, *149*, 134−141.

(103) Sarkisov, L.; Harrison, A. Computational Structure Character-isation Tools in Application to Ordered and Disordered Porous Materials. *Mol. Simul.* **2011**, *37*, 1248−1257.

(104) First, E. L.; Gounaris, C. E.; Wei, J.; Floudas, C. A. Computational Characterization of Zeolite Porous Networks: An Automated Approach. *Phys. Chem. Chem. Phys.* **2011**, *13*, 17339−17358.

(105) First, E. L.; Floudas, C. A. Mofomics: Computational Pore Characterization of Metal-Organic Frameworks. *Microporous Mesoporous Mater.* **2013**, *165*, 32−39.

(106) Keskin, S.; Sholl, D. S. Screening Metal-Organic Framework Materials for Membrane-Based Methane/Carbon Dioxide Separations. *J. Phys. Chem. C* **2007**, *111*, 14055−14059.

(107) Erucar, I.; Keskin, S. Screening Metal-Organic Framework-Based Mixed-Matrix Membranes for CO_2/CH_4 Separations. *Ind. Eng. Chem. Res.* **2011**, *50*, 12606−12616.

(108) Erucar, I.; Keskin, S. Computational Screening of Metal Organic Frameworks for Mixed Matrix Membrane Applications. *J. Membr. Sci.* **2012**, *407−408*, 221−230.

(109) Yilmaz, G.; Keskin, S. Predicting the Performance of Zeolite Imidazolate Framework/Polymer Mixed Matrix Membranes for CO_2, CH_4, and H_2 Separations Using Molecular Simulations. *Ind. Eng. Chem. Res.* **2012**, *51*, 14218−14228.

(110) Kim, J.; Abouelnasr, M.; Lin, L.-C.; Smit, B. Large-Scale Screening of Zeolite Structures for CO_2 Membrane Separations. *J. Am. Chem. Soc.* **2013**, *135*, 7545−7552.

(111) Baerlocher, C.; McCusker, L. B. *Database of Zeolite Structures.* International Zeolite Association: http://www.iza-structure.org/databases/, 2020.

(112) Pophale, R.; Cheeseman, P. A.; Deem, M. W. A Database of New Zeolite-Like Materials. *Phys. Chem. Chem. Phys.* **2011**, *13*, 12407−12412.

(113) Wilmer, C. E.; Kim, K. C.; Snurr, R. Q. An Extended Charge Equilibration Method. *J. Phys. Chem. Lett.* **2012**, *3*, 2506−2511.

(114) Campañá, C.; Mussard, B.; Woo, T. K. Electrostatic Potential Derived Atomic Charges for Periodic Systems Using a Modified Error Functional. *J. Chem. Theory Comput.* **2009**, *5*, 2866−2878.

(115) Li, S.; Chung, Y. G.; Simon, C. M.; Snurr, R. Q. High-Throughput Computational Screening of Multivariate Metal-Organic Frameworks (Mtv-Mofs) for CO_2 Capture. *J. Phys. Chem. Lett.* **2017**, *8*, 6135−6141.

(116) Nalaparaju, A.; Khurana, M.; Farooq, S.; Karimi, I. A.; Jiang, J. W. CO_2 Capture in Cation-Exchanged Metal-Organic Frameworks: Holistic Modeling from Molecular Simulation to Process Optimization. *Chem. Eng. Sci.* **2015**, *124*, 70−78.

(117) Haghpanah, R.; Majumder, A.; Nilam, R.; Rajendran, A.; Farooq, S.; Karimi, I. A.; Amanullah, M. Multiobjective Optimization of a Four-Step Adsorption Process for Postcombustion CO_2 Capture Via Finite Volume Simulation. *Ind. Eng. Chem. Res.* **2013**, *52*, 4249−4265.

(118) Maring, B. J.; Webley, P. A. A New Simplified Pressure/Vacuum Swing Adsorption Model for Rapid Adsorbent Screening for CO_2 Capture Applications. *Int. J. Greenhouse Gas Control* **2013**, *15*, 16−31.

(119) Krishnamurthy, S.; Rao, V. R.; Guntuka, S.; Sharratt, P.; Haghpanah, R.; Rajendran, A.; Amanullah, M.; Karimi, I. A.; Farooq, S. CO_2 Capture from Dry Flue Gas by Vacuum Swing Adsorption: A Pilot Plant Study. *AIChE J.* **2014**, *60*, 1830−1842.

(120) Estupiñan Perez, L.; Sarkar, P.; Rajendran, A. Experimental Validation of Multi-Objective Optimization Techniques for Design of Vacuum Swing Adsorption Processes. *Sep. Purif. Technol.* **2019**, *224*, 553−563.

(121) Subramanian Balashankar, V.; Rajendran, A. Process Optimization-Based Screening of Zeolites for Post-Combustion CO_2 Capture by Vacuum Swing Adsorption. *ACS Sustainable Chem. Eng.* **2019**, *7*, 17747−17755.

(122) Farmahini, A. H.; Friedrich, D.; Brandani, S.; Sarkisov, L. Exploring New Sources of Efficiency in Process-Driven Materials Screening for Post-Combustion Carbon Capture. *Energy Environ. Sci.* **2020**, *13*, 1018−1037.

(123) Ga, S.; Jang, H.; Lee, J. H. New Performance Indicators for Adsorbent Evaluation Derived from a Reduced Order Model of an Idealized Psa Process for CO_2 Capture. *Comput. Chem. Eng.* **2017**, *102*, 188−212.

(124) Burns, T. D.; Pai, K. N.; Subraveti, S. G.; Collins, S. P.; Krykunov, M.; Rajendran, A.; Woo, T. K. Prediction of MOF Performance in Vacuum Swing Adsorption Systems for Postcombustion CO_2 Capture Based on Integrated Molecular Simulations, Process Optimizations, and Machine Learning Models. *Environ. Sci. Technol.* **2020**, *54*, 4536−4544.

(125) Danaci, D.; Bui, M.; Mac Dowell, N.; Petit, C. Exploring the Limits of Adsorption-Based CO_2 Capture Using Mofs with Pvsa - from Molecular Design to Process Economics. *Mol. Syst. Des. Eng.* **2020**, *5*, 212−231.

(126) Yancy-Caballero, D.; Leperi, K. T.; Bucior, B. J.; Richardson, R. K.; Islamoglu, T.; Farha, O. K.; You, F.; Snurr, R. Q. Process-Level Modelling and Optimization to Evaluate Metal-Organic Frameworks for Post-Combustion Capture of CO_2. *Mol. Syst. Des. Eng.* **2020**, *5*, 1205.

(127) Pai, K. N.; Prasad, V.; Rajendran, A. Generalized, Adsorbent-Agnostic, Artificial Neural Network Framework for Rapid Simulation, Optimization and Adsorbent-Screening of Adsorption Processes. *Ind. Eng. Chem. Res.* **2020**, *59*, 16730.

(128) Yaghi, O. M.; Li, H. Hydrothermal Synthesis of a Metal-Organic Framework Containing Large Rectangular Channels. *J. Am. Chem. Soc.* **1995**, *117*, 10401−10402.

(129) Li, H.; Eddaoudi, M.; O'Keeffe, M.; Yaghi, O. M. Design and Synthesis of an Exceptionally Stable and Highly Porous Metal-Organic Framework. *Nature* **1999**, *402*, 276−279.

(130) Eddaoudi, M.; Kim, J.; Rosi, N.; Vodak, D.; Wachter, J.; Keeffe, M.; Yaghi, O. M. Systematic Design of Pore Size and Functionality in Isoreticular Mofs and Their Application in Methane Storage. *Science* **2002**, *295*, 469.

(131) Yaghi, O. M.; O'Keeffe, M.; Ockwig, N. W.; Chae, H. K.; Eddaoudi, M.; Kim, J. Reticular Synthesis and the Design of New Materials. *Nature* **2003**, *423*, 705−714.

(132) Li, A.; Bueno-Perez, R.; Wiggin, S.; Fairen-Jimenez, D. Enabling Efficient Exploration of Metal-Organic Frameworks in the Cambridge Structural Database. *CrystEngComm* **2020**, *22*, 7152.

(133) Huang, X.; Zhang, J.; Chen, X. [Zn(Bim)2] · (H₂O)1.67: A Metal-Organic Open-Framework with Sodalite Topology. *Chin. Sci. Bull.* **2003**, *48*, 1531−1534.

(134) Tian, Y.-Q.; Chen, Z.-X.; Weng, L.-H.; Guo, H.-B.; Gao, S.; Zhao, D. Y. Two Polymorphs of Cobalt(Ii) Imidazolate Polymers Synthesized Solvothermally by Using One Organic Template N,N-Dimethylacetamide. *Inorg. Chem.* **2004**, *43*, 4631−4635.

(135) Park, K. S.; Ni, Z.; Côté, A. P.; Choi, J. Y.; Huang, R.; Uribe-Romo, F. J.; Chae, H. K.; O'Keeffe, M.; Yaghi, O. M. Exceptional Chemical and Thermal Stability of Zeolitic Imidazolate Frameworks. *Proc. Natl. Acad. Sci. U. S. A.* **2006**, *103*, 10186.

(136) Pimentel, B. R.; Parulkar, A.; Zhou, E. K.; Brunelli, N. A.; Lively, R. P. Zeolitic Imidazolate Frameworks: Next-Generation Materials for Energy-Efficient Gas Separations. *ChemSusChem* **2014**, *7*, 3202−3240.

(137) Ding, S. Y.; Wang, W. Covalent Organic Frameworks (Cofs): From Design to Applications. *Chem. Soc. Rev.* **2013**, *42*, 548−568.

(138) Marsh, H.; Rodríguez-Reinoso, F. *Activated Carbon*; Elsevier Science Ltd: Oxford, 2006; p 554.

(139) Presser, V.; Heon, M.; Gogotsi, Y. Carbide-Derived Carbons - from Porous Networks to Nanotubes and Graphene. *Adv. Funct. Mater.* **2011**, *21*, 810−833.

(140) McKeown, N. B. Polymers of Intrinsic Microporosity. *ISRN Materials Science* **2012**, *2012*, 1−16.

(141) Ben, T.; Qiu, S. Porous Aromatic Frameworks: Synthesis, Structure and Functions. *CrystEngComm* **2013**, *15*, 17−26.

(142) Newsam, J. M.; Treacy, M. M. J. Zeofile: A Stack of Zeolite Structure Types. *Zeolites* **1993**, *13*, 183−186.

(143) Reacy, M. M. J.; Rao, S.; Rivin, I. A Combinatorial Method for Generating New Zeolite Frameworks. In *Proceedings from the Ninth International Zeolite Conference*; von Ballmoos, R., Higgins, J. B., Treacy, M. M. J., Eds.; Butterworth-Heinemann: 1993; pp 381−388.

(144) Wells, S. A.; Foster, M. D.; Treacy, M. M. J. A Simple Geometric Structure Optimizer for Accelerated Detection of Infeasible Zeolite Graphs. *Microporous Mesoporous Mater.* **2006**, *93*, 151−157.

(145) Earl, D. J.; Deem, M. W. Toward a Database of Hypothetical Zeolite Structures. *Ind. Eng. Chem. Res.* **2006**, *45*, 5449−5454.

(146) Moosavi, S. M.; Xu, H.; Chen, L.; Cooper, A. I.; Smit, B. Geometric Landscapes for Material Discovery within Energy-Structure-Function Maps. *Chemical Science* **2020**, *11*, 5423.

(147) Moosavi, S. M.; Nandy, A.; Jablonka, K. M.; Ongari, D.; Janet, J. P.; Boyd, P. G.; Lee, Y.; Smit, B.; Kulik, H. J. Understanding the Diversity of the Metal-Organic Framework Ecosystem. *Nat. Commun.* **2020**, *11*, 4068.

(148) Sartbaeva, A.; Wells, S. A.; Treacy, M. M. J.; Thorpe, M. F. The Flexibility Window in Zeolites. *Nat. Mater.* **2006**, *5*, 962−965.

(149) Boyd, P. G.; Lee, Y.; Smit, B. Computational Development of the Nanoporous Materials Genome. *Nat. Rev. Mater.* **2017**, *2*, 17037.

(150) Groom, C. R.; Bruno, I. J.; Lightfoot, M. P.; Ward, S. C. The Cambridge Structural Database. *Acta Crystallogr., Sect. B: Struct. Sci., Cryst. Eng. Mater.* **2016**, *72*, 171−179.

(151) Chung, Y. G.; Camp, J.; Haranczyk, M.; Sikora, B. J.; Bury, W.; Krungleviciute, V.; Yildirim, T.; Farha, O. K.; Sholl, D. S.; Snurr, R. Q. Computation-Ready, Experimental Metal-Organic Frameworks: A Tool to Enable High-Throughput Screening of Nanoporous Crystals. *Chem. Mater.* **2014**, *26*, 6185−6192.

(152) Gómez-Gualdrón, D. A.; Colón, Y. J.; Zhang, X.; Wang, T. C.; Chen, Y.-S.; Hupp, J. T.; Yildirim, T.; Farha, O. K.; Zhang, J.; Snurr, R. Q. Evaluating Topologically Diverse Metal-Organic Frameworks for Cryo-Adsorbed Hydrogen Storage. *Energy Environ. Sci.* **2016**, *9*, 3279−3289.

(153) Martin, R. L.; Simon, C. M.; Smit, B.; Haranczyk, M. In Silico Design of Porous Polymer Networks: High-Throughput Screening for Methane Storage Materials. *J. Am. Chem. Soc.* **2014**, *136*, 5006−5022.

(154) Moghadam, P. Z.; Li, A.; Wiggin, S. B.; Tao, A.; Maloney, A. G. P.; Wood, P. A.; Ward, S. C.; Fairen-Jimenez, D. Development of a Cambridge Structural Database Subset: A Collection of Metal-Organic Frameworks for Past, Present, and Future. *Chem. Mater.* **2017**, *29*, 2618−2625.

(155) Sikora, B. J.; Winnegar, R.; Proserpio, D. M.; Snurr, R. Q. Textural Properties of a Large Collection of Computationally Constructed Mofs and Zeolites. *Microporous Mesoporous Mater.* **2014**, *186*, 207−213.

(156) Boyd, P. G.; Woo, T. K. A Generalized Method for Constructing Hypothetical Nanoporous Materials of Any Net Topology from Graph Theory. *CrystEngComm* **2016**, *18*, 3777−3792.

(157) Boyd, P. G.; Chidambaram, A.; García-Díez, E.; Ireland, C. P.; Daff, T. D.; Bounds, R.; Gładysiak, A.; Schouwink, P.; Moosavi, S. M.; Maroto-Valer, M. M.; Reimer, J. A.; Navarro, J. A. R.; Woo, T. K.; Garcia, S.; Stylianou, K. C.; Smit, B. Data-Driven Design of Metal-Organic Frameworks for Wet Flue Gas CO₂ Capture. *Nature* **2019**, *576*, 253−256.

(158) Rappe, A. K.; Goddard, W. A. Charge Equilibration for Molecular Dynamics Simulations. *J. Phys. Chem.* **1991**, *95*, 3358−3363.

(159) Kadantsev, E. S.; Boyd, P. G.; Daff, T. D.; Woo, T. K. Fast and Accurate Electrostatics in Metal Organic Frameworks with a Robust Charge Equilibration Parameterization for High-Throughput Virtual Screening of Gas Adsorption. *J. Phys. Chem. Lett.* **2013**, *4*, 3056−3061.

(160) Colón, Y. J.; Gómez-Gualdrón, D. A.; Snurr, R. Q. Topologically Guided, Automated Construction of Metal-Organic Frameworks and Their Evaluation for Energy-Related Applications. *Cryst. Growth Des.* **2017**, *17*, 5801−5810.

(161) Goldsmith, J.; Wong-Foy, A. G.; Cafarella, M. J.; Siegel, D. J. Theoretical Limits of Hydrogen Storage in Metal-Organic Frameworks: Opportunities and Trade-Offs. *Chem. Mater.* **2013**, *25*, 3373−3382.

(162) Panella, B.; Hirscher, M.; Roth, S. Hydrogen Adsorption in Different Carbon Nanostructures. *Carbon* **2005**, *43*, 2209−2214.

(163) Nazarian, D.; Camp, J. S.; Sholl, D. S. A Comprehensive Set of High-Quality Point Charges for Simulations of Metal-Organic Frameworks. *Chem. Mater.* **2016**, *28*, 785−793.

(164) Nazarian, D.; Camp, J. S.; Chung, Y. G.; Snurr, R. Q.; Sholl, D. S. Large-Scale Refinement of Metal-Organic Framework Structures Using Density Functional Theory. *Chem. Mater.* **2017**, *29*, 2521−2528.

(165) Chung, Y. G.; Haldoupis, E.; Bucior, B. J.; Haranczyk, M.; Lee, S.; Zhang, H.; Vogiatzis, K. D.; Milisavljevic, M.; Ling, S.; Camp, J. S.; Slater, B.; Siepmann, J. I.; Sholl, D. S.; Snurr, R. Q. Advances, Updates, and Analytics for the Computation-Ready, Experimental Metal-Organic Framework Database: Core Mof 2019. *J. Chem. Eng. Data* **2019**, *64*, 5985−5998.

(166) Deem, M. W.; Pophale, R.; Cheeseman, P. A.; Earl, D. J. Computational Discovery of New Zeolite-Like Materials. *J. Phys. Chem. C* **2009**, *113*, 21353−21360.

(167) Mercado, R.; Fu, R.-S.; Yakutovich, A. V.; Talirz, L.; Haranczyk, M.; Smit, B. In Silico Design of 2d and 3d Covalent Organic Frameworks for Methane Storage Applications. *Chem. Mater.* **2018**, *30*, 5069−5086.

(168) Tong, M.; Lan, Y.; Yang, Q.; Zhong, C. Exploring the Structure-Property Relationships of Covalent Organic Frameworks for Noble Gas Separations. *Chem. Eng. Sci.* **2017**, *168*, 456−464.

(169) Grimme, S. Semiempirical Gga-Type Density Functional Constructed with a Long-Range Dispersion Correction. *J. Comput. Chem.* **2006**, *27*, 1787−1799.

(170) Tong, M.; Lan, Y.; Yang, Q.; Zhong, C. *CoRE-COF Database*, ver. 4.0. 25/02/2020; https://github.com/core-cof/CoRE-COF-Database, 2020.

(171) Ongari, D.; Yakutovich, A. V.; Talirz, L.; Smit, B. Building a Consistent and Reproducible Database for Adsorption Evaluation in Covalent-Organic Frameworks. *ACS Cent. Sci.* **2019**, *5*, 1663−1675.

(172) Fraux, G.; Chibani, S.; Coudert, F.-X. Modelling of Framework Materials at Multiple Scales: Current Practices and Open Questions. *Philos. Trans. R. Soc., A* **2019**, *377*, 20180220.

(173) Simon, C. M.; Kim, J.; Gomez-Gualdron, D. A.; Camp, J. S.; Chung, Y. G.; Martin, R. L.; Mercado, R.; Deem, M. W.; Gunter, D.; Haranczyk, M.; Sholl, D. S.; Snurr, R. Q.; Smit, B. The Materials Genome in Action: Identifying the Performance Limits for Methane Storage. *Energy Environ. Sci.* **2015**, *8*, 1190−1199.

(174) Martin, R. L.; Simon, C. M.; Medasani, B.; Britt, D. K.; Smit, B.; Haranczyk, M. In Silico Design of Three-Dimensional Porous Covalent

Organic Frameworks Via Known Synthesis Routes and Commercially Available Species. *J. Phys. Chem. C* **2014**, *118*, 23790−23802.

(175) Thyagarajan, R.; Sholl, D. S. A Database of Porous Rigid Amorphous Materials. *Chem. Mater.* **2020**, *32*, 8020.

(176) Keen, D. A.; Bennett, T. D. Structural Investigations of Amorphous Metal-Organic Frameworks Formed Via Different Routes. *Phys. Chem. Chem. Phys.* **2018**, *20*, 7857−7861.

(177) Nguyen, T. X.; Cohaut, N.; Bae, J.-S.; Bhatia, S. K. New Method for Atomistic Modeling of the Microstructure of Activated Carbons Using Hybrid Reverse Monte Carlo Simulation. *Langmuir* **2008**, *24*, 7912−7922.

(178) Farmahini, A. H.; Opletal, G.; Bhatia, S. K. Structural Modelling of Silicon Carbide-Derived Nanoporous Carbon by Hybrid Reverse Monte Carlo Simulation. *J. Phys. Chem. C* **2013**, *117*, 14081−14094.

(179) Farmahini, A. H.; Bhatia, S. K. Hybrid Reverse Monte Carlo Simulation of Amorphous Carbon: Distinguishing between Competing Structures Obtained Using Different Modeling Protocols. *Carbon* **2015**, *83*, 53−70.

(180) Farmahini, A. H.; Bhatia, S. K. Effect of Structural Anisotropy and Pore-Network Accessibility on Fluid Transport in Nanoporous Ti3sic2 Carbide-Derived Carbon. *Carbon* **2016**, *103*, 16−27.

(181) de Tomas, C.; Suarez-Martinez, I.; Vallejos-Burgos, F.; López, M. J.; Kaneko, K.; Marks, N. A. Structural Prediction of Graphitization and Porosity in Carbide-Derived Carbons. *Carbon* **2017**, *119*, 1−9.

(182) de Tomas, C.; Suarez-Martinez, I.; Marks, N. A. Carbide-Derived Carbons for Dense and Tunable 3d Graphene Networks. *Appl. Phys. Lett.* **2018**, *112*, 251907.

(183) Zhang, D.; Dutzer, M. R.; Liang, T.; Fonseca, A. F.; Wu, Y.; Walton, K. S.; Sholl, D. S.; Farmahini, A. H.; Bhatia, S. K.; Sinnott, S. B. Computational Investigation on CO_2 Adsorption in Titanium Carbide-Derived Carbons with Residual Titanium. *Carbon* **2017**, *111*, 741−751.

(184) Hart, K. E.; Colina, C. M. Estimating Gas Permeability and Permselectivity of Microporous Polymers. *J. Membr. Sci.* **2014**, *468*, 259−268.

(185) Hart, K. E.; Abbott, L. J.; McKeown, N. B.; Colina, C. M. Toward Effective CO_2/CH_4 Separations by Sulfur-Containing Pims Via Predictive Molecular Simulations. *Macromolecules* **2013**, *46*, 5371−5380.

(186) Hart, K. E.; Colina, C. M. Ionomers of Intrinsic Microporosity: In Silico Development of Ionic-Functionalized Gas-Separation Membranes. *Langmuir* **2014**, *30*, 12039−12048.

(187) Kupgan, G.; Demidov, A. G.; Colina, C. M. Plasticization Behavior in Polymers of Intrinsic Microporosity (Pim-1): A Simulation Study from Combined Monte Carlo and Molecular Dynamics. *J. Membr. Sci.* **2018**, *565*, 95−103.

(188) Abbott, L. J.; Colina, C. M. Formation of Microporosity in Hyper-Cross-Linked Polymers. *Macromolecules* **2014**, *47*, 5409−5415.

(189) Tang, D.; Kupgan, G.; Colina, C. M.; Sholl, D. S. Rapid Prediction of Adsorption Isotherms of a Diverse Range of Molecules in Hyper-Cross-Linked Polymers. *J. Phys. Chem. C* **2019**, *123*, 17884−17893.

(190) Kupgan, G.; Liyana-Arachchi, T. P.; Colina, C. M. Pore Size Tuning of Poly(Styrene-Co-Vinylbenzyl Chloride-Co-Divinylbenzene) Hypercrosslinked Polymers: Insights from Molecular Simulations. *Polymer* **2016**, *99*, 173−184.

(191) Bousige, C.; Ghimbeu, C. M.; Vix-Guterl, C.; Pomerantz, A. E.; Suleimenova, A.; Vaughan, G.; Garbarino, G.; Feygenson, M.; Wildgruber, C.; Ulm, F.-J.; Pellenq, R. J. M.; Coasne, B. Realistic Molecular Model of Kerogen's Nanostructure. *Nat. Mater.* **2016**, *15*, 576−582.

(192) Pellenq, R. J.; Kushima, A.; Shahsavari, R.; Van Vliet, K. J.; Buehler, M. J.; Yip, S.; Ulm, F.-J. A Realistic Molecular Model of Cement Hydrates. *Proc. Natl. Acad. Sci. U. S. A.* **2009**, *106*, 16102.

(193) Sarkisov, L.; Kim, J. Computational Structure Characterization Tools for the Era of Material Informatics. *Chem. Eng. Sci.* **2015**, *121*, 322−330.

(194) Coudert, F.-X.; Fuchs, A. H. Computational Characterization and Prediction of Metal-Organic Framework Properties. *Coord. Chem. Rev.* **2016**, *307*, 211−236.

(195) Sarkisov, L.; Bueno-Perez, R.; Sutharson, M.; Fairen-Jimenez, D. Material Informatics with Poreblazer V4.0 and Csd Mof Database. *Chem. Mater.* **2020**, *32*, 9849.

(196) Opletal, G.; Petersen, T. C.; Russo, S. P.; Barnard, A. S. Porosityplus: Characterisation of Defective, Nanoporous and Amorphous Materials. *Journal of Physics: Materials* **2018**, *1*, 016002.

(197) Foster, M. D.; Rivin, I.; Treacy, M. M. J.; Delgado Friedrichs, O. A Geometric Solution to the Largest-Free-Sphere Problem in Zeolite Frameworks. *Microporous Mesoporous Mater.* **2006**, *90*, 32−38.

(198) Dubbeldam, D.; Calero, S.; Ellis, D. E.; Snurr, R. Q. Raspa: Molecular Simulation Software for Adsorption and Diffusion in Flexible Nanoporous Materials. *Mol. Simul.* **2016**, *42*, 81−101.

(199) Yang, Q.; Liu, D.; Zhong, C.; Li, J. R. Development of Computational Methodologies for Metal-Organic Frameworks and Their Application in Gas Separations. *Chem. Rev.* **2013**, *113*, 8261−8323.

(200) Smit, B.; Maesen, T. L. M. Molecular Simulations of Zeolites: Adsorption, Diffusion, and Shape Selectivity. *Chem. Rev.* **2008**, *108*, 4125−4184.

(201) Allen, M. P.; Tildesley, D. J. *Computer Simulation of Liquids*, 2nd ed.; Oxford University Press: 2017.

(202) Frenkel, D.; Smit, B. Monte Carlo Simulations. In *Understanding Molecular Simulation*, 2nd ed.; Frenkel, D., Smit, B., Eds.; Academic Press: San Diego, 2002; Chapter 3, pp 23−61.

(203) Frenkel, D.; Smit, B. Monte Carlo Simulations in Various Ensembles. In *Understanding Molecular Simulation*, 2nd ed.; Frenkel, D., Smit, B., Eds.; Academic Press: San Diego, 2002; Chapter 5, pp 111−137.

(204) Dubbeldam, D.; Torres-Knoop, A.; Walton, K. S. On the Inner Workings of Monte Carlo Codes. *Mol. Simul.* **2013**, *39*, 1253−1292.

(205) Zhang, J.-P.; Zhou, H.-L.; Zhou, D.-D.; Liao, P.-Q.; Chen, X.-M. Controlling Flexibility of Metal-Organic Frameworks. *National Science Review* **2018**, *5*, 907−919.

(206) Agrawal, M.; Sholl, D. S. Effects of Intrinsic Flexibility on Adsorption Properties of Metal-Organic Frameworks at Dilute and Nondilute Loadings. *ACS Appl. Mater. Interfaces* **2019**, *11*, 31060−31068.

(207) Gee, J. A.; Sholl, D. S. Effect of Framework Flexibility on C8 Aromatic Adsorption at High Loadings in Metal-Organic Frameworks. *J. Phys. Chem. C* **2016**, *120*, 370−376.

(208) Witman, M.; Ling, S.; Jawahery, S.; Boyd, P. G.; Haranczyk, M.; Slater, B.; Smit, B. The Influence of Intrinsic Framework Flexibility on Adsorption in Nanoporous Materials. *J. Am. Chem. Soc.* **2017**, *139*, 5547−5557.

(209) Daou, A. S. S.; Findley, J. M.; Fang, H.; Boulfelfel, S. E.; Ravikovitch, P. I.; Sholl, D. S. Quantifying Impact of Intrinsic Flexibility on Molecular Adsorption in Zeolites. *J. Phys. Chem. C* **2021**, *125*, 5296−5305.

(210) Brandani, S.; Mangano, E.; Sarkisov, L. Net, Excess and Absolute Adsorption and Adsorption of Helium. *Adsorption* **2016**, *22*, 261−276.

(211) Torres-Knoop, A.; Poursaeidesfahani, A.; Vlugt, T. J. H.; Dubbeldam, D. Behavior of the Enthalpy of Adsorption in Nanoporous Materials Close to Saturation Conditions. *J. Chem. Theory Comput.* **2017**, *13*, 3326−3339.

(212) Ghosh, P.; Kim, K. C.; Snurr, R. Q. Modeling Water and Ammonia Adsorption in Hydrophobic Metal-Organic Frameworks: Single Components and Mixtures. *J. Phys. Chem. C* **2014**, *118*, 1102−1110.

(213) Coudert, F.-X. Responsive Metal-Organic Frameworks and Framework Materials: Under Pressure, Taking the Heat, in the Spotlight, with Friends. *Chem. Mater.* **2015**, *27*, 1905−1916.

(214) Sweatman, M. B. Preface to the Special Issue on 'Monte Carlo Codes, Tools and Algorithms'. *Mol. Simul.* **2013**, *39*, 1123−1124.

(215) Gowers, R. J.; Farmahini, A. H.; Friedrich, D.; Sarkisov, L. Automated Analysis and Benchmarking of GCMC Simulation Programs in Application to Gas Adsorption. *Mol. Simul.* **2018**, *44*, 309−321.

(216) Walton, K. S.; Millward, A. R.; Dubbeldam, D.; Frost, H.; Low, J. J.; Yaghi, O. M.; Snurr, R. Q. Understanding Inflections and Steps in Carbon Dioxide Adsorption Isotherms in Metal-Organic Frameworks. *J. Am. Chem. Soc.* **2008**, *130*, 406−407.

(217) Gowers, R. J.; Farmahini, A. H.; Friedrich, D.; Sarkisov, L. *Gcmc Benchmarks.* https://github.com/SarkisovGroup/gcmcbenchmarks, 2018.

(218) Shah, J. K.; Marin-Rimoldi, E.; Mullen, R. G.; Keene, B. P.; Khan, S.; Paluch, A. S.; Rai, N.; Romanielo, L. L.; Rosch, T. W.; Yoo, B.; Maginn, E. J. Cassandra: An Open Source Monte Carlo Package for Molecular Simulation. *J. Comput. Chem.* **2017**, *38*, 1727−1739.

(219) Purton, J. A.; Crabtree, J. C.; Parker, S. C. Dl_Monte: A General Purpose Program for Parallel Monte Carlo Simulation. *Mol. Simul.* **2013**, *39*, 1240−1252.

(220) Gupta, A.; Chempath, S.; Sanborn, M. J.; Clark, L. A.; Snurr, R. Q. Object-Oriented Programming Paradigms for Molecular Modeling. *Mol. Simul.* **2003**, *29*, 29−46.

(221) Martin, M. G. Mcccs Towhee: A Tool for Monte Carlo Molecular Simulation. *Mol. Simul.* **2013**, *39*, 1212−1222.

(222) Chempath, S.; Düren, T.; Sarkisov, L.; Snurr, R. Q. Experiences with the Publicly Available Multipurpose Simulation Code, Music. *Mol. Simul.* **2013**, *39*, 1223−1232.

(223) Martin, M. G. *Mcccs Towhee,* http://towhee.sourceforge.net/ (accessed 26/06/2020).

(224) Zhang, J.; Xu, F.; Hong, Y.; Xiong, Q.; Pan, J. A Comprehensive Review on the Molecular Dynamics Simulation of the Novel Thermal Properties of Graphene. *RSC Adv.* **2015**, *5*, 89415−89426.

(225) Hollingsworth, S. A.; Dror, R. O. Molecular Dynamics Simulation for All. *Neuron* **2018**, *99*, 1129−1143.

(226) Ma, Z.; Ranjith, P. G. Review of Application of Molecular Dynamics Simulations in Geological Sequestration of Carbon Dioxide. *Fuel* **2019**, *255*, 115644.

(227) Sliwoski, G.; Kothiwale, S.; Meiler, J.; Lowe, E. W. Computational Methods in Drug Discovery. *Pharmacol. Rev.* **2014**, *66*, 334.

(228) Singh, A.; Vanga, S. K.; Orsat, V.; Raghavan, V. Application of Molecular Dynamic Simulation to Study Food Proteins: A Review. *Crit. Rev. Food Sci. Nutr.* **2018**, *58*, 2779−2789.

(229) Dubbeldam, D.; Snurr, R. Q. Recent Developments in the Molecular Modeling of Diffusion in Nanoporous Materials. *Mol. Simul.* **2007**, *33*, 305−325.

(230) Boulfelfel, S. E.; Ravikovitch, P. I.; Sholl, D. S. Modeling Diffusion of Linear Hydrocarbons in Silica Zeolite Lta Using Transition Path Sampling. *J. Phys. Chem. C* **2015**, *119*, 15643−15653.

(231) Verploegh, R. J.; Nair, S.; Sholl, D. S. Temperature and Loading-Dependent Diffusion of Light Hydrocarbons in Zif-8 as Predicted through Fully Flexible Molecular Simulations. *J. Am. Chem. Soc.* **2015**, *137*, 15760−15771.

(232) Frenkel, D.; Smit, B. Molecular Dynamics Simulations. In *Understanding Molecular Simulation*, 2nd ed.; Frenkel, D., Smit, B., Eds.; Academic Press: San Diego, 2002; Chapter 4, pp 63−107.

(233) Frenkel, D.; Smit, B. Molecular Dynamics in Various Ensembles. In *Understanding Molecular Simulation*, 2nd ed.; Frenkel, D., Smit, B., Eds.; Academic Press: San Diego, 2002; Chapter 6, pp 139−163.

(234) Gubbins, K. E.; Liu, Y.-C.; Moore, J. D.; Palmer, J. C. The Role of Molecular Modeling in Confined Systems: Impact and Prospects. *Phys. Chem. Chem. Phys.* **2011**, *13*, 58−85.

(235) Sholl, D. S. Understanding Macroscopic Diffusion of Adsorbed Molecules in Crystalline Nanoporous Materials Via Atomistic Simulations. *Acc. Chem. Res.* **2006**, *39*, 403−411.

(236) Verlet, L. Computer "Experiments" on Classical Fluids. I. Thermodynamical Properties of Lennard-Jones Molecules. *Phys. Rev.* **1967**, *159*, 98−103.

(237) Hinchliffe, A. *Molecular Modelling for Beginners*, 2nd ed.; Wiley-Blackwell: Oxford, 2008.

(238) Hockney, R. W. *Computer Simulation Using Particles*, special student edition; Hilger: Bristol, 1988.

(239) Hertäg, L.; Bux, H.; Caro, J.; Chmelik, C.; Remsungnen, T.; Knauth, M.; Fritzsche, S. Diffusion of CH_4 and H_2 in Zif-8. *J. Membr. Sci.* **2011**, *377*, 36−41.

(240) Zheng, B.; Sant, M.; Demontis, P.; Suffritti, G. B. Force Field for Molecular Dynamics Computations in Flexible Zif-8 Framework. *J. Phys. Chem. C* **2012**, *116*, 933−938.

(241) Zhang, L.; Wu, G.; Jiang, J. Adsorption and Diffusion of CO_2 and CH_4 in Zeolitic Imidazolate Framework-8: Effect of Structural Flexibility. *J. Phys. Chem. C* **2014**, *118*, 8788−8794.

(242) Pantatosaki, E.; Megariotis, G.; Pusch, A.-K.; Chmelik, C.; Stallmach, F.; Papadopoulos, G. K. On the Impact of Sorbent Mobility on the Sorbed Phase Equilibria and Dynamics: A Study of Methane and Carbon Dioxide within the Zeolite Imidazolate Framework-8. *J. Phys. Chem. C* **2012**, *116*, 201−207.

(243) Keskin, S.; Liu, J.; Rankin, R. B.; Johnson, J. K.; Sholl, D. S. Progress, Opportunities, and Challenges for Applying Atomically Detailed Modeling to Molecular Adsorption and Transport in Metal-Organic Framework Materials. *Ind. Eng. Chem. Res.* **2009**, *48*, 2355−2371.

(244) Huang, B. L.; McGaughey, A. J. H.; Kaviany, M. Thermal Conductivity of Metal-Organic Framework 5 (Mof-5): Part I. Molecular Dynamics Simulations. *Int. J. Heat Mass Transfer* **2007**, *50*, 393−404.

(245) Schelling, P. K.; Phillpot, S. R.; Keblinski, P. Comparison of Atomic-Level Simulation Methods for Computing Thermal Conductivity. *Phys. Rev. B: Condens. Matter Mater. Phys.* **2002**, *65*, 144306.

(246) Ning, F. L.; Glavatskiy, K.; Ji, Z.; Kjelstrup, S.; H. Vlugt, T. J. Compressibility, Thermal Expansion Coefficient and Heat Capacity of CH_4 and CO_2 Hydrate Mixtures Using Molecular Dynamics Simulations. *Phys. Chem. Chem. Phys.* **2015**, *17*, 2869−2883.

(247) Chempath, S.; Krishna, R.; Snurr, R. Q. Nonequilibrium Molecular Dynamics Simulations of Diffusion of Binary Mixtures Containing Short N-Alkanes in Faujasite. *J. Phys. Chem. B* **2004**, *108*, 13481−13491.

(248) Skoulidas, A. I.; Sholl, D. S. Molecular Dynamics Simulations of Self-Diffusivities, Corrected Diffusivities, and Transport Diffusivities of Light Gases in Four Silica Zeolites to Assess Influences of Pore Shape and Connectivity. *J. Phys. Chem. A* **2003**, *107*, 10132−10141.

(249) Skoulidas, A. I.; Sholl, D. S. Self-Diffusion and Transport Diffusion of Light Gases in Metal-Organic Framework Materials Assessed Using Molecular Dynamics Simulations. *J. Phys. Chem. B* **2005**, *109*, 15760−15768.

(250) Ford, D. C.; Dubbeldam, D.; Snurr, R. Q.; Künzel, V.; Wehring, M.; Stallmach, F.; Kärger, J.; Müller, U. Self-Diffusion of Chain Molecules in the Metal-Organic Framework Irmof-1: Simulation and Experiment. *J. Phys. Chem. Lett.* **2012**, *3*, 930−933.

(251) Farmahini, A. H.; Shahtalebi, A.; Jobic, H.; Bhatia, S. K. Influence of Structural Heterogeneity on Diffusion of CH_4 and CO_2 in Silicon Carbide-Derived Nanoporous Carbon. *J. Phys. Chem. C* **2014**, *118*, 11784−11798.

(252) Farmahini, A. H.; Bhatia, S. K. Differences in the Adsorption and Diffusion Behaviour of Water and Non-Polar Gases in Nanoporous Carbon: Role of Cooperative Effects of Pore Confinement and Hydrogen Bonding. *Mol. Simul.* **2015**, *41*, 432−445.

(253) García-Sánchez, A.; Dubbeldam, D.; Calero, S. Modeling Adsorption and Self-Diffusion of Methane in Lta Zeolites: The Influence of Framework Flexibility. *J. Phys. Chem. C* **2010**, *114*, 15068−15074.

(254) Leroy, F.; Rousseau, B.; Fuchs, A. H. Self-Diffusion of N-Alkanes in Silicalite Using Molecular Dynamics Simulation: A Comparison between Rigid and Flexible Frameworks. *Phys. Chem. Chem. Phys.* **2004**, *6*, 775−783.

(255) Heffelfinger, G. S.; Swol, F. V. Diffusion in Lennard-Jones Fluids Using Dual Control Volume Grand Canonical Molecular Dynamics Simulation (Dcv-Gcmd). *J. Chem. Phys.* **1994**, *100*, 7548−7552.

(256) Swol, F. V.; Heffelfinger, G. S. Gradient-Driven Diffusion Using Dual Control Volume Grand Canonical Molecular Dynamics (Dcv-Gcmd). *MRS Proceedings* **1995**, *408*, 299.

(257) Krishna, R.; Wesselingh, J. A. The Maxwell-Stefan Approach to Mass Transfer. *Chem. Eng. Sci.* **1997**, *52*, 861−911.

(258) Kärger, J.; Ruthven, D. M. Diffusion in Nanoporous Materials: Fundamental Principles, Insights and Challenges. *New J. Chem.* **2016**, *40*, 4027−4048.

(259) Kärger, J. R.; Ruthven, D. M.; Theodorou, D. N. *Diffusion in Nanoporous Materials*; John Wiley & Sons: Hoboken, 2012.

(260) Wang, Y.; LeVan, M. D. Mixture Diffusion in Nanoporous Adsorbents: Development of Fickian Flux Relationship and Concentration-Swing Frequency Response Method. *Ind. Eng. Chem. Res.* **2007**, *46*, 2141−2154.

(261) Shen, C.; Grande, C. A.; Li, P.; Yu, J.; Rodrigues, A. E. Adsorption Equilibria and Kinetics of CO_2 and N_2 on Activated Carbon Beads. *Chem. Eng. J.* **2010**, *160*, 398−407.

(262) Haghpanah, R.; Rajendran, A.; Farooq, S.; Karimi, I. A. Optimization of One- and Two-Staged Kinetically Controlled CO_2 Capture Processes from Postcombustion Flue Gas on a Carbon Molecular Sieve. *Ind. Eng. Chem. Res.* **2014**, *53*, 9186−9198.

(263) Sedova, A.; Eblen, J. D.; Budiardja, R.; Tharrington, A.; Smith, J. C. High-Performance Molecular Dynamics Simulation for Biological and Materials Sciences: Challenges of Performance Portability. *2018 IEEE/ACM International Workshop on Performance, Portability and Productivity in HPC (P3HPC)*; IEEE: Dallas, TX, USA, 2018.

(264) Phillips, J. C.; Braun, R.; Wang, W.; Gumbart, J.; Tajkhorshid, E.; Villa, E.; Chipot, C.; Skeel, R. D.; Kalé, L.; Schulten, K. Scalable Molecular Dynamics with Namd. *J. Comput. Chem.* **2005**, *26*, 1781−1802.

(265) Brooks, B. R.; Bruccoleri, R. E.; Olafson, B. D.; States, D. J.; Swaminathan, S.; Karplus, M. Charmm: A Program for Macromolecular Energy, Minimization, and Dynamics Calculations. *J. Comput. Chem.* **1983**, *4*, 187−217.

(266) Plimpton, S. Fast Parallel Algorithms for Short-Range Molecular Dynamics. *J. Comput. Phys.* **1995**, *117*, 1−19.

(267) Abraham, M. J.; Murtola, T.; Schulz, R.; Páll, S.; Smith, J. C.; Hess, B.; Lindahl, E. Gromacs: High Performance Molecular Simulations through Multi-Level Parallelism from Laptops to Supercomputers. *SoftwareX* **2015**, *1−2*, 19−25.

(268) Todorov, I. T.; Smith, W.; Trachenko, K.; Dove, M. T. Dl_Poly_3: New Dimensions in Molecular Dynamics Simulations Via Massive Parallelism. *J. Mater. Chem.* **2006**, *16*, 1911−1918.

(269) Dubbeldam, D.; Walton, K. S.; Vlugt, T. J. H.; Calero, S. Design, Parameterization, and Implementation of Atomic Force Fields for Adsorption in Nanoporous Materials. *Adv. Theory Simul.* **2019**, *2*, 1900135.

(270) Weiner, P. K.; Kollman, P. A. Amber: Assisted Model Building with Energy Refinement. A General Program for Modeling Molecules and Their Interactions. *J. Comput. Chem.* **1981**, *2*, 287−303.

(271) Weiner, S. J.; Kollman, P. A.; Case, D. A.; Singh, U. C.; Ghio, C.; Alagona, G.; Profeta, S.; Weiner, P. A New Force Field for Molecular Mechanical Simulation of Nucleic Acids and Proteins. *J. Am. Chem. Soc.* **1984**, *106*, 765−784.

(272) Weiner, S. J.; Kollman, P. A.; Nguyen, D. T.; Case, D. A. An All Atom Force Field for Simulations of Proteins and Nucleic Acids. *J. Comput. Chem.* **1986**, *7*, 230−252.

(273) Cornell, W. D.; Cieplak, P.; Bayly, C. I.; Gould, I. R.; Merz, K. M.; Ferguson, D. M.; Spellmeyer, D. C.; Fox, T.; Caldwell, J. W.; Kollman, P. A. A Second Generation Force Field for the Simulation of Proteins, Nucleic Acids, and Organic Molecules. *J. Am. Chem. Soc.* **1995**, *117*, 5179−5197.

(274) Maier, J. A.; Martinez, C.; Kasavajhala, K.; Wickstrom, L.; Hauser, K. E.; Simmerling, C. Ff14sb: Improving the Accuracy of Protein Side Chain and Backbone Parameters from Ff99sb. *J. Chem. Theory Comput.* **2015**, *11*, 3696−3713.

(275) Wang, L.-P.; McKiernan, K. A.; Gomes, J.; Beauchamp, K. A.; Head-Gordon, T.; Rice, J. E.; Swope, W. C.; Martínez, T. J.; Pande, V. S. Building a More Predictive Protein Force Field: A Systematic and Reproducible Route to Amber-Fb15. *J. Phys. Chem. B* **2017**, *121*, 4023−4039.

(276) Salomon-Ferrer, R.; Case, D. A.; Walker, R. C. An Overview of the Amber Biomolecular Simulation Package. *WIREs Computational Molecular Science* **2013**, *3*, 198−210.

(277) Rappe, A. K.; Casewit, C. J.; Colwell, K. S.; Goddard, W. A.; Skiff, W. M. Uff, a Full Periodic Table Force Field for Molecular Mechanics and Molecular Dynamics Simulations. *J. Am. Chem. Soc.* **1992**, *114*, 10024−10035.

(278) Coupry, D. E.; Addicoat, M. A.; Heine, T. Extension of the Universal Force Field for Metal-Organic Frameworks. *J. Chem. Theory Comput.* **2016**, *12*, 5215−5225.

(279) Jaillet, L.; Artemova, S.; Redon, S. Im-Uff: Extending the Universal Force Field for Interactive Molecular Modeling. *J. Mol. Graphics Modell.* **2017**, *77*, 350−362.

(280) Mayo, S. L.; Olafson, B. D.; Goddard, W. A. Dreiding: A Generic Force Field for Molecular Simulations. *J. Phys. Chem.* **1990**, *94*, 8897−8909.

(281) Mulliken, R. S. Electronic Population Analysis on Lcao-Mo Molecular Wave Functions. I. *J. Chem. Phys.* **1955**, *23*, 1833−1840.

(282) Manz, T. A.; Sholl, D. S. Chemically Meaningful Atomic Charges That Reproduce the Electrostatic Potential in Periodic and Nonperiodic Materials. *J. Chem. Theory Comput.* **2010**, *6*, 2455−2468.

(283) Breneman, C. M.; Wiberg, K. B. Determining Atom-Centered Monopoles from Molecular Electrostatic Potentials. The Need for High Sampling Density in Formamide Conformational Analysis. *J. Comput. Chem.* **1990**, *11*, 361−373.

(284) Watanabe, T.; Manz, T. A.; Sholl, D. S. Accurate Treatment of Electrostatics During Molecular Adsorption in Nanoporous Crystals without Assigning Point Charges to Framework Atoms. *J. Phys. Chem. C* **2011**, *115*, 4824−4836.

(285) Sladekova, K.; Campbell, C.; Grant, C.; Fletcher, A. J.; Gomes, J. R. B.; Jorge, M. The Effect of Atomic Point Charges on Adsorption Isotherms of CO_2 and Water in Metal Organic Frameworks. *Adsorption* **2020**, *26*, 663−685.

(286) Kancharlapalli, S.; Gopalan, A.; Haranczyk, M.; Snurr, R. Q. Fast and Accurate Machine Learning Strategy for Calculating Partial Atomic Charges in Metal-Organic Frameworks. *J. Chem. Theory Comput.* **2021**, *17*, 3052.

(287) Raza, A.; Sturluson, A.; Simon, C. M.; Fern, X. Message Passing Neural Networks for Partial Charge Assignment to Metal-Organic Frameworks. *J. Phys. Chem. C* **2020**, *124*, 19070−19082.

(288) Dubbeldam, D.; Calero, S.; Vlugt, T. J. H.; Krishna, R.; Maesen, T. L. M.; Smit, B. United Atom Force Field for Alkanes in Nanoporous Materials. *J. Phys. Chem. B* **2004**, *108*, 12301−12313.

(289) Martin, M. G.; Siepmann, J. I. Transferable Potentials for Phase Equilibria. 1. United-Atom Description of N-Alkanes. *J. Phys. Chem. B* **1998**, *102*, 2569−2577.

(290) Martin, M. G.; Siepmann, J. I. Novel Configurational-Bias Monte Carlo Method for Branched Molecules. Transferable Potentials for Phase Equilibria. 2. United-Atom Description of Branched Alkanes. *J. Phys. Chem. B* **1999**, *103*, 4508−4517.

(291) Chen, B.; Siepmann, J. I. Transferable Potentials for Phase Equilibria. 3. Explicit-Hydrogen Description of Normal Alkanes. *J. Phys. Chem. B* **1999**, *103*, 5370−5379.

(292) Wick, C. D.; Martin, M. G.; Siepmann, J. I. Transferable Potentials for Phase Equilibria. 4. United-Atom Description of Linear and Branched Alkenes and Alkylbenzenes. *J. Phys. Chem. B* **2000**, *104*, 8008−8016.

(293) Potoff, J. J.; Siepmann, J. I. Vapor-Liquid Equilibria of Mixtures Containing Alkanes, Carbon Dioxide, and Nitrogen. *AIChE J.* **2001**, *47*, 1676−1682.

(294) Chen, B.; Potoff, J. J.; Siepmann, J. I. Monte Carlo Calculations for Alcohols and Their Mixtures with Alkanes. Transferable Potentials for Phase Equilibria. 5. United-Atom Description of Primary, Secondary, and Tertiary Alcohols. *J. Phys. Chem. B* **2001**, *105*, 3093−3104.

(295) García-Sánchez, A.; Ania, C. O.; Parra, J. B.; Dubbeldam, D.; Vlugt, T. J. H.; Krishna, R.; Calero, S. Transferable Force Field for Carbon Dioxide Adsorption in Zeolites. *J. Phys. Chem. C* **2009**, *113*, 8814−8820.

(296) Martin-Calvo, A.; Gutiérrez-Sevillano, J. J.; Parra, J. B.; Ania, C. O.; Calero, S. Transferable Force Fields for Adsorption of Small Gases in Zeolites. *Phys. Chem. Chem. Phys.* **2015**, *17*, 24048−24055.

(297) Bludský, O.; Rubeš, M.; Soldán, P.; Nachtigall, P. Investigation of the Benzene-Dimer Potential Energy Surface: Dft/Ccsd(T) Correction Scheme. *J. Chem. Phys.* **2008**, *128*, 114102.

(298) Fang, H.; Kamakoti, P.; Zang, J.; Cundy, S.; Paur, C.; Ravikovitch, P. I.; Sholl, D. S. Prediction of CO_2 Adsorption Properties in Zeolites Using Force Fields Derived from Periodic Dispersion-Corrected Dft Calculations. *J. Phys. Chem. C* **2012**, *116*, 10692−10701.

(299) Fang, H.; Kamakoti, P.; Ravikovitch, P. I.; Aronson, M.; Paur, C.; Sholl, D. S. First Principles Derived, Transferable Force Fields for CO_2 Adsorption in Na-Exchanged Cationic Zeolites. *Phys. Chem. Chem. Phys.* **2013**, *15*, 12882−12894.

(300) Fang, H.; Kulkarni, A.; Kamakoti, P.; Awati, R.; Ravikovitch, P. I.; Sholl, D. S. Identification of High-CO_2-Capacity Cationic Zeolites by Accurate Computational Screening. *Chem. Mater.* **2016**, *28*, 3887−3896.

(301) Fang, H.; Findley, J.; Muraro, G.; Ravikovitch, P. I.; Sholl, D. S. A Strong Test of Atomically Detailed Models of Molecular Adsorption in Zeolites Using Multilaboratory Experimental Data for CO_2 Adsorption in Ammonium Zsm-5. *J. Phys. Chem. Lett.* **2020**, *11*, 471−477.

(302) Vishnyakov, A.; Ravikovitch, P. I.; Neimark, A. V.; Bülow, M.; Wang, Q. M. Nanopore Structure and Sorption Properties of Cu-Btc Metal-Organic Framework. *Nano Lett.* **2003**, *3*, 713−718.

(303) Chen, L.; Morrison, C. A.; Düren, T. Improving Predictions of Gas Adsorption in Metal-Organic Frameworks with Coordinatively Unsaturated Metal Sites: Model Potentials, Ab Initio Parameterization, and Gcmc Simulations. *J. Phys. Chem. C* **2012**, *116*, 18899−18909.

(304) Dzubak, A. L.; Lin, L.-C.; Kim, J.; Swisher, J. A.; Poloni, R.; Maximoff, S. N.; Smit, B.; Gagliardi, L. Ab Initio Carbon Capture in Open-Site Metal-Organic Frameworks. *Nat. Chem.* **2012**, *4*, 810−816.

(305) Fischer, M.; Gomes, J. R. B.; Jorge, M. Computational Approaches to Study Adsorption in Mofs with Unsaturated Metal Sites. *Mol. Simul.* **2014**, *40*, 537−556.

(306) Becker, T. M.; Lin, L.-C.; Dubbeldam, D.; Vlugt, T. J. H. Polarizable Force Field for CO_2 in M-Mof-74 Derived from Quantum Mechanics. *J. Phys. Chem. C* **2018**, *122*, 24488−24498.

(307) Becker, T. M.; Heinen, J.; Dubbeldam, D.; Lin, L.-C.; Vlugt, T. J. H. Polarizable Force Fields for CO_2 and CH_4 Adsorption in M-Mof-74. *J. Phys. Chem. C* **2017**, *121*, 4659−4673.

(308) Borycz, J.; Lin, L.-C.; Bloch, E. D.; Kim, J.; Dzubak, A. L.; Maurice, R.; Semrouni, D.; Lee, K.; Smit, B.; Gagliardi, L. CO_2 Adsorption in Fe2(Dobdc): A Classical Force Field Parameterized from Quantum Mechanical Calculations. *J. Phys. Chem. C* **2014**, *118*, 12230−12240.

(309) Haldoupis, E.; Borycz, J.; Shi, H.; Vogiatzis, K. D.; Bai, P.; Queen, W. L.; Gagliardi, L.; Siepmann, J. I. Ab Initio Derived Force Fields for Predicting CO_2 Adsorption and Accessibility of Metal Sites in the Metal-Organic Frameworks M-Mof-74 (M = Mn, Co, Ni, Cu). *J. Phys. Chem. C* **2015**, *119*, 16058−16071.

(310) Mercado, R.; Vlaisavljevich, B.; Lin, L.-C.; Lee, K.; Lee, Y.; Mason, J. A.; Xiao, D. J.; Gonzalez, M. I.; Kapelewski, M. T.; Neaton, J. B.; Smit, B. Force Field Development from Periodic Density Functional Theory Calculations for Gas Separation Applications Using Metal-Organic Frameworks. *J. Phys. Chem. C* **2016**, *120*, 12590−12604.

(311) Schneemann, A.; Bon, V.; Schwedler, I.; Senkovska, I.; Kaskel, S.; Fischer, R. A. Flexible Metal-Organic Frameworks. *Chem. Soc. Rev.* **2014**, *43*, 6062−6096.

(312) Chang, Z.; Yang, D.-H.; Xu, J.; Hu, T.-L.; Bu, X.-H. Flexible Metal-Organic Frameworks: Recent Advances and Potential Applications. *Adv. Mater.* **2015**, *27*, 5432−5441.

(313) Verploegh, R. J.; Kulkarni, A.; Boulfelfel, S. E.; Haydak, J. C.; Tang, D.; Sholl, D. S. Screening Diffusion of Small Molecules in Flexible Zeolitic Imidazolate Frameworks Using a Dft-Parameterized Force Field. *J. Phys. Chem. C* **2019**, *123*, 9153−9167.

(314) Greathouse, J. A.; Allendorf, M. D. The Interaction of Water with Mof-5 Simulated by Molecular Dynamics. *J. Am. Chem. Soc.* **2006**, *128*, 10678−10679.

(315) Dubbeldam, D.; Walton, K. S.; Ellis, D. E.; Snurr, R. Q. Exceptional Negative Thermal Expansion in Isoreticular Metal-Organic Frameworks. *Angew. Chem.* **2007**, *119*, 4580−4583.

(316) Heinen, J.; Dubbeldam, D. On Flexible Force Fields for Metal-Organic Frameworks: Recent Developments and Future Prospects. *Wiley Interdiscip. Rev.: Comput. Mol. Sci.* **2018**, *8*, No. e1363.

(317) Salles, F.; Ghoufi, A.; Maurin, G.; Bell, R. G.; Mellot-Draznieks, C.; Férey, G. Molecular Dynamics Simulations of Breathing Mofs: Structural Transformations of Mil-53(Cr) Upon Thermal Activation and CO_2 Adsorption. *Angew. Chem., Int. Ed.* **2008**, *47*, 8487−8491.

(318) Miller, W.; Smith, C. W.; Mackenzie, D. S.; Evans, K. E. Negative Thermal Expansion: A Review. *J. Mater. Sci.* **2009**, *44*, 5441−5451.

(319) Gor, G. Y.; Huber, P.; Bernstein, N. Adsorption-Induced Deformation of Nanoporous Materials—a Review. *Appl. Phys. Rev.* **2017**, *4*, 011303.

(320) Schmid, R. An Electric Field Induced Breath for Metal-Organic Frameworks. *ACS Cent. Sci.* **2017**, *3*, 369−371.

(321) Babaei, H.; Wilmer, C. E. Mechanisms of Heat Transfer in Porous Crystals Containing Adsorbed Gases: Applications to Metal-Organic Frameworks. *Phys. Rev. Lett.* **2016**, *116*, 025902.

(322) Kapil, V.; Wieme, J.; Vandenbrande, S.; Lamaire, A.; Van Speybroeck, V.; Ceriotti, M. Modeling the Structural and Thermal Properties of Loaded Metal-Organic Frameworks. An Interplay of Quantum and Anharmonic Fluctuations. *J. Chem. Theory Comput.* **2019**, *15*, 3237−3249.

(323) Bristow, J. K.; Skelton, J. M.; Svane, K. L.; Walsh, A.; Gale, J. D. A General Forcefield for Accurate Phonon Properties of Metal-Organic Frameworks. *Phys. Chem. Chem. Phys.* **2016**, *18*, 29316−29329.

(324) Bristow, J. K.; Tiana, D.; Walsh, A. Transferable Force Field for Metal-Organic Frameworks from First-Principles: Btw-Ff. *J. Chem. Theory Comput.* **2014**, *10*, 4644−4652.

(325) Vanduyfhuys, L.; Vandenbrande, S.; Verstraelen, T.; Schmid, R.; Waroquier, M.; Van Speybroeck, V. Quickff: A Program for a Quick and Easy Derivation of Force Fields for Metal-Organic Frameworks from Ab Initio Input. *J. Comput. Chem.* **2015**, *36*, 1015−1027.

(326) Vanduyfhuys, L.; Vandenbrande, S.; Wieme, J.; Waroquier, M.; Verstraelen, T.; Van Speybroeck, V. Extension of the Quickff Force Field Protocol for an Improved Accuracy of Structural, Vibrational, Mechanical and Thermal Properties of Metal-Organic Frameworks. *J. Comput. Chem.* **2018**, *39*, 999−1011.

(327) Boyd, P. G.; Moosavi, S. M.; Witman, M.; Smit, B. Force-Field Prediction of Materials Properties in Metal-Organic Frameworks. *J. Phys. Chem. Lett.* **2017**, *8*, 357−363.

(328) Ruthven, D. M. *Principles of Adsorption and Adsorption Processes*; John Wiley & Sons: 1984.

(329) Ruthven, D. M.; Farooq, S.; Knaebel, K. S. *Pressure Swing Adsorption*; John Wiley & Sons: New York, 1993; pp 352, XXIV.

(330) Bird, R. B.; Stewart, W. E.; Lightfoot, E. N. *Transport Phenomena*, 2nd ed.; Wiley: New York, 2002.

(331) Ilavský, J.; Brunovská; Hlaváček, V. Experimental Observation of Temperature Gradients Occurring in a Single Zeolite Pellet. *Chem. Eng. Sci.* **1980**, *35*, 2475−2479.

(332) Zhao, Q.; Wu, F.; He, Y.; Xiao, P.; Webley, P. A. Impact of Operating Parameters on CO_2 Capture Using Carbon Monolith by Electrical Swing Adsorption Technology (Esa). *Chem. Eng. J.* **2017**, *327*, 441−453.

(333) Krishnamurthy, S.; Haghpanah, R.; Rajendran, A.; Farooq, S. Simulation and Optimization of a Dual-Adsorbent, Two-Bed Vacuum Swing Adsorption Process for CO_2 Capture from Wet Flue Gas. *Ind. Eng. Chem. Res.* **2014**, *53*, 14462−14473.

(334) Beck, J.; Friedrich, D.; Brandani, S.; Fraga, E. S. Multi-Objective Optimisation Using Surrogate Models for the Design of Vpsa Systems. *Comput. Chem. Eng.* **2015**, *82*, 318−329.

(335) Glueckauf, E. Theory of Chromatography. Part 10.—Formulæ for Diffusion into Spheres and Their Application to Chromatography. *Trans. Faraday Soc.* **1955**, *51*, 1540−1551.

(336) Abanades, J. C.; Arias, B.; Lyngfelt, A.; Mattisson, T.; Wiley, D. E.; Li, H.; Ho, M. T.; Mangano, E.; Brandani, S. Emerging CO_2 Capture Systems. *Int. J. Greenhouse Gas Control* **2015**, *40*, 126−166.

(337) Hindmarsh, A. C.; Brown, P. N.; Grant, K. E.; Lee, S. L.; Serban, R.; Shumaker, D. E.; Woodward, C. S. Sundials: Suite of Nonlinear and Differential/Algebraic Equation Solvers. *ACM Trans. Math. Softw.* **2005**, *31*, 363−396.

(338) Myers, A. L. Activity Coefficients of Mixtures Adsorbed on Heterogeneous Surfaces. *AIChE J.* **1983**, *29*, 691−693.

(339) Hefti, M.; Joss, L.; Bjelobrk, Z.; Mazzotti, M. On the Potential of Phase-Change Adsorbents for CO_2 Capture by Temperature Swing Adsorption. *Faraday Discuss.* **2016**, *192*, 153−179.

(340) Pai, K. N.; Baboolal, J. D.; Sharp, D. A.; Rajendran, A. Evaluation of Diamine-Appended Metal-Organic Frameworks for Post-Combustion CO_2 Capture by Vacuum Swing Adsorption. *Sep. Purif. Technol.* **2019**, *211*, 540−550.

(341) Haghpanah, R.; Rajendran, A.; Farooq, S.; Karimi, I. A.; Amanullah, M. Discrete Equilibrium Data from Dynamic Column Breakthrough Experiments. *Ind. Eng. Chem. Res.* **2012**, *51*, 14834−14844.

(342) Forssén, P.; Fornstedt, T. A Model Free Method for Estimation of Complicated Adsorption Isotherms in Liquid Chromatography. *J. Chromatogr. A* **2015**, *1409*, 108−115.

(343) Rajendran, A.; Maruyama, R. T.; Landa, H. O. R.; Seidel-Morgenstern, A. Modelling Binary Non-Linear Chromatography Using Discrete Equilibrium Data. *Adsorption* **2020**, *26*, 973.

(344) Myers, A. L.; Prausnitz, J. M. Thermodynamics of Mixed-Gas Adsorption. *AIChE J.* **1965**, *11*, 121−127.

(345) Hu, X.; Mangano, E.; Friedrich, D.; Ahn, H.; Brandani, S. Diffusion Mechanism of CO_2 in 13x Zeolite Beads. *Adsorption* **2014**, *20*, 121−135.

(346) Medved', I.; Černý, R. Surface Diffusion in Porous Media: A Critical Review. *Microporous Mesoporous Mater.* **2011**, *142*, 405−422.

(347) Kärger, J.; Ruthven, D. M. *Diffusion in Zeolites and Other Microporous Solids*; John Wiley: New York, 1992.

(348) Ko, D.; Siriwardane, R.; Biegler, L. T. Optimization of Pressure Swing Adsorption and Fractionated Vacuum Pressure Swing Adsorption Processes for CO_2 Capture. *Ind. Eng. Chem. Res.* **2005**, *44*, 8084−8094.

(349) Haghpanah, R.; Nilam, R.; Rajendran, A.; Farooq, S.; Karimi, I. A. Cycle Synthesis and Optimization of a Vsa Process for Postcombustion CO_2capture. *AIChE J.* **2013**, *59*, 4735−4748.

(350) Nilchan, S.; Pantelides, C. C. On the Optimisation of Periodic Adsorption Processes. *Adsorption* **1998**, *4*, 113−147.

(351) Kumar, R.; Fox, V. G.; Hartzog, D. G.; Larson, R. E.; Chen, Y. C.; Houghton, P. A.; Naheiri, T. A Versatile Process Simulator for Adsorptive Separations. *Chem. Eng. Sci.* **1994**, *49*, 3115−3125.

(352) Effendy, S.; Farooq, S.; Ruthven, D. M. A Rigorous Criterion for Approach to Cyclic Steady-State in Psa Simulations. *Chem. Eng. Sci.* **2017**, *160*, 313−320.

(353) Sharma, I.; Friedrich, D.; Golden, T.; Brandani, S. Monolithic Adsorbent-Based Rapid-Cycle Vacuum Pressure Swing Adsorption Process for Carbon Capture from Small-Scale Steam Methane Reforming. *Ind. Eng. Chem. Res.* **2020**, *59*, 7109−7120.

(354) Khurana, M.; Farooq, S. Simulation and Optimization of a 6-Step Dual-Reflux Vsa Cycle for Post-Combustion CO_2 Capture. *Chem. Eng. Sci.* **2016**, *152*, 507−515.

(355) Fiandaca, G.; Fraga, E. S.; Brandani, S. A Multi-Objective Genetic Algorithm for the Design of Pressure Swing Adsorption. *Engineering Optimization* **2009**, *41*, 833−854.

(356) Hadka, D. Platypus - Multiobjective Optimization in Python, https://github.com/Project-Platypus/Platypus, 2017.

(357) Hadka, D. *Moea Framework - a Free and Open Source Java Framework for Multiobjective Optimization*, v. 2.13; http://moeaframework.org/, 2015.

(358) Hadka, D.; Reed, P. Borg: An Auto-Adaptive Many-Objective Evolutionary Computing Framework. *Evolutionary Computation* **2013**, *21*, 231−259.

(359) Smith, O. J.; Westerberg, A. W. Acceleration of Cyclic Steady State Convergence for Pressure Swing Adsorption Models. *Ind. Eng. Chem. Res.* **1992**, *31*, 1569−1573.

(360) Ding, Y.; LeVan, M. D. Periodic States of Adsorption Cycles Iii. Convergence Acceleration for Direct Determination. *Chem. Eng. Sci.* **2001**, *56*, 5217−5230.

(361) Friedrich, D.; Ferrari, M.-C.; Brandani, S. Efficient Simulation and Acceleration of Convergence for a Dual Piston Pressure Swing Adsorption System. *Ind. Eng. Chem. Res.* **2013**, *52*, 8897−8905.

(362) Pai, K. N.; Prasad, V.; Rajendran, A. Experimentally Validated Machine Learning Frameworks for Accelerated Prediction of Cyclic Steady State and Optimization of Pressure Swing Adsorption Processes. *Sep. Purif. Technol.* **2020**, *241*, 116651.

(363) Subramanian Balashankar, V.; Rajagopalan, A. K.; de Pauw, R.; Avila, A. M.; Rajendran, A. Analysis of a Batch Adsorber Analogue for Rapid Screening of Adsorbents for Postcombustion CO_2 Capture. *Ind. Eng. Chem. Res.* **2019**, *58*, 3314−3328.

(364) Biegler, L. T.; Grossmann, I. E.; Westerberg, A. W. A Note on Approximation Techniques Used for Process Optimization. *Comput. Chem. Eng.* **1985**, *9*, 201−206.

(365) Sant Anna, H. R.; Barreto, A. G.; Tavares, F. W.; de Souza, M. B. Machine Learning Model and Optimization of a Psa Unit for Methane-Nitrogen Separation. *Comput. Chem. Eng.* **2017**, *104*, 377−391.

(366) Leperi, K. T.; Yancy-Caballero, D.; Snurr, R. Q.; You, F. 110th Anniversary: Surrogate Models Based on Artificial Neural Networks to Simulate and Optimize Pressure Swing Adsorption Cycles for CO_2 Capture. *Ind. Eng. Chem. Res.* **2019**, *58*, 18241−18252.

(367) Subraveti, S. G.; Li, Z.; Prasad, V.; Rajendran, A. Machine Learning-Based Multiobjective Optimization of Pressure Swing Adsorption. *Ind. Eng. Chem. Res.* **2019**, *58*, 20412−20422.

(368) Ding, Y.; T. Croft, D.; LeVan, M. D. Periodic States of Adsorption Cycles Iv. Direct Optimization. *Chem. Eng. Sci.* **2002**, *57*, 4521−4531.

(369) Jiang, L.; Biegler, L. T.; Fox, V. G. Simulation and Optimization of Pressure-Swing Adsorption Systems for Air Separation. *AIChE J.* **2003**, *49*, 1140−1157.

(370) Process Systems Enterprise, *Gproms*, https://www.psenterprise.com/products/gproms, 1997−2020.

(371) Liu, Z.; Grande, C. A.; Li, P.; Yu, J.; Rodrigues, A. E. Multi-Bed Vacuum Pressure Swing Adsorption for Carbon Dioxide Capture from Flue Gas. *Sep. Purif. Technol.* **2011**, *81*, 307−317.

(372) Mondino, G.; Spjelkavik, A. I.; Didriksen, T.; Krishnamurthy, S.; Stensrød, R. E.; Grande, C. A.; Nord, L. O.; Blom, R. Production of Mof Adsorbent Spheres and Comparison of Their Performance with Zeolite 13x in a Moving-Bed Tsa Process for Postcombustion CO_2 Capture. *Ind. Eng. Chem. Res.* **2020**, *59*, 7198−7211.

(373) Nikolaidis, G. N.; Kikkinides, E. S.; Georgiadis, M. C. Modelling and Optimization of Pressure Swing Adsorption (Psa) Processes for Post-Combustion CO_2 Capture from Flue Gas. In *Process Systems and Materials for CO_2 Capture*; Papadopoulos, A. I., Seferlis, P., Eds.; Wiley: 2017; pp 343−369.

(374) Nikolić, D.; Kikkinides, E. S.; Georgiadis, M. C. Optimization of Multibed Pressure Swing Adsorption Processes. *Ind. Eng. Chem. Res.* **2009**, *48*, 5388−5398.

(375) Aspentech *Aspen Adsorption*; https://www.aspentech.com/en/products/pages/aspen-adsorption, 1981−2020.

(376) Wood, K. R.; Liu, Y. A.; Yu, Y. *Design, Simulation, and Optimization of Adsorptive and Chromatographic Separations: A Hands-on Approach*; Wiley-VCH: 2018; p 432.

(377) Ntiamoah, A.; Ling, J.; Xiao, P.; Webley, P. A.; Zhai, Y. CO_2 Capture by Vacuum Swing Adsorption: Role of Multiple Pressure Equalization Steps. *Adsorption* **2015**, *21*, 509−522.

(378) Bhatt, T. S.; Storti, G.; Rota, R. Detailed Simulation of Dual-Reflux Pressure Swing Adsorption Process. *Chem. Eng. Sci.* **2015**, *122*, 34−52.

(379) Li, D.; Zhou, Y.; Shen, Y.; Sun, W.; Fu, Q.; Yan, H.; Zhang, D. Experiment and Simulation for Separating CO_2/N_2 by Dual-Reflux Pressure Swing Adsorption Process. *Chem. Eng. J.* **2016**, *297*, 315−324.

(380) Shen, Y.; Zhou, Y.; Li, D.; Fu, Q.; Zhang, D.; Na, P. Dual-Reflux Pressure Swing Adsorption Process for Carbon Dioxide Capture from Dry Flue Gas. *Int. J. Greenhouse Gas Control* **2017**, *65*, 55−64.

(381) Fontalvo Alzate, J. Using User Models in Matlab within the Aspen Plus Interface with an Excel Link. *Ing. Invest.* **2014**, *34*, 39−43.

(382) *Prosim Dac: Dynamic Adsorption Column Simulator*, https://www.prosim.net/en/product/prosim-dac-dynamic-adsorption-column-simulation/, 1989−2020.

(383) Brown, P. N.; Byrne, G. D.; Hindmarsh, A. C. Vode: A Variable-Coefficient Ode Solver. *SIAM Journal on Scientific and Statistical Computing* **1989**, *10*, 1038−1051.

(384) Webley, P. A.; He, J. Fast Solution-Adaptive Finite Volume Method for Psa/Vsa Cycle Simulation; 1 Single Step Simulation. *Comput. Chem. Eng.* **2000**, *23*, 1701−1712.

(385) Todd, R. S.; He, J.; Webley, P. A.; Beh, C.; Wilson, S.; Lloyd, M. A. Fast Finite-Volume Method for Psa/Vsa Cycle Simulation-Experimental Validation. *Ind. Eng. Chem. Res.* **2001**, *40*, 3217−3224.

(386) Xiao, P.; Wilson, S.; Xiao, G.; Singh, R.; Webley, P. Novel Adsorption Processes for Carbon Dioxide Capture within a Igcc Process. *Energy Procedia* **2009**, *1*, 631−638.

(387) Xiao, P.; Zhang, J.; Webley, P.; Li, G.; Singh, R.; Todd, R. Capture of CO_2 from Flue Gas Streams with Zeolite 13x By vacuum-Pressure Swing Adsorption. *Adsorption* **2008**, *14*, 575−582.

(388) Zhang, J.; Webley, P. A. Cycle Development and Design for CO_2 Capture from Flue Gas by Vacuum Swing Adsorption. *Environ. Sci. Technol.* **2008**, *42*, 563−569.

(389) Ling, J.; Ntiamoah, A.; Xiao, P.; Webley, P. A.; Zhai, Y. Effects of Feed Gas Concentration, Temperature and Process Parameters on Vacuum Swing Adsorption Performance for CO_2 Capture. *Chem. Eng. J.* **2015**, *265*, 47−57.

(390) Jiang, Y.; Ling, J.; Xiao, P.; He, Y.; Zhao, Q.; Chu, Z.; Liu, Y.; Li, Z.; Webley, P. A. Simultaneous Biogas Purification and CO_2 Capture by Vacuum Swing Adsorption Using Zeolite Nausy. *Chem. Eng. J.* **2018**, *334*, 2593−2602.

(391) Friedrich, D.; Mangano, E.; Brandani, S. Automatic Estimation of Kinetic and Isotherm Parameters from Zlc Experiments. *Chem. Eng. Sci.* **2015**, *126*, 616−624.

(392) Dang, W.; Friedrich, D.; Brandani, S. Dual-Piston Pressure Swing Adsorption System: Instrumentation and Characterisation with Pure Gas Experiments. *Chem. Eng. Sci.* **2020**, *214*, 115423.

(393) Deb, K.; Pratap, A.; Agarwal, S.; Meyarivan, T. A Fast and Elitist Multiobjective Genetic Algorithm: Nsga-Ii. *IEEE Transactions on Evolutionary Computation* **2002**, *6*, 182−197.

(394) Deb, K. *Multi-Objective Optimization Using Evolutionary Algorithms*; Wiley: 2001.

(395) Tonda, A. Inspyred: Bio-Inspired Algorithms in Python. *Genetic Programming and Evolvable Machines* **2020**, *21*, 269−272.

(396) Sharma, I.; Mennitto, R.; Friedrich, D.; Brandani, S. Combining the Nonuniform Structure and Flow Maldistribution for the Accurate Prediction of the Process Performance of Monolithic Adsorbent Systems. *Ind. Eng. Chem. Res.* **2020**, *59*, 3162−3172.

(397) Sircar, S.; Golden, T. C. Purification of Hydrogen by Pressure Swing Adsorption. *Sep. Sci. Technol.* **2000**, *35*, 667−687.

(398) Reynolds, S. P.; Ebner, A. D.; Ritter, J. A. Stripping Psa Cycles for CO_2 Recovery from Flue Gas at High Temperature Using a Hydrotalcite-Like Adsorbent. *Ind. Eng. Chem. Res.* **2006**, *45*, 4278−4294.

(399) Reynolds, S. P.; Mehrotra, A.; Ebner, A. D.; Ritter, J. A. Heavy Reflux Psa Cycles for CO_2 Recovery from Flue Gas: Part i. performance Evaluation. *Adsorption* **2008**, *14*, 399−413.

(400) Shen, C.; Liu, Z.; Li, P.; Yu, J. Two-Stage Vpsa Process for CO_2 Capture from Flue Gas Using Activated Carbon Beads. *Ind. Eng. Chem. Res.* **2012**, *51*, 5011−5021.

(401) Wang, L.; Yang, Y.; Shen, W.; Kong, X.; Li, P.; Yu, J.; Rodrigues, A. E. CO_2 Capture from Flue Gas in an Existing Coal-Fired Power Plant by Two Successive Pilot-Scale Vpsa Units. *Ind. Eng. Chem. Res.* **2013**, *52*, 7947−7955.

(402) Diagne, D.; Goto, M.; Hirose, T. New Psa Process with Intermediate Feed Inlet Position Operated with Dual Refluxes: Application to Carbon Dioxide Removal and Enrichment. *J. Chem. Eng. Jpn.* **1994**, *27*, 85−89.

(403) Diagne, D.; Goto, M.; Hirose, T. Parametric Studies on CO_2 Separation and Recovery by a Dual Reflux Psa Process Consisting of Both Rectifying and Stripping Sections. *Ind. Eng. Chem. Res.* **1995**, *34*, 3083−3089.

(404) Rossi, E.; Paloni, M.; Storti, G.; Rota, R. Modeling Dual Reflux-Pressure Swing Adsorption Processes: Numerical Solution Based on the Finite Volume Method. *Chem. Eng. Sci.* **2019**, *203*, 173−185.

(405) Kikkinides, E. S.; Yang, R. T.; Cho, S. H. Concentration and Recovery of Carbon Dioxide from Flue Gas by Pressure Swing Adsorption. *Ind. Eng. Chem. Res.* **1993**, *32*, 2714−2720.

(406) Chue, K. T.; Kim, J. N.; Yoo, Y. J.; Cho, S. H.; Yang, R. T. Comparison of Activated Carbon and Zeolite 13x for CO_2 Recovery from Flue Gas by Pressure Swing Adsorption. *Ind. Eng. Chem. Res.* **1995**, *34*, 591−598.

(407) Ishibashi, M.; Ota, H.; Akutsu, N.; Umeda, S.; Tajika, M.; Izumi, J.; Yasutake, A.; Kabata, T.; Kageyama, Y. Technology for Removing Carbon Dioxide from Power Plant Flue Gas by the Physical Adsorption Method. *Energy Convers. Manage.* **1996**, *37*, 929−933.

(408) Park, J.-H.; Beum, H.-T.; Kim, J.-N.; Cho, S.-H. Numerical Analysis on the Power Consumption of the Psa Process for Recovering CO_2 from Flue Gas. *Ind. Eng. Chem. Res.* **2002**, *41*, 4122−4131.

(409) Merel, J.; Clausse, M.; Meunier, F. Experimental Investigation on CO_2 Post-Combustion Capture by Indirect Thermal Swing Adsorption Using 13x and 5a Zeolites. *Ind. Eng. Chem. Res.* **2008**, *47*, 209−215.

(410) Zhang, J.; Webley, P. A.; Xiao, P. Effect of Process Parameters on Power Requirements of Vacuum Swing Adsorption Technology for CO_2 Capture from Flue Gas. *Energy Convers. Manage.* **2008**, *49*, 346−356.

(411) Li, G.; Xiao, P.; Webley, P.; Zhang, J.; Singh, R.; Marshall, M. Capture of CO_2 from High Humidity Flue Gas by Vacuum Swing Adsorption with Zeolite 13x. *Adsorption* **2008**, *14*, 415−422.

(412) Zhang, J.; Xiao, P.; Li, G.; Webley, P. A. Effect of Flue Gas Impurities on CO_2 Capture Performance from Flue Gas at Coal-Fired Power Stations by Vacuum Swing Adsorption. *Energy Procedia* **2009**, *1*, 1115−1122.

(413) Shen, C.; Yu, J.; Li, P.; Grande, C. A.; Rodrigues, A. E. Capture of CO_2 from Flue Gas by Vacuum Pressure Swing Adsorption Using Activated Carbon Beads. *Adsorption* **2011**, *17*, 179−188.

(414) Clausse, M.; Merel, J.; Meunier, F. Numerical Parametric Study on CO_2 Capture by Indirect Thermal Swing Adsorption. *Int. J. Greenhouse Gas Control* **2011**, *5*, 1206−1213.

(415) Delgado, J. A.; Uguina, M. A.; Sotelo, J. L.; Águeda, V. I.; Sanz, A.; Gómez, P. Numerical Analysis of CO_2 Concentration and Recovery from Flue Gas by a Novel Vacuum Swing Adsorption Cycle. *Comput. Chem. Eng.* **2011**, *35*, 1010−1019.

(416) Wang, L.; Liu, Z.; Li, P.; Yu, J.; Rodrigues, A. E. Experimental and Modeling Investigation on Post-Combustion Carbon Dioxide Capture Using Zeolite 13x-Apg by Hybrid Vtsa Process. *Chem. Eng. J.* **2012**, *197*, 151−161.

(417) Wang, L.; Liu, Z.; Li, P.; Wang, J.; Yu, J. CO_2 Capture from Flue Gas by Two Successive Vpsa Units Using 13xapg. *Adsorption* **2012**, *18*, 445−459.

(418) Liu, Z.; Wang, L.; Kong, X.; Li, P.; Yu, J.; Rodrigues, A. E. Onsite CO_2 Capture from Flue Gas by an Adsorption Process in a Coal-Fired Power Plant. *Ind. Eng. Chem. Res.* **2012**, *51*, 7355−7363.

(419) Nikolaidis, G. N.; Kikkinides, E. S.; Georgiadis, M. C. Model-Based Approach for the Evaluation of Materials and Processes for Post-Combustion Carbon Dioxide Capture from Flue Gas by Psa/Vsa Processes. *Ind. Eng. Chem. Res.* **2016**, *55*, 635−646.

(420) Leperi, K. T.; Snurr, R. Q.; You, F. Optimization of Two-Stage Pressure/Vacuum Swing Adsorption with Variable Dehydration Level

for Postcombustion Carbon Capture. *Ind. Eng. Chem. Res.* **2016**, *55*, 3338−3350.

(421) Khurana, M.; Farooq, S. Integrated Adsorbent-Process Optimization for Carbon Capture and Concentration Using Vacuum Swing Adsorption Cycles. *AIChE J.* **2017**, *63*, 2987−2995.

(422) Hefti, M.; Mazzotti, M. Postcombustion CO_2 Capture from Wet Flue Gas by Temperature Swing Adsorption. *Ind. Eng. Chem. Res.* **2018**, *57*, 15542−15555.

(423) Rajagopalan, A. K.; Rajendran, A. The Effect of Nitrogen Adsorption on Vacuum Swing Adsorption Based Post-Combustion CO_2 Capture. *Int. J. Greenhouse Gas Control* **2018**, *78*, 437−447.

(424) Krishnamurthy, S.; Lind, A.; Bouzga, A.; Pierchala, J.; Blom, R. Post Combustion Carbon Capture with Supported Amine Sorbents: From Adsorbent Characterization to Process Simulation and Optimization. *Chem. Eng. J.* **2021**, *406*, 127121.

(425) Krishnamurthy, S.; Boon, J.; Grande, C.; Lind, A.; Blom, R.; Boer, R.; Willemsen, H.; de Scheemaker, G. Screening Supported Amine Sorbents in the Context of Post-Combustion Carbon Capture by Vacuum Swing Adsorption. *Chem. Ing. Tech.* **2021**, *93*, 929.

(426) Pai, K. N.; Prasad, V.; Rajendran, A. Practically Achievable Process Performance Limits for Pressure-Vacuum Swing Adsorption-Based Postcombustion CO_2 Capture. *ACS Sustainable Chem. Eng.* **2021**, *9*, 3838−3849.

(427) Bobbitt, N. S.; Chen, J.; Snurr, R. Q. High-Throughput Screening of Metal-Organic Frameworks for Hydrogen Storage at Cryogenic Temperature. *J. Phys. Chem. C* **2016**, *120*, 27328−27341.

(428) Jorgensen, W. L.; Maxwell, D. S.; Tirado-Rives, J. Development and Testing of the Opls All-Atom Force Field on Conformational Energetics and Properties of Organic Liquids. *J. Am. Chem. Soc.* **1996**, *118*, 11225−11236.

(429) Garberoglio, G.; Skoulidas, A. I.; Johnson, J. K. Adsorption of Gases in Metal Organic Materials: Comparison of Simulations and Experiments. *J. Phys. Chem. B* **2005**, *109*, 13094−13103.

(430) Vandenbrande, S.; Verstraelen, T.; Gutiérrez-Sevillano, J. J.; Waroquier, M.; Van Speybroeck, V. Methane Adsorption in Zr-Based Mofs: Comparison and Critical Evaluation of Force Fields. *J. Phys. Chem. C* **2017**, *121*, 25309−25322.

(431) Zang, J.; Nair, S.; Sholl, D. S. Prediction of Water Adsorption in Copper-Based Metal-Organic Frameworks Using Force Fields Derived from Dispersion-Corrected Dft Calculations. *J. Phys. Chem. C* **2013**, *117*, 7519−7525.

(432) Chen, L.; Grajciar, L.; Nachtigall, P.; Düren, T. Accurate Prediction of Methane Adsorption in a Metal-Organic Framework with Unsaturated Metal Sites by Direct Implementation of an Ab Initio Derived Potential Energy Surface in Gcmc Simulation. *J. Phys. Chem. C* **2011**, *115*, 23074−23080.

(433) Lennox, M. J.; Bound, M.; Henley, A.; Besley, E. The Right Isotherms for the Right Reasons? Validation of Generic Force Fields for Prediction of Methane Adsorption in Metal-Organic Frameworks. *Mol. Simul.* **2017**, *43*, 828−837.

(434) Garberoglio, G. Computer Simulation of the Adsorption of Light Gases in Covalent Organic Frameworks. *Langmuir* **2007**, *23*, 12154−12158.

(435) Yazaydın, A. Ö.; Snurr, R. Q.; Park, T.-H.; Koh, K.; Liu, J.; LeVan, M. D.; Benin, A. I.; Jakubczak, P.; Lanuza, M.; Galloway, D. B.; Low, J. J.; Willis, R. R. Screening of Metal-Organic Frameworks for Carbon Dioxide Capture from Flue Gas Using a Combined Experimental and Modeling Approach. *J. Am. Chem. Soc.* **2009**, *131*, 18198−18199.

(436) Pérez-Pellitero, J.; Amrouche, H.; Siperstein, F. R.; Pirngruber, G.; Nieto-Draghi, C.; Chaplais, G.; Simon-Masseron, A.; Bazer-Bachi, D.; Peralta, D.; Bats, N. Adsorption of CO_2, CH_4, and N_2 on Zeolitic Imidazolate Frameworks: Experiments and Simulations. *Chem. - Eur. J.* **2010**, *16*, 1560−1571.

(437) McDaniel, J. G.; Li, S.; Tylianakis, E.; Snurr, R. Q.; Schmidt, J. R. Evaluation of Force Field Performance for High-Throughput Screening of Gas Uptake in Metal-Organic Frameworks. *J. Phys. Chem. C* **2015**, *119*, 3143−3152.

(438) Fang, H.; Demir, H.; Kamakoti, P.; Sholl, D. S. Recent Developments in First-Principles Force Fields for Molecules in Nanoporous Materials. *J. Mater. Chem. A* **2014**, *2*, 274−291.

(439) Farmahini, A. H.; Sholl, D. S.; Bhatia, S. K. Fluorinated Carbide-Derived Carbon: More Hydrophilic, yet Apparently More Hydrophobic. *J. Am. Chem. Soc.* **2015**, *137*, 5969−5979.

(440) McDaniel, J. G.; Schmidt, J. R. Robust, Transferable, and Physically Motivated Force Fields for Gas Adsorption in Functionalized Zeolitic Imidazolate Frameworks. *J. Phys. Chem. C* **2012**, *116*, 14031−14039.

(441) Li, W.; Grimme, S.; Krieg, H.; Möllmann, J.; Zhang, J. Accurate Computation of Gas Uptake in Microporous Organic Molecular Crystals. *J. Phys. Chem. C* **2012**, *116*, 8865−8871.

(442) Vujić, B.; Lyubartsev, A. P. Transferable Force-Field for Modelling of CO_2, N_2, O_2 and Ar in All Silica and Na+Exchanged Zeolites. *Modell. Simul. Mater. Sci. Eng.* **2016**, *24*, 045002.

(443) Liu, B.; Smit, B. Molecular Simulation Studies of Separation of CO_2/N_2, CO_2/CH_4, and CH_4/N_2 by Zifs. *J. Phys. Chem. C* **2010**, *114*, 8515−8522.

(444) Karra, J. R.; Walton, K. S. Molecular Simulations and Experimental Studies of CO_2, Co, and N_2 Adsorption in Metal-Organic Frameworks. *J. Phys. Chem. C* **2010**, *114*, 15735−15740.

(445) Siderius, D.; Allison, T. C.; Shen, V. K. *Effect of Partial Charge Calculation Method on Adsorption Thermodynamics in Metal-Organic Frameworks*; National Institute of Standards and Technology (NIST): 2016.

(446) Gagliardi, L.; Lindh, R.; Karlström, G. Local Properties of Quantum Chemical Systems: The Loprop Approach. *J. Chem. Phys.* **2004**, *121*, 4494−4500.

(447) Altintas, C.; Keskin, S. Role of Partial Charge Assignment Methods in High-Throughput Screening of Mof Adsorbents and Membranes for CO_2/CH_4 Separation. *Mol. Syst. Des. Eng.* **2020**, *5*, 532−543.

(448) Ioannidis, J. P. A.; Greenland, S.; Hlatky, M. A.; Khoury, M. J.; Macleod, M. R.; Moher, D.; Schulz, K. F.; Tibshirani, R. Increasing Value and Reducing Waste in Research Design, Conduct, and Analysis. *Lancet* **2014**, *383*, 166−175.

(449) Moher, D.; Glasziou, P.; Chalmers, I.; Nasser, M.; Bossuyt, P. M. M.; Korevaar, D. A.; Graham, I. D.; Ravaud, P.; Boutron, I. Increasing Value and Reducing Waste in Biomedical Research: Who's Listening? *Lancet* **2016**, *387*, 1573−1586.

(450) National Academies of Sciences, Engineering, and Medicine *Reproducibility and Replicability in Science*; The National Academies Press: Washington, DC, 2019; p 256.

(451) Nichols, J. D.; Oli, M. K.; Kendall, W. L.; Boomer, G. S. Opinion: A Better Approach for Dealing with Reproducibility and Replicability in Science. *Proc. Natl. Acad. Sci. U. S. A.* **2021**, *118*, No. e2100769118.

(452) Allison, D. B.; Shiffrin, R. M.; Stodden, V. Reproducibility of Research: Issues and Proposed Remedies. *Proc. Natl. Acad. Sci. U. S. A.* **2018**, *115*, 2561−2562.

(453) Han, R.; Walton, K. S.; Sholl, D. S. Does Chemical Engineering Research Have a Reproducibility Problem? *Annu. Rev. Chem. Biomol. Eng.* **2019**, *10*, 43−57.

(454) Agrawal, M.; Han, R.; Herath, D.; Sholl, D. S. Does Repeat Synthesis in Materials Chemistry Obey a Power Law? *Proc. Natl. Acad. Sci. U. S. A.* **2020**, *117*, 877−882.

(455) Goodman, A. L.; Busch, A.; Duffy, G. J.; Fitzgerald, J. E.; Gasem, K. A. M.; Gensterblum, Y.; Krooss, B. M.; Levy, J.; Ozdemir, E.; Pan, Z.; Robinson, R. L., Jr.; Schroeder, K.; Sudibandriyo, M.; White, C. M. An Inter-Laboratory Comparison of CO_2 Isotherms Measured on Argonne Premium Coal Samples. *Energy Fuels* **2004**, *18*, 1175−1182.

(456) Hurst, K. E.; Gennett, T.; Adams, J.; Allendorf, M. D.; Balderas-Xicohténcatl, R.; Bielewski, M.; Edwards, B.; Espinal, L.; Fultz, B.; Hirscher, M.; Hudson, M. S. L.; Hulvey, Z.; Latroche, M.; Liu, D.-J.; Kapelewski, M.; Napolitano, E.; Perry, Z. T.; Purewal, J.; Stavila, V.; Veenstra, M.; White, J. L.; Yuan, Y.; Zhou, H.-C.; Zlotea, C.; Parilla, P. An International Laboratory Comparison Study of Volumetric and

Gravimetric Hydrogen Adsorption Measurements. *ChemPhysChem* **2019**, *20*, 1997−2009.

(457) Bingel, L. W.; Chen, A.; Agrawal, M.; Sholl, D. S. Experimentally Verified Alcohol Adsorption Isotherms in Nanoporous Materials from Literature Meta-Analysis. *J. Chem. Eng. Data* **2020**, *65*, 4970−4979.

(458) Park, J.; Howe, J. D.; Sholl, D. S. How Reproducible Are Isotherm Measurements in Metal-Organic Frameworks? *Chem. Mater.* **2017**, *29*, 10487−10495.

(459) Goodman, A. L.; Busch, A.; Bustin, R. M.; Chikatamarla, L.; Day, S.; Duffy, G. J.; Fitzgerald, J. E.; Gasem, K. A. M.; Gensterblum, Y.; Hartman, C.; Jing, C.; Krooss, B. M.; Mohammed, S.; Pratt, T.; Robinson, R. L.; Romanov, V.; Sakurovs, R.; Schroeder, K.; White, C. M. Inter-Laboratory Comparison Ii: CO₂ Isotherms Measured on Moisture-Equilibrated Argonne Premium Coals at 55 °C and up to 15 mpa. *Int. J. Coal Geol.* **2007**, *72*, 153−164.

(460) Gensterblum, Y.; van Hemert, P.; Billemont, P.; Busch, A.; Charriére, D.; Li, D.; Krooss, B. M.; de Weireld, G.; Prinz, D.; Wolf, K. H. A. A. European Inter-Laboratory Comparison of High Pressure CO₂ Sorption Isotherms. I: Activated Carbon. *Carbon* **2009**, *47*, 2958−2969.

(461) Gasparik, M.; Rexer, T. F. T.; Aplin, A. C.; Billemont, P.; De Weireld, G.; Gensterblum, Y.; Henry, M.; Krooss, B. M.; Liu, S.; Ma, X.; Sakurovs, R.; Song, Z.; Staib, G.; Thomas, K. M.; Wang, S.; Zhang, T. First International Inter-Laboratory Comparison of High-Pressure CH₄, CO₂ and C₂H₆ Sorption Isotherms on Carbonaceous Shales. *Int. J. Coal Geol.* **2014**, *132*, 131−146.

(462) Broom, D. P.; Hirscher, M. Irreproducibility in Hydrogen Storage Material Research. *Energy Environ. Sci.* **2016**, *9*, 3368−3380.

(463) Siderius, D. W.; Shen, V. K.; Johnson, R. D., III; van Zee, R. D. *Nist/Arpa-E Database of Novel and Emerging Adsorbent Materials*; National Institute of Standards and Technology, 2016.

(464) Cai, X.; Gharagheizi, F.; Bingel, L. W.; Shade, D.; Walton, K. S.; Sholl, D. S. A Collection of More Than 900 Gas Mixture Adsorption Experiments in Porous Materials from Literature Meta-Analysis. *Ind. Eng. Chem. Res.* **2021**, *60*, 639−651.

(465) Mostafa, A. T. M. G.; Eakman, J. M.; Montoya, M. M.; Yarbro, S. L. Prediction of Heat Capacities of Solid Inorganic Salts from Group Contributions. *Ind. Eng. Chem. Res.* **1996**, *35*, 343−348.

(466) Kloutse, F. A.; Zacharia, R.; Cossement, D.; Chahine, R. Specific Heat Capacities of Mof-5, Cu-Btc, Fe-Btc, Mof-177 and Mil-53 (Al) over Wide Temperature Ranges: Measurements and Application of Empirical Group Contribution Method. *Microporous Mesoporous Mater.* **2015**, *217*, 1−5.

(467) Nath, P.; Plata, J. J.; Usanmaz, D.; Al Rahal Al Orabi, R.; Fornari, M.; Nardelli, M. B.; Toher, C.; Curtarolo, S. High-Throughput Prediction of Finite-Temperature Properties Using the Quasi-Harmonic Approximation. *Comput. Mater. Sci.* **2016**, *125*, 82−91.

(468) Kamencek, T.; Bedoya-Martínez, N.; Zojer, E. Understanding Phonon Properties in Isoreticular Metal-Organic Frameworks from First Principles. *Phys. Rev. Mater.* **2019**, *3*, 116003.

(469) Togo, A.; Tanaka, I. First Principles Phonon Calculations in Materials Science. *Scr. Mater.* **2015**, *108*, 1−5.

(470) Knoop, F.; Purcell, T. A. R.; Scheffler, M.; Carbogno, C. Anharmonicity Measure for Materials. *arXiv*, https://arxiv.org/abs/2006.14672, 2020.

(471) Sircar, S. Comments on Practical Use of Langmuir Gas Adsorption Isotherm Model. *Adsorption* **2017**, *23*, 121−130.

(472) Ritter, J. A.; Bhadra, S. J.; Ebner, A. D. On the Use of the Dual-Process Langmuir Model for Correlating Unary Equilibria and Predicting Mixed-Gas Adsorption Equilibria. *Langmuir* **2011**, *27*, 4700−4712.

(473) Ritter, J. A.; Bumiller, K. C.; Tynan, K. J.; Ebner, A. D. On the Use of the Dual Process Langmuir Model for Binary Gas Mixture Components That Exhibit Single Process or Linear Isotherms. *Adsorption* **2019**, *25*, 1511−1523.

(474) Fehr, J.; Heiland, J.; Himpe, C.; Saak, J. Best Practices for Replicability, Reproducibility and Reusability of Computer-Based Experiments Exemplified by Model Reduction Software. *AIMS Mathematics* **2016**, *1*, 261−281.

(475) Peng, R. D. Reproducible Research in Computational Science. *Science* **2011**, *334*, 1226.

(476) Dang, W.; Friedrich, D.; Brandani, S. Characterisation of an Automated Dual Piston Pressure Swing Adsorption (Dp-Psa) System. *Energy Procedia* **2013**, *37*, 57−64.

(477) Gibson, J. A. A.; Mangano, E.; Shiko, E.; Greenaway, A. G.; Gromov, A. V.; Lozinska, M. M.; Friedrich, D.; Campbell, E. E. B.; Wright, P. A.; Brandani, S. Adsorption Materials and Processes for Carbon Capture from Gas-Fired Power Plants: Ampgas. *Ind. Eng. Chem. Res.* **2016**, *55*, 3840−3851.

(478) Hartzog, D. G.; Sircar, S. Sensitivity of Psa Process Performance to Input Variables. *Adsorption* **1995**, *1*, 133−151.

(479) Shih, C.; Park, J.; Sholl, D. S.; Realff, M. J.; Yajima, T.; Kawajiri, Y. Hierarchical Bayesian Estimation for Adsorption Isotherm Parameter Determination. *Chem. Eng. Sci.* **2020**, *214*, 115435.

(480) McDonald, T. M.; Mason, J. A.; Kong, X.; Bloch, E. D.; Gygi, D.; Dani, A.; Crocellà, V.; Giordanino, F.; Odoh, S. O.; Drisdell, W. S.; Vlaisavljevich, B.; Dzubak, A. L.; Poloni, R.; Schnell, S. K.; Planas, N.; Lee, K.; Pascal, T.; Wan, L. F.; Prendergast, D.; Neaton, J. B.; Smit, B.; Kortright, J. B.; Gagliardi, L.; Bordiga, S.; Reimer, J. A.; Long, J. R. Cooperative Insertion of CO₂ in Diamine-Appended Metal-Organic Frameworks. *Nature* **2015**, *519*, 303−308.

(481) Reichenbach, C.; Kalies, G.; Lincke, J.; Lässig, D.; Krautscheid, H.; Moellmer, J.; Thommes, M. Unusual Adsorption Behavior of a Highly Flexible Copper-Based Mof. *Microporous Mesoporous Mater.* **2011**, *142*, 592−600.

(482) Rogacka, J.; Formalik, F.; Triguero, A. L.; Firlej, L.; Kuchta, B.; Calero, S. Intermediate States Approach for Adsorption Studies in Flexible Metal-Organic Frameworks. *Phys. Chem. Chem. Phys.* **2019**, *21*, 3294−3303.

(483) Mu, B.; Li, F.; Huang, Y.; Walton, K. S. Breathing Effects of CO₂ Adsorption on a Flexible 3d Lanthanide Metal-Organic Framework. *J. Mater. Chem.* **2012**, *22*, 10172−10178.

(484) Rogge, S. M. J.; Goeminne, R.; Demuynck, R.; Gutiérrez-Sevillano, J. J.; Vandenbrande, S.; Vanduyfhuys, L.; Waroquier, M.; Verstraelen, T.; Van Speybroeck, V. Modeling Gas Adsorption in Flexible Metal-Organic Frameworks Via Hybrid Monte Carlo/Molecular Dynamics Schemes. *Adv. Theory Simul.* **2019**, *2*, 1800177.

(485) Remy, T.; Baron, G. V.; Denayer, J. F. M. Modeling the Effect of Structural Changes During Dynamic Separation Processes on Mofs. *Langmuir* **2011**, *27*, 13064−13071.

(486) Verbraeken, M. C.; Brandani, S. Predictions of Stepped Isotherms in Breathing Adsorbents by the Rigid Adsorbent Lattice Fluid. *J. Phys. Chem. C* **2019**, *123*, 14517−14529.

(487) Nandi, S.; Collins, S.; Chakraborty, D.; Banerjee, D.; Thallapally, P. K.; Woo, T. K.; Vaidhyanathan, R. Ultralow Parasitic Energy for Postcombustion CO₂ Capture Realized in a Nickel Isonicotinate Metal-Organic Framework with Excellent Moisture Stability. *J. Am. Chem. Soc.* **2017**, *139*, 1734−1737.

(488) Burtch, N. C.; Jasuja, H.; Walton, K. S. Water Stability and Adsorption in Metal-Organic Frameworks. *Chem. Rev.* **2014**, *114*, 10575−10612.

(489) *Handbook of Zeolite Science and Technology*; M. Dekker: New York, 2003.

(490) Singh, A.; Stéphenne, K. Shell Cansolv CO₂ Capture Technology: Achievement from First Commercial Plant. *Energy Procedia* **2014**, *63*, 1678−1685.

(491) Britt, D.; Furukawa, H.; Wang, B.; Glover, T. G.; Yaghi, O. M. Highly Efficient Separation of Carbon Dioxide by a Metal-Organic Framework Replete with Open Metal Sites. *Proc. Natl. Acad. Sci. U. S. A.* **2009**, *106*, 20637.

(492) Yang, D.-A.; Cho, H.-Y.; Kim, J.; Yang, S.-T.; Ahn, W.-S. CO₂ Capture and Conversion Using Mg-Mof-74 Prepared by a Sonochemical Method. *Energy Environ. Sci.* **2012**, *5*, 6465−6473.

(493) Kizzie, A. C.; Wong-Foy, A. G.; Matzger, A. J. Effect of Humidity on the Performance of Microporous Coordination Polymers as Adsorbents for CO₂ Capture. *Langmuir* **2011**, *27*, 6368−6373.

(494) Tan, K.; Zuluaga, S.; Gong, Q.; Canepa, P.; Wang, H.; Li, J.; Chabal, Y. J.; Thonhauser, T. Water Reaction Mechanism in Metal

Organic Frameworks with Coordinatively Unsaturated Metal Ions: Mof-74. *Chem. Mater.* **2014**, *26*, 6886−6895.

(495) Bon, V.; Kavoosi, N.; Senkovska, I.; Kaskel, S. Tolerance of Flexible Mofs toward Repeated Adsorption Stress. *ACS Appl. Mater. Interfaces* **2015**, *7*, 22292−22300.

(496) Wang, C.; Liu, X.; Keser Demir, N.; Chen, J. P.; Li, K. Applications of Water Stable Metal-Organic Frameworks. *Chem. Soc. Rev.* **2016**, *45*, 5107−5134.

(497) Howarth, A. J.; Liu, Y.; Li, P.; Li, Z.; Wang, T. C.; Hupp, J. T.; Farha, O. K. Chemical, Thermal and Mechanical Stabilities of Metal-Organic Frameworks. *Nature Reviews* **2016**, *1*, 15018.

(498) Liu, X.; Wang, X.; Kapteijn, F. Water and Metal-Organic Frameworks: From Interaction toward Utilization. *Chem. Rev.* **2020**, *120*, 8303−8377.

(499) Shimizu, G.; Vaidhyanathan, R.; Iremonger, S.; Deakin, K.; Lin, J.-B.; Dawson, K. W. Metal Organic Framework, Production and Use Thereof - Cross-Reference to Related Applications. International Patent WO2014138878A1, 2014.

(500) Qazvini, O. T.; Telfer, S. G. A Robust Metal-Organic Framework for Post-Combustion Carbon Dioxide Capture. *J. Mater. Chem. A* **2020**, *8*, 12028−12034.

(501) Batra, R.; Chen, C.; Evans, T. G.; Walton, K. S.; Ramprasad, R. Prediction of Water Stability of Metal-Organic Frameworks Using Machine Learning. *Nature Machine Intelligence* **2020**, *2*, 704−710.

(502) Zoelle, A.; Keairns, D.; Pinkerton, L.; Turner, M.; Woods, M.; Kuehn, N.; Shah, V.; Chou, V. Cost and Performance Baseline for Fossil Energy Plants Vol. 1a: Bituminous Coal (Pc) and Natural Gas to Electricity Revision 3, DOE/NETL-2015/1723, National Energy Technology Laboratory (NETL), 2015.

(503) Murray, J. Profiling the Five Largest Coal Power Plants in China. *NS ENERGY* https://www.nsenergybusiness.com/features/largest-coal-plants-china/, 2021.

(504) Rubio-Martinez, M.; Avci-Camur, C.; Thornton, A. W.; Imaz, I.; Maspoch, D.; Hill, M. R. New Synthetic Routes Towards Mof Production at Scale. *Chem. Soc. Rev.* **2017**, *46*, 3453−3480.

(505) DeSantis, D.; Mason, J. A.; James, B. D.; Houchins, C.; Long, J. R.; Veenstra, M. Techno-Economic Analysis of Metal-Organic Frameworks for Hydrogen and Natural Gas Storage. *Energy Fuels* **2017**, *31*, 2024−2032.

(506) Letourneau, C.; Dreyer, D. *Lafargeholcim and Svante: Preparing for the Future Carbon Economy*; Edwards, P., Ed.; Global Cement Magazine: 2020; pp 20−24.

(507) Ghaffari-Nika, O.; Mariacb, L.; Liua, A.; Henkela, B.; Marxd, S.; Hovington, P. Rapid Cycle Temperature Swing Adsorption Process Using Solid Structured Sorbent for CO_2 Capture from Cement Flue Gas. Presented at the 15th International Conference on Greenhouse Gas Control Technologies (GHGT-15), Abu Dhabi, UAE, March 2021.

(508) Schmidt, J.; Marques, M. R. G.; Botti, S.; Marques, M. A. L. Recent Advances and Applications of Machine Learning in Solid-State Materials Science. *npj Computational Materials* **2019**, *5*, 83.

(509) Ruthven, D. M.; Thaeron, C. Performance of a Parallel Passage Adsorbent Contactor. *Sep. Purif. Technol.* **1997**, *12*, 43−60.

(510) Cho, S.-H., et al. A 2-stage PSA process for the recovery of CO2 from flue gas and its power consumption, in Studies in Surface Science and Catalysis; Park, S.-E., Chang, J.-S., Lee, K.-W., Editors. 2004, Elsevier. pp 405−410, https://doi.org/10.1016/S0167-2991(04)80287-8.